UNIVERSIDADE DE LISBOA
FACULDADE DE CIÊNCIAS

UNIVERSIDADE FEDERAL DO
RIO DE JANEIRO
INSTITUTO DE GEOCIÊNCIAS

Compound Drought and Heatwaves over South America: Land–atmosphere processes, atmospheric driving mechanisms and impacts in a changing world

" Documento Definitivo"

Doutoramento em Ciências Geofísicas e da Geoinformação
Meteorologia
Programa de Pós-Graduação em Meteorologia
Meteorologia

João Lucas Marcelino Geirinhas

Tese orientada por:
Professora Doutora Ana Cristina Machado Russo
Professora Doutora Renata Libonati dos Santos
Professor Doutor Diego Gonzalez Miralles

Documento especialmente elaborado para a obtenção do grau de doutor

2024

UNIVERSIDADE DE LISBOA
FACULDADE DE CIÊNCIAS

UNIVERSIDADE FEDERAL DO
RIO DE JANEIRO
INSTITUTO DE GEOCIÊNCIAS

Compound Drought and Heatwaves over South America: Land–atmosphere processes, atmospheric driving mechanisms and impacts in a changing world

Doutoramento em Ciências Geofísicas e da Geoinformação
Meteorologia
Programa de Pós-Graduação em Meteorologia
Meteorologia

João Lucas Marcelino Geirinhas

Tese orientada por:

Professora Doutora Ana Cristina Machado Russo

Professora Doutora Renata Libonati dos Santos

Professor Doutor Diego Gonzalez Miralles

Júri:
Presidente:

- Miguel Centeno da Costa Ferreira Brito, Professor Associado com Agregação e Presidente do Departamento de Engenharia Geográfica, Geofísica e Energia da Faculdade de Ciências da Universidade de Lisboa

Vogais:

- Doutor Gutemberg Borges França, Professor Titular do Departamento de Meteorologia da Universidade Federal do Rio de Janeiro, Brasil
- Doutor David Barriopedro Cepero, Research Professor do Instituto de Geociencias (IGEO) da Universidad Complutense de Madrid, Espanha
- Doutora Margarida da Conceição Rasteiro Magano Lopes Rodrigues Liberato, Professora Associada da Escola de Ciências e Tecnologia da Universidade de Trás-os-Montes e Alto Douro
- Doutora Ana Cristina Machado Russo, Investigadora do Instituto Dom Luiz da Faculdade de Ciências da Universidade de Lisboa (orientadora)
- Doutora Rita Margarida Antunes de Paula Cardoso Tavares, Investigadora do Instituto Dom Luiz da Faculdade de Ciências da Universidade de Lisboa

Tese financiada pela Fundação para a Ciência e Tecnologia com a bolsa 2020.05198.BD

Documento especialmente elaborado para a obtenção do grau de Doutor

2024

Acknowledgments

First of all, I would like to thank my supervisors Ana Russo, Renata Libonati and Diego Miralles for their constructive supervision, expertise, know-how and vision. They were absolutely key for the accomplishment of this milestone in my life, always showing a great availability and willingness to provide their best support. They never left me alone during these four years. I also acknowledge the opportunity they gave me to establish new lines of collaboration. They were important to enhance the quality and interest of the outcomes produced by this project. In particular, I would like to thank Ana Russo for including me in the project DHEFEUS (https://doi.org/10.54499/2022.09185.PTDC), which co-funded this PhD program together with the grant 2020.05198.BD from Fundação para a Ciência e Tecnologia (FCT).

I am also grateful to all the colleagues and researchers from Instituto Dom Luiz, the Federal University of Rio de Janeiro and the University of Ghent who followed my steps and contributed, each in their own way, for this project. A special thanks goes for Ricardo Trigo, Pedro Sousa, Alexandre Ramos, Daniela Lima and Carlos da Camara. Without their contribution and support, I have to say that none of the published papers presented in this thesis would have reached such a satisfactory level.

I am deeply grateful to my family and, in particular, to my parents. They always encouraged me to pursue my goals and to devote my energy to this project, knowing that this was far from being the easiest option to my personal and professional life.

I am also grateful to my long-time friends who have always shown an interest in my academic life and wanted me to succeed. These four years have helped me to realize that friends are essential for the emotional balance in our lives. Work becomes easier and more enjoyable when you have someone close to you that will help you keep things in perspective.

Finally, thank you Tamara. I'm sure I would never been able to do this without your support. I know that this journey has also forced you to make some sacrifices. Although your name is not on the list of authors, this thesis was also done by you.

Abstract

Recent decades in South America (SA) have been marked by an increase in the frequency and magnitude of hot and dry spells. This changing pattern is unequivocally tied to an unsustainable level of anthropogenic greenhouse emissions. Future climate change projections indicate a further aggravation of this trend, representing a serious threat to ecosystem sustainability and to human well-being. Over the past few years, the scientific community has been joining efforts to improve the knowledge around this topic. Even so, a thorough characterization of droughts and heatwaves, particularly when their occur in a compound event manner, is still lacking for SA. The assessment, under a climate change context, of the atmospheric forcing mechanisms and of the land–atmosphere feedbacks that control the intensification and propagation of hot and dry spells, is still missing for the region.

This thesis aims to fill these gaps and to provide solid answers to the following main research questions: (i) What was the historical evolution of compound drought and heatwave (CDHW) conditions over SA? (ii) What are the physical mechanisms driving these compound events? (iii) What should we expect in a future climate change scenario?

Results show that vast areas in SA have recorded a significant increase in the number of CDHW episodes. Recent summer periods have witnessed strong soil moisture–temperature coupling conditions that triggered record-breaking temperatures and outstanding 'mega-heatwave' episodes. A long-term soil drying trend resulting from a joint contribution of natural variability, via large-scale tropical and subtropical dynamics, and climate change, via increasing temperatures, has predisposed some regions in SA to face unprecedented droughts, temperatures and devastating wildfires in the recent years. An overall increment of these compound episodes is expected in the future, partially due to an enhancement of the soil moisture–temperature coupling in some regions of SA. This thesis highlights the complex interplay between distinct physical mechanisms that modulate the occurrence of CDHW conditions, and calls attention to under-examined feedback processes that need to be properly addressed by climate models, setting ground for a more effective design of mitigation measures by authorities.

Keywords: South America; Climate Change; Droughts; Heatwaves; Compound events

Resumo

Nas últimas décadas a América do Sul tem sido marcada por uma tendência crescente do número de ocorrências, duração e intensidade de eventos extremos de calor e seca. Este é um padrão de alteração semelhante ao observado em diversas outras regiões do planeta e que se encontra inequivocamente ligado à libertação excessiva de gases de efeito de estufa causada pela atividade humana no pós revolução industrial. Este desiquilibrio antropogénico resulta numa tendência de aquecimento global que se reflecte não só em alterações na termodinâmica do sistema climático e em particular numa intensificação do ciclo da água, mas também em alterações na própria dinâmica do escoamento atmosférico. Assim, o aumento médio da temperatura junto à superfície pode aliar-se, através destes dois tipos de alterações, a uma maior variabilidade temporal e espacial da temperatura e precipitação, bem como a uma maior covariância entre estas duas variáveis. Em teoria todo este processo poderá, em última análise, resultar num aumento generalizado do número de eventos de seca e onda de calor bem como numa maior interligação entre estes dois extremos, permitindo a sua amplificação mútua. De acordo com a maioria dos cenários futuros de alterações climáticas, é expectável que esta tendência se mantenha, havendo inclusive a possibilidade de uma intensificação até ao final do século. Por consequência, a sustentabilidade de grande parte dos ecossistemas assim como o bem-estar e a própria vida humana encontram-se seriamente em risco.

Ao longo dos últimos anos, a comunidade científica tem-se focado no aprofundamento da análise em torno deste tópico. Contudo, o esforço imprimido para uma melhor caracterização e compreensão deste assunto está longe de ser o mesmo para todas as regiões do globo. A América do Sul destaca-se precisamente como uma das regiões do planeta onde uma caracterização profunda e detalhada deste tipo de episódios extremos de calor e seca está ainda em falta. Esta ausência de conhecimento científico torna-se ainda mais clara quando, na literatura, é difícil encontrar algum tipo de informação relativamente à ocorrência acoplada destes dois extremos, aos processos atmosféricos e de superfície–atmosfera que estão subjacentes ao seu forçamento, e aos impactos naturais e socioeconómicos gerados.

Esta tese de doutoramento procura assim colmatar estas falhas no conhecimento científico e contribuir de forma significativa para o estudo da temática no continente sul americano. Como tal, pretende-se dar resposta às seguintes questões: (i) Qual foi o padrão de evolução ao longo das últimas décadas dos eventos compostos de seca e onda de calor na América do Sul? (ii)

Quais os principais mecanismos físicos por detrás da ocorrência, propagação e amplificação deste tipo de episódios? (iii) O que podemos esperar num contexto futuro de alterações climáticas?

Os resultados indicam que vastas áreas no continente sul Americano têm registado um aumento significativo do número de eventos compostos de seca e onda de calor. Este incremento explica-se não só à luz das tendências de aquecimento global mas também por via de um aumento da variabilidade e da covariância entre a precipitação e a temperatura. Isto gera, por um lado, uma maior probabilidade de ocorrência dos dois extremos e, por outro, uma maior hipótese de estes se originarem de forma simultânea e tomarem um comportamento acoplado. Durante alguns períodos de verão mais recentes, acentuadas condições de seca sobrepostas a fortes taxas de aquecimento radiativo resultaram num forte acoplamento entre a humidade do solo e a temperatura. Este regime de acoplamento, associado a uma substituição gradual dos níveis de evaporação por um maior fluxo de calor sensível da superfície para a atmosfera, foi responsável por uma amplificação das condições pré-existentes de seca e pelo escalamento dos valores de temperatura para níveis record. O carácter excepcional de alguns eventos de mega-onda de calor que se fizeram sentir em algumas regiões da América do Sul durantes estes verões e que estiveram associados a níveis de *stress* térmico extremo em algumas regiões metropolitanas, deveu-se em grande medida, a uma sobreposição entre estes mecanismos de interação superfície–atmosfera e um forçamento atmosférico previamente estabelecido.

Nas últimas décadas, algumas áreas mais centrais da América do Sul têm vindo a observar um padrão persistente caracterizado pela redução do conteúdo de água disponível nos solos. Os resultados demonstraram que este decréscimo é, por um lado, produto do aumento dos níveis de evaporação suportado pelas tendências lineares de aquecimento global e, por outro, resultado de uma diminuição ao longo das últimas décadas dos níveis de precipitação causada pela variabilidade natural do sistema climático. Este padrão culminou na ocorrência de um episódio de seca extrema entre os anos de 2019 e 2022 com características excepcionais dada a sua duração, intensidade e expressão espacial. Níveis mínimos de humidade do solo cobriram uma extensa área no centro da América do Sul com cerca de 100.000 km^2 e estiveram associados à propagação de incêndios devastadores na região. Do ponto de vista atmosférico, foi ainda possível observar que a ocorrência destas anomalias expressivas da humidade do solo tiveram a sua origem numa complexa e interligada rede de mecanismos forçadores com diferentes escalas espaciais e temporais. Primeiro, prolongados *deficits* de precipitação estabeleceram-se

sobre a região em resultado de uma circulação anómala tropical associada a um intenso episódio de La Niña. Posteriormente, episódios de *flash drought* relacionados com condições extremas de onda de calor, sobrepuseram-se ao já existente evento de seca através do estabelecimento de um padrão ondulatório de teleconexão subtropical, tipicamente conhecido como Ondas de Rossby.

A tese revela ainda que num contexto futuro de alterações climáticas, perspectiva-se uma maior probabilidade de ocorrência deste tipo de eventos compostos de seca e de onda de calor. Ainda que esta seja uma tendência expectável para a generalidade do continente sul Americano, as maiores alterações estimam-se que ocorram nas regiões tropicais. É também a latitude mais baixas que se espera um fortalecimento mais acentuado do regime de acoplamento entre a humidade do solo e a temperatura. De facto, a atual ligação entre a intensidade deste regime de retro-alimentação entre a superfície e a atmosfera, e o estabelecimento de condições compostas de seca e onda de calor é clara para algumas destas regiões mais tropicais. Perspectiva-se, inclusive, que esta conexão se torne ainda mais intensa até ao final do século, o que indica uma potencial relação de causalidade entre estes dois parâmetros cuja análise deverá ser aprofundada em trabalhos futuros.

Assim, esta tese explora com carácter inovador o efeito que mecanismos não lineares e menos explorados podem ter na definição de uma trajetória crescente de eventos de seca e onda de calor. Destaca-se ainda a complexa rede de processos físicos que está por detrás da ocorrência e dinâmica deste tipo de extremos climáticos. Com isto, torna-se evidente a necessidade de compreender e modelar de forma mais eficaz o efeito conjunto que as alterações e a variabilidade climática podem ter nesta multitude de processos atmosféricos e de interacção entre a superfície e a atmosfera. Só conhecendo todos os meandros do sistema climático, será possível quantificar de forma exacta os efeitos causados pelas alterações climáticas e assim evitar uma eventual subestimação dos seus impactos nas décadas futuras. É ainda importante salientar o grau de novidade e relevância que as conclusões aqui obtidas representam para o conhecimento científico, considerando a vulnerabilidade e as fragilidades dos ecossistemas e do tecido socioeconómico de grande parte dos países da América do Sul.

Palavras-chave: América do Sul; Alterações Climáticas; Secas; Ondas de Calor; Eventos Compostos

Contents

List of Acronyms and Abbreviations

CDHW	Compound Drought and Heatwave
SA	South America
GHG	Greenhouse Gas
RQ	Research Question
SEB	Southeast Brazil
SP	São Paulo
RJ	Rio de Janeiro
MG	Minas Gerais
GLEAM	Global Land Evaporation Amsterdam Model
SPI	Standardized Precipitation Index
DJF	December, January, February
CDH	Compound Dry and Hot
UASP	Urban Area of São Paulo
UACT	Urban Area of Curitiba
VPD	Vapor Pressure Deficit
INMET	Brazilian National Institute of Meteorology
ECMWF	European Centre of Medium-Range Weather Forecast
CESA	Central-East South America
ENSO	El Niño–Southern Oscillation
MJO	Madden–Julian Oscillation
AMM	Atlantic Meridional Mode
AZM	Atlantic Zonal Mode
SALLJ	South America Low-Level Jet
VIMC	Vertically Integrated Moisture Convergence
IVT	Vertically Integrated Water Vapor Transport
PDO	Pacific Decadal Oscillation
SOI	Southern Oscillation Index
ONI	Oceanic Niño Index

RWS	Rossby Wave Source
SST	Sea Surface Temperature
EOF	Empirical Orthogonal Function
SAM	Southern Annular Mode
IPCC	Intergovernmental Panel on Climate Change
ESGF	Earth System Grid Federation
RMSE	Root Mean Square Error
NWS	Northwest South America
NSA	North South America
NES	Northeast South America
SAM	South America Monsoon Region
SES	Southeast South America
SWS	Southwest South America
SSA	South South America
RCP	Representative Concentration Pathway

List of Symbols

T_{max}	Maximum Temperature
T_{mean}	Mean Temperature
Z500	500 hPa geopotential height
lat	latitude
lon	longitude
p	p-value
HWF	Number of summer day under a heatwave regime
HWD	Duration of the longest ever recorded summer heatwave
HWN	Number of summer heatwaves
HWMId	Heatwave Magnitude Index
π	Soil Moisture–temperature coupling
T	Near surface air temperature
E	Evaporation
E_p	Potential Evaporation
T'	Daily anomalies of T
H	Sensible heat Flux
H_p	Potential sensible heat flux
H'	Daily anomalies of H
H'_p	Daily anomalies of H_p
λE	Latent Heat Flux
R_n	Surface net radiation
λ	latitude
ϕ	longitude
t	time
Δ	Finite difference

v	Horizontal wind speed
T	Temperature
ω	Vertical Velocity
θ	Potential Temperature
R	Pearson's Correlation Coefficient
kg	Kilogram
m	meter
s	second
mm	Millimeter
Pa	Pascal
hPa	hectopascal
P	Precipitation
km^2	Square kilometer
°C	Degrees Celsius
°W	Degree West
°S	Degree South
m^3	Cubit meter
Q_λ	Zonal transport of specific humidity
Q_ϕ	Meridional transport of specific humidity
q	Specific humidity
u	Zonal wind
v	Meridional wind
g	Gravitational acceleration
dp	Infinitesimal element of vertical pressure
ζ	Absolute vorticity
ν_x	Non-rotational wind vector component

∇	Gradient
Π	Soil Moisture–temperature coupling
$CDHW_{days}$	Mean number of summer days under CDHW conditions
R^2	Explained Variance
CO_2	Carbon Dioxide

List of Figures

List of Tables

Chapter 1
Introduction

1. Introduction

In this section, a general overview of compound drought and heatwave (CDHW) events is presented, considering the current and future climate change scenario and the numerous natural and socioeconomic impacts over South America (SA). The aim is to provide an overall conceptualization of the problem, highlighting the main physical concepts and exploring the relevance of the topic. The following chapters are *ipsis verbis* versions of published (Chapters 2, 3 and 4) and under review (Chapter 5) studies, and the body of their original version is preserved. Chapters 2, 3, 4 and 5 include the respective introduction, data and methods section, followed by results, discussion and conclusions. This applies also to the contents of the appendix sections (Appendix A, B and C). To some extent, repetition in the description of concepts, datasets and methods is unavoidable. Chapter 1 provides a general contextualization of the research questions addressed in the succeeding chapters. More detailed information about the research objectives and the thesis structure follows in the last part of this opening section.

1.1 General Context

The greenhouse gas (GHG) emissions from human activities have been leading to a sharp and unprecedented warming trend, resulting in global surface temperatures higher by 1.1 °C in 2011–2020 compared to the pre-industrial (1850–1900) period (IPCC 2023). This anthropogenic forcing has been responsible for pronounced changes not only in temperature but also in precipitation distribution and, ultimately, in the frequency, magnitude and spatiotemporal patterns of extreme events such as heatwaves (Perkins-Kirkpatrick and Lewis 2020; Rousi et al. 2022) and droughts (Wu et al. 2022). Climate change has also strengthened the synchronisation in space and time of such extremely hot and dry conditions (Mukherjee et al. 2023) triggering more frequent and severe CDHW events in recent decades (Figure 1.1) (Hao et al. 2018a; Geirinhas et al. 2021; Mukherjee and Mishra 2021). Further global warming will likely pave the way for a continuous escalation of such co-occurring conditions (Mukherjee and Mishra 2021), posing severe threats to ecosystem sustainability (Yin et al. 2023; Xu et al. 2024), economy (García-León et al. 2021), food security (Ribeiro et al. 2020a) and human well-being (Ballester et al. 2023), as CDHW events often lead to more devastating impacts than isolated extremes (Zscheischler and Seneviratne 2017; Zscheischler et al. 2018; Yin et al. 2023).

Recent studies have shown that anomalous synoptic circulation patterns are the main initiator of CDHW events (Schumacher et al. 2019; Sousa et al. 2020; Geirinhas et al. 2022), that are further amplified, spatially and temporally, due to enhanced background warming caused by the GHG emissions (Alizadeh et al. 2020; Collazo et al. 2024). Nonetheless, the impact of climate change in the escalation of CDHW episodes goes beyond the one promoted by the anthropogenic warming trends that increase the likelihood of temperature extremes, or by other straightforward thermodynamical effects (Rahmstorf and Coumou 2011; Christidis et al. 2015). More complex mechanisms that are also sensitive to climate change, involving soil moisture imbalances and dynamical processes embedded in the internal variability of climate, may further intensify the climate change impacts, as they lead to more persistent large-scale circulation anomalies (Kornhuber et al. 2019; Rousi et al. 2022; White et al. 2022) and positive land–atmosphere feedbacks (Miralles et al. 2019; Qiao et al. 2023) (Figure 1.1). In this context, planetary wave resonance, associated with high-amplitude quasi-stationary Rossby waves, has been linked to the occurrence of extreme hot and dry events in the Northern Hemisphere (Kornhuber et al. 2019; Rousi et al. 2022). Although projections from climate models regarding this topic are bound to a relatively high level of uncertainty, future increases in the jet stream meandering and in these slow-moving amplified Rossby waves are foreseen, favoring the occurrence of CDHW conditions (Mann et al. 2017, 2018). Climate change has also led to an intensification of Earth's water cycle and to more frequent and severe episodes of extreme wet and dry climate (Allan et al. 2020; Chagas et al. 2022; Ficklin et al. 2022). Resulting disturbances in the land-surface water balance might amplify the land–atmosphere interactions and the level of influence of soil moisture in the portioning of surface energy and, therefore, in temperature variability (Seneviratne et al. 2010; Miralles et al. 2012). Such synergy between the land surface and the atmosphere can occur at a local scale (Geirinhas et al. 2022; Lemus-Canovas et al. 2024), with a progressive multi-day heat entrainment and accumulation in the atmospheric boundary layer (Miralles et al. 2014). It can also enhance downwind influences through the advection of sensible heat, enabling the spatial propagation of droughts and heatwaves (Schumacher et al. 2019).

Although the problem around CDHW events and all the previously mentioned physical mechanisms has already been addressed for many regions and case studies in the Northern Hemisphere, for the Southern Hemisphere and, particularly for SA, there is still a relatively large knowledge gap (Libonati et al. 2022b). Despite countries in SA being responsible for only 8% of all GHG emissions globally (Watch 2024), they are especially vulnerable to climate hazards due to marked socioeconomic inequalities, a sharp population growth, an increasing urban population density, a low average income, and fragile public health systems unable to

protect people from more frequent and severe weather extremes (Libonati et al. 2022b; Hartinger et al. 2023; dos Santos et al. 2024). Furthermore, several regions within SA have been witnessing an increasing trend in the frequency and magnitude of extreme hot events (Ceccherini et al. 2016; Geirinhas et al. 2018a; Feron et al. 2019). This enhancement is expected to be maintained or even amplified under a future climate change scenario, particularly in tropical regions (Feron et al. 2019). An escalation of dry conditions has also been observed. However, the recent decades have been characterized by an absence of a coherent changing pattern, in space and time, of precipitation over the continent (Geirinhas et al. 2023; Tomasella et al. 2023). This clearly points to an active role played by global warming in leading to higher variability in soil moisture due to enhanced evaporation rates. Meanwhile, there is a strong indication that the future will hold an amplified hydrological cycle, with more frequent and intense drought episodes, explained by increasingly heavy-tailed precipitation distributions and a rightward shifted temperature distribution (Almazroui et al. 2021). However, the consequences of these future changes for the soil moisture availability and for the land–atmosphere feedbacks, are not yet fully understood.

South America is home to some of the world's most vital and diverse natural ecosystems, including the Amazon rainforest, the Brazilian Atlantic Forest, the Brazilian savanna (Cerrado), the Patagonian ecosystems and the Pantanal, which is the largest contiguous wetland of the world (Bergier and Assine 2016). All these ecosystems are characterized by a large variety of plants and animals, including several endangered species that are threatened by climate

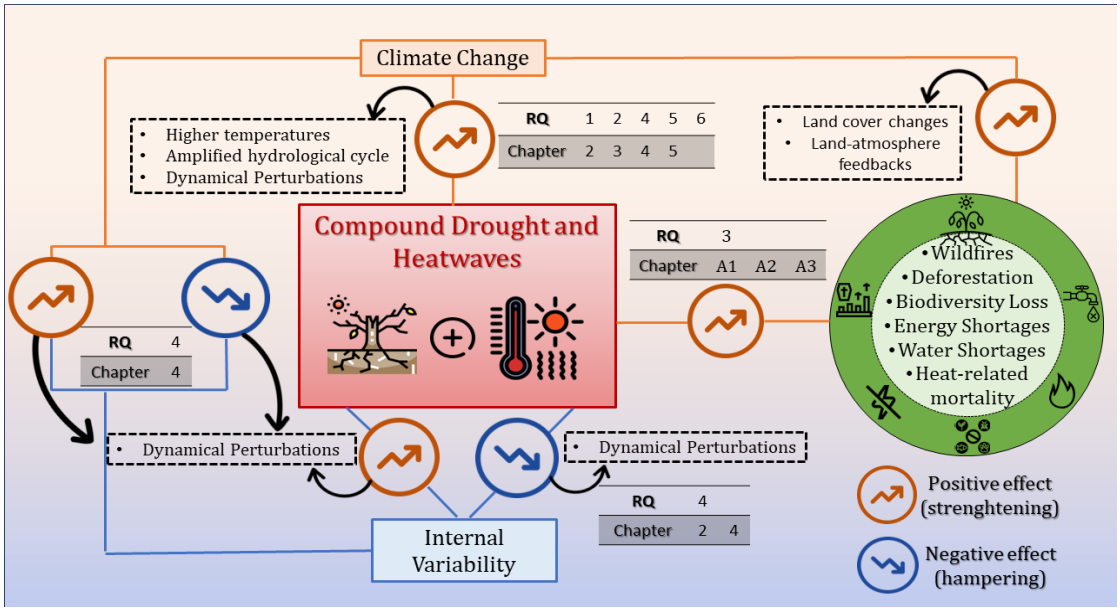

Figure 1.1 Illustrative and schematic conceptualization of the main research topic under analysis in the PhD project, highlighting the intricate links between CDHW conditions, climate change and internal variability, through a framework of cascading climate impacts and positive feedback mechanisms. The inset tables indicate the associated Research Questions and the Chapter of thesis in which the illustrated processes are analyzed.

extremes (Gatti et al. 2021), wildfires (Tomas et al. 2021), agriculture expansion (Lopes dos Santos et al. 2021) and the unsustainable extraction of wood for economic purposes (Matricardi et al. 2020). Moreover, these ecosystems play a key role in the global carbon cycle. From 2001 to 2021, Brazil lost almost 63 Mha of tree cover which corresponds to a 12% decrease and 34.5 Gt of CO_2 emissions (Global Forest Watch, 2024). Climate change via increasing trends in the frequency and magnitude of drought and heatwave events, has been leading to a rising forest stress and to extensive pulses of tree mortality (Park Williams et al. 2013; Yan et al. 2024). A positive feedback may then be established as this decline in tree cover can affect climate itself through the amplification of the upstream anthropogenic disturbances resulting from global warming (Figure 1.1). In this context, tree mortality and deforestation have been linked to less moisture of Amazon origin, resulting in precipitation reductions over local and downwind regions of SA, including the main breadbaskets of the continent (Eiras-Barca et al. 2020; Li et al. 2023).

The transport and convergence of moisture coming from the Amazon region determines, with the contribution of several dynamical mechanisms embedded in the South America Monsoon System (SAMS) and in the natural variability of climate system (de Carvalho and Cavalcanti 2016; Montini et al. 2019; Geirinhas et al. 2023), the spatiotemporal patterns of precipitation and temperature in SA (Figure 1.1). The complex network of climate features associated with SAMS is influenced by several global interannual and intraseasonal climate modes of variability, such as the El Niño-Southern Oscillation (ENSO) and the Madden-Julian Oscillation (MJO), via perturbations in the Walker circulation and Rossby waves (Cai et al. 2020; Fernandes and Grimm 2023). Disturbances in this moisture transport and convergence, responsible for long-term and slow-evolving droughts in SA, are, in some instances, associated with the establishment of quasi-stationary anticyclonic anomalies in the atmosphere prone to the occurrence of heatwaves, enhanced evaporation rates and sharp decreases in soil moisture (Geirinhas et al. 2023). These compound conditions constitute the ideal ingredients for the occurrence of severe CDHW episodes, flash droughts and wildfires (Otkin et al. 2018; Geirinhas et al. 2021, 2023; Libonati et al. 2022a), hampering the public water supply, hydropower generation, agriculture production and the fluvial transport in SA (Gomes et al. 2021; Marengo et al. 2021).

In addition to these environmental impacts, evidence has been mounting that the extreme heat-stress conditions felt during CDHW events have clear impacts on public health, particularly on excessive mortality rates, hospitalizations, preterm births, human cognitive

performance, mental health and work-related injuries (Figure 1.1). This is particularly evident in low-income regions such as the case of SA, with growing populations (Cole et al. 2023), fragile infrastructures (Cui et al. 2024) and health care (dos Santos et al. 2024). Currently, four-fifths of the South American population live in urban areas of mega-cities like São Paulo, Buenos Aires and Rio de Janeiro (Hartinger et al. 2023), being particularly susceptible to climate and environmental conditions. Some regions within SA with a tropical climate, have been witnessing several dengue mosquito outbreaks during heatwave episodes, that are more severe over mega-metropolitan areas due to the urban heat island effect (Jia et al. 2019; He et al. 2021). Another cascading impact generated by CDHW conditions on human health, may rise through increases in the vegetation flammability and the occurrence of severe wildfires that release a large amount of particulate matter and gases into the atmosphere, causing severe respiratory illnesses (Machado-Silva et al. 2020) (Figure 1.1).

The still open questions about the intricate interplay between CDHW events, climate dynamics, land–atmosphere processes and the numerous natural and socioeconomic impacts driven by these compound conditions, warrant the need for studies aiming to better understand the problem in a future climate change perspective. Figure 1.1 illustrates this complex network of inter-links wrapped up in a non-linear chain of processes that might reflect a self-amplifying cycle. This is even more important when the region under consideration has, so far, received little attention from the scientific community and has all the previously enumerated rich, unique, global-impact environmental features and socioeconomic gaps. With this in mind, the importance of the analysis presented in this thesis for science, local authorities and policy makers becomes clear and unquestionable.

1.2 Goals and research objectives

This thesis focuses on investigating hot and dry extremes over SA from both past and future climate change perspectives, their underlying atmospheric forcing mechanisms, and the associated land–atmosphere feedbacks. The main goal is to understand the nexus between these two extremes and to analyze their co-occurrence, mutual amplification, and impacts on the region. Throughout this thesis, the following research questions (RQ) are addressed sequentially:

RQ1. How has climate change contributed in recent decades to a spatiotemporal increase in the CDHW conditions over SA?

RQ2. What is the exact role played by land–atmosphere interactions and particularly by soil moisture–temperature coupling in the occurrence, amplification and propagation of CDHWs over SA?

RQ3. If these land–atmosphere interactions are proven to amplify CDHW events and to trigger enhanced heat stress conditions and flammability levels in vegetation, are there any cascading impacts, particularly on public health and wildfire occurrence?

RQ4. What are the main local and large-scale atmospheric processes behind hot and dry events in SA? What is the role played by climate change and internal variability in the dynamical forcing mechanisms? Can climate change background amplify/hamper the influence of internal variability in these driving circulation patterns and therefore affect CDHW conditions?

RQ5. What are the future expected trends regarding CDHWs over SA? How will climate change reshape the occurrence in space and time of these compound conditions beyond the direct impact promoted by the increasing trends in temperature?

RQ6. Can future perturbations in land–atmosphere feedbacks and, more specifically, in the moisture–temperature coupling, explain the estimated changing patterns in CDHW conditions?

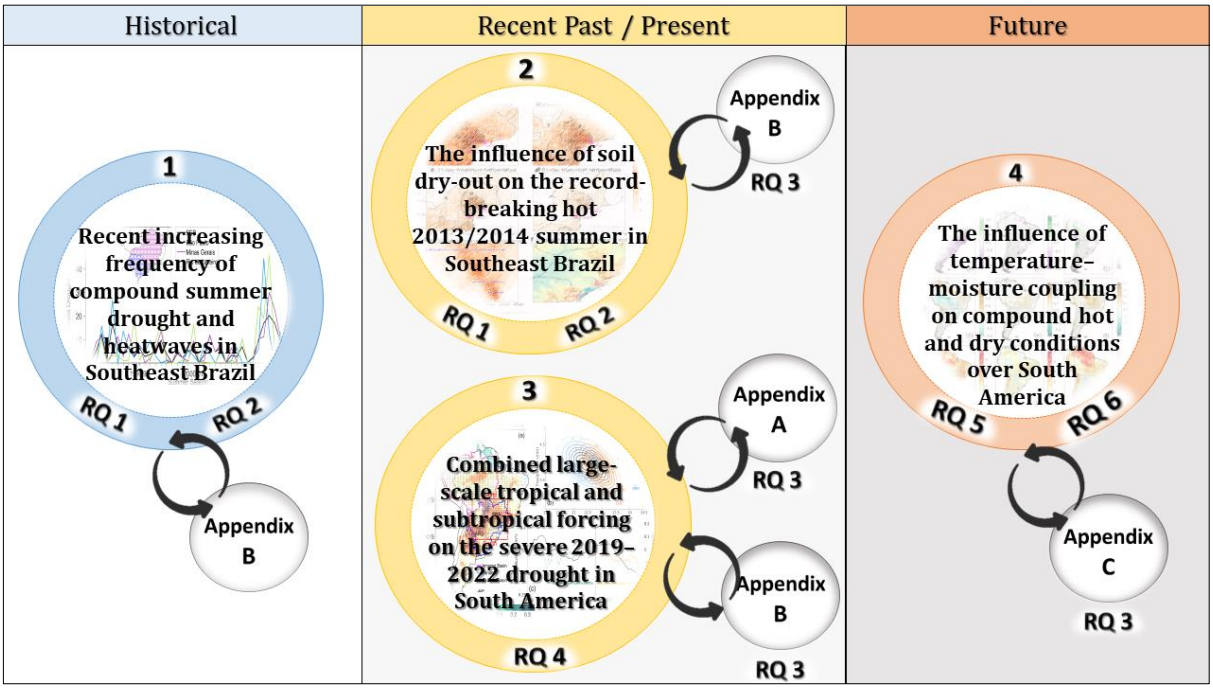

Figure 1.2 Schematic overview of the thesis structure.

This thesis aims to cast light on each one of these research questions and therefore to contribute to the state-of-the-art knowledge on the analysis of CDHW episodes. Figure 1.1 shows, schematically, how each one of these points addresses distinct stages of the main research topic and of the complex link between CDHWs and the climate system. From an operational point of view, the main goal is to help South American policy and decision-makers, as well as other stakeholders within several sectors of society and economy, to design proper mitigation measures and improve the individual and community preparedness for the future challenges imposed by climate change. Considering the demand for scientific knowledge regarding this topic for SA, this analysis aims to present a valuable contribution to filling this gap.

1.3 Thesis structure

The structure of the thesis relies on four core chapters framed by an opening and closing chapter. These core sections are followed by three other complementary works carried out during the PhD and included as Appendices. These additional results are aligned with the thesis framework and were essential to improve the level of detail with which the previously mentioned research questions were addressed. Figure 1.2 presents an illustrative and schematic overview of the thesis structure, based on the following chapters that aim to address the above stated RQs:

- **Chapter 1.** Presents an overall introduction to the research topic and states the research goals.

- **Chapter 2.** Investigates the historical evolution of CDHW events in the heavily populated region of Southeast Brazil (SEB) over the past four decades.

- **Chapter 3.** Undertakes a detailed characterization of the record-breaking dry and hot 2013/2014 austral summer season over SEB, emphasizing the role played by anomalous atmospheric circulation patterns at several spatial and temporal scales and of land–atmosphere coupling in the temperature escalation.

- **Chapter 4.** Provides a detailed spatiotemporal characterization of the unprecedented 2019–2022 drought in SA, exploring the historical context of the event, assessing the

exceptionality of the soil moisture anomalies, and describing the large-scale atmospheric forcing mechanisms associated with climate change and internal climate variability.

- **Chapter 5.** Quantifies the future expected changes in CDHW conditions over SA and evaluates the extent to which these changes are explained by perturbations in soil moisture–temperature coupling dynamics.

- **Chapter 6.** Summarizes the main findings of the PhD project, presenting closing considerations about the main achievements and deliverables, as well as several future research lines.

- **Appendix A.** Estimates, from a cascading natural hazard approach, the contribution of CDHW conditions and land–atmosphere feedbacks to the extreme wildfires that affected the Brazilian Pantanal biome during 2020.

- **Appendix B.** Synthesizes the emerging progress in the understanding of CDHW patterns in Brazil, providing insights about the impacts on fire occurrence and public health.

- **Appendix C.** Explores the influence of extreme hot conditions on fire occurrence in Pantanal from a historical and future climate change perspective.

Chapter 2

Recent increasing frequency of compound summer drought and heatwaves in Southeast Brazil

***Geirinhas JL**, Russo A, Libonati R, Sousa PM, Miralles DG, Trigo RM. (2021). Recent increasing frequency of compound summer drought and heatwaves in Southeast Brazil. Environ Res Lett 16: https://doi.org/10.1088/1748-9326/abe0eb.*

***João Lucas Geirinhas contributions:** conceptualization of the study; preparation of the data; computation, analysis and interpretation of the results; production of all the figures and coordination of the manuscript writing.*

Abstract

An increase in the frequency of extremely hot and dry events has been experienced over the past few decades in South America, and particularly in Brazil. Regional climate change projections indicate a future aggravation of this trend. However, a comprehensive characterization of drought and heatwave compound events, as well as of the main land–atmosphere mechanisms involved, is still lacking for most of South America. This study aims to fill this gap, assessing for the first time the historical evolution of compound summer drought and heatwave events for the heavily populated region of Southeast Brazil and for the period of 1980–2018. The main goal is to undertake a detailed analysis of the surface and synoptic conditions, as well as of the land–atmosphere coupling processes that led to the occurrence of individual and compound dry and hot extremes. Our results confirm that the São Paulo, Rio de Janeiro and Minas Gerais states have recorded pronounced and statistically significant increases in the number of compound summer drought and heatwave episodes. In particular, the last decade was characterized by two austral summer seasons (2013/14 and 2014/15) with outstanding concurrent drought and heatwave conditions stemmed by severe precipitation deficits and a higher-than-average occurrence of blocking patterns. As a result of these land and atmosphere conditions, a high coupling (water-limited) regime was imposed, promoting the re-amplification of hot spells that resulted in mega heatwave episodes. Our findings reveal a substantial contribution of persistent dry conditions to heatwave episodes, highlighting the vulnerability of the region to climate change.

Keywords: Southeast Brazil, compound events, droughts, heatwaves, climate extremes.

2. Recent increasing frequency of compound drought and heatwaves in Southeast Brazil

2.1 Introduction

Positive trends in the frequency and severity of compound drought and heatwave (CDHW) events have been reported for numerous regions of the world, including USA (Mazdiyasni and AghaKouchak 2015; Alizadeh et al. 2020), Europe (Manning et al. 2019; Russo et al. 2019), Australia (Seneviratne et al. 2012) and China (Liu et al. 2015; Lu et al. 2018). The progressive intensification of these compound extremes represents one of the largest challenges in climate change (Dosio et al. 2018; Rasmijn et al. 2018), and may be responsible for a wide range of natural and socioeconomic impacts, such as heat-related mortality (Gasparrini et al. 2017), severe wildfires (Brando et al. 2014), air pollution (Shaposhnikov et al. 2014), agricultural losses (Zipper et al. 2016), and water and energy shortages (Zscheischler et al. 2018; Coffel et al. 2019).

It is now accepted that the univariate analysis of a single climate event typically underestimates the effect of the combination of climatic extremes over different spatial and temporal scales (Mazdiyasni and AghaKouchak 2015; Zscheischler et al. 2020). In the case of hot and dry extreme episodes, the influence of local (Miralles et al. 2014) and remote (Schumacher et al. 2019) land–atmosphere feedbacks contribute to their simultaneous occurrence. These feedbacks control the local temperature escalation via surface sensible heat from the drying soils; moreover, temperature anomalies can be propagated downwind via heat advection (Miralles et al. 2019; Schumacher et al. 2019). The inter-links between droughts and heatwaves are however, still under study, both in terms of atmospheric drivers and land–atmosphere coupling (Miralles et al. 2019). Recent studies have characterized hot and dry compound extremes based on distinct approaches, including event coincidence analysis (Rammig et al. 2015; Donges et al. 2016), frequency of simultaneous occurrences of multiple extremes (Wu et al. 2019), or copula analyzes (Ribeiro et al. 2020b).

South America (SA), and particularly Southeast Brazil (SEB), has experienced over the past few decades an increase in the frequency, intensity and duration of extremely hot and dry events (IPCC 2014; Hao et al. 2018). Recently, Perkins-Kirkpatrick and Lewis (2020) showed

that significant positive trends regarding the intensity and duration of the longest heatwaves per year were recorded for SA, and particularly SEB, over the period 1950–2014. Silva Dias et al. (2013), showed a temperature increase of more than 3℃ between 1940 and 2010 for the SEB mega-city of São Paulo (SP), that after the 80s decade also registered a significant increase in the number of heatwaves (Geirinhas et al. 2018a). Positive trends in vapor pressure deficit have been also observed during the past decades in the Southeast Amazon region and SEB, pointing for a higher influence of land– atmosphere coupling under warmer climate (Barkhordarian et al. 2019). Cunha et al. (2019) demonstrated that most Brazilian regions experienced in the last decade the most severe droughts over the past 60 years. This concentration of events involved unprecedented drought conditions in SEB during the austral summer seasons of 2013/14 and 2014/15 (Coelho et al. 2016a, b). These prolonged periods with lack of precipitation were responsible for catastrophic impacts in water availability for human consumption and hydropower generation (Coelho et al. 2016b). Between January 2014 and February 2015, an unprecedented number of forest fires were recorded in the mountainous region of Rio de Janeiro (RJ) (Rodrigues et al. 2018). Additionally, a dramatic excess of fatalities was recorded in the region due to a severe dengue fever outbreak, linked to home water storage tanks installed by the population (Brown et al. 2014; BBC 2015). The severe water scarcity in SEB also led to significant impacts on economy, with the coffee production sector suffering great losses (Watson 2014; Rodrigues et al. 2019).

Climate projections indicate a continuing intensification of these extreme events in a separate mode and, particularly, in a compound manner (IPCC, 2014; Hao et al. 2018a). Despite the scientific progress to date, the full comprehension of the mechanistic links between heatwaves and drought is in its early stages (Miralles et al. 2019). Conceptual and technical barriers remain, such as the ambiguity in drought and heatwave definitions (Perkins and Alexander 2013), limitations of data products (Seneviratne et al. 2012), and challenges in the characterization of causal links across the land– atmosphere interplay (Miralles et al. 2019). This is paramount for the SEB region considering that, despite a few recent exceptions (Geirinhas et al. 2019), the region still lacks a comprehensive assessment of CDHW events and their impacts. In addition, SEB is a heavily populated area responsible for 60% of the total Brazilian gross domestic product. In 2018, the population in SEB—which encompasses the Mega Metropolitan Regions of SP, RJ, and Belo Horizonte, capitals of SP, RJ and Minas Gerais (MG) states, respectively—reached 87 million, representing 42% of the total Brazilian population (IBGE 2018).

This study aims to (a) analyze the historical evolution of CDHW events in SEB, (b) characterize the land and atmosphere conditions, and (c) disentangle the physical land–atmosphere coupling mechanisms, enabled by the atmospheric and surface conditions analyzed in (b), that were responsible for the observed record-breaking dry and hot events recorded during the 2013/2014 and 2014/2015 summers.

2.2 Data and Methods

2.2.1 Data

Daily and hourly meteorological data, including maximum temperature (Tmax), precipitation, 500 hPa geopotential height (Z500), surface net solar radiation and surface sensible heat flux values were extracted from the European Centre of Medium range Weather Forecast ERA-5 reanalysis datasets (Copernicus Climate Change Service — C2S, 2017) (Hersbach et al. 2020). Soil moisture data were obtained from the Global Land Evaporation Amsterdam Model (GLEAM v3.3a) (Miralles et al. 2011; Martens et al. 2017). All variables were retrieved for the summer season (December–February) using the 1980–2018 base period, at a gridded 0.25°×0.25° spatial resolution, and for a selected area encompassing SEB (14–26° S, 54–38° W) (Figure 2.1).

2.2.2 Compound drought and heatwave definition and indices

Drought conditions were defined at a monthly scale and considering 3-month Standardized Precipitation Index (SPI) values <−1 (Svoboda et al. 2012). Heatwave events were identified using a relative threshold methodology (Perkins and Alexander 2013), considering periods of consecutive days with T_{max} values above a certain percentile of T_{max} for the particular calendar day (calculated on a 15 day window). Different percentiles (80th, 90th, 95th) and durations (3–4 days, 5–7 days, >7 days) were considered. In order to isolate T_{max} values from the global warming effect, the linear trend was removed from the entire time series by applying a 1st degree polynomial regression technique. Considering the above-mentioned criteria for the definition of monthly drought and daily heatwave periods, a CDHW event was defined as a heatwave episode that occurs during a month under drought conditions (i.e., a month with an associated 3-month SPI value <−1). This is a simple and effective compound event metric that was already used in previous studies (Mazdiyasni and AghaKouchak 2015) and that safeguards the inherent and different time-scales linked to the definition of both extremes. To quantify the

historical change of CDHW events for each SEB grid-cell, we derived a percent (%) change index. This percent change is defined as the difference between the number of compound events recorded during the 1999/00–2017/18 and 1980/81–1998/99 summer seasons, normalized by the total number of events identified throughout the whole analysis period. In order to assess the statistical robustness of the above mentioned percent change values, a non-parametric Wilcoxon Rank Sum test (Hollander et al. 2015) was computed. This statistical test assesses the significance between pairs of data that are non-normally distributed. In this particular analysis, the annual CDHW events observed during the 1980/81–1998/99 and 1999/00–2017/18 summer seasons were defined as the pairs of data to be tested. Finally, the percent change values were considered as statistically significant if they were result of two pairs of data with different median values. The percentage of total summer pixels under a compound regime was also analyzed. This methodology follows the approach applied to the USA by Mazdiyasni and AghaKouchak (2015), and it is obtained by calculating the percentage of total number of pixels for each summer season that are in CDHW conditions:

$$pixels_{total} = pixels_{lat} \times pixels_{lon} \times pixels_{time} \qquad (2.1)$$

lat and *lon* represent, respectively, the number of pixels in latitude and longitude, and time represents the number of days within each summer season. For instance, a percentage of 100% indicates that concurrence conditions were recorded for the entire SEB area as well as during all summer days.

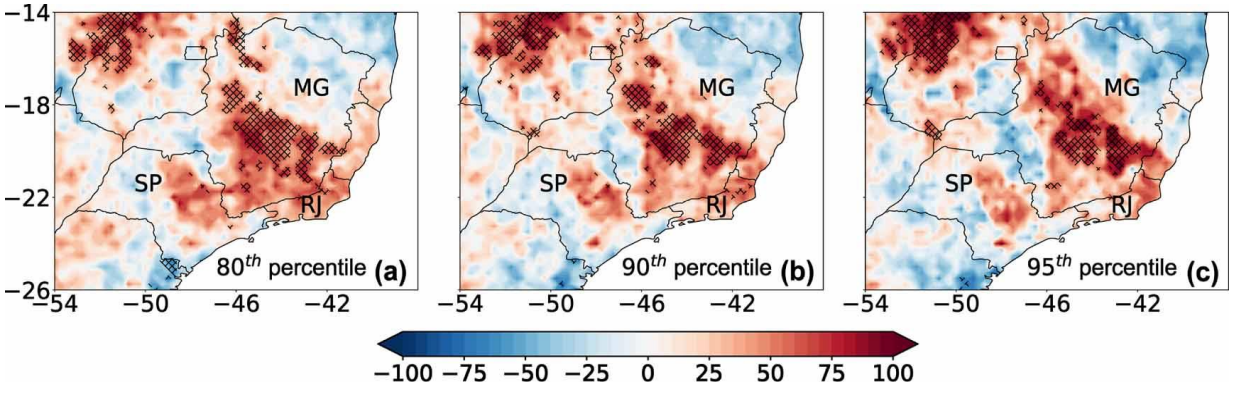

Figure 2.1 Percent change (%) in CDH events (all events considered, with durations of at least three consecutive days) during 1999/00–2017/18 summer seasons (DJF) relative to 1980/81–1998/99 summer seasons. Each panel shows a different heatwave severity, based on (**a**) 80th, (**b**) 90th and (**c**) 95th temperature percentile thresholds. Statistically significant ($p < 0.05$) percentage changes are identified by thin black crosses.

2.2.3 Definition of atmospheric blocking anomalies

Regional atmospheric blocking was detected by searching reversals of the usual Z500 gradient. Instantaneous (at the daily scale) local blocking was defined by detecting grid-cells presenting simultaneously negative Z500 gradient towards 15° north and 15° south, i.e., meridional maxima of Z500 (Mendes et al. 2012). These daily detections were used to compute monthly and seasonal climatological frequencies of regional blocking occurrence, and, subsequently, to derive monthly and seasonal relative anomalies with respect to the 1980–2018 base period.

2.3 Results

2.3.1 Historical evolution of compound episodes

We started by analyzing the percent change of CDHW events, considering all the summer heatwave episodes with durations above three consecutive days and three different thresholds (80th, 90th, 95th percentiles) (Figure 2.1). During the 1999/00–2017/18 period, concurrences increased substantially (values between 50% and 100%) over the northwestern SEB section, the central and southern areas of MG, and the northeastern section of RJ. This increase is statistically significant over large swaths when compared to the 1980/81–1998/99 period. Positive values were also observed in some areas of SP, however a general absence of statistical significance was evident. All the remaining areas presented near-zero or even negative values, mostly not statistically significant. The spatial variability pattern of the percent change was very similar throughout the considered temperature thresholds.

In addition to considering different thresholds, we also assessed the percent change for different heatwave durations (Figure 2.2). Despite some slight differences regarding the spatial pattern of percent change values distribution throughout all the combinations of drought and heatwave, in general, severe and long compound events have become more frequent than those short and mild. This is particularly evident for the SEB northwestern section and MG central and southern areas. For compound event durations of 3–4 days (Figure 2.2a-c), large parts of SEB presented positive and statistically significant ($p < 0.05$) percent changes, with the highest values in the MG central region. Regarding compound events with a duration of 5–7 days (Figure 2.2d-f), the pattern was very similar, despite the higher absolute values of percent change. As we consider even longer heatwaves and higher intensity thresholds, the SEB area

with negative percent change values also increases, although the values are typically non-statistically significant. Taking into account the longest compound heatwave events (Figure 2.2g-i), the regions with higher positive and statistically significant values were located within MG, which is in fact, the only SEB area that presented a robust and consistent pattern of positive % change throughout all the combinations of severity and duration of compound heatwaves. Regions such as the coastal section of RJ and some interior land parts of SP also presented positive changes close to 100%. However, the interpretation of these results requires a careful consideration due to their lack of statistical significance.

We looked in detail at the critical summer seasons that contributed more to the positive changes in SEB. In each one of the three most populated states (namely SP, MG and RJ), the percentage values of total summer pixels under a compound regime were also analyzed (see section 2.2.2 and Figure 2.3). To consider as many compound events as possible, the percentage levels were computed using the lowest heatwave percentile threshold (80th) and a duration of at least 3 days. Considering the whole SEB area, the most critical summer seasons in terms of

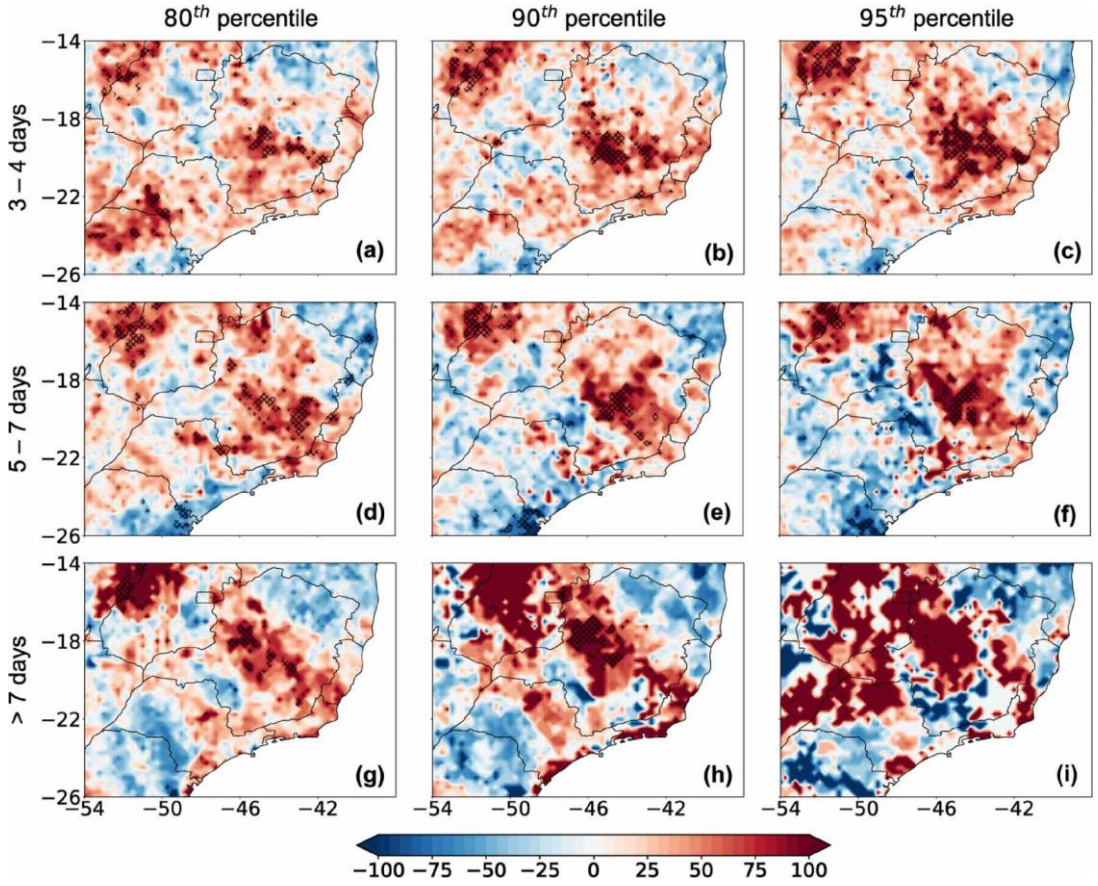

Figure 2.2 Percent change (%) in the occurrence of summer (DJF) CDHW events during 1999/00–2017/18 relative to 1980/81–1998/99. The rows correspond to different heatwave durations (3–4, 5–6, >7 days). The columns show different heatwave severities (80th, 90th and 95th percentiles). Statistically significant ($p < 0.05$) percentage changes are identified by black crosses.

concurrence percentage were observed during the last decade of the period under analysis, particularly during the summer seasons of 2013/14, 2014/15 and 2015/16, when the combined values were about 20% (Figure 2.3, black curve).

2.3.2 The record-breaking 2013/14 and 2014/15 summer seasons

The unprecedented CDHW situation observed during 2013/14, particularly for SP, and during 2014/15 particularly for RJ and MG, deserves the analysis of the atmospheric synoptic conditions, the land surface drivers and the soil–atmosphere coupling mechanisms. Figure 2.4a represents the yearly summer precipitation anomalies from 1980/81 to 2017/18. During the last quarter of the analysis period, the three states presented a marked correspondence between drought–heatwave concurrence and precipitation deficits (Figure 2.3 and 2.4). For SP, the negative association was more evident for the 2013/14 summer season, when the lowest ever recorded negative precipitation anomaly (Figure 2.4a) corresponded to the highest concurrence percentage (Figure 2.3). Regarding the states of MG and RJ, this particular summer season was also characterized by an extreme absence of precipitation. In fact, the precipitation anomaly in RJ was very similar to that in SP, however, the SP percentage of concurrence was far greater (Figure 2.3). Figure 2.4b shows a different perspective on surface dryness for the different states. Severe and historically unprecedented drought conditions were observed over SP in 2013/14, while in MG and RJ soil moisture anomalies were closer to zero, or even positive in some areas. This indicates that, although these regions experienced similar conditions in terms

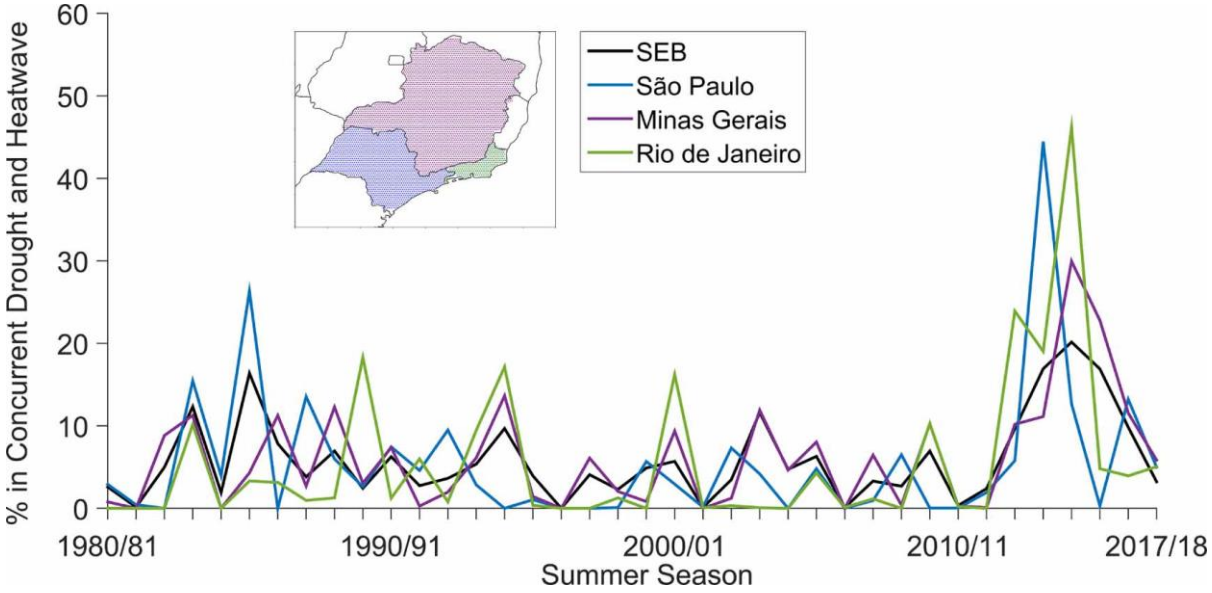

Figure 2.3 Percentage of total yearly summer pixels (%) under a CDHW regime (heatwave defined using a 80th percentile threshold and a duration of at least three consecutive days) from 1980/81 to 2017/18 and for different spatial domains: whole SEB, the states of São Paulo, Rio de Janeiro, and Minas Gerais (black, blue, green and purple lines, respectively).

of mean summer precipitation deficits (Figure 2.4a), the surface was considerably drier in SP. This asymmetry between the three states was likely due the occurrence of different precipitation episodes in these three states and to greater evaporation rates in SP, promoted by higher shortwave radiance incidence at surface. The later was linked to anticyclonic conditions promoting clear skies and high diabatic heating (Figure 2.4d and S2.1). In fact, looking at the large-scale atmospheric circulation, we found that during the 2013/14 summer season SP experienced a higher than normal percentage of days under atmospheric blocking than MG and RJ (Figure 4d). These quasi-stationary anticyclonic circulation patterns are prone to higher than average incidence levels of solar radiation at the surface (Meehl and Tebaldi 2004; Sousa et al. 2018b), and ideal to foster evaporation—as long as soil moisture is still available—progressively drying the soils and favoring the escalation of temperatures through diabatic heating (Sousa et al. 2018b). Figure S2.1 corroborates this point, showing the incidence of high levels of solar incoming radiation, particularly over SP. Therefore, the different synoptic atmospheric conditions experienced by SP, MG and RJ were essential to explain the differences among soil moisture levels (Figure 2.4b), the number of heatwaves, and the percentages of concurrence (Figure 2.3). For MG and RJ, the lowest (highest) recorded precipitation anomaly (percentage of concurrence) was observed during the 2014/15 summer season. Despite this, the precipitation anomaly values were not so different compared to 2013/14. By contrast, soil moisture anomalies (Figure 2.4c) were much stronger and widespread in MG and RJ when compared to the 2013/14 season (Figure 2.4b). This difference reflects the fact that during the period between the 2013/14 and 2014/15 summer seasons, pronounced precipitation deficits were maintained, particularly for MG and RJ (Nobre et al. 2016). Consequently, the soil moisture values continued to decrease at a faster rate in these two states, compared to SP. Secondly, the synoptic atmospheric circulation pattern in MG and RJ, contrary to SP, induced clear sky conditions and strong diabatic heating, leveraging initially high evaporation rates (until soil dry-out) and the occurrence of several heatwave periods, and, consequently, compound events. During the 2014/15 season the predominant atmospheric blocking pattern (Figure 2.4e) moved northeast, affecting a broader area in RJ and MG when compared to the 2013/14 season (Figure 2.4d). Consequently, clear sky conditions were predominant over these two states, offering the ideal conditions (radiative forcing and diabatic heating) for boosting the development of heatwaves over RJ and MG, rather than over SP (Figure S2.1). Analyzing the isohypses at 500 hpa during the 2014/15 summer season (Figure 2.4e), it is possible to observe a well-defined wave pattern of the mid-atmosphere circulation spanning from the central south

Pacific Ocean to the western South Atlantic Ocean and to the vicinities of south and southeastern coast of Brazil. This ridge-trough sequence was a clear signature of a large-scale teleconnection wave train that was also identified (although with less intensity) during the 2013/14 (Figure 2.4d). This Rossby wave train was induced by an equatorial Pacific heat source north of Australia (Coelho et al. 2016a).

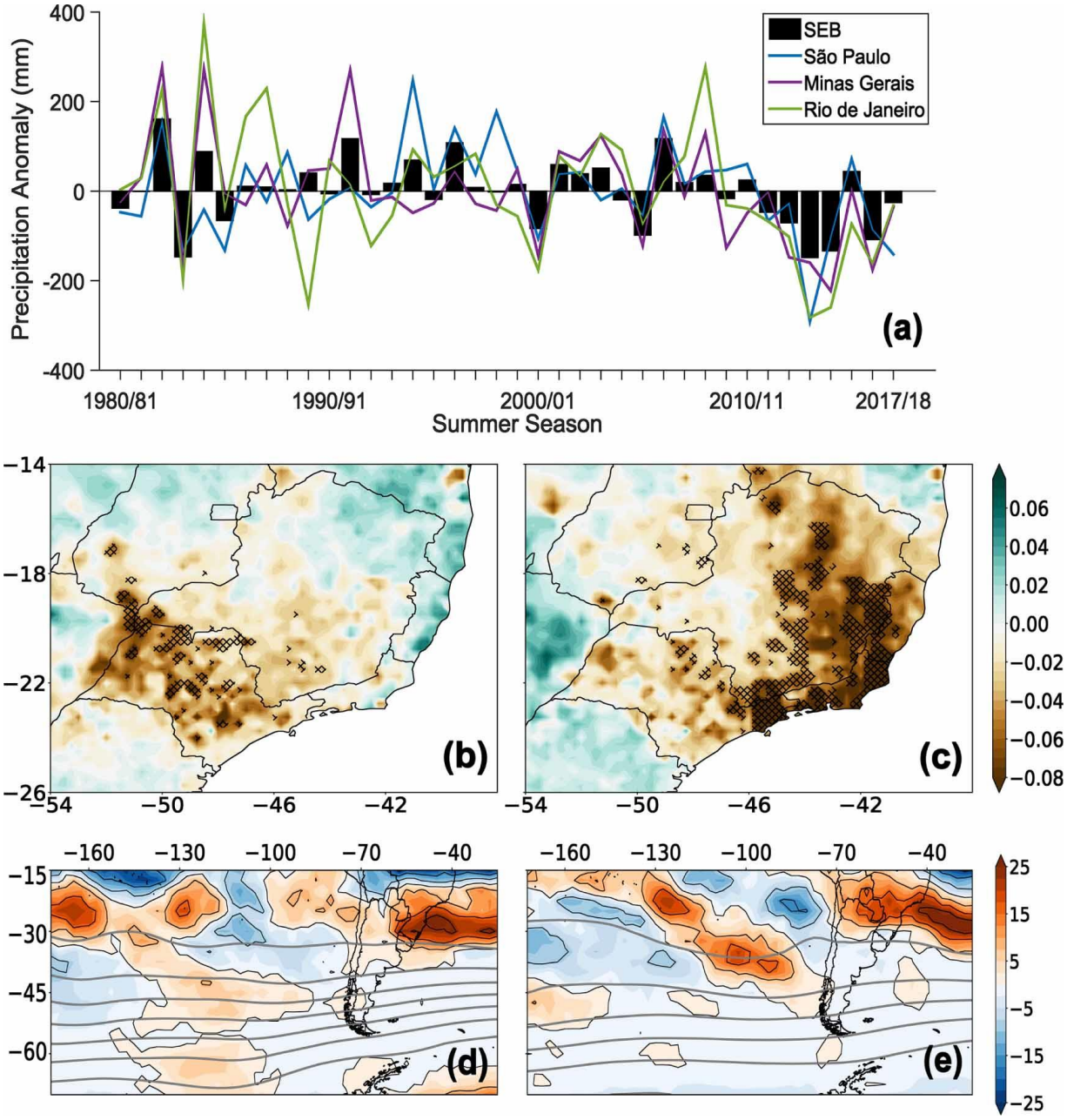

Figure 2.4 (**a**) Area average austral summer precipitation anomaly time series for SEB, SP, RJ and MG. (**b**) and (**c**) Soil moisture anomaly values regarding summer climatology (m^3_{water}/m^3_{soil}) during the 2013/14 (**b**) and the 2014/15 (**c**) summer seasons. Regions marked with crosses denote the areas in which the negative anomalies where the lowest ever recorded within the analysis period (1980–2018). (**d**) and (**e**) Relative anomaly in the percentage of summer days (colors, %) affected by atmospheric blocking conditions and summer averaged 500 hpa geopotential height field (gray contour lines delimitating equal geopotential areas) during the 2013/14 (**d**) and the 2014/15 (**e**) summer seasons, respectively.

To characterize the land–atmosphere interactions responsible for the potential reinforcement of hot and dry events (Miralles et al. 2014, 2019; Mazdiyasni and AghaKouchak 2015), the anomaly time series of the near surface air temperature, surface net solar radiation, soil moisture and sensible heat flux were analyzed in detail for the three SEB states. Figure 2.5 shows the results of this analysis for the 2013/14 summer season, highlighting several periods defined by positive anomalies of 2m air temperature, particularly in SP. The first period appeared during the first days of December 2013 (3rd–5th) and was primarily promoted by a strong diabatic process represented by positive anomalies of surface net solar radiation. The summer season started with positive soil moisture anomalies and, consequently, negative anomalies of sensible heat fluxes were not recorded. It is important to note that ECMWF convention for vertical radiative fluxes is negative upwards and positive downwards. The summer season progressed under a pronounced lack of precipitation, especially over SP, promoting a steady decrease in soil moisture. From the last days of December until mid-January another hot period was recorded, presenting a close association with positive anomalies of surface net solar radiation. The meteorological situation of clear sky conditions and precipitation deficits remained until the mega-heatwave event over SP, from January 20th to February 15th. The pronounced variation of the accumulated values from all the analyzed parameters reflects the magnitude of this episode (see bold lines in Figure 2.5). Initially, the positive temperature anomalies were induced by strong diabatic contributions that promoted a sharp decrease in soil moisture due to a high evaporative demand. As the availability of water on the surface reduced, the surface started to deliver part of the available radiative energy back to the atmosphere through sensible heat fluxes, further intensifying the temperatures. During 2014/15, the role played by land–atmosphere coupling was larger in RJ and MG compared to SP (Figure S2.2).

In contrast to the 2013/14 summer season, the soil moisture anomalies during the beginning of the 2014/15 season were already negative, reflecting antecedent precipitation anomalies, and continued to decrease as the season progressed. This led to pronounced anomalies in surface sensible heat fluxes. This land–atmosphere coupling was evident for RJ during the whole month of December and January, especially when diabatic forcing conditions were met. Regarding MG, the coupling process was more intense throughout the entire month of January 2015.

2.4 Discussion and Conclusions

Until this study, the physical mechanisms responsible for triggering the amplification of CDHW events remained unclear for SEB, particularly with respect to (a) the level to which heatwaves, as recurrent isolated events causing heat-stress, could enhance already established drought conditions, (b) the extent to which prolonged drought and subsequent surface sensible heat fluxes can amplify heatwaves, and (c) the degree to which (a) and (b) can concur. The summer seasons of 2013/14 and 2014/15 were clear examples of such an association between drought and heatwave in this important region of Brazil. This inter-relationship was controlled by two soil– atmosphere coupling regimes that were predominant during distinct periods of both summer seasons, and defined by pronounced evaporative demands and different evaporation levels and soil moisture availability (Pendergrass et al. 2020). The first regime (energy-limited), characterized by a low coupling, occurred during the first half of both summer seasons, in which consecutive hot periods coupled with long-term precipitation deficits were important to induce the dry surface conditions. During the hot periods, the demand of the atmosphere induced by the clear sky conditions and low humidity levels was satisfied by increasing evaporation rates and, consequently, the soil moisture availability suffered an accelerated decrease (Figure 2.5c and S2.2). The ideal synoptic conditions for high levels of shortwave radiation incidence were maintained and, due to a severe dryness of the surface, a

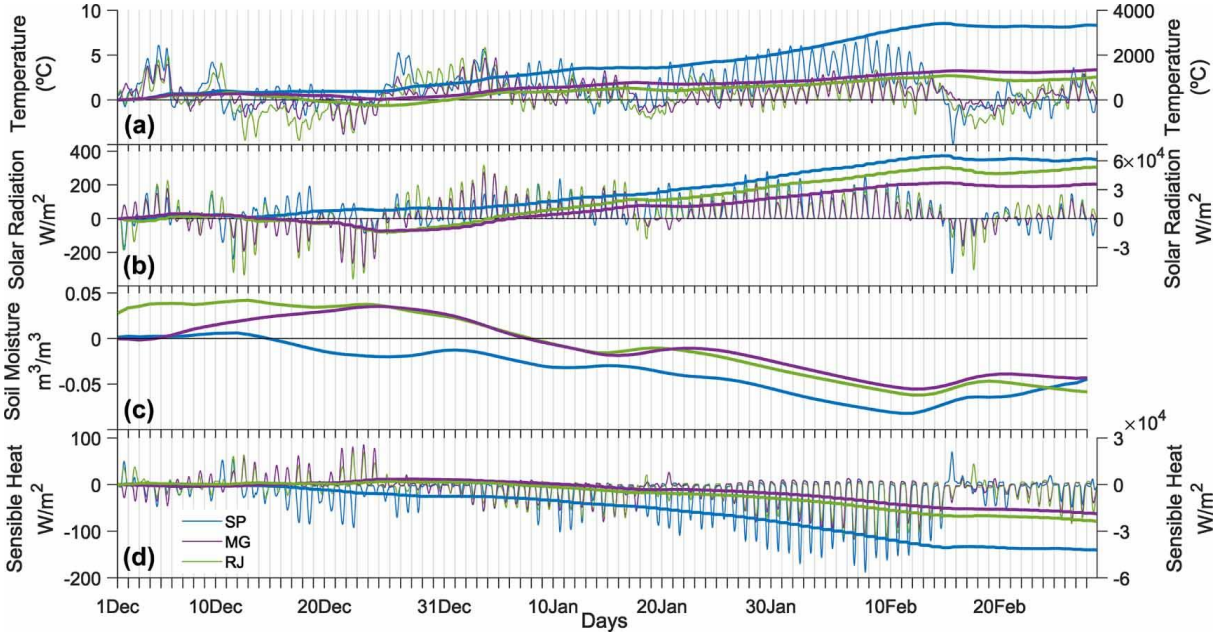

Figure 2.5 Anomalies (left y-axis) from 1st December of 2013 to 28th February of 2014, of (**a**) surface 2m temperature (at an hourly scale), (**b**) surface net solar radiation (at an hourly scale), (**c**) soil moisture (at a daily scale) and (**d**) surface sensible heat flux (at an hourly scale) for SP (blue line), MG (purple line) and RJ (green line). The respective colored bold lines represent the accumulated values of each variable since 1st December (right y-axis).

high coupling regime (water-limited) was imposed, in which the heatwave events were amplified by the simultaneous drought conditions. In this second regime, the evaporative demand continued to increase. However, contrary to the first regime, evaporation rapidly decreased. This was due to an absence of soil water availability, and so, the surface started to lose its capability to meet the atmospheric water demand.

Relying in previous conducted analysis, it is likely that the transpiration declined as plant stomata closed to prevent desiccation (Miralles et al. 2019; Buckley 2019), not just as a response to the low soil water content, but also to the high atmospheric vapour pressure deficit. At this stage, the surface started to disproportionally dissipate the incoming radiation as sensible heat, instead of latent heat (evaporation). Consequently, near surface atmospheric temperatures further escalated, increasing the severity of the events, and leading to mega-heatwaves such as the ones we recorded for SEB. Therefore, the presence of the observed higher-than-average blocking patterns over SEB during the 2013/14 and 2014/15 summer seasons — responsible for reduced cloudiness, large precipitation deficits, advection of warm air and a high atmospheric demand for humidity — proved to be essential for soil moisture depletion, yielding large fluxes of sensible heat and a subsequent reduction in evaporative cooling. These persistent synoptic conditions likely resulted, therefore, in the progressive intensification of drought and heatwave conditions. For Europe, it has been demonstrated that conditions of dry soil can also intensify heat entrainment from the top of the atmospheric boundary layer and favour the near-surface multiday storage of heat in the residual boundary layer (Miralles et al. 2014). Model experiments have also shown the potential of soil dryness to sustain anticyclones, and consequently intensify heatwave periods (Fischer et al. 2007). Moreover, soil desiccation upwind has also been shown to increase the temperature escalation in downwind locations via heat advection (Vautard et al. 2007; Schumacher et al. 2019). Most of these previous studies have concentrated in Europe, North America and Australia (Seneviratne et al. 2012; Mazdiyasni and AghaKouchak 2015; Manning et al. 2019; Russo et al. 2019; Alizadeh et al. 2020). While heatwave–drought concurrence over SEB has been much less studied, recent analyzes have shown that the synoptic-scale high-pressure conditions are required to generate these compound events in SEB (Geirinhas et al. 2018a, 2019a). In addition, these events are related to teleconnections perturbations of inter-tropical oceanic/atmospheric modes, such as the Madden–Julian oscillation (Shimizu and Ambrizzi 2016) and the El Niño–Southern oscillation (Rodrigues et al. 2019; Cai et al. 2020).

Regarding the historical evolution of these events, it is possible to conclude from our analyzes that, besides the northwestern SEB section, also central MG, RJ and some areas of SP close to MG and RJ, experienced an increase in frequency. This concurrence increase proved to be more intense as we considered the most extreme and longer-lasting heatwave classes. However, a careful consideration should be raised to the lack of statistical robustness among the observed percent change values, particularly for the severest and longest CDHW events. Considering that the linear positive effect of global warming in T_{max} levels was accounted by removing the trend from the time series, this result indicates an increase of daily T_{max} extreme values through an increase of the time series variability. This could be explained by a growing role by dry surface conditions in generating and enhancing temperature extremes over the last years. Therefore, one of the main conclusions is that over the last decades temperatures and extreme dry and hot conditions have intensified over the densely populated SEB. These results are in accordance with previous studies for other regions worldwide (IPCC 2014; Geirinhas et al. 2018; Cunha et al. 2019; de Abreu et al. 2019).

Nowadays it is well known the existence of a wide-range of impacts associated to CDHW events, not just within natural sectors and ecosystems, but also for humans and particularly in what concerns public health (Gasparrini et al. 2017; Guo et al. 2018; Zscheischler et al. 2018). All these impacts are expected to be exacerbated in a future hotter climate scenario triggered by the emissions of Greenhouse gases and other anthropogenic factors (Gasparrini et al. 2017; Zscheischler et al. 2018). For instance, Gasparrini et al. (2017) estimated that populations living in regions like Europe, Southeast Asia and South America will record a sharp surge in heat-related impacts. This will be especially true for areas where heat-stress conditions are expected to be exacerbated due to a joint effect of a global warming trend, a higher contribution of local and or remote drought condition to temperature extremes (Miralles et al. 2014; Schumacher et al. 2019), and also due to a regional urban heat-island effect (Peres et al. 2018). In regards to SEB, an increment on the occurrence of compound hot and dry events is expected, particularly in the absence of a serious decrease in the emissions of Greenhouse gases. In order to provide scientific support to policy making, studies of this type are of extreme relevance and should be further supported by national and international funding agencies.

Supplementary Material

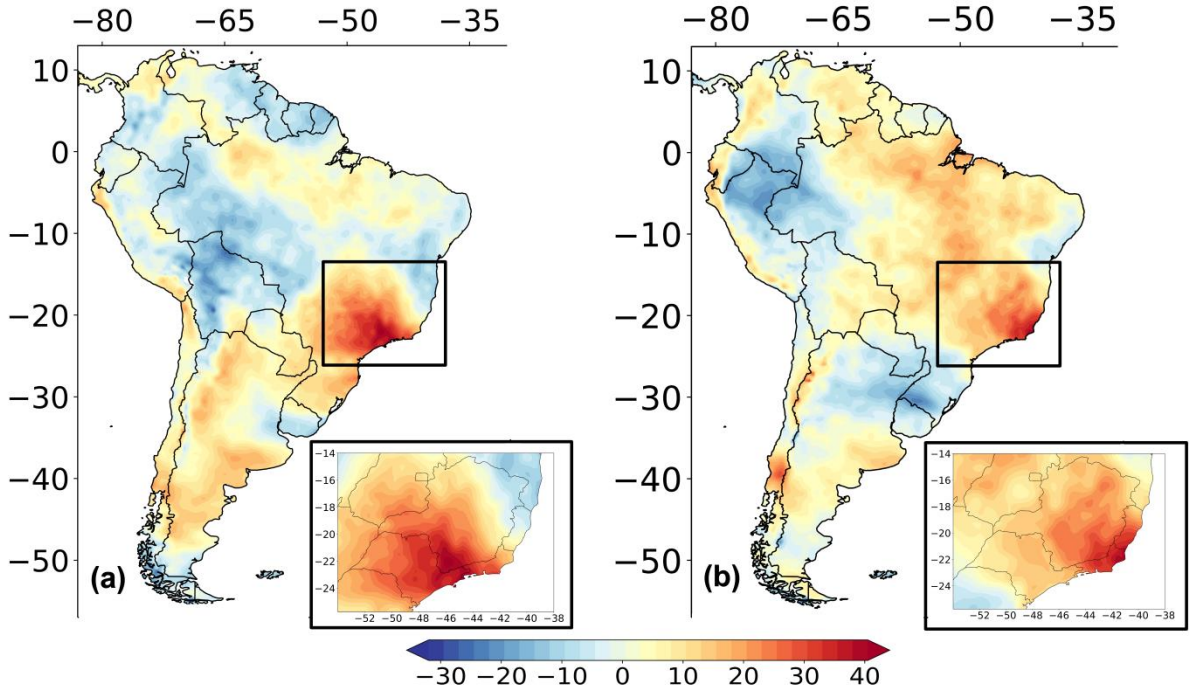

Figure S2.1 Anomaly composite fields of surface net solar radiation (w/m^2) for South America and particularly for SEB (inset panel), regarding 2013/14 (**a**) and 2014/15 (**b**) summer seasons.

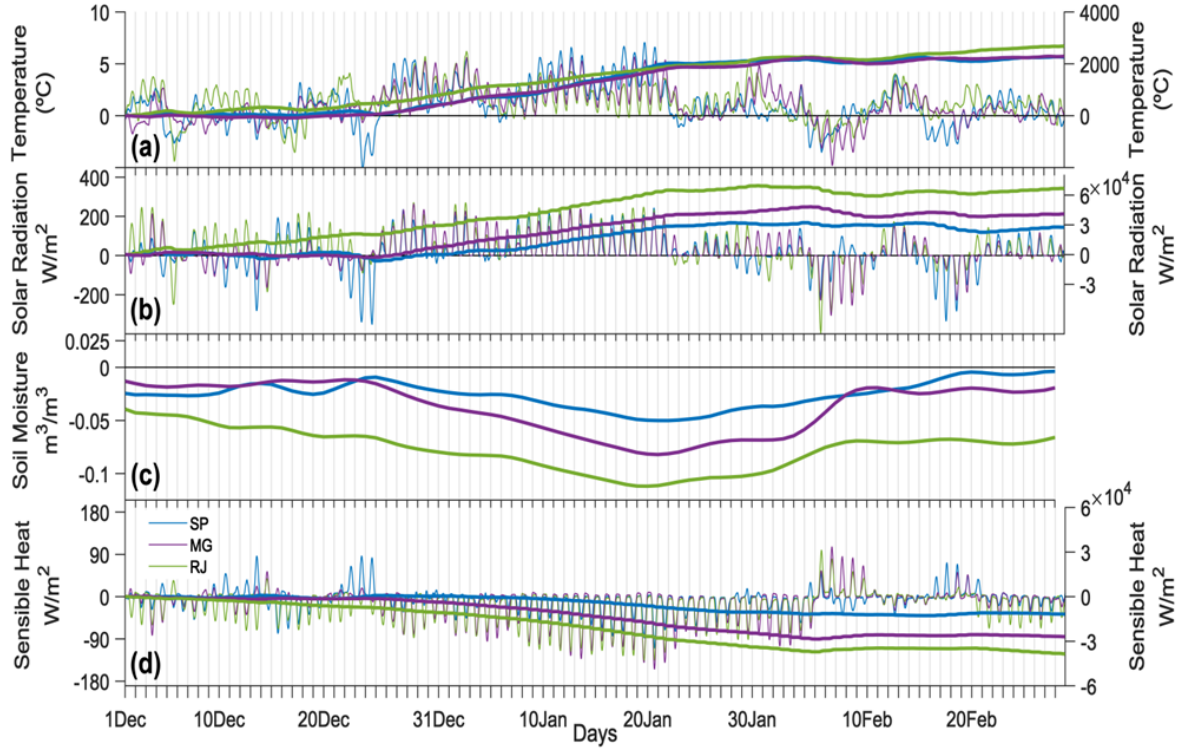

Figure S2.2 As in Figure 2.5 but for 2014/15 summer season.

Chapter 3

The influence of soil dry-out on the record-breaking hot 2013/2014 summer in Southeast Brazil

***Geirinhas JL**, Russo AC, Libonati R, Miralles DG, Sousa PM, Wouters H, Trigo RM. (2022) The influence of soil dry-out on the record-breaking hot 2013/2014 summer in Southeast Brazil. Sci Rep 12:5836. https://doi.org/10.1038/s41598-022-09515-z*

***João Lucas Geirinhas contributions:** conceptualization of the study; preparation of the data; computation, analysis and interpretation of the results; production of all the figures and coordination of the manuscript writing.*

Abstract

The 2013/2014 summer in Southeast Brazil was marked by historical unprecedented compound dry and hot (CDH) conditions with profound socio-economic impacts. The synoptic drivers for this event have already been analyzed, and its occurrence within the context of the increasing trend of CDH conditions in the area evaluated. However, so far, the causes for these record temperatures remain poorly understood. Here, a detailed characterization of the 2013/2014 austral summer season over Southeast Brazil is proposed, emphasizing the role played by land–atmosphere interactions in temperature escalation. We demonstrate that a strong soil moisture–temperature coupling regime promoted record-breaking temperatures levels exceeding almost 5 °C over the previous highest record, and played a key role in triggering an outstanding 'mega-heatwave' that lasted for a period of around 20 days. This pronounced soil desiccation occurred within a current climate change trend defined by drier and hotter conditions in the region. The soil dry-out, coupled with strong radiative processes and low entrainment of cooler air masses through mesoscale sea-breeze circulation processes, led to a water-limited regime and to an enhancement of sensible heat fluxes that, ultimately, resulted in a sharp increase of surface temperatures.

3. The influence of soil dry-out on the record-breaking hot 2013/2014 summer in Southeast Brazil

3.1 Introduction

The global warming trend has led to the recent occurrence of historically unprecedented heatwaves and record-breaking temperatures (Russo et al. 2015; Perkins-Kirkpatrick and Gibson 2017). These mega-heatwave episodes have been responsible for a massive number of heat-related deaths (Grynszpan 2003), high levels of air pollution from severe wildfires (Shaposhnikov et al. 2014), peaks in energy consumption (Pechan and Eisenack 2014), exacerbation of drought events (Miralles et al. 2014), and reduced crop yields (Bastos et al. 2014). Several studies have shown that the escalation of temperatures during recent episodes in Europe could not be explained by atmospheric circulation anomalies alone, and that the combined effect of local soil dryness and high heat advection is a necessary ingredient (Miralles et al. 2012, 2014; Sousa et al. 2020; Dirmeyer et al. 2021). Soil desiccation leads to a reduction in the evaporative cooling and an increase in the sensible heat flux between surface and atmosphere (Seneviratne et al. 2010). A more complex effect of soil moisture on temperature was identified by (Miralles et al. 2014) for the 2010 Russian mega-heatwave, when the observed temperature anomalies were triggered by horizontal heat advection and warming from soil dry-out conditions, combined with a progressive entrainment of warm and dry air from higher levels of the atmosphere into to the atmospheric boundary layer, also driven by drying soils. This effect is not just local, as heatwaves can also propagate through horizontal heat advection, fueled by upwind soil drought (Schumacher et al. 2019). Such compound dry and hot (CDH) conditions were also recently observed in North America (Mazdiyasni and AghaKouchak 2015), Asia (Yu and Zhai 2020; Seo et al. 2021) and Australia (Herold et al. 2016). Future climate projections suggest that events with a magnitude similar to the recent mega-heatwaves will become the norm by the end of the century (Russo et al. 2014, 2015; Molina et al. 2020). This is in part due to critical changes in precipitation and evaporation leading to transitions from energy-limited to water-limited regimes, increasing the likelihood of CDH events (Seneviratne et al. 2013; Soares et al. 2019).

Despite recent efforts to understand the occurrence of CDH extremes, particularly on the mid-latitude regions of the Northern Hemisphere (Schumacher et al. 2019; Mukherjee et al. 2020; Mukherjee and Mishra 2021; Benson and Dirmeyer 2021), the Southern Hemisphere region still lacks a similar detailed analysis of these compound conditions. To the best of our knowledge, in what concerns South America, and specifically Brazil, only recently a few preliminary assessments started to be undertaken (Coronato et al. 2020; Geirinhas et al. 2021; Marengo et al. 2021). Moreover, certain regions of Southeast Brazil (SEB) have been experiencing a clear increase in the number and severity of heatwaves and droughts over the last decades (Geirinhas et al. 2018a; Cunha et al. 2019; Gozzo et al. 2019), and positive trends in the number of CDH events (Geirinhas et al. 2021). The historically unprecedented drought conditions recorded during the austral summer seasons (December to February) of 2013/2014 and 2014/2015 have contributed substantially to the drying trend recently observed in SEB (Coelho et al. 2016b; Nobre et al. 2016; Geirinhas et al. 2021). The inhabitants of the metropolitan region of São Paulo, the fourth most populated megacity in the world (United Nations, 2018), faced a dramatic water supply crisis as a result of this severe drought during the 2013/2014 summer (Coelho et al. 2016a). The water scarcity led to serious shortages in agricultural irrigation and in energy production from hydropower plants.

Several studies have looked into this extreme summer to identify the large-scale and synoptic conditions leading to the occurrence of the drought and hot event (Seth et al. 2015; Coelho et al. 2016b; Rodrigues et al. 2019; Finke et al. 2020); others have investigated how this season fits into an increasing trend of CDH conditions in the area (Geirinhas et al. 2021). However, so far, none of these assessments has explored and quantified the long-term record nature of the observed hot conditions and their true spatial extent. The critical role played by land–atmosphere interactions and by strong soil moisture–atmosphere coupling conditions in temperature escalation remains poorly described. In addition, little attention has been given to assessing the mesoscale atmospheric processes that triggered the warm conditions observed in some of the urban areas of SEB, such as the urban areas of São Paulo (UASP) and Curitiba (UACT), where heat-stress levels are known to cause critical impacts in public health (Son et al. 2016; United Nations, 2018).

In light of climate projections, which point to a warmer and drier future in the region (Feron et al. 2019; Llopart et al. 2020; Rusticucci and Zazulie 2021), it is therefore crucial to enhance the knowledge about the key processes and feedbacks associated with such extreme

compound events. Here, we aim to quantify in detail the exceptionality of the warm temperature levels experienced during the 2013/2014 austral summer season over SEB, and analyze the role of land–atmosphere interactions in temperature escalation. We also intend to assess, in a high spatial resolution, the mesoscale atmospheric mechanisms that triggered the outstanding near-surface temperature anomalies over SEB.

3.2 Data and Methods

3.2.1 Data

Daily maximum temperature (hereafter, Tmax) and precipitation data from two meteorological stations located within the UASP were used. The first station (23.50° S, 46.63° W) belongs to the Brazilian National Institute of Meteorology (INMET) and was used to assess the daily precipitation record for the UASP from 1980 to 2020. The second station (23.65° S, 46.62° W) belongs to the University of São Paulo and provides a long-term Tmax record from 1933 to 2020. Accordingly, the Tmax analyzed for the UASP and for the period from 1980 to 2020, resulted from daily averages between the Tmax values observed in these two meteorological stations. On the other hand, the daily precipitation record analyzed for the UASP belongs to the INMET station only. Regarding the UACT, precipitation and Tmax data from an INMET station (25.40° S, 49.23° W) were used for the period from 1980 to 2020. Other daily meteorological data, including surface net radiation, geopotential height, near-surface temperature, as well as temperature and zonal and meridional wind at several pressure levels, were extracted from the European Centre of Medium-range Weather Forecast (ECMWF) ERA5 reanalysis (Copernicus Climate Change Service, C3S) (Hersbach et al. 2020). Daily surface variables including soil moisture and evaporation were extracted from the Global Land Evaporation Amsterdam Model (GLEAM v3.3a) (Miralles et al. 2011; Martens et al. 2017). Both ERA5 and GLEAM data share a 0.25°×0.25° horizontal resolution. Anomalies were computed with respect to the climatological seasonal cycle (1981–2010).

3.2.2 Record-breaking temperature definition

To identify record-breaking temperature anomalies in a particular summer, we define the respective historical period which contains all the summer days (December to January) from 1980 up to the year of the given event. In order to identify record-breaking temperature values we adopted, similarly to Barriopedro et al. (2011), the following rationale: (1) the running means of daily anomalies for different time scales centered on each summer day are calculated, allowing superposition (e.g., for a 5-day time scale and for February 6th the period to be considered for the running mean goes from February 4th to February 8th); (2) for each grid-point and time-scale, the maximum value of the n×90 sample is retained as historical maximum, with *n* being the number of years from 1980 to the year before the summer season in consideration and 90 corresponding to the total number of days within the summer season; (3) a record-breaking temperature is identified if the maximum anomaly for a given summer period surpasses the historical maximum for the corresponding temporal scale. For instance, for a 5-day time scale and for a specific grid-point, if the highest temperature anomaly recorded for the summer season of 2013/2014 is higher than the maximum anomaly ever recorded for the historical period (containing the n×90 summer days from 1980 up to the 2013/2014 summer), then this particular grid-point experienced during the 2013/2014 summer a record-breaking temperature anomaly. The data used for these calculations corresponded to the daily mean near-surface temperature from ERA5 reanalysis.

3.2.3 Heatwave definition

Heatwaves were defined as periods of three or more consecutive days with daily Tmax values above the climatological (1981–2010) 90th percentile, calculated based on a 15-day moving window centered in the specific calendar day (Perkins and Alexander 2013; Geirinhas et al. 2021). Hot periods were defined by grouping several heatwaves separated by short periods of heat-stress relief. Based on this criterion, the heatwave incidence per summer season (December–February, 1980–2020) was explored by assessing the values of several heatwave parameters: the number of heatwave episodes (HWN), the sum of participating heatwave days (HWF), and the length (in days) of the longest heatwave event (HWD). To account for both heatwave duration and intensity, values of the heatwave magnitude index daily (HWMId) (Russo et al. 2015) were also computed for each summer season (more information regarding the HWMId metric can be found in the Supplementary Material). The data used for these

calculations correspond to in situ daily Tmax records from two meteorological stations located within the UASP and UACT.

3.2.4 Soil moisture–temperature coupling

The π diagnostic proposed by (Miralles et al. 2012) was used to assess and quantify the magnitude of soil moisture–temperature coupling. This metric estimates two terms based on near surface air temperature (*T*), evaporation (*E*), potential evaporation (E_p) and surface net radiation (R_n). π is defined as the product of a temperature term (T') and an energy term ($H' - H'_p$):

$$\pi = \left(H' - H'_p\right) T' \quad (3.1)$$

where *H* quantifies the actual sensible heat resulting from the estimated evaporation and surface net radiation levels, and H_p quantifies the sensible heat that would occur assuming potential evaporation:

$$\left(H' - H'_p\right) = (R_n - \lambda E)' - \left(R_n - \lambda E_p\right)' \quad (3.2)$$

T', H' and H'_p indicates, respectively, the daily anomalies of *T*, *H* and H_p expressed in the number of standard deviations relative to their expectation, and λE the latent heat flux calculated as a function of T and R_n. The energy term $H' - H'_p$ represents, therefore, the short-term potential of soil moisture to affect T through changes in the partitioning of the available radiative energy. When soil moisture is sufficient to meet the atmospheric demand for water, evaporation equals the potential evaporation, and the energy term is zero. Under dry conditions, as atmospheric water demand increases and soil moisture gradually decreases, the energy term increases. Ultimately the soil moisture–temperature coupling (π) will be high when positive values of T'concur with high levels of $H' - H'_p$. This method was developed and validated by Miralles et al. (2012). Since then, it has been widely used in many published studies focusing on different regions of the globe and where the soil moisture–temperature coupling conditions were assessed through different perspectives (e.g. Miralles et al. 2014; Ford et al. 2018; Gevaert et al. 2018).

3.2.5 Contribution of temperature advection and radiative processes to the near-surface temperature variation

The near-temperature variation for each grid-cell can be determined by the contribution of the temperature advection (horizontally and vertically) and local radiative processes using a fixed space (point-by-point) Eulerian approach.

$$\left(\frac{\Delta T}{\Delta t}\right)_h (\lambda, \phi, t) = -\vec{v} \cdot \nabla_p T \quad (3.3)$$

$$\left(\frac{\Delta T}{\Delta t}\right)_v (\lambda, \phi, t) = -\omega \frac{T}{\theta} \frac{\partial \theta}{\partial p} \quad (3.4)$$

Where λ, ϕ, t represent latitude, longitude and time, respectively, v indicates horizontal wind speed, T temperature, ω vertical velocity and θ potential temperature. The temperature advection by the horizontal wind can be calculated by (3.3), while (3.4) represents the temperature advection by vertical motion. Temperature changes due to sensible heat advected from remote regions (Schumacher et al. 2019) is, according to this Eulerian approach, comprised in the horizontal and vertical temperature advection terms. Both contributions were computed at an hourly scale, in constant pressure coordinates, and according to particular pressure levels available in the ERA5 reanalysis datasets that correspond to the local near-surface atmospheric layer (from 950hPa to 900hPa). The temperature change rate due to diabatic processes, including local sensible heat fluxes induced by local soil desiccation, was estimated as a residual from the previous two terms based on the temperature tendency equation (3.5):

$$\left(\frac{\Delta T}{\Delta t}\right)_d (\lambda, \phi, t) = \frac{\Delta T}{\Delta t} - \left(\frac{\Delta T}{\Delta t}\right)_h - \left(\frac{\Delta T}{\Delta t}\right)_v \quad (3.5)$$

The determination of the diabatic process as a residual term involves some careful considerations. Different factors, such as sub-grid turbulent mixing, analysis increments or even other numerical errors, may contribute to this residual term (Sousa et al. 2018b). This analysis was performed by computing average values of the ERA5 model grid points located within UASP and UACT (Figure 3.1f).

3.3 Results

3.3.1 The historically unprecedented hot and dry 2013/2013 summer season

During the 2013/2014 summer season, SEB witnessed exceptional surface warm conditions at different temporal scales, ranging from weekly to seasonal (Figure 3.1a–d). The state of São Paulo was the center of the highest maximum of temperature anomalies for all temporal scales. The anomalies for this particular region exceeded the mean by 4 standard deviations for all the temporal scales, underlining the massive amplitude and persistence of the induced temperature extremes. The strongest anomalies were observed for the 15-day average periods (up to 8 °C in some areas), with most of the state of São Paulo witnessing historically unprecedented hot temperatures, sometimes representing an exceedance of almost 5 °C over the previous highest record. The area covered by record-breaking temperatures for all temporal scales (Figure 3.1) extended from the state of São Paulo towards more southern regions. Figure 3.1e displays the temporal evolution during the 2013/2014 summer of the spatial extent of areas, within the grey box depicted in Figure 3.1a-d, experiencing record-breaking temperatures. For shorter time scales, temperature records were established during two distinct periods of the summer season: the first, less intense, took place from the end of December until the first half of January; the second, much stronger, developed from the end of January until the first half of February. For the 15-day period time scale, February 5th was the day witnessing the highest area with record-breaking temperatures, with around 450,000 km^2. It is important to stress that this value underestimates the real spatial extent of the warm conditions since it was restricted to the area within the grey box. Finally, the record-breaking pattern was not symmetric in time, indicating that the warm conditions that started in mid-January ceased abruptly after mid-February (Figure 3.1e).

It is important to acknowledge that the data from the ERA5 reanalysis datasets used here, only goes back to 1980 (see “Data and methods” section), which undermines the statistical significance of these record-breaking temperature conditions. Thus, we also used a long-term daily maximum temperature record since 1933, from the University of São Paulo meteorological station, located within the city of São Paulo (see “Data and methods” section). This much longer time series allowed us to observe that, in fact, the 2013/2014 summer witnessed the highest temperature since 1933 for different temporal scales (Figure S3.1).

Although this result was computed for a single point over SEB, it confirms the analysis obtained using the reanalysis datasets for the region and provides additional reliable information on the true temporal extent of these outstanding warm conditions.

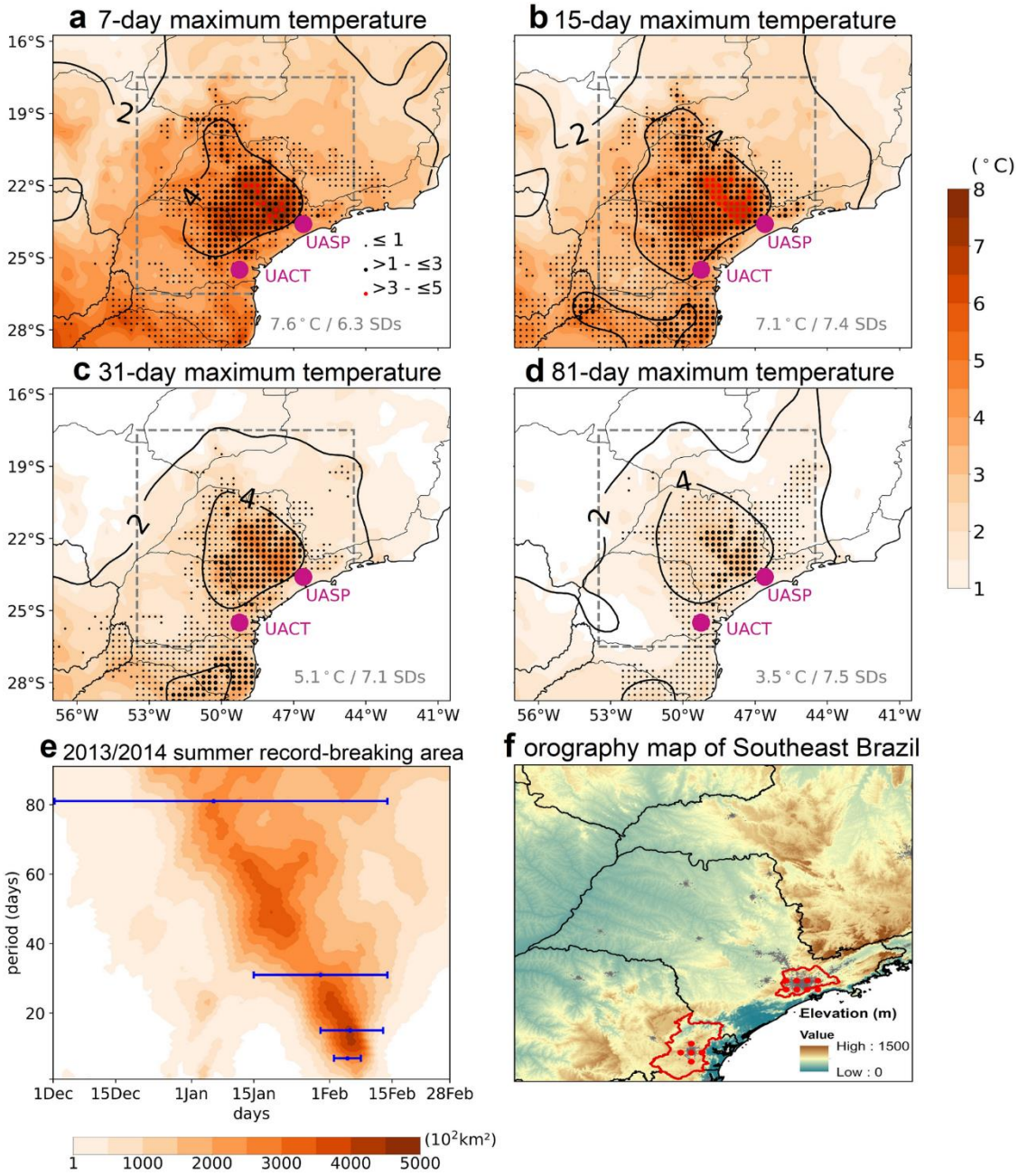

Figure 3.1 Spatio-temporal characterization of the record-breaking 2013/2014 summer. Maximum surface temperature anomalies (°C, relative to 1981–2010) during the 2013/2014 summer for 7-day (**a**), 15-day (**b**), 31-day (**c**) and 81-day average periods (**d**). Contour lines depict the anomaly divided by the corresponding standard deviation of all summer days of the reference period. The dots highlight record-breaking temperature anomalies with the size and the color being proportional to the exceedance over the previous period. The magenta dots indicate the location of the UASP and UACT. The maximum temperature anomaly is shown in the bottom right corner. Temporal evolution of the spatial extent (in 10^2 km^2) of areas experiencing record-breaking temperatures at different time scales during the 2013/2014 summer (**e**). Only the grid points within the grey box shown in the previous panels are considered. Blue bars indicate the period of maximum extension for the time scales represented in the previous panels. Orography map of the region within the grey box (**f**). The limits of the UASP and the UACT are shown by the red polygons. The grey shade highlights the urbanized areas and the red dots indicate the ERA5 and GLEAM grid-points considered to compute area averages for these particular urban areas.

The synoptic analysis conducted for this summer shows that such record-breaking temperatures were triggered by quasi-stationary anticyclonic circulation anomalies over the eastern branch of south Atlantic Ocean, near the southeast coast of Brazil (Figure 3.2). This high-pressure configuration favors the escalation of temperatures in the region due to a combination of mechanisms, including diabatic heating, strong subsidence and warm air advection (Sousa et al. 2019, 2020; Zschenderlein et al. 2019). Figure 3.2 shows the anomalous atmospheric pattern observed during the days with the largest spatial extension affected by record-breaking temperatures for the four temporal scales considered in Figure 3.1e (see blue lines). In particular, time scales compatible with synoptic disturbances (7 and 15 day) clearly show that a high-pressure system was established in the region. Such quasi-stationary circulation anomaly led to a strong adiabatic heating mechanism that was particularly intense over the coastal land section of SEB and over the state of São Paulo, where most of the record-breaking temperature values were observed. This finds support in the spatial signature of the 850-hPa temperature anomalies that shows a slight westward shift regarding the pressure anomaly center and a pronounced continental penetration towards these land areas.

The 2013/2014 season was, at the time, the hottest ever recorded summer for the region bounded by the grey box in Figures 3.1 and 3.2 (Figure 3.3a), only recently surpassed by the 2018/2019 summer. In fact, the four hottest summers were recorded during the short 8-year period from 2013 to 2020, reflecting a pronounced warming trend in the last decade of the analysis period. Regarding soil moisture, one can observe that the values recorded, although not being record-breaking, were extremely low during the 2013/2014 summer (Figure 3.3b). Such dry conditions occurred within a pronounced decreasing trend of the mean monthly summer soil moisture levels ($-0.032\ m^3_{water}/m^3_{soil}$ per decade, statistically significant at a 5% level) that started during the 2009/2010 summer (breakpoint obtained from an iterative process described in Supplementary Material) and has contributed, since then, to a total estimated mean monthly decrease of $0.036\ m^3_{water}/m^3_{soil}$. This can be explained, in part, by the occurrence of higher evaporation rates supported by the recent summer warming trend (Figure 3.3a). On the other hand, the extreme hot conditions experienced during the 2013/2014 summer triggered record-breaking vapor pressure deficit (VPD) values, indicating the high evaporative demand observed during this period and how the low soil moisture was partially due to large evaporative rates (Figure 3c). Similarly to soil moisture, the outstanding VPD observed during this summer season occurred within an increasing trend of the mean monthly

summer VPD for the region. Such trend started in 1997/1998 summer (0.096 kPa per decade, statistically significant at a 5% level) and, since then, has contributed to a total estimated mean monthly increase of 0.2208 kPa. As a result of such concurring soil desiccation, enhanced evaporative demand and severe warm conditions, a strong soil moisture–temperature coupling was observed in the region during this summer (Figure 3.3d), indicating that when the hot temperature anomalies occurred a strong soil moisture deficit was present, leading to a large flux of sensible heat from surface to the atmosphere. In fact, such soil moisture–temperature coupling levels only find parallel in the values recorded during the summer of 1985/1986. This reinforces the interest of analyzing in detail the exceptional concurring conditions of extreme

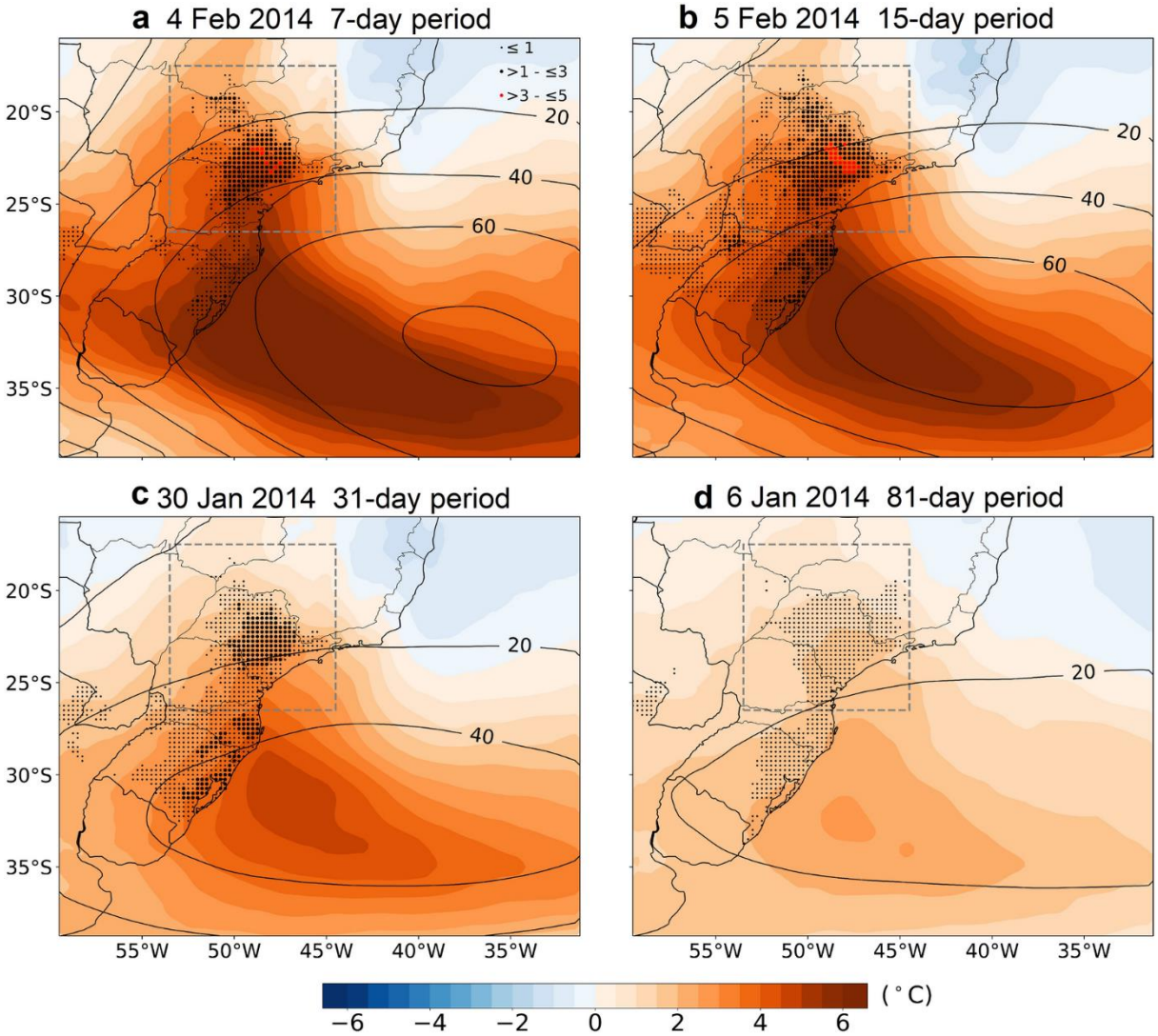

Figure 3.2 Characterization of the synoptic conditions for the 2013/2014 summer during the days having a maximum area covered by record-breaking temperatures at different temporal scales. Shading shows the spatial distribution of the 850-hPa temperature (°C) anomalies and contours the spatial distribution of the 500-hpa geopotential height (gpm) anomalies (relative to the 1981–2010 period) for 7-day (**a**), 15-day (**b**), 31-day (**c**) and 81-day average periods (**d**) centered on the day indicate at the top of each panel. The dots highlight the grid-points with record-breaking land surface temperature anomalies during the respective average periods. The size and the color are proportional to the exceedance over the previous period.

heat, soil desiccation and strong soil moisture–atmosphere coupling witnessed during the 2013/2014 summer.

3.3.2 The outstanding 2013/2014 summer in the UASP and UACT in a historical context

The historical evolution of several summer heatwave parameters from 1980 to 2020 reveals that extreme temperatures were particularly experienced over the UASP and UACT during the 2013/2014 summer season (Figure 3.4). For the UASP, the maximum HWF (number of summer days under a heatwave regime) was observed during this period, reaching 61 days. Regarding the UACT, this summer witnessed the second highest HWF with 35 days, a value that was only shortly exceeded by the one recorded during the 2018/2019 summer (36 days). The longest ever recorded heatwave (HWD) was also observed for both urban areas during the 2013/2014 summer season, when the UASP (UACT) was affected by an outstanding episode that lasted for 26 (19) consecutive days. Similarly, the highest value of the heatwave magnitude index daily (HWMId) was observed during this period, revealing the unprecedented magnitude of this heatwave. Moreover, the 2013/2014 summer was also subject to the occurrence of several hot spells with an almost perfect temporal match between cities, despite them being more than 300 km apart from each other (Figure 3.1f). Three hot periods (grey shaded areas in Figure 3.4b,d) were defined by grouping several heatwaves separated by short periods of mild temperatures. Accordingly, the first hot period occurred during the first days of December; the second from the end of December to mid-January; and the third corresponds to a mega-heatwave episode, from mid-January to mid-February. These two last hot periods identified for both urban areas correspond to those previously identified in Fig. 1e when analyzing the areas covered by record-breaking temperatures. In fact, the days having the highest land extension covered by record-breaking temperatures when considering 7-day (February 4th), 15-day (February 5th) and 31-day (January 31st) average periods are all included in this massive mega-heatwave identified for both urban areas. It is important to note that these results, obtained from *in situ* meteorological data are in agreement with the previous analysis obtained using the ERA5 datasets. This indicates once again that the data from the reanalysis model is reliable to

reconstruct the warm conditions of this summer, particularly for the urban areas considered here.

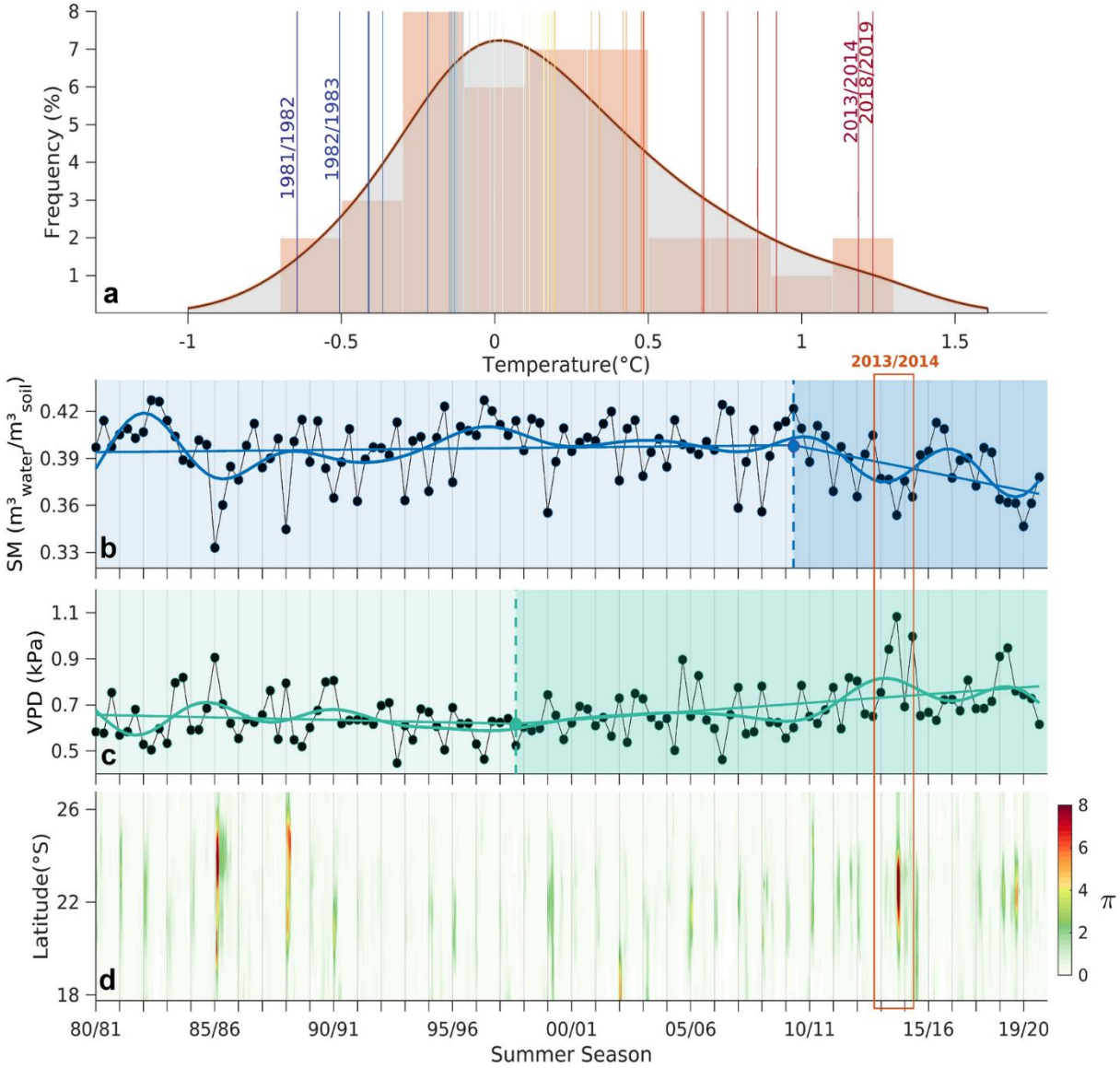

Figure 3.3 Analysis of the extreme summer hot and dry conditions during the 2013/2014 summer in a historical evolution perspective. Kernel distribution function for the average summer temperature anomalies (°C) from 1980 to 2020 observed for the region within the grey box shown in Figures 3.1 and 3.2 (**a**). The vertical colored lines indicate the mean surface temperature anomaly values for each summer season. Historical evolution from 1980 to 2020 of monthly mean summer soil moisture (m^3_{water}/m^3_{soil}) and vapor pressure deficit (kPa) values (**b**, **c**, respectively). The bold lines result from the application of a 10-year low-pass Lanczos filter and a linear regression model with two segmented (i.e., piecewise) linear relationships separated by a break point (obtained from an iterative process described in Supplementary Material) highlighted by the filled colored dot. The monthly mean values result from area averages applied for the region within the grey box in Figures 3.1 and 3.2. Mean daily π coupling metric per each 0.25° latitude within the grey box shown in Figures 3.1 and 3.2, for the summer seasons from 1980 to 2020 (**d**).

3.3.3 Soil moisture–temperature coupling during the 2013/2014 summer

The spatial signature over SEB and the temporal evolution for the UASP and UACT of the two soil moisture–temperature coupling terms analyzed here (T': temperature term; $H' - H'_p$: energy term) reveal that several independent periods were defined by distinct anomalies in both terms (Figure 3.5). In fact, the occurrence of these anomalies matches the hot periods identified and discussed previously for these urban areas in Figure 3.4, which suggests an influence of land–atmosphere feedbacks on temperature anomalies. Accordingly, four periods were defined: (i) from December 1st to 9th (corresponding to the first hot period defined during the analysis of Figure 3.4), (ii) from December 11th to 22nd, (iii) from December 24th to January 14th (which corresponds to the second hot period) and (iv) from January 19th to February 13th, corresponding to the mega-heatwave episode. During the first period, some SEB regions, and particularly the UASP and UACT, were marked by positive values of both terms (Figure 3.5a,e,f). This is indicative of a high coupling regime (i.e. high π; see Figure S3.2), in which the temperature anomalies are influenced by a pronounced evaporative stress linked to a strong soil desiccation and large amounts of shortwave radiative energy available at surface (i.e., large values of $H' - H'_p$). During the second period (Figure 3.5b,e,f), large values of the energy term concurred with negative temperature anomalies, indicating that although dry conditions and large amounts of incoming radiative energy at surface concurred, air temperature (likely driven by advection of cooler air masses) was not anomalously positive, pointing to a low coupling regime (i.e. low π; see Figure S3.2). During the third period (Figure 3.5c,e,f), relatively low soil moisture–temperature coupling conditions were maintained (Figure S3.2), although they were explained by an opposite behavior in what concerns the contributions of the temperature and energy terms. By contrast to the preceding days, positive temperature anomalies concurred with a relatively low energy term, indicating that although the atmosphere warmed, the soil moisture restriction relaxed. This was evident for the UASP and UACT, and resulted from the occurrence of brief precipitation events (Figure S3.3). Finally, the fourth period, corresponding to the mega-heatwave event, was marked by a positive contribution from the energy and temperature terms throughout most of SEB and particularly over its central region, where the warmest conditions were recorded (Figures 3.1, 3.3d). This triggered a strong coupling regime over the UASP, UACT and the north and northwestern surrounding regions (Figure 3.5d–f, Figure S3.2). Therefore, the observed record-breaking temperature anomalies

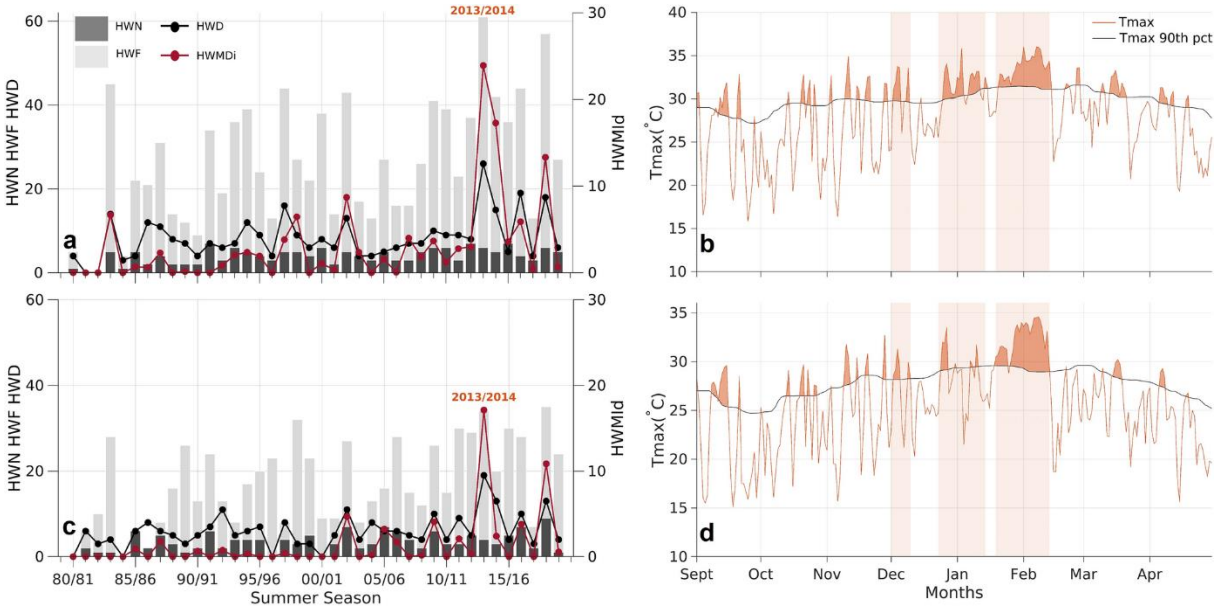

Figure 3.4 Analysis of the heatwave conditions over the UASP and UACT. Temporal evolution for the summers from 1980 to 2020 of the heatwave parameters: HWN, HWF, HWD and HWMId (see "Data and methods" section) for the UASP (**a**) and UACT (**c**). Daily maximum temperature values (°C, orange line) and the respective 90th calendar day climatological (1981–2010 reference period) percentile (black line) from September 2013 to April 2014 over the UASP (**b**) and UACT (**d**). The results for the UASP were obtained using the averages between the daily maximum temperature values observed at two meteorological stations located within the UASP (see "Data and methods" section). The results for the UACT were also obtained using a maximum temperature record from a single meteorological station located within the UACT.

and the outstanding magnitude of this mega-heatwave were somewhat driven by a pronounced soil moisture imbalance that forced the surface to start delivering part of the available radiative energy back to the atmosphere through sensible heat flux. This suggests that dry conditions were likely the extra ingredient that defined this episode as a historically unprecedented mega-heatwave rather than a regular heatwave with shorter duration and less intense temperature anomalies.

3.3.4 Mesoscale meteorological drivers of heatwave conditions over the UASP and UACT

In order to disentangle the mesoscale atmospheric mechanisms that triggered such anomalies in temperature and land–atmosphere coupling over the UASP and UACT, we zoom in on the heatwave event at hourly time scales. The hourly evolution of area-averaged values in near-surface temperature variation, the contribution of the diabatic processes, and horizontal and vertical temperature advection to this temperature variation was assessed for the UASP (Figure 3.6) and UACT (Figure S3.4). These area-averaged values were computed considering the ERA5 model grid points located within both urban areas (highlighted by the red dots in Figure 3.1f). The heat-stress conditions observed during the first hot period over the UASP, were triggered by a pronounced atmospheric heating rate during the first days of December

2013 (Figure 3.6a). This was the outcome of a positive balance between the contribution of the diabatic term (positive) and the horizontal temperature advection term (negative), explaining the positive energy coupling term depicted in Figure 3.5, which highly depends on the available shortwave radiative energy at the surface. During the second period (encompassing the days defined by a temperature cooling between the first and second hot periods—see Figures 3.4a, 3.5e), a pronounced atmospheric cooling (see black line in Figure 3.6a) was observed. This resulted from a strong negative contribution of both horizontal and vertical temperature advection terms, combined with a positive contribution of local radiative processes (Figure 3.6b). This can be observed by analyzing the consistent decreasing trend in the cumulative values of vertical and horizontal temperature advection (green and blue bold lines in Figure 3.6b) and the mean hourly negative contribution of these two processes to the temperature variation (bar plots in Figure 3.6b). Thus, although clear sky conditions were

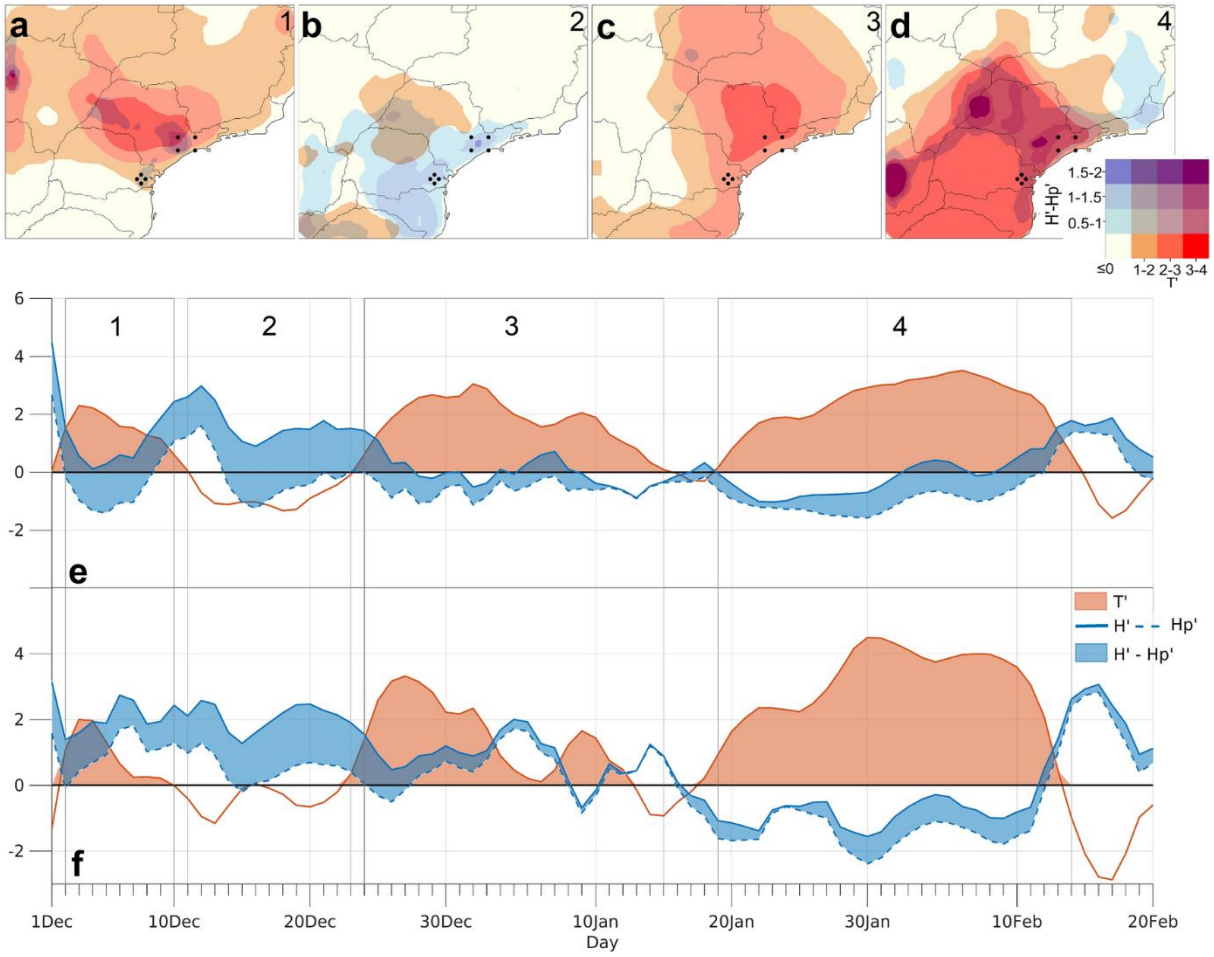

Figure 3.5 Soil moisture–temperature coupling during the 2013/2014 summer. Spatial distribution over SEB of the temperature and energy coupling anomalies throughout the four previously defined periods within the 2013/2014 summer season (**a–d**) and chronologically defined in (**e**) and (**f**) by grey boxes. Time series for the 2013/2014 summer season of spatial average values of the temperature and energy coupling terms over the UASP (**e**) and UACT (**f**). Black dots on the top panels mark the geographical limits of these two urban areas. The location of the model grid-points considered for the computation of these area averaged time series for the two urban areas is shown in Figure 3.1f.

maintained, the lower troposphere suffered an intense cooling due to a continental penetration of oceanic air masses. The influence throughout the UASP of this cooler air coming from the South Atlantic is evidenced by the observed values of the zonal and meridional wind components (Figure 3.6c), that indicate the dominant presence of southeasterly winds (see black arrow in Figure 3.6c).

Therefore, although diabatic heating remained, explaining the positive energy coupling term (Figure 3.5b,e), the coupling temperature term was negative, resulting in a weak soil moisture–atmosphere coupling over the UASP. The third period was marked again by a pronounced atmospheric heating that occurred mostly between the last days of December and the first days of January (Figure 3.6a), which was supported by a dominant positive contribution of diabatic processes and of vertical temperature advection mechanisms from December 28th to January 4th (see tick and bold green lines in Figure 3.6b). Such intense contribution from the vertical temperature advection term is associated with the predominance of north and northwesterly winds (Figure 3.6c). Analyzing the orography of the UASP and of the surrounding regions (Figure 3.1f), it is possible to observe that these north and northwesterly offshore winds brought air masses from more elevated regions towards the UASP, generating an adiabatic air compression mechanism responsible for a near-surface heating. These conditions concurred with relatively lower negative contribution of horizontal temperature advection (blue line in Figure 3.6b) and relatively lower diabatic contribution when compared to other periods. Thus, although clear-sky conditions were present, part of the atmospheric heating process resulted from katabatic winds explaining the previously identified relatively low (high) energy (temperature) coupling term for the region during this period (Figure 3.5c,e). Finally, during the fourth period, strong positive coupling conditions were observed for the UASP (Figure 3.5). The mega-heatwave event recorded during this period was generated by a pronounced atmospheric heating from January 19th to 22nd and later from January 27th to 31st (Figure 3.6a). These periods of temperature escalation were strongly promoted by local diabatic processes and by residual contributions from the vertical and horizontal advection mechanisms. Thus, clear-sky conditions coupled with a relatively low entrainment of cooler oceanic air masses towards the UASP triggered the observed temperature anomalies. In fact, Figure S3.5 shows that the region of interest within SEB (highlighted by the grey rectangle) as well as both urban areas, was not affected by the advection of warmer air masses from remote regions. When analyzing the anomaly wind pattern, one may conclude that the observed wind configuration during both the whole summer

season and during the mega-heatwave episode was anomalously eastward (Figure S3.5c,f), promoting the advection towards the UASP, UACT and the surrounding regions of slightly colder air masses (Figure S3.5a,b,d,e). On the other hand, Figure S3.6 shows that the anomalies of the surface net solar radiation over this area were remarkably positive during both periods, indicating that the diabatic contribution was always the dominant mesoscale mechanism fueling the temperature variation. Such strong contribution of radiative processes for the temperature escalation explains the high energy coupling term as well as the high temperature coupling term identified for the region (Figure 3.5d,e), with the last one receiving an extra boost due to a breaking of the sea-land breeze mesoscale regime.

The corresponding analysis for the UACT (Figure S3.4) is very similar. Due to the smoother orography of the UACT and of the surrounding regions (Figure 3.1f), the vertical temperature advection mechanisms were always residual, and so, the near-surface temperature variation was mainly controlled by the balance resulting from the diabatic and the horizontal temperature advection processes.

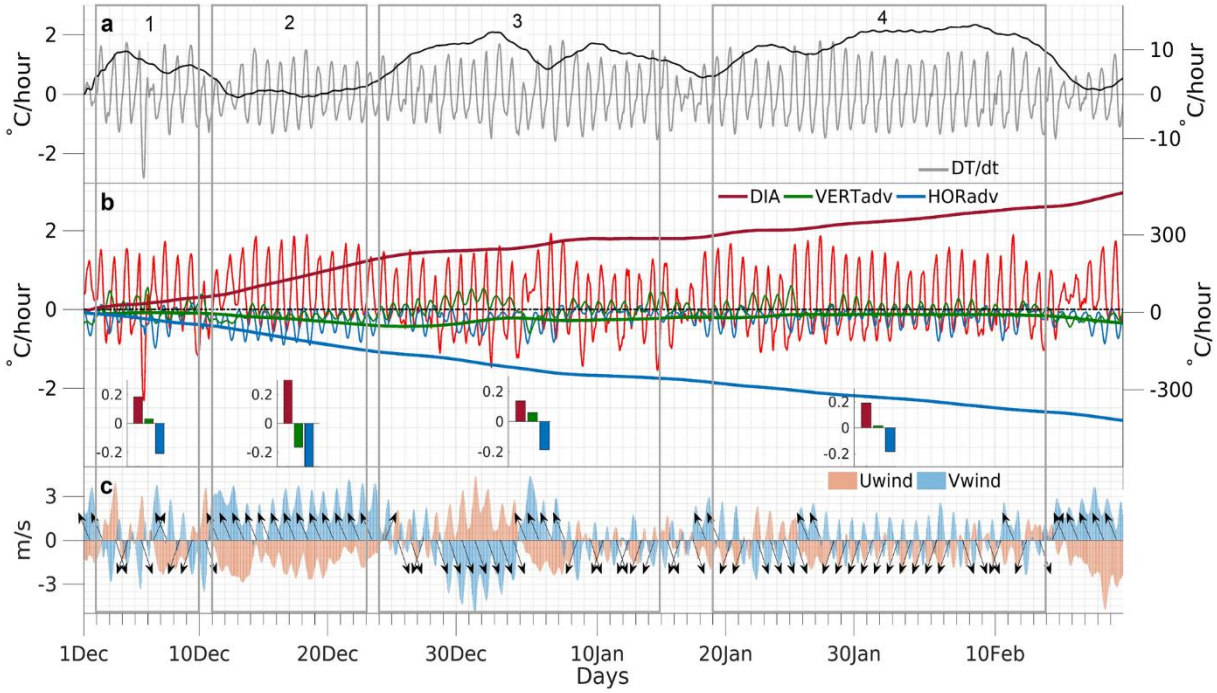

Figure 3.6 Atmospheric mesoscale characterization of the 2013/2014 summer over the UASP. Time series of area average values computed (at an hourly scale) for the UASP and throughout the 2013/2014 summer season of several regional high resolution meteorological parameters. 925-hPa (local near-surface) temperature variation rate (grey line) and respective cumulative values (accumulated over time, black line) (**a**). Contribution of the diabatic term (red), of vertical (green) and horizontal (blue) temperature advection terms for the observed 925-hpa temperature variation rate (see "Data and methods" section) (**b**). Ticker lines indicate the cumulative values. The inset bar plots show the mean hourly contribution of each mechanism during each one of the four previously defined periods within the summer season. Time series of zonal (Uwind) and meridional (Vwind) wind components (colors) (**c**). Arrows indicate the daily predominant wind direction. The location of the model grid-points considered for the computation of these area averaged time series for the UASP is shown in Figure 3.1f

3.4 Discussion and Conclusions

During the outstanding 2013/2014 summer season, SEB experienced a historically unprecedented heatwave. It was the longest and most severe summer heatwave episode ever recorded over both the UASP and UACT for the past four decades, and was responsible for an increase in the numbers of heat-related mortality (Son et al. 2016; Diniz et al. 2020). The obtained high HWMId values for this season revealed the exceptional magnitude of this particular event that occurred during a record-breaking summer season, which finds parallel in its magnitude and extent with the remarkable 2003 European and 2010 Russian summers (Barriopedro et al. 2011; Russo et al. 2015, 2017). The hot periods recorded over SEB concurred with pronounced drought conditions which were already described in recent studies (Seth et al. 2015; Coelho et al. 2016b, a; Finke et al. 2020; Geirinhas et al. 2021). Here we show that the occurrence of dry surface conditions, triggered by higher VPD and lower precipitation levels (Geirinhas et al. 2021) has been increasing for the region during the last decade. A permanent soil moisture decreasing trend in the near-future could lead soil moisture to reach values lower than the so-called critical level (Seneviratne et al. 2010). Accordingly, this would enhance the role played by the surface in constraining evaporation and in influencing the land energy and water balances. In this context, there is an increased likelihood for the occurrence of strong soil moisture–temperature coupling conditions such as the one described during this 2013–2014 event. Figure S3.7 shows the difference of the correlation values obtained between soil moisture and the evaporative fraction for two sub-periods encompassing, respectively, the summers for the 1981–2000 and 2001–2020 periods. One can observe that in some regions of SEB (namely the center of São Paulo state), the correlation coefficient values have increased significantly between the early period (1981–2000) and the latter period (2001–2020). This highlights that soil moisture has been gaining more influence in the partitioning of incoming energy to latent and sensible heat fluxes. However, we acknowledge that some caution must be taken due to the short period considered, and therefore this particular topic deserves further analysis. Nevertheless, this process is something already expected to occur in some regions of the globe under several climate change scenarios (Seneviratne et al. 2013; Soares et al. 2019).

Previous studies have shown that the observed long-term precipitation deficit and the severe high temperatures observed in SEB were induced due to a suppression of the South Atlantic Convergence Zone (Coelho et al. 2016b), which agrees with the quasi-stationary anticyclonic pattern identified over SEB and highlighted here in Figure 3.2. These synoptic

conditions were triggered by anomalous convective activity in the equatorial sections of both the Indian and Pacific oceans near Australia (Coelho et al. 2016b; Rodrigues et al. 2019; Finke et al. 2020) , that imposed a large perturbation in the tropical zonal Walker cell and in the extratropical meridional Hadley cell, establishing a stationary Rossby wave spanning from west Pacific to South Atlantic Ocean. The eastern signature of this large wave pattern was the occurrence of the quasi-stationary anticyclone structure identified in the present work (Figure 3.2).

The analysis of the soil moisture–temperature coupling terms and of the mesoscale atmospheric mechanisms that led to the near-surface temperature increase over the UASP and the UACT, revealed that the relationship between the soil dryness conditions and heatwaves was marked by distinct phases. Although dry conditions were present during almost the entire summer season, a positive soil moisture–temperature coupling, leveraged by enhanced diabatic heating processes and a suppression of the normal atmospheric cooling by sea breezes, was only observed during two distinct periods, being one the discussed mega-heatwave. Thus, the observed concurring drought conditions were important for the amplification and maintenance of this mega-heatwave through the establishment of a water-limited regime and an increase in the sensible heat flux between surface and atmosphere. The high values obtained for the soil moisture–temperature coupling over SEB were similar to the ones obtained for the 2003 European and 2010 Russian mega-heatwaves (Miralles et al. 2012, 2014) which indicates the historical relevance of this episode.

Although several previous studies have already characterized the main synoptic drivers for this summer season (Seth et al. 2015; Coelho et al. 2016b; Rodrigues et al. 2019; Finke et al. 2020), to the best of our knowledge, none had explored and quantified in detail the exceptionality of the induced warm conditions in such a high temporal and spatial scale. Therefore, our results and conclusions highlighted a chapter about this historical summer season that remained so far unexplored, by showing that the observed record-breaking warm conditions weren't explained by synoptic circulation anomalies alone and that land–atmosphere feedbacks and their inter-links with mesoscale processes played a crucial role.

Useful metrics to perform a thorough characterization and quantification of the magnitude of CDH events could also be drawn using the results presented here. This would allow for a more robust comparison between these compound episodes throughout periods defined by a climate change context. Moreover, they would represent a guideline for predicting future

episodes of this kind and mitigate the associated natural, socio-economic and public health impacts for Brazil. The increased heat-related impact observed during the 2013/2014 summer (Son et al. 2016; Diniz et al. 2020) should encourage political, health and civil protection authorities to seek tools and mitigation measures to improve the control of illnesses related to hot periods, particularly in megacities in developing countries like Brazil (Hajat and Kosatky 2010; United Nations, 2018). Finally, robust projections indicate a future climate scenario controlled by hotter and drier conditions in South America and specifically in Brazil (Feron et al. 2019; Llopart et al. 2020; Rusticucci and Zazulie 2021) and, consequently, by an increasing frequency of more intense and longer lasting CDH episodes.

Supplementary Material

HWMId definition:

The HWMId was defined as the maximum magnitude of HWs in the summer season. The magnitude of each HW event is the sum of the magnitude of the consecutive days composing the episode. The daily magnitude is calculated as follows:

$$M_d(T_d) = \begin{cases} \dfrac{T_d - T_{30y25p}}{T_{30y75p} - T_{30y25p}}, & if\ T_d > T_{30y25p} \\ 0, & if\ T_d \leq T_{30y25p} \end{cases}$$

with T_d being the daily Tmax on the heatwave day d, T_{30y25p} and T_{30y75p} the 25th and 75th percentiles, respectively, of the time series composed of 30-year maximum temperatures within the reference period (1981-2010). The HWMId definition here presented, corresponds to a slight adaptation from the one proposed by Russo et al. (2015), where the HWMId was defined as the maximum magnitude of HWs in a year: here we defined it as the maximum magnitude of HWs in a summer season. Theoretically the summer season encompasses the most severe HW events with the highest observed Tmax values. Therefore, we believe that this slight adaptation in the index originally proposed by Russo et al. (2015) does not imply considerable changes in the results.

Segmented linear regression model with breakpoints

The estimation of the generalized linear models with two segmented relationships in the linear predictor presented in Figure 3.3, was obtained using the r-package "segmented" (https://cran.r-project.org/web/packages/segmented/segmented.pdf). The package estimates the slopes and breakpoints along with standard errors. The algorithm corresponds to an iterative procedure described in Muggeo (2003). Hypothesis testing (about the existence of the breakpoint) and confidence intervals are performed via appropriate methods and functions Muggeo (2016, 2017).

Supplementary Figures

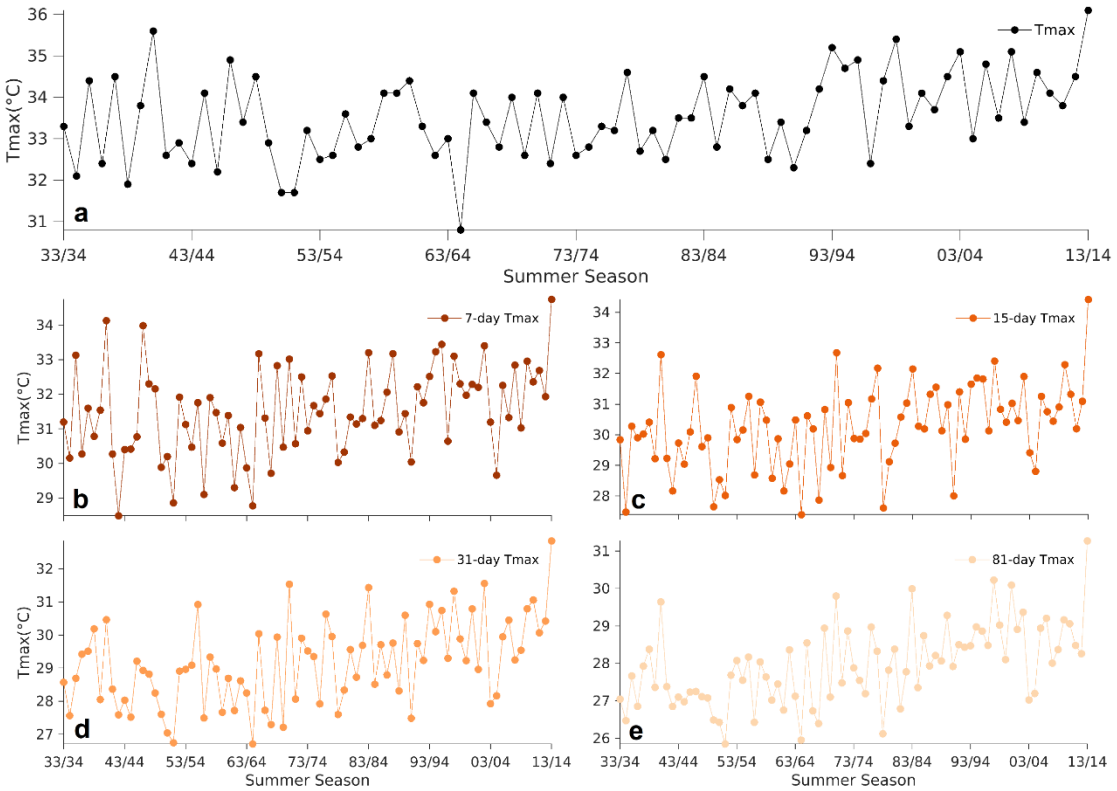

Figure S3.1 Time series of the mean maximum temperature for the summers between 1933/1934 and 2013/2014 considering raw daily temperature values (**a**), 7-day (**b**), 15-day (**c**), 31-day (**d**) and 81-day (**e**) average periods. These results were obtained using the long-term data from the meteorological station of the University of São Paulo (see Data and Methods).

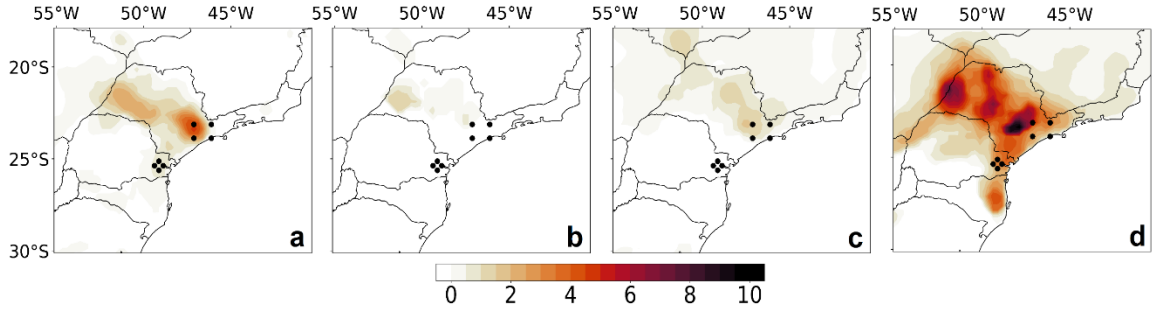

Figure S3.2 Soil moisture–temperature coupling (π) during the four defined hot periods within the 2013/2014 summer season and chronologically defined in Figure 3.5e and 3.5f by the grey boxes.

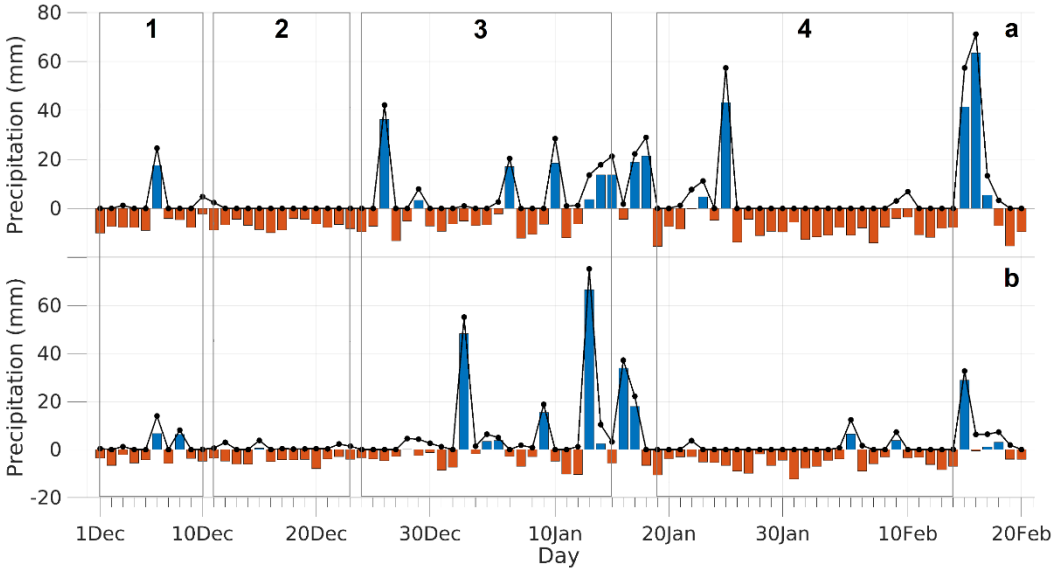

Figure S3.3 Time series for the 2013/2014 summer season of daily accumulated precipitation (black line) and respective anomaly values (bars) for the UASP (**a**) and UACT (**b**). Results computed using daily precipitation levels recorded from two meteorological stations located in both urban areas (see Data and Methods).

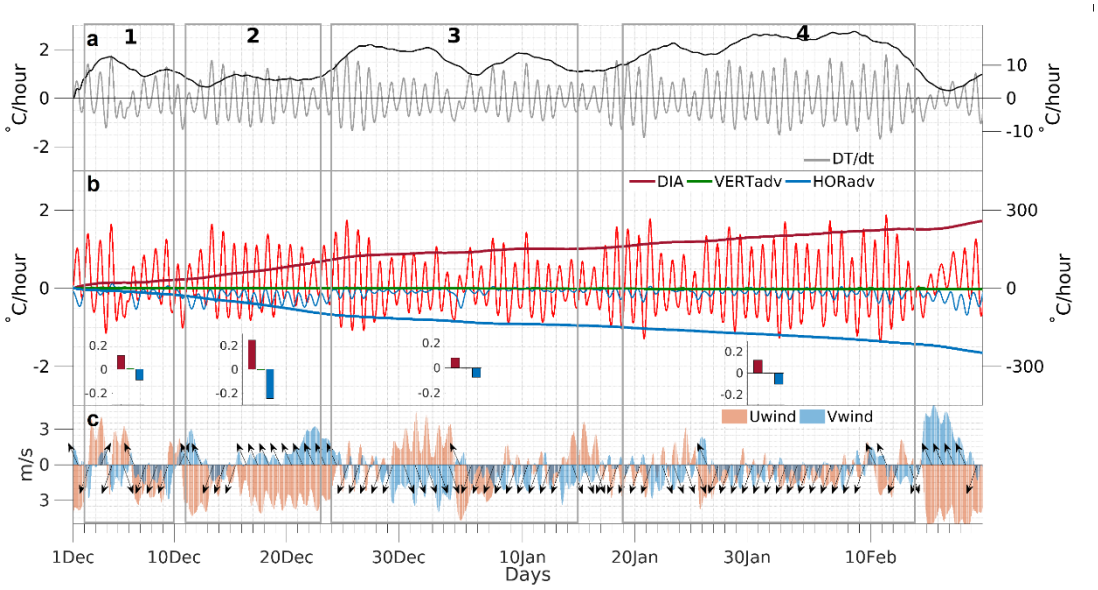

Figure S3.4 As in Figure 3.6 but for the UACT.

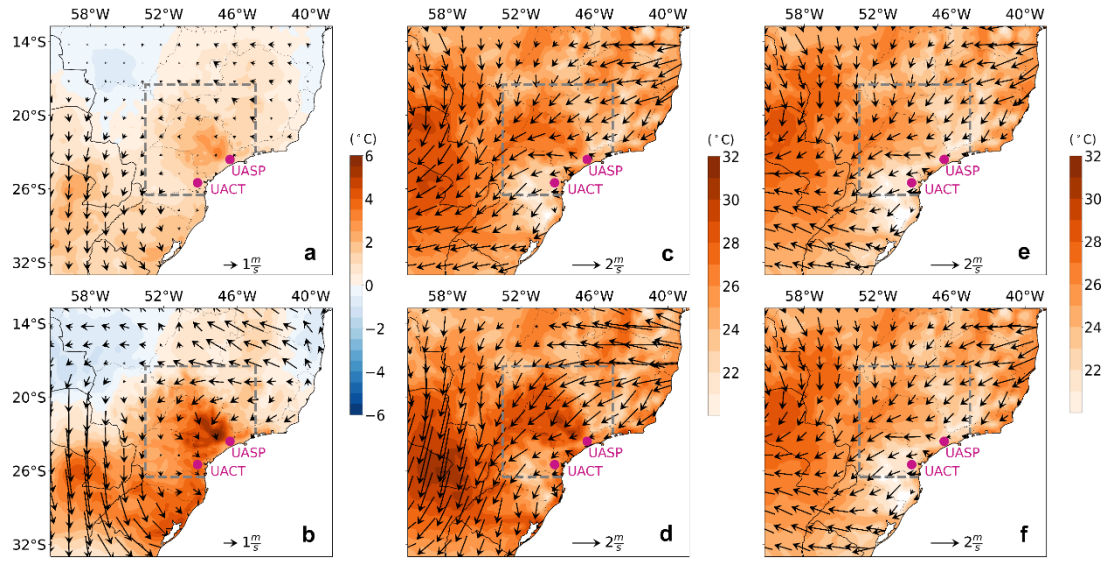

Figure S3.5 Mean anomaly composite fields over Southeast Brazil of the daily mean surface temperature (ºC, colors) and wind pattern (vectors, m/s) computed for the 2013/2014 summer (**a**) and for the mega-heatwave episode – from January 19th to February 13th 2014 (**b**). Mean observed values over Southeast Brazil of the same meteorological parameters during the 2013/2014 summer (**c**) and during the mega-heatwave episode (**d**). Climatological field (1981–2010 base period) of the same meteorological parameters represented in the previous panels, for the austral summer season (December–February) (**e**) and for the summer period encompassing the mega-heatwave episode (**f**).

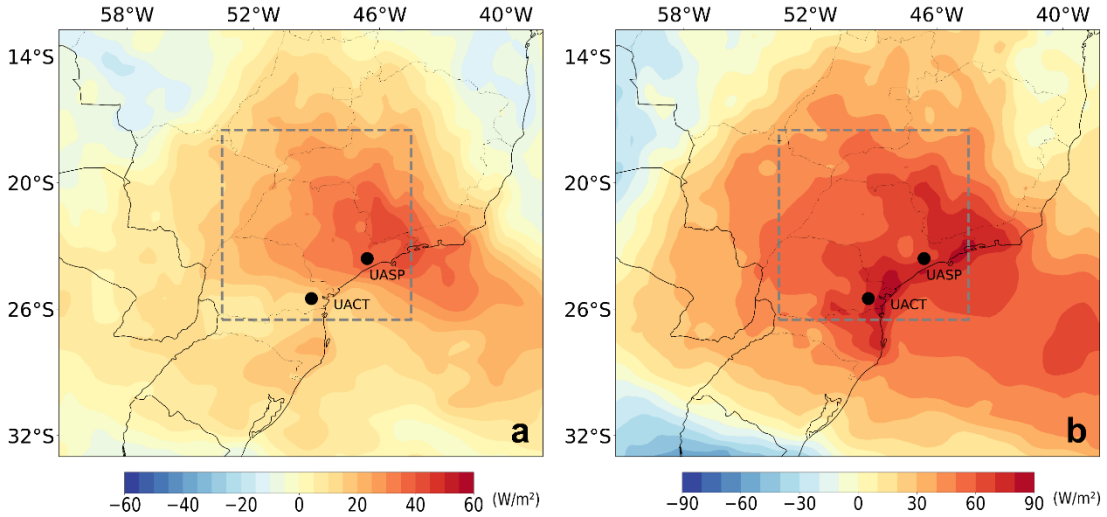

Figure S3.6 Anomaly composite fields of surface net solar radiation (W/m^2) over Southeast Brazil computed for the 2013/2014 summer (**a**) and for the mega-heatwave episode - from January 19th to February 14th 2014 (**b**).

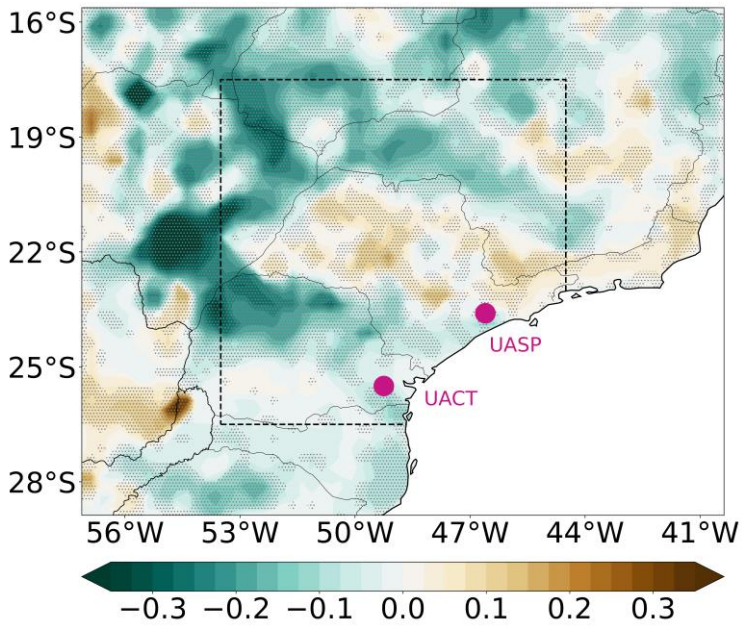

Figure S3.7 Spatial distribution of correlation coefficient differences between the period encompassing the summers of 2000/2001 to 2019/2020 and the period encompassing the summers from 1980/1981 to 1999/2000. The correlation coefficients were computed between daily soil moisture and evaporative fraction values. The grey dots highlight the grid-points in which the differences were statistically significant at a 5% level.

Chapter 4

Combined large-scale tropical and subtropical forcing on the severe 2019–2022 drought in South America

***Geirinhas JL**, Russo AC, Libonati R, Miralles DG, Ramos AM, Gimeno L, Trigo RM. (2023) Combined large-scale tropical and subtropical forcing on the severe 2019–2022 drought in South America. npj Clim Atmos Sci 6:185. https://doi.org/10.1038/s41612-023-00510-3*

***João Lucas Geirinhas contributions:** conceptualization of the study; preparation of the data; computation, analysis and interpretation of the results; production of all the figures and coordination of the manuscript writing.*

Abstract

Changes in the frequency and magnitude of dry spells have been recorded over the past few decades due to an intensification of the global water cycle. A long-term soil drying trend resulting from a joint contribution of natural decadal variability in precipitation levels and increasing temperatures, predisposed central-east South America (CESA) to experience during 2019–2022 a period of outstanding soil desiccation. Flash droughts led to large areas (~100.000 km^2) in CESA covered by record-breaking soil dryness. April 2020 witnessed the most severe conditions, when over 30% of the region experienced negative soil moisture anomalies larger than two standard deviations. Internal variability, particularly El Niño–Southern Oscillation, explained the dynamical forcing of this extreme drought. Large precipitation deficits and enhanced evaporation in CESA resulted from a coupled tropical and subtropical forcing associated to pronounced changes in the normal Walker and Hadley Cells' circulation and to the establishment of a Rossby wave extending from west south Pacific towards South America. These findings highlight the intricate interplay between different mechanisms in the occurrence of climate extremes, stressing the need for an adequate representation of the dynamical processes associated with daily-to-multiyear timescales in climate models.

4. Combined large-scale tropical and subtropical forcing on the severe 2019–2022 drought in South America

4.1 Introduction

Climate change is expected to cause, through both thermodynamic and dynamical mechanisms, a strengthening of the global water cycle and thus profound changes in the frequency and magnitude of dry and wet spells (Donat et al. 2016; Wang et al. 2017b; Chagas et al. 2022). This poses great pressure on global freshwater availability (Haddeland et al. 2014; Konapala et al. 2020), food security (Lesk et al. 2016) and sustainability of natural ecosystems (Seddon et al. 2016). Higher levels of lower-tropospheric water vapor promoted by increasing temperatures are linked to changes in the balance between evaporation and precipitation (E–P) that ultimately determines soil moisture, groundwater recharge and total water available for runoff (Trenberth 2011; Kumar et al. 2014; Zhou et al. 2021). Long-term drying trends can influence the atmospheric water budget, particularly over drylands, by limiting evaporation and reducing moisture recycling for precipitation (Jung et al. 2010; Dirmeyer et al. 2014; Miralles et al. 2016; Zhou et al. 2021). On the other hand, reduced soil moisture conditions may also enhance, through convective instability, the atmospheric moisture convergence contributing to a higher frequency of extreme precipitation episodes from convective storms (Taylor et al. 2011, 2012; Miralles et al. 2019; Zhou et al. 2021). In parallel, under a large atmospheric evaporative demand, a strong soil moisture imbalance may also play a major role in the surface energy partitioning by constraining surface latent heat fluxes, leading to an above-normal accumulation of sensible heat in the atmosphere and to the escalation of temperatures (Miralles et al. 2014; Santanello et al. 2018; Geirinhas et al. 2022). Thus, the interplay between soil moisture, atmospheric water budget and temperature is part of a large and complex framework of feedbacks that are modulated by climate change (i.e., increasing temperatures, changes in vegetation and in atmospherics dynamics), and that may also affect the climate trends themselves (Douville et al. 2013; Miralles et al. 2019; Zhou et al. 2021).

So far, relatively little attention has been given to the simultaneous assessment of temperature, precipitation and soil moisture trends over South America (SA) (Libonati et al.

2022b). According to the last report from the Intergovernmental Panel on Climate Change (IPCC 2021), most of the continent has warmed up at a rate between 0.1 °C and 0.4 °C per decade during the 1981–2020 period, with tropical SA experiencing the largest warming trends. Previous studies have also pointed to a significant increase in the frequency of warm extremes during the 1961–2018 period (de Barros Soares et al. 2017; Regoto et al. 2021). Regarding precipitation, the conclusions are less spatially coherent and the projections for SA indicate a dipole pattern of drier conditions centered in the Amazon, while wetter conditions prevail in central-eastern parts of the continent, i.e., over La Plata Basin (Reboita et al. 2014; Llopart et al. 2020). The evaporation from the Amazon and La Plata basins (Figure 4.1a), the two largest watersheds of SA, is crucial for the regional hydroclimate and for precipitation through local moisture recycling and moisture transport between both (Drumond et al. 2014; Zanin and Satyamurty 2020; Chug et al. 2022). Other external moisture sources are also important for the atmospheric water budget over these two watersheds, such as the large quantities of water vapor transported from the Atlantic into the Amazon Basin by the trade winds (Zanin and Satyamurty 2020; Chug et al. 2022). All these hydrological processes are modulated by a complex interplay between large-scale oceanic–atmospheric modes of variability such as the El Niño–Southern Oscillation (ENSO) (Cai et al. 2020; Taschetto et al. 2020), the Madden–Julian Oscillation (MJO) (Alvarez et al. 2016; Grimm 2019) and the Atlantic Meridional and Zonal Modes (AMM and AZM, respectively) (Drumond et al. 2014). These climate variability modes influence semi-permanent and transient systems that play a key role for precipitation and evaporation in SA, namely the Inter-Tropical Convergence Zone, the South Atlantic Convergence Zone, the South America Low Level Jet (SALLJ), mid-latitude cold fronts, cyclones and quasi-stationary anticyclonic systems (Coelho et al. 2016b; Cai et al. 2020).

More recently, La Plata basin and Pantanal in central-east South America (CESA), have been affected by a severe drought whose first signs were noticed during mid-2018 in Southeast Brazil (Thielen et al. 2021). However, soil dryness rapidly extended to adjacent areas in Paraguay, Bolivia, and later over northern Argentina, where millions of hectares of wheat production were affected (Gomes et al. 2021). In Paraguay, Uruguay and Southern Brazil, huge agricultural losses in maize, wheat and soybean production were also recorded and many Brazilian farmers were forced to request economic assistance (Gomes et al. 2021). Alongside, extremely low levels in discharge in both Paraná and Paraguay rivers were observed, leading to serious constraints in the hydropower generation and water supply, and to the interruption of waterways that are essential for the fluvial transport and economy of these countries (Gomes et

al. 2021; Marengo et al. 2021). This prolonged and intense drought also affected, particularly during 2020, the Pantanal biome, which is the largest contiguous wetland on the planet and home to a large variety of animal and plant species (Libonati et al. 2020). Pronounced soil dry-out in the region coincided with several heatwaves, leading to periods characterized by a rapid and sudden intensification of the drought conditions and a large evaporative stress (Geirinhas et al. 2022; Libonati et al. 2022a). This short-term (weekly to monthly) periods, marked by a rapid rate of intensification of the already established dry conditions, are usually referred as flash droughts and are often linked to more severe impacts than the slowly evolving droughts (Qing et al. 2022). In Pantanal, these flash droughts raised fire danger to levels not seen since 1980 and led to devastating fires (Libonati et al. 2022a), resulting in one-third of the biome burnt and economic losses of around USD 3.6 billion (Libonati et al. 2022a). The extreme

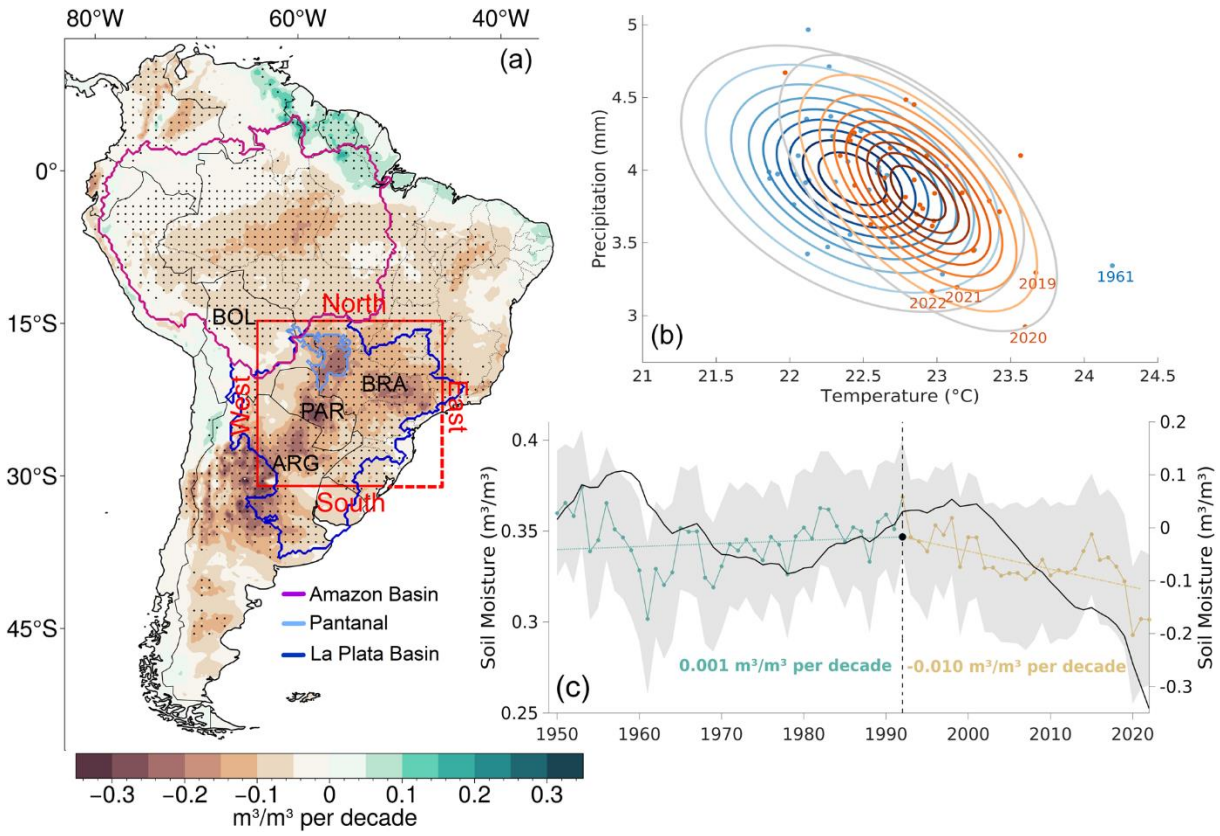

Figure 4.1 (**a**) Spatial distribution over SA of soil moisture trends (m^3/m^3 per decade) over the 1990–2022 period. The black dots depict regions with statistically significant trends at a 5% level, according to the non-parametric Mann–Kendall two-tailed test. The limits of the Amazon basin, La Plata Basin and the Pantanal biome are marked by the purple, blue and turquoise lines, respectively. The red box delimitates the region of interest covering CESA. (**b**) Bivariate Gaussian probability distribution functions of mean annual surface temperatures (°C) and daily accumulated precipitation levels (mm) averaged over CESA, for the 1959–1989 (blue ellipses) and the 1990–2022 periods (orange ellipses). The gray ellipses show the 95% level of the probability distribution. (**c**) Time series (1951–2022) of mean annual soil moisture levels, spatially averaged over CESA (green and yellow lines, left y-axis), and of the time accumulated soil moisture anomalies regarding the climatological period of 1981–2010 (black line, right y-axis). The dash green and yellow lines result from a regression model with two segmented (i.e., piecewise) linear relationships separated by a break point (obtained from an iterative process described in Supplementary Material) highlighted by the filled black dot. The respective trend values are shown in the bottom part of the panel.

drought lasted until the end of 2022, spreading from Pantanal to wider areas in CESA (Getirana et al. 2021).

This study seeks to provide a detailed spatiotemporal characterization of the unprecedented 2019–2022 drought in CESA, exploring the historical context of the event, assessing the exceptionality of the soil moisture anomalies and describing the atmospheric mechanisms involved from a daily to multiyear timescale perspective. Overall, we aim to contribute to a better understanding of the dynamical processes associated with internal variability, and thus to improve the predictability of climate extremes in future.

4.2 Data and Methods

4.2.1 Data

Daily data from several meteorological parameters at surface and at different pressure levels, such as precipitation, temperature, specific humidity, zonal and meridional wind, geopotential and vertical velocity were extracted from the European Centre of Medium-range Weather Forecast ERA-5 reanalysis datasets (Copernicus Climate Change Service, C2S, 2017) for the 1959–2022 period (Hersbach et al. 2020). Daily soil moisture levels (0 – 7 cm soil depth) for the 1951–2022 period were obtained from the ERA5-Land reanalysis which replaced the land component of the ERA5 model providing a better representation of the hydrological cycle (Muñoz-Sabater et al. 2021). ERA5-Land shows a good performance in estimating soil moisture levels when compared to other datasets, including satellite products and other models with and without data assimilation (Beck et al. 2021). ERA5-Land soil moisture data is obtained using meteorological fields, such as precipitation and temperature, given by ERA5 that has incorporated a data assimilation scheme (Muñoz-Sabater et al. 2021). ERA5 and ERA5-Land show for CESA smaller biases in precipitation than other known reanalysis such as JRA-55 and MERRA-2 (Hassler and Lauer 2021). The same is observed regarding the performance of ERA5 in estimating temperature extremes and the persistence of hot days (Coronato et al. 2020; Balmaceda-Huarte et al. 2021). Although ERA5-Land, as a reanalysis product, has some disparities regarding observations, it provides the most reliable dataset for analysis of this kind on very long time periods and over wide regions such as SA and particularly CESA, where observations for variables such as soil moisture are unavailable (Baker et al. 2021).

4.2.2 Bivariate gaussian distributions

In order to estimate temperature–precipitation distributions for the two halves of the total period of analysis (1959–2022) and thus assess long-term changes in the bivariate distribution of these variables, two probability density functions assuming a bivariate gaussian distribution were computed for pairs of mean annual temperature and precipitation averaged over the red box in Figure 4.1 (CESA) and during the periods of 1959–1989 and 1990–2022. Similarly to Bevacqua et al. (2022), we assume that a bivariate Gaussian distribution is acceptable for mean annual values of these two variables allowing for a simple understanding of their compound effect on soil moisture levels, with the hypothesis that in some particular grid-points both precipitation and temperature datasets may have a skewed (Gamma) distribution.

4.2.3 The vertically integrated water vapor transport

The vertically integrated water vapor transport (IVT) quantifies the total horizontal moisture transport by integrating over the vertical column of the atmosphere the zonal (Q_λ) and meridional (Q_ϕ) transport of specific humidity, defined as follows (Peixoto and Oort 1992):

$$IVT\left[\left(\frac{1}{g}\int_{SURF}^{TOA} qudp\right)^2 + \left(\frac{1}{g}\int_{SURF}^{TOA} qvdp\right)^2\right]^{\frac{1}{2}} \quad (4.1)$$

with,

$$Q_\lambda = \frac{1}{g}\int_{SURF}^{TOA} qudp \quad (4.2)$$

$$Q_\phi = \frac{1}{g}\int_{SURF}^{TOA} qvdp \quad (4.3)$$

where *q* is the specific humidity, *u* and *v* are the zonal and meridional components of wind, respectively, g is the gravitational acceleration and dp an infinitesimal element of vertical pressure.

Considering this definition for the meridional and zonal components of the IVT, the vertically integrated moisture divergence can be computed using finite differences as follows:

$$\nabla . \vec{Q} = \frac{\partial Q_\lambda}{\partial x} + \frac{\partial Q_\emptyset}{dy} \quad (4.4)$$

Accordingly, when the divergence is positive (negative) the atmospheric circulation is acting to decrease (increase) the water vapor transport over all the column of the atmosphere.

4.2.4 The water vapor balance over CESA

According to previous studies (Peixoto and Oort 1992; Peixoto 1973) the total (net) vertically integrated moisture convergence (VIMC) over CESA, whose area is geographically defined in Figure 4.1 (see red box), can be obtained as a line integral that accounts for the IVT across the western (F_w), the northern (F_N), the eastern (F_E) and the southern (F_S) borders:

$$VIMC = F_w + F_N + F_E + F_S \quad (4.5)$$

with,

$$F_W = \int_{\emptyset=31°S}^{\emptyset=15°S} Q_\lambda d\phi\,, \quad \lambda = 64°W \quad (4.6)$$

$$F_E = -\int_{\emptyset=31°S}^{\emptyset=15°S} Q_\lambda d\phi\,, \quad \lambda = 44°W \quad (4.7)$$

$$F_N = -\int_{\lambda=64°W}^{\lambda=44°W} Q_\phi d\lambda\,, \quad \phi = 15°S \quad (4.8)$$

$$F_S = \int_{\lambda=64°W}^{\lambda=44°W} Q_\phi d\lambda\,, \quad \phi = 31°S \quad (4.9)$$

Analyzing equation (4.9) and neglecting the water storage changes ($\frac{\partial w}{\partial t}$), when VIMC > 0, the region experiences a moisture flux convergence and acts as moisture sink if $P - E > 0$, or $E - P < 0$. On the other hand, when VIMC < 0, the region witnesses a moisture flux divergence and acts as moisture source if $P - E < 0$, or $E - P > 0$:

$$VIMC = P - E + \frac{\partial w}{\partial t} \quad (4.10)$$

The area-averaged precipitation rate due to moisture convergence ($P_{convergence}$) over SESA can be obtained dividing VIMC by the total area of the red box depicted in Figure 4.1a (*A*):

$$P_{convergence} = \frac{VIMC}{A} \quad (4.11)$$

Accordingly, the contribution of moisture convergence to the total area averaged precipitation (P_{total}) can be computed by $\frac{P_{convergence}}{P_{total} \times 100}$, while the contribution of local moisture recycling due to evaporation can be obtained by:

$$100 \times \frac{\left(P_{total} - P_{convergence}\right)}{P_{total}} \quad (4.12)$$

4.2.5 R-index: ranking soil moisture anomalies

The R-index is defined here as an adaptation of a metric initially proposed by Hart and Grumm (2001) and used in several studies (Ramos et al. 2014; Liberato et al. 2021) to rank precipitation events on a daily basis. The exact same rationale was adopted here but considering soil moisture levels in CESA as input. First, daily standardized soil moisture anomalies regarding the seasonal climatology (1981–2010) were computed for each grid point within CESA and then filtered using a 31-day running mean filter. Thus, for each day of the analysis period (1951–2022) and for each grid-point within CESA we attained a normalized soil moisture departure value from the climatology. Ultimately, the R-index quantifies and ranks, on a daily basis, the magnitude of the soil moisture anomalies over CESA by multiplying (1) the area of CESA (in percentage) that experiences soil moisture anomalies lower than two standard deviations ("Spatial Extent") by (2) the mean soil moisture anomaly obtained by considering only the grid-points that recorded anomalies lower than two standard deviations ("Mean Anomaly").

Therefore, severe drought conditions are diagnosed when R-index reaches extremely low levels. Weekly to monthly peaks of this metric are linked to a sudden and rapid onset development of dry conditions and thus to flash drought episodes.

4.2.6 Rossby wave source

The Rossby Wave Source (RWS) was computed considering the barotropic vorticity equation in pressure coordinates (Sardeshmukh and Hoskins 1988; Holton and Hakim 2012):

$$RWS = -\zeta D - v_x . \nabla \zeta \quad (4.13)$$

Where ζ is the absolute vorticity, obtained by summing the relative vorticity with the Coriolis parameter, and v_x is the non-rotational (i.e., divergent) wind vector component. The first term denotes the vortex stretching and accounts for the changing rate of vorticity, while the second term denotes the advection of vorticity by the divergent flow. Therefore, the Rossby Wave forcing tends to be higher in regions where divergence, divergent wind, absolute vorticity and the gradient of absolute vorticity is large. For instance, regions in the Western Pacific, at east and south of Australia, located on the edge of strong diabatic tropical heating and over the passage of the subtropical jet stream, where there are co-occurring conditions of high divergence, enhanced absolute vorticity and a high gradient of vorticity, reunite all the ideal conditions for a strong Rossby Wave forcing (Shimizu and de Albuquerque Cavalcanti 2011).

4.3 Results

4.3.1 The 2019–2022 drought in a historical context

Most of SA has been witnessing, particularly after the 1990's decade, a significant land surface drying trend, with CESA (limited by the red box shown in Figure 4.1a), revealing the steepest soil moisture decrease, particularly over the Pantanal, Southeast Brazil, central Paraguay and northern Argentina (Figure 4.1a). When analyzing long-term changes in climate for CESA (Figure 4.1b and Figure S4.1), a pronounced shift towards higher temperatures from the first half of the analysis period (1959–1989) into the second half (1990–2022) is observed – see blue and orange ellipses in Fig. 4.1b. Regarding precipitation, there is a less pronounced contrast in the distribution between both periods. However, a skewed distribution is observed during the second half of the period, indicating a few periods characterized by extreme low and high precipitation levels during recent decades. The correlation between precipitation and temperature is stronger for the second half (R= –0.63) than for the first half (R= –0.43), indicating that during the last three decades, dry years were more often associated with extremely warm conditions. This recent warmer and drier conditions explain a continuous decrease in soil moisture levels (Figure 4.1c), particularly after 1990's decade (–0.010 per decade, statistically significant at a 5% level according to the Mann–Kendall two-tailed test), paving the way for the outstanding 2019–2022 drought. In fact, this 4-year period finds no parallel with any other period in the historical record, being unprecedented in terms of dryness intensity and duration.

When analyzing the total precipitation anomalies (gray and black lines in Figure 4.2a) as well as the precipitation anomalies caused only by the vertically integrated moisture convergence (VIMC) (blue bars and line in Figure 4.2a) in CESA for the 1959–2022 historical period, one can observed that they were characterized by a marked decadal variability and by

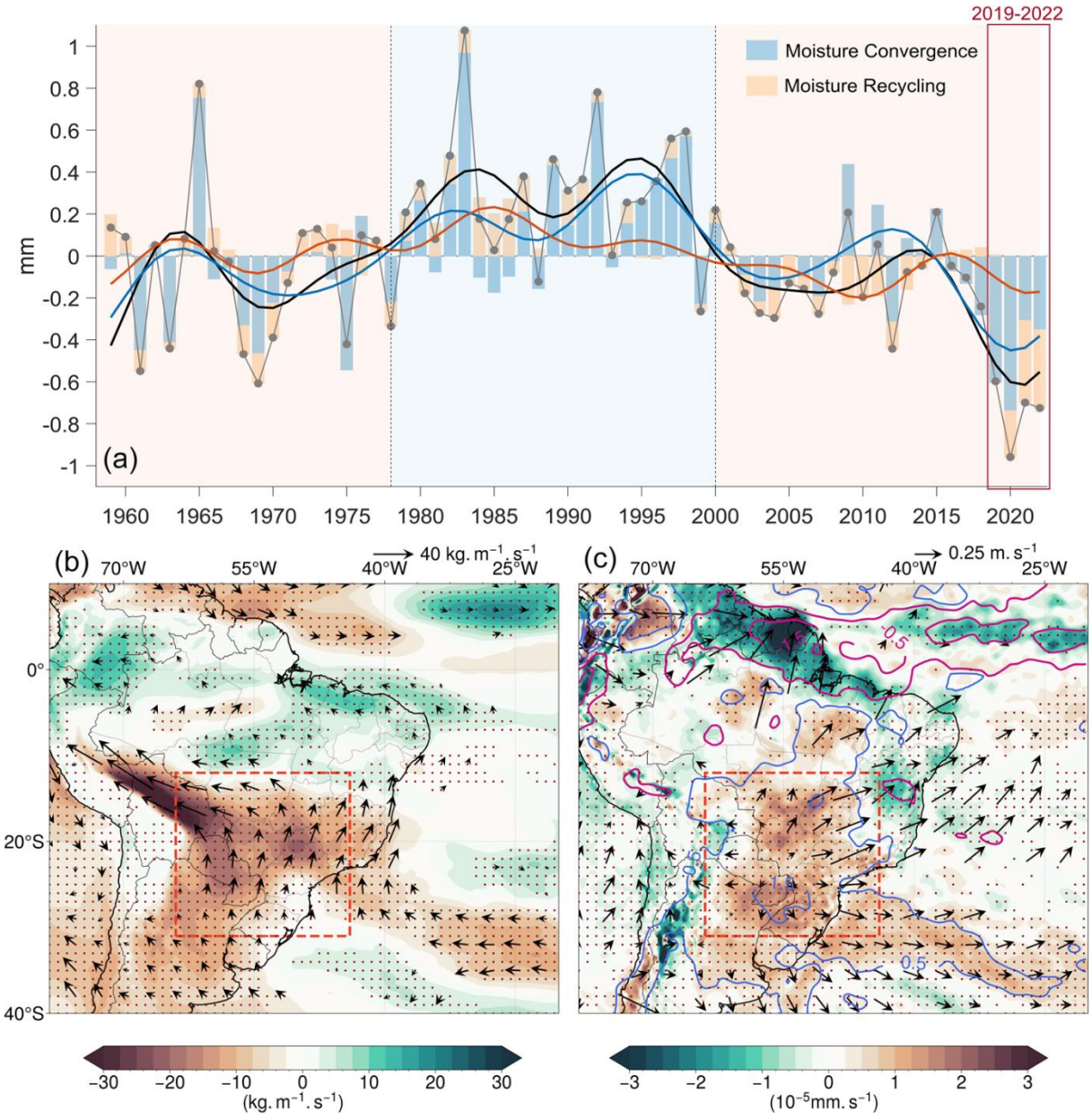

Figure 4.2 (**a**) Time series of mean annual anomalies over CESA of daily accumulated precipitation (gray line, mm), and daily accumulated precipitation due to vertically integrated moisture convergence (blue bars, mm) and due to moisture recycling (orange bars, mm). The bold lines depict the respective time series filtered by a 10-year low pass Lanczos filter. Light orange and blue background colors highlight decadal periods defined by drier and wetter condition, respectively. (**b**) Anomaly composites (regarding the 1981–2010 climatology) of IVT obtained considering the mean observed conditions during the 2019–2022 drought period (color shading, $kg.m^{-1}.s^{-1}$), and direction (vector – only the statistically significant anomalies at a 5% level are shown according to the Student's two-tailed *t* test). (**c**) Anomaly composites for the 2019–2022 period of the vertical integral of divergence of moisture flux (color shading, $mm.s^{-1}$) and of the divergent wind field at the 850hPa level (vectors, $m.s^{-1}$). Blue and magenta contours delimitate regions covered by positive and negative anomalies of the daily evaporation minus precipitation balance, respectively. Red dots in (**b**) and (**c**) mark the statistically significant anomalies at a 5% level according to the Student's two-tailed *t* test.

the occurrence of a drier period during the first and last two decades and a wetter period during the 1980's and 1990's. The two variables present a Spearman's correlation coefficient of 0.92 over the entire period, statistically significant at a 5% level, showing that long-term disturbances in moisture convergence in CESA are strongly reflected in the total amount of precipitation in the region. On the other hand, moisture recycling seems to be less important in explaining inter-annual changes of precipitation anomalies as it shows a less pronounced decadal variability and a lower correlation coefficient ($R = 0.62$, statistically significant at a 5% level). The precipitation anomalies caused by moisture recycling show a decreasing trend after the 1980's (statistically significant at the 5% level), which likely results from the previously observed progressive reduction in soil moisture in the region (see Figure 4.1c). In particular, the drought years of 2019 and 2020 experienced the two lowest ever recorded VIMC levels, while 2021 and 2022 observed the two lowest contributions of moisture recycling for total precipitation.

The boxplots shown in Figure S4.2 highlight the statistical distribution of the mean annual values of daily vertically integrated water vapor transport (IVT) across each one of the four CESA borders depicted in Figure 4.1a, with positive (negative) values indicating moisture inflow (outflow) to (from) CESA. The inflow of moisture occurs mostly throughout the northern and western borders while the outflow occurs mainly throughout the eastern and southern borders. The 2019–2022 drought years were defined by a lower than normal northern and western moisture inflow, which clearly contrasts with the higher-than-normal moisture inflow throughout these two limits during the four wettest years (1965, 1983, 1992 and 1998, see Figure S4.2). In fact, the correlation coefficients for 1959–2022 between the mean annual IVT over each one of the four frontiers and the mean annual VIMC over CESA (inset table in Figure S4.2), are positive and statistically significant at a 5% level for the northern ($R = 0.70$) and western borders ($R = 0.55$), indicating that the moisture convergence and precipitation anomalies are mostly determined by the amount of moisture inflow from Amazon. In contrast, the amount of moisture outflow through the eastern and southern borders does not play a significant role in moisture convergence in CESA. These results are corroborated when analyzing from a spatial perspective the anomalous IVT over SA, which shows an anomalous southeast–northwest orientation pattern during the 2019–2022 drought period (Figure 4.2b), and an anomalous northwest–southeast orientation during the four wettest years (Figure S4.3a). Comparing with climatological conditions (see Figure S4.4), the IVT configuration observed during the 2019–2022 period points to a weakening of the expected northwest–southeast

moisture transport from the Amazon basin towards CESA that is mostly supported by the SALLJ (Marengo et al. 2002).

Precipitation anomalies are determined not only by moisture availability but also by convergence patterns in the atmosphere. Accordingly, the positive anomalies of the vertical integral of divergence of moisture flux in CESA, reveal that during the 2019–2022 drought the region was characterized by a lower-than-normal moisture convergence (Figure 4.2c). The anomalous low tropospheric (850hPa) wind field shows enhanced divergence and air spread from CESA towards the surrounding regions, highlighting pronounced subsidence and clear sky conditions. These conditions were responsible for large precipitation deficits in CESA and thus for positive anomalies in evaporation minus precipitation (E–P) in the region (see blue contours in Figure 4.2c). Moreover, this divergence implied anomalous advection from CESA towards north SA, where pronounced moisture convergence and negative anomalies in E–P prevailed. The mean observed conditions during the wettest years show a clear contrasting pattern (Figure S4.3b). The regression maps shown in Figure S4.5 support this relationship, indicating that throughout the 1959–2022 period, increasing IVT and decreasing levels of the vertically integrated divergence over CESA were associated with enhanced local precipitation.

4.3.2 A closer insight into the 2019–2022 drought: evolution, exceptionality and spatial extent

The time series for the 2019–2022 period of the R-index, a metric defined to rank extreme and widespread drought events using soil moisture anomalies (see "Methods section"), presents a relatively large variability resulting from pronounced fluctuations of both the drought intensity and spatial extent. At the beginning of 2019, marked dry conditions started to affect CESA (Figure 4.3a). The R-index peaks for the first time on January 26th (9th and 36th in the ranking classification considering the short 2019–2022 and the long 1951–2022 periods, respectively), highlighting a rapid and pronounced soil desiccation and the occurrence of a flash drought over southeast Brazil and the Pantanal biome (see left panel of Figure 4.3c). Analyzing Figure 4.3b and the color shading level intercepted by the purple line which depicts the 31-day time scale (the time scale used to obtain the running mean filtered soil moisture anomalies that were input for the R-index), one can observe that this period was characterized by several areas within CESA experiencing record-breaking low soil moisture levels (with a total extension of around 100 000 km^2). Later, during the following months, there was a clear amelioration of the

drought, with R-index reaching values closer to zero. However, the year 2020 witnessed the most critical conditions with the occurrence of several flash drought episodes, particularly during the months of March, April, October, November and December, when many regions in CESA experienced a record-breaking soil dry-out (Figure 4.3b). In fact, the five most severe R-index peaks occurred within each of these particular months, with April 26th (peak #1) witnessing the lowest R-index on record (since 1951). More than 30% of CESA experienced soil moisture anomalies larger than two standard deviations on that day (see purple shaded area in Figure 4.3a) and a total of around 100 000 km^2 was affected by record-breaking drying conditions (Figure 4.3b). When considering longer temporal scales (seasonal and annual), the amount of CESA covered by unprecedented low soil moisture increases, underlying the exceptional duration of the event. For instance, for temporal scales between 300 and 365 days, more than 700 000 km^2 (20% of the total area of CESA) witnessed record-breaking soil

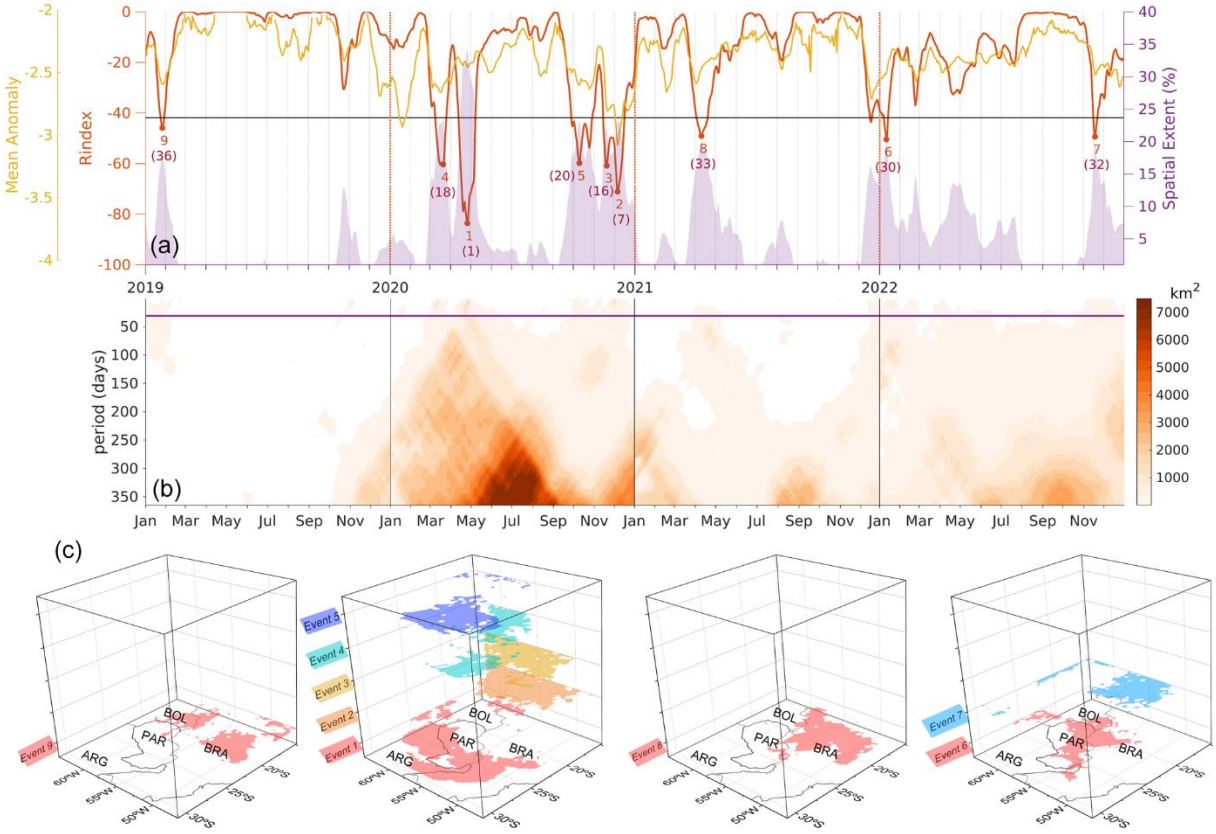

Figure 4.3 (**a**) Time series of the R-index (red line, left y-axis) and of the two sub-indexes: mean anomaly (yellow line, left y-axis) and spatial extent (lilac shade, right y-axis) for the 2019–2022 drought in CESA (for more information see the "Methods" section). The black line depicts the 2.5th percentile of the R-index considering all the analysis period from ERA5-land dataset (1951–2022). The red filled dots identify the nine most extreme peaks of low R-index levels observed during the 4-yr period. The red numbers rank the peaks according to their intensity. The ones out of brackets show the rankings only considering the R-index levels obtained during the 4-year drought period, while the numbers inside brackets consider the R-index levels for all the analysis period. (**b**) Daily temporal evolution of the spatial extend (in $10^2 km^2$) of areas within CESA experiencing record-breaking low soil moisture anomalies, computed for several time-scales by applying a running mean filter with time windows between 1-day and 365-day. (**c**) Three-dimensional framework showing the location of the grid-points within CESA that observed daily negative soil moisture anomalies higher than two standard deviations during each of the nine extreme peaks of the R-index.

dryness. Moreover, the spatial signature of the drought throughout 2020 was considerably variable (Figure 4.3c). Marked dry conditions started to be recorded in March over Pantanal and southern Brazil (see the turquoise shading in the second panel of Figure 4.3c, associated with peak #4). Later, during April, the drought signal expanded south and eastwards, towards south Brazil, north Argentina and central Paraguay as shown by the red color shadings associated with peak #1 in the middle panel of Figure 4.3c. In October and during the flash drought marked by the peak #5 (October 10th), the soil dry-out pattern moved slightly northwards affecting more the central CESA. During the last two months of 2020, when peak #3 and #2 occurred, soil dryness dominated over the northern section of CESA and Pantanal. Later, the year of 2021 started with a slight weakening of the drought signal (Figure 4.3a), however a strong amplification occurred in April with pronounced soil desiccation being recorded over Pantanal (red area in the third panel of Figure 4.3c). Finally, the year of 2022 witnessed a new intensification of the pre-established drought conditions, mainly during the 1st half of the year and the final months of November and December. The right panel in Figure 4.3c highlights that, once again, Pantanal and the northward surrounding region were the most affected areas in CESA during the occurrence of the two most extreme flash drought events recorded in 2022 (peak #6 and #7).

4.3.3 The influence of large-scale tropical and subtropical atmospheric forcing on the 2019–2022 drought

Decadal-scale variability such as the one observed when analyzing the long-term inter-annual variability of precipitation and VIMC over CESA (Figure 4.2a), is often associated with slowly varying atmospheric and/or oceanic conditions (e.g., sea surface temperature, atmospheric pressure) described by a particular large-scale atmospheric-oceanic variability mode. Figure 4.4a provides the spatial correlation between the mean annual SST's and the mean annual IVT across the northern border of CESA, which controls the amount of moisture convergence and precipitation in the region. The central and southeast tropical Pacific reveal pronounced positive and statistically significant correlations, indicating that mean annual wet conditions over CESA are associated with warmer SSTs in these areas of the Pacific Ocean and with ENSO. Statistically significant negative correlations were also observed over the equatorial Atlantic Ocean, as well as over the southwest and northwest Pacific, pointing for a potential link between CESA moisture conditions and the Pacific Decadal Oscillation (PDO). When analyzing the decadal variability of the Southern Oscillation Index (SOI) and of Oceanic

Niño Index (ONI) (see Supplementary Material), we observe that multi-year dry periods in CESA were defined by positive values of SOI and negatives levels of ONI, thus to La Niña conditions (Figure 4.4b). Moreover, a lead-lag relationship between these time series seems to be present. The correlation between these ENSO indicators and the IVT across the northern border of CESA, was high and statistically significant during the autumn, winter and spring seasons, while during summer, residual and non-statistically significant correlations were obtained (see inset table in Figure 4.4). From an annual perspective and filtering all signals with a 10-yr low pass filter, correlations reach higher levels than the ones obtained considering the non-filtered time series (see Figure 4.4 inset table). The same is observed with PDO (table S4.1). This points for a stronger link between CESA precipitation and all these Modes of variability when considering long-term decadal oscillations. Regarding the Atlantic Ocean, the variability of precipitation levels in CESA appears to be negatively correlated with the Atlantic

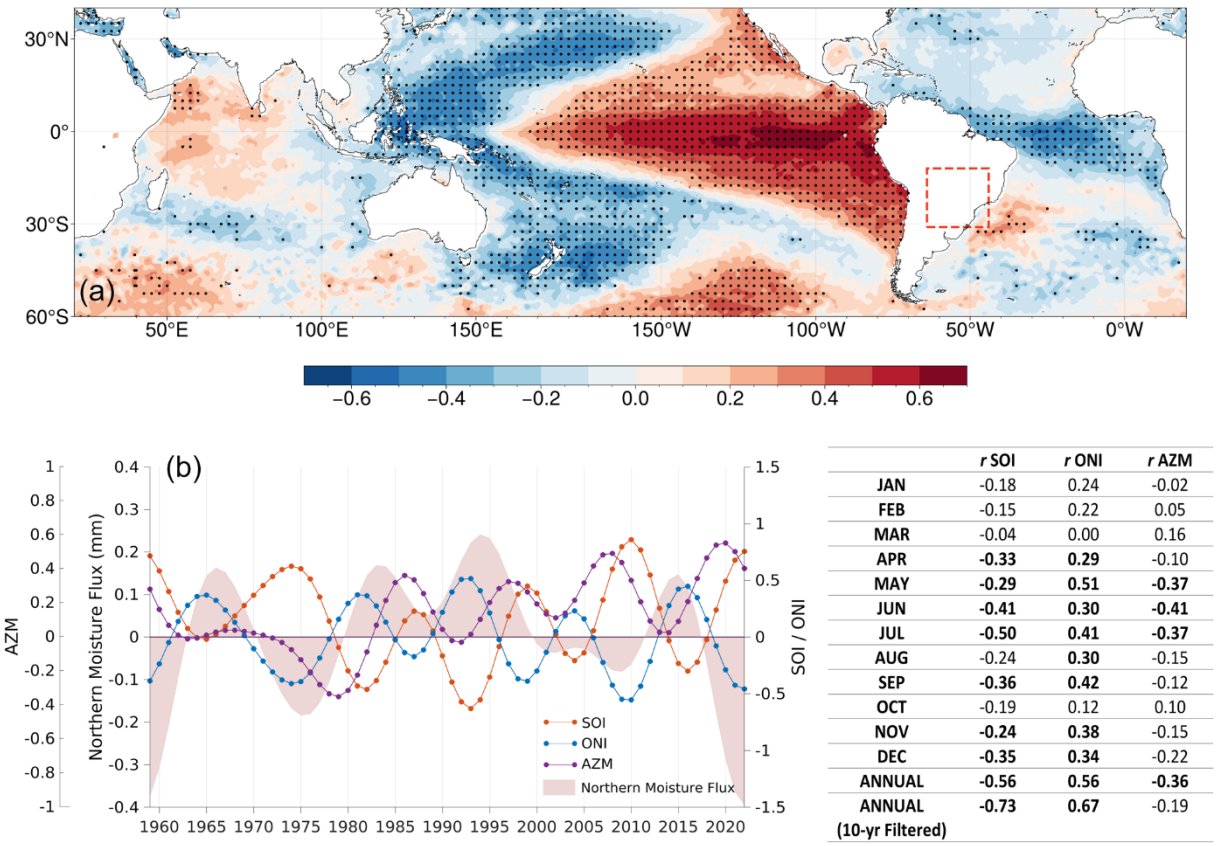

	r SOI	*r* ONI	*r* AZM
JAN	-0.18	0.24	-0.02
FEB	-0.15	0.22	0.05
MAR	-0.04	0.00	0.16
APR	**-0.33**	**0.29**	-0.10
MAY	**-0.29**	**0.51**	**-0.37**
JUN	**-0.41**	**0.30**	**-0.41**
JUL	**-0.50**	**0.41**	**-0.37**
AUG	-0.24	**0.30**	-0.15
SEP	**-0.36**	**0.42**	-0.12
OCT	-0.19	0.12	0.10
NOV	**-0.24**	**0.38**	-0.15
DEC	**-0.35**	**0.34**	-0.22
ANNUAL	**-0.56**	**0.56**	**-0.36**
ANNUAL (10-yr Filtered)	**-0.73**	**0.67**	-0.19

Figure 4.4 (**a**) Spatial distribution of Spearman's correlation coefficients between the mean annual SST and the IVT across the northern border of CESA obtained for the 1959–2022 period. (**b**) Time series from 1959 to 2022 of the mean annual anomaly levels of daily IVT across the northern border of CESA (shaded area; left y-axis), of the Atlantic Zonal Mode (purple line; left y-axis), the Southern Oscillation Index (orange line; right y-axis) and the Oceanic Niño index (blue line; right y-axis) filtered by a 10-year low pass Lanczos filter. The inset right table highlights the annual and monthly Spearman's correlation coefficients obtained between the non-filtered time series of three indexes and the northern moisture transport over CESA for the 1959–2022 period. The last row shows the correlations obtained considering the times series filtered by a 10-year low pass Lanczos filter. In bold are shown the statistically significant correlation coefficients at a 5% significant level according to the Student's two-tailed *t* test.

Zonal Mode (AZM), although this relation is, in general, less pronounced compared to the other two modes of variability in Pacific.

The spatial distribution of the observed SST anomalies during the 2019–2022 drought period shows cold SSTs in tropical central and southeast Pacific associated to enhanced low tropospheric air divergence (Figure 4.5). Such anomalous divergence pattern (see vectors in the lower panel of Figure 4.5) is a signature of above-normal subsidence as shown by the positive anomalies of the vertical velocity over central tropical Pacific and northwest SA (middle panel in Figure 4.5). The subsidence over northwest SA represents the descending branch of an eastward shifted Walker Cell (descending blue arrow in Figure 4.5), strongly connected to anomalous convergence at the top of the atmosphere, as shown by the positive anomalies of velocity potential (Figure 4.5, top panel). The corresponding ascending branch, linked with divergence at the top of the atmosphere and convection, was located in the equatorial Atlantic near northeast SA (see ascending blue arrow in Figure 4.5), supporting the low tropospheric moisture convergence patterns and the negative anomalies of E–P balance that were previously identified for this region (see Figure 4.2d). Moreover, Figure 4.5 shows that this large-scale anomalous zonal circulation was strongly connected with subtropical SA, through the establishment of an amplified meridional Hadley Cell (see purple lines in Figure 4.5) with its descending branch associated with clear sky conditions, strong diabatic and adiabatic heating rates and moisture divergence, located over CESA. Accordingly, this descending branch promoted the low tropospheric spread of large amounts of moisture from CESA towards the surrounding regions and particularly towards northeast SA, where it converged, explaining the positive anomalies of the E–P balance that were previously identified in Figure 4.2d. The three wettest years were characterized by a contrasting tropical zonal and meridional circulation, with the establishment over CESA of a Hadley cell's ascending branch associated with strong moisture convergence and supply from the Amazon basin (Figure S4.6).

In addition to this anomalous tropical circulation responsible for the long-term precipitation deficits in CESA during the 2019–2022 drought, at synoptic scales, the subtropical dynamic may also have played a key role in explaining the occurrence of the flash droughts identified by the R-index peaks. Accordingly, we computed spatial anomaly composites considering the nine most extreme R-index peaks (Figure 4.3a) and regarding several meteorological parameters (Figure 4.6). Pronounced negative soil moisture anomalies are clearly visible all over CESA (Figure 4.6a). The mid-level atmospheric circulation was defined

by the occurrence of positive 500hPa geopotential height anomalies and by exceptional warm conditions in the low troposphere, likely promoted by strong air subsidence, enhanced adiabatic and diabatic heating rates (Figure 4.6b). The occurrence of positive anomalies of the vertical integral of divergence of moisture flux (see color shading in Figure 4.6c) and the spreading out of air masses from CESA to the surrounding regions, as indicated by the anomalous low tropospheric divergent wind field (see arrows in Figure 4.6c), is evident. This points to the establishment over CESA of exceptional clear-sky conditions and strong shortwave radiation incidence at the surface that led to large evaporation rates. From a large-scale perspective and in agreement with Figure 4.5, it is possible to observe the establishment of a meridional Hadley cell (Figure 4.6d) with enhanced divergence at the top of the atmosphere over northeast SA (see the negative anomalies of potential velocity represented by the color shading in Figure 4.6d), and its descending branch over CESA. Regarding the mid-latitude atmospheric circulation, the anomalous meridional wind field at the 200 hPa level shows a clear sequence of divergence/convergence patterns in the top of the troposphere spanning from west-central south Pacific to south Atlantic (Figure 4.6e). This is a clear signature of a Rossby wave train

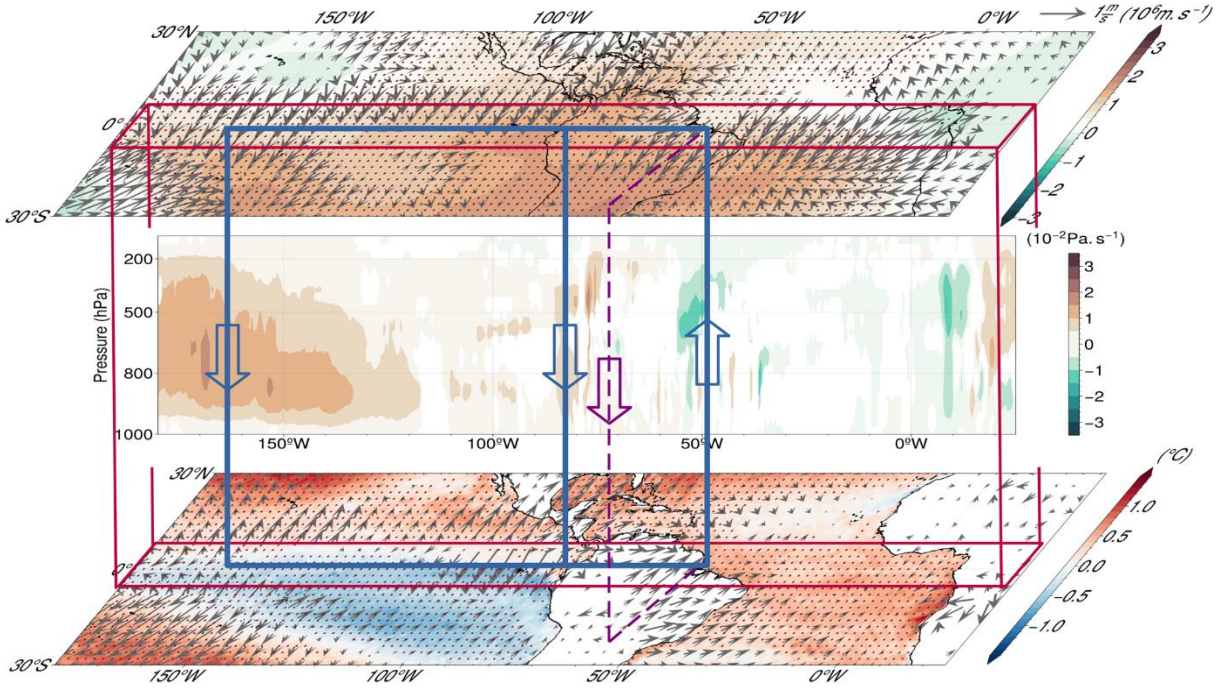

Figure 4.5 Three-dimensional schematic framework of the oceanic and atmospheric mean anomalous conditions observed during the 2019–2022 drought. The lower panel highlights the SST anomalies (color shading, °C) and the mean anomalous pattern of the low-tropospheric (850hPa) divergent wind field (vectors, $m.s^{-1}$). The middle panel shows a zonal-vertical circulation in a latitudinal band between 5°N and 5°S, with the color shading depicting the mean anomalies in vertical wind velocity ($10^{-2}Pa.s^{-1}$). Only the statistically significant anomalies (p value < 0.05) are shown according to the Student's two-tailed *t* test. The top panel illustrates the mean anomalous field of velocity potential (color shading, $10^6 m.s^{-1}$) and of the 200hPa divergent wind (vectors, $m.s^{-1}$). The anomalies were filtered using a 31-day running mean filter. Red dots and vectors shown in the top and bottom panels mark the statistically significant anomalies at a 5% level, according to the Student's two-tailed *t* test).

(wavenumber 3) embedded in a jet stream that experienced an anomalous poleward shift over southeast South Pacific, near SA (see contours in Figure 4.6e) (White et al. 2022). A large Rossby wave source region was recorded in west-central Pacific, at east and south Australia, where the Rossby wave train was formed (Figure 4.6f). At east of Australia, the Rossby wave forcing was mostly due to the advection of absolute vorticity by the divergent flow (see Figure S4.7a) and to strong convection in the Indo-Pacific warm pool, while at south of Australia only dynamic factors were involved (Figure S4.7b) which agrees with Shimizu and de Albuquerque Cavalcanti (2011). Finally, from a long-term perspective, this 4-yr drought was characterized by a clear zonal expansion of the subtropical quasi-stationary high-pressure system in the south Atlantic, with a higher-than-normal continental penetration towards SA when compared to the mean climatology. This points for a higher influence of this system in modulating precipitation deficits mainly in the eastern section of CESA (Figure S4.8). A similar zonal expansion of the south Pacific high-pressure system was observed, leading to pronounced positive mean sea level pressure anomalies in South Pacific, over 150°W and 100°W, in a latitudinal band between 35°S and 45°S (see color shading in Figure S4.8). This suggests an increased ridging activity in the region (Sousa et al. 2018a). Consequently, the mean position of the subtropical Southern Hemisphere jet stream suffered a poleward shift over southeast south Pacific, near SA, reducing the passage of cyclones and frontal systems over the southernmost regions of CESA.

4.4 Discussion and Conclusions

Despite the outstanding amplitude and length of the 2019–2022 drought, it is paramount to stress that it occurred within the context of a prolonged drying trend observed over the past three decades in CESA, that resulted from a joint contribution of natural decadal variability in precipitation levels and increasing temperatures. The observed decadal variability in precipitation was found to be mainly controlled by ENSO, with La Niña events, such as the recent one extending from 2020 to 2022 (NASA 2022), being associated to precipitation deficits over CESA. A lead-lag relationship between ENSO indicators and CESA precipitation appears to be present (Figure 4.4b). However, there is a weak consistency of the leading and lagging time series throughout the analysis period, which motivates further investigation for a better understating. An association between PDO and precipitation in CESA was also found, particularly when considering decadal oscillations (Table S4.1 and Figure S4.9). Previous studies have shown that PDO influences El Niño teleconnections over South America

particularly during the warm season. According to Kayano and Andreoli (2007), rainfall anomalies over SA are enhanced when a negative (positive) phase of the PDO concurs with La Niña (El Niño) conditions in a situation similar to the one during the 2019–2022 period (Figure S4.9). The observed negative SST anomalies in eastern tropical Pacific were found to promote large-scale disturbances in the location and intensity of the Walker cell modulating the

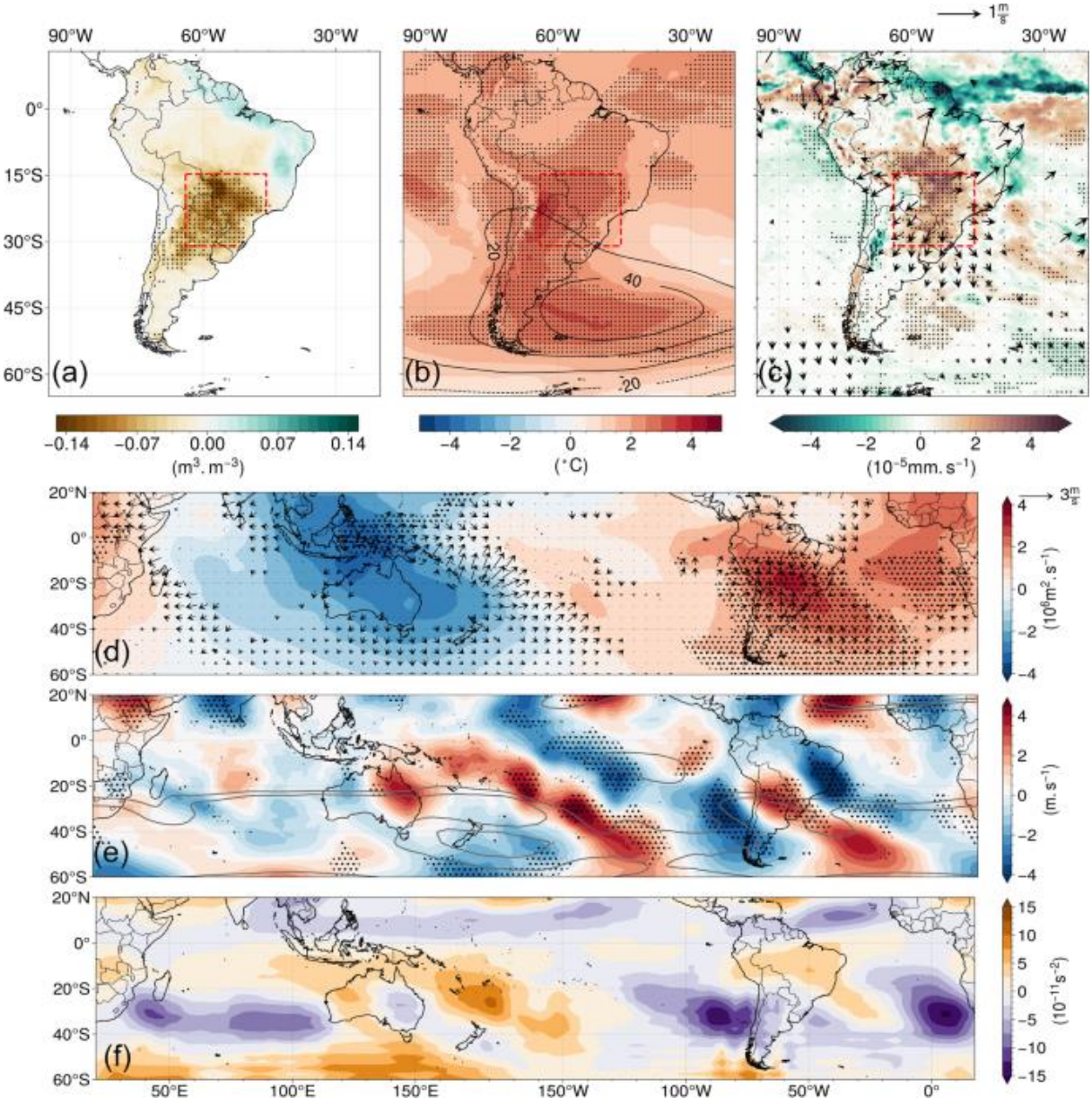

Figure 4.6 Spatial distribution of composite anomalies and mean observed values during the days that recorded the nine lowest R-index peaks (see Fig. 4.3a) of several land and meteorological parameters: (**a**) Anomalies of soil moisture (color shading, m^3/m^3); (**b**) Anomalies of the 500hPa geopotential height (contours, gpm) and of the 850hPa temperature (color shading, °C); (**c**) Anomalies of the Vertical Integral of divergence of moisture flux (color shading, $10^{-5} mm.s^{-1}$) and of the divergent wind field at the 850hPa level (vectors, $m.s^{-1}$); (**d**) Anomalies of the velocity potential (color shading, $10^6 m.s^{-1}$) and of divergent wind field at the 200hPa level (vector, $m.s^{-1}$); (**e**) Anomalies of the 200hPa meridional wind (color shading, $m.s^{-1}$). The gray solid lines show the mean observed 200hPa zonal wind pattern (contour levels: 25, 35, 45 $m.s^{-1}$). (**f**) Rossby wave source (color shading, $10^{-11} s^{-2}$). The anomalies and the mean observed values were filtered using a 31-day running mean filter. Black dots and vectors highlight the respective statistically significant anomalies at a 5% level according to the student's two-tailed *t* test.

southwards moisture transport from the Amazon and the water vapor convergence over SA. Disturbances in these two hydrological processes are reflected in the amount of precipitation over CESA (Drumond et al. 2014; Zanin and Satyamurty 2020; Chug et al. 2022). This agrees with previous studies that demonstrated an influence of La Niña conditions in precipitation over SA through a similar tropical pathway (Sasaki et al. 2015; Cai et al. 2020). Our study adds another layer to this known tropical teleconnection by showing how the anomalous Walker circulation trigger a secondary meridional circulation and strong subsidence over CESA.

On the other hand, deforestation has been associated to less moisture of Amazonian origin and to precipitation reductions in non-deforested parts of the western Amazon and in regions further downstream, mainly CESA (Boers et al. 2017; Eiras-Barca et al. 2020). Therefore, recent deforestation may have enhanced the impact of La Niña on precipitation deficits over the last two decades in CESA, paving the way for the outstanding 2019–2022 drought. Soil moisture anomalies during this 4-yr period were defined by a large spatiotemporal variability. Flash droughts in 2020 affected multiple regions such as Pantanal, Bolivia, Paraguay and North Argentina, and led to large areas covered by record-breaking soil moisture anomalies (~100.000 km^2) and warm temperatures fueled by strong soil moisture–temperature coupling (Libonati et al. 2022a). Such severe drought conditions can cause devastating losses in agriculture and livestock production, depletion of water resources, reduction of air quality and exacerbated wildfire risk (Otkin et al. 2018; Christian et al. 2020). The Pantanal's catastrophic wildfires recorded during the spring months of October and November 2020 clearly expose this link (Libonati et al. 2020, 2022a; Geirinhas et al. 2021). In fact, the most severe drought conditions, associated with record-breaking soil desiccation, were observed during autumn and spring in 2019–2022 (Figure 4.3a), hence during the months before and after winter, when climatological soil water content in CESA reaches the lowest levels (Figure S4.10).

To summarize the tropical and mid-latitude mechanisms mentioned in the previous sections we propose a conceptual scheme (Figure 4.7) that aims to capture the coupled large-scale tropical and subtropical atmospheric dynamics responsible for the historically unprecedented soil desiccation in CESA during the 2019–2022 drought. Enhanced surface air convergence over northeast SA and tropical Atlantic Ocean, linked to negative SST anomalies in tropical Pacific and to an anomalous ascending branch of an eastward shifted Walker Cell, was responsible for precipitation deficits and large evaporation rates in CESA via two distinct processes. First, enhanced deep convection in northern Brazil and equatorial Atlantic led to a

decrease in this region of moisture available to be advected and a weakening of the northeast trade winds, causing a reduction of the SALLJ activity (Marengo et al. 2002). Secondly, this eastward shifted Walker Cell induced a meridional Hadley cell and enhanced subsidence over CESA, resulting in the suppression of moisture convergence and precipitation. The SALLJ is defined as a low tropospheric northerly jet along the eastern slopes of the Andes responsible for the transport of large amounts of moisture from the Amazon to the subtropics (Marengo et al. 2002; Oliveira et al. 2018; Montini et al. 2019). In agreement with our results, previous studies have shown that at interannual timescales, this jet is strongly modulated by ENSO, and La Niña conditions are associated with weaker and less frequent jet days (Drumond et al. 2014; Montini et al. 2019). Here we demonstrated that negative precipitation anomalies in CESA were also found to be related to AZM and so to positive SST anomalies in tropical Atlantic. Although we did not explore in detail this association, our results corroborate Barreiro and Tippmann (2008) showing that positive phases of the AZM induce equatorial westerlies, leading to a weakening of the SALLJ activity and therefore to long-term precipitation deficits over CESA. During the flash drought episodes, when soil desiccation reached its maximum intensity and spatial extent, a Rossby wave pattern, reinforced the subsidence over CESA and the already established descending branch of the meridional Hadley Cell. This compound mechanism connecting the tropical and subtropical anomalous dynamics resulted in the establishment over CESA of a quasi-stationary anticyclonic circulation known to enhance evaporation and reduce soil moisture levels (Geirinhas et al. 2022). This Rossby wave train was forced at east and south of Australia in regions known to bring together the ideal conditions for the development of such atmospheric patterns (Shimizu and de Albuquerque Cavalcanti 2011; Coelho et al. 2016b; Rodrigues et al. 2019; Gelbrecht et al. 2023). These Rossby wave source regions were closely linked to strong convection in the western tropical Pacific and to local warm SST's, typically associated with La Niña episodes (Figure 4.7). Our results support previous works that had shown the capability of ENSO to modulate precipitation over CESA through such an extratropical pathway, known as the Pacific–South American pattern (Silva and Ambrizzi 2006; Cai et al. 2020; Gelbrecht et al. 2023). Particular phases of the MJO were also linked to these Rossby Wave trains and so to warm and dry extremes in SA (Grimm 2019; Rodrigues et al. 2019). MJO and ENSO are both influenced by SST anomalies in the western Pacific although both modes are defined by distinct times scales. ENSO, as a key slowly-varying "external" forcing, regulates the background mean state (i.e., the lower-tropospheric winds and humidity) capable to modulate MJO, which is the dominant mode of tropical intraseasonal variability on

which these weekly to monthly Rossby Wave Patterns express their main temporal signature (Deng and Li 2016; Wei and Ren 2022). Moreover, the trajectory of these extratropical wave structures as well as the passage of transient systems particularly over the southernmost regions of CESA is influenced by the southern Hemisphere westerlies and by the subtropical jet stream. Although no relevant correlations were obtained between the Southern Annular Mode and the tropical moisture inflow towards CESA (Table S4.1), this mode of variability in the Southern Hemisphere might influence the westerlies and the positioning and intensity of the subtropical jet stream current, leading to precipitation changes in the more extratropical areas of CESA (Swart et al. 2015). In this context, we have shown that during 2019–2022 there was a clear zonal expansion of the South Pacific high-pressure system associated to a poleward shift of the jet stream (Figure S4.8). A similar change in the trajectory of the jet stream has been associated to positive SAM phases such as the one that has been characterizing the last two decades (Figure S4.9) (Thompson et al. 2011; Swart et al. 2015).

The findings, summarized in a conceptual model in Figure 4.7, highlight the effect of internal variability in the occurrence of climate extremes, providing a guideline to characterize

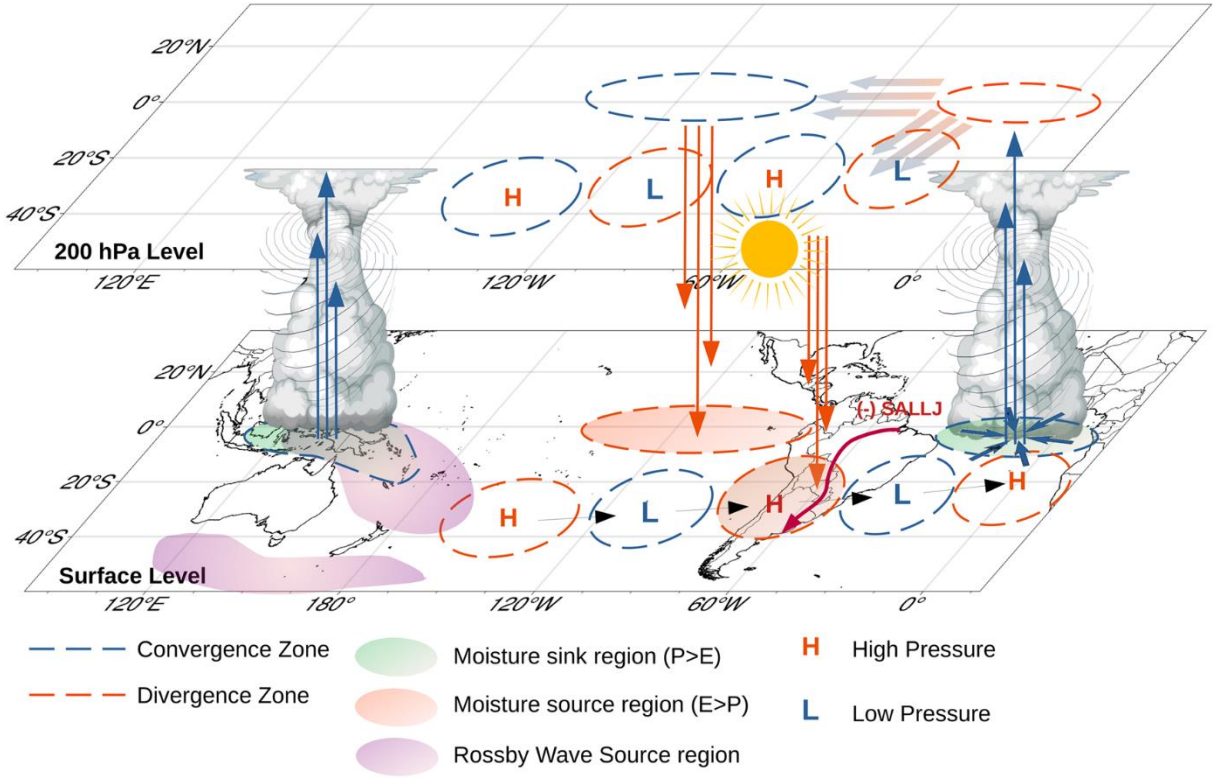

Figure 4.7 Conceptual model showing in an illustrative and schematic framework the coupled tropical and subtropical atmospheric forcing responsible for the 2019–2022 drought and for the record-breaking soil desiccation.

other historical drought events and to predict the occurrence of future extreme dry spells together with climate models capable to simulate such dynamical processes in tropical and subtropical regions. Moreover, previous studies have identified CESA as a region with strong soil moisture–temperature and soil moisture–precipitation feedbacks (Ruscica et al. 2014, 2015). In fact, recent hot extremes (e.g., 2020 in Pantanal and 2013/2014 in Southeast Brazil) resulted from a joint contribution of large-scale atmospheric circulation anomalies and a strong soil moisture imbalance (Geirinhas et al. 2022; Libonati et al. 2022a). Libonati et al. (2022a) demonstrated how CESA was affected during 2020 by a strong soil moisture–temperature coupling regime and how the co-occurring conditions of pronounced soil desiccation and shortwave radiation incidence led to an increase of the sensible heat flux between surface and atmosphere. An amplification of temperature extremes and of the drought conditions, initially triggered by the atmospheric dynamics highlighted here, resulted in exceptional flammability conditions. However, it is important to stress that Libonati et al. (2022a) only explored a particular section of the total area in SA affected by the 2019–2022 drought (i.e., Pantanal). Therefore, further studies employing an extended spatial analysis and addressing more closely the link between the multiple atmospheric forcing mechanisms shown here and the amplification of the drought conditions through these land–atmosphere feedbacks, appear necessary.

Future climate change projections regarding land–atmosphere interactions in regions such as CESA, where soil moisture is a driving factor, are shrouded in large uncertainty (Ruscica et al. 2015; Bieri et al. 2021). Recent studies suggest that CESA will remain a land–atmosphere coupling hotspot, with some regions (namely the Pantanal and Brazilian Highlands) witnessing a change from energy-limited to water-limited regimes, and a higher concurrence of dry and hot spells (Ruscica et al. 2016; Olmo et al. 2022). Moreover, these results highlight how internal variability represents a key factor for the occurrence of long-term dry and wet periods in SA, stressing the need of climate models to better simulated the atmospheric dynamics associated to this climate variability. This is particularly relevant when considering precipitation projections at a local scale for which internal climate variability is the dominant source of uncertainty (Fatichi et al. 2016; Peleg et al. 2019). Some studies have shown disparities between state-of-the-art climate models and observations regarding the effect of global warming in the tropical Pacific dynamics and particularly in the Walker Circulation (Seager et al. 2019; Lee et al. 2022). This points for a critical failure of models to correctly modulate key features of ENSO and other atmospheric dynamics linked to climate variability that, as we have shown here, influences

long-term changes in precipitation and evaporation in South America, putting into question the known projections of these variables for the continent. Accordingly, this study provides robust guidelines to better predict the occurrence of future dry extremes, stressing the urgent need to improve the representation of the dynamical processes associated with daily-to-multiyear time-scales in climate models. We believe these findings will be of interest to the international community in the context of natural hazards characterization and prediction under a climate change scenario.

Supplementary Material

Supplementary Methods

There are many indexes to measure and monitor ENSO (Anthony Barnston 2015), due to the complexity of the atmospheric and oceanic coupled mechanism evolved. Overall, the most used indices can be separated into two main groups: the air pressure indexes and the sea surface temperature (SST) indexes. Regarding the air pressure indexes the most commonly used metric is the so-called Southern Oscillation Index (SOI), which is a standardized index based on the differences between the sea level pressure at Tahiti (central South Pacific) and at Darwin (north Australia). During El Niño (La Niña) the SOI is negative (positive). Regarding the SST indexes there is a wide variety of metrics that consider different sections of the equatorial Pacific to measure SST anomalies (e.g., Niño1, Niño2, Niño3, Niño4). However, the most representative region is the so-called the Niño3.4 (Bamston et al. 1997), that corresponds to the area between Niño3 and Niño4. The Oceanic Niño index (ONI) is the official ENSO indicator for NOAA and considers the SST anomalies in Niño 3.4, defining El Niño (La Niña) episodes when SST anomalies are higher (lower) than 0.5ºC (-0.5ºC) in this particular region. The Pacific Decadal Oscillation (PDO) is defined by the leading Empirical Orthogonal Function (EOF) of the SST anomalies in the North Pacific basin, and so, positive (negative) values of the PDO index correspond to negative (positive) SST anomalies in central and western North Pacific and positive (negative) SST anomalies in the eastern North Pacific (Mantua et al. 1997).

Similarly, to ENSO, the Atlantic Zonal Mode (AZM) also known as Atlantic Niño is a mode of natural variability occurring in the equatorial Atlantic. The AZM index was computed as the domain averages SST anomaly over the equatorial Atlantic Ocean (3°N– 3°S, 0–20°W) (Nnamchi et al. 2015). The Southern Annular Mode (SAM) was evaluated using the Marshall

Southern Annular Mode which is a station-based index based on the zonal pressure difference between the latitudes of 45ºS and 65ºS (Marshall 2003). Thus, positive values of SAM are linked to above than normal pressure levels over Antarctica and vice-versa.

The estimation of the generalized linear models with two segmented relationships in the linear predictor presented in Figure 4.1, was obtained using the rpackage "segmented" (https://cran.r-project.org/web/packages/segmented/segmented.pdf). The package estimates the slopes and breakpoints along with standard errors. The algorithm corresponds to an iterative procedure described in Muggeo (2003). Hypothesis testing (about the existence of the breakpoint) and confidence intervals are performed via appropriate methods and functions (Muggeo 2016, 2017).

Supplementary Figures

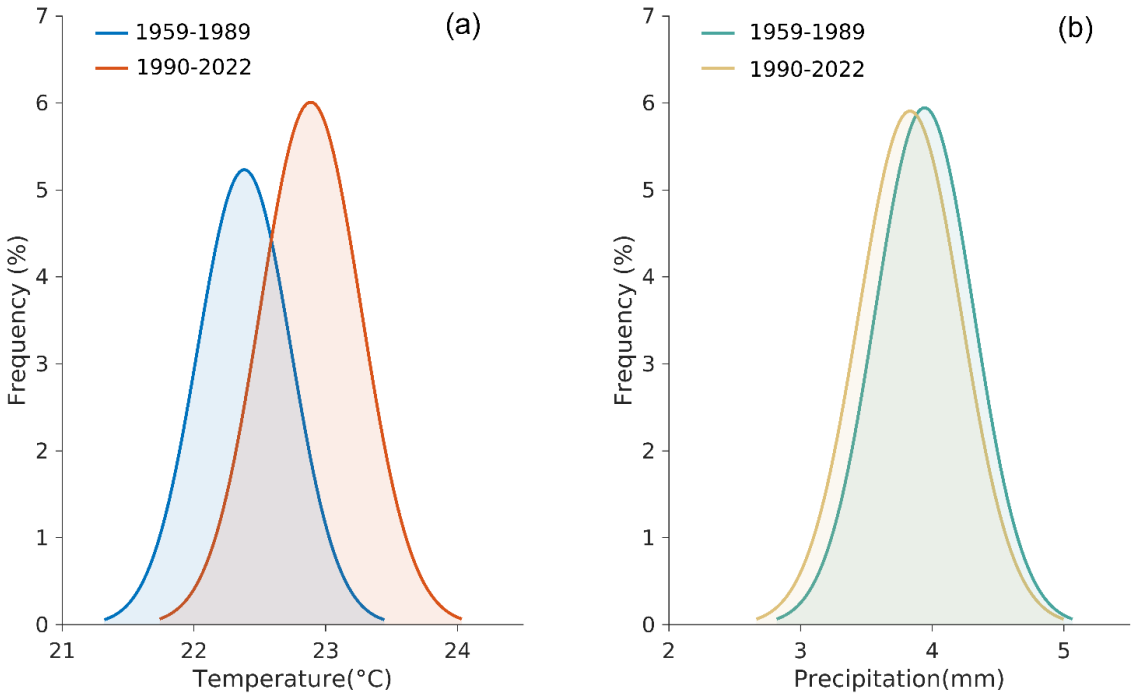

Figure S4.1 Probability density functions assuming a normal fit for the mean annual temperature (**a**) and precipitation (**b**) levels spatially averaged over CESA, over the two periods of: 1959-1989 and 1990-2022.

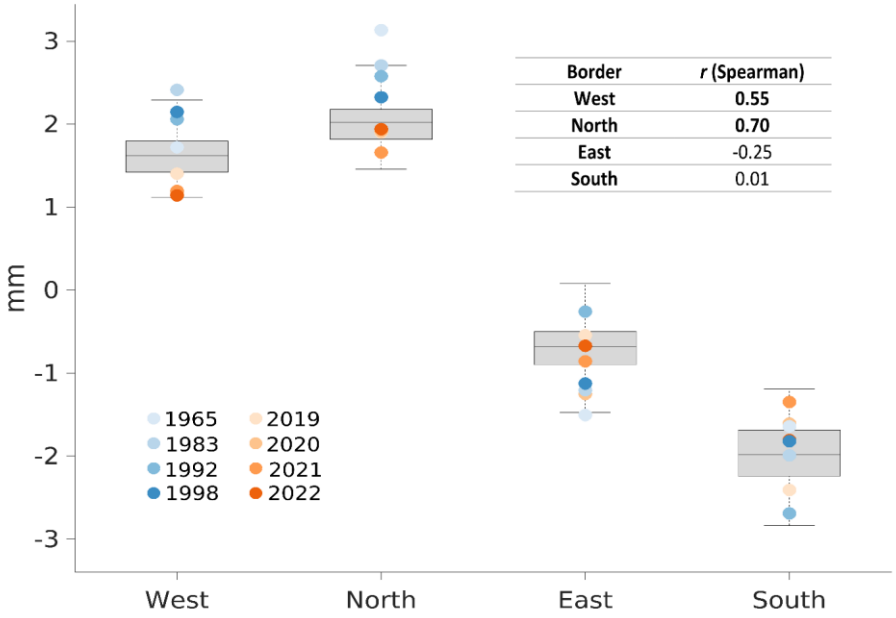

Figure S4.2 Boxplots of mean annual values of daily vertically integrated water vapor transport (IVT, mm) across the four CESA borders shown in Figure 4.1a. The boxes correspond to the interquartile range and whiskers extend to the most extreme data points not considered as outliers. The dots highlight the observed mean value for a particular year (see left-bottom legend). The inset table shows the Spearman's correlation coefficients obtained for the 1959–2022 period between the mean annual VIMC over SESA and the mean annual IVT across the four CESA borders. In bold are shown the statistically significant correlation coefficients at a 5% significant level according to the student's two-tailed *t* test.

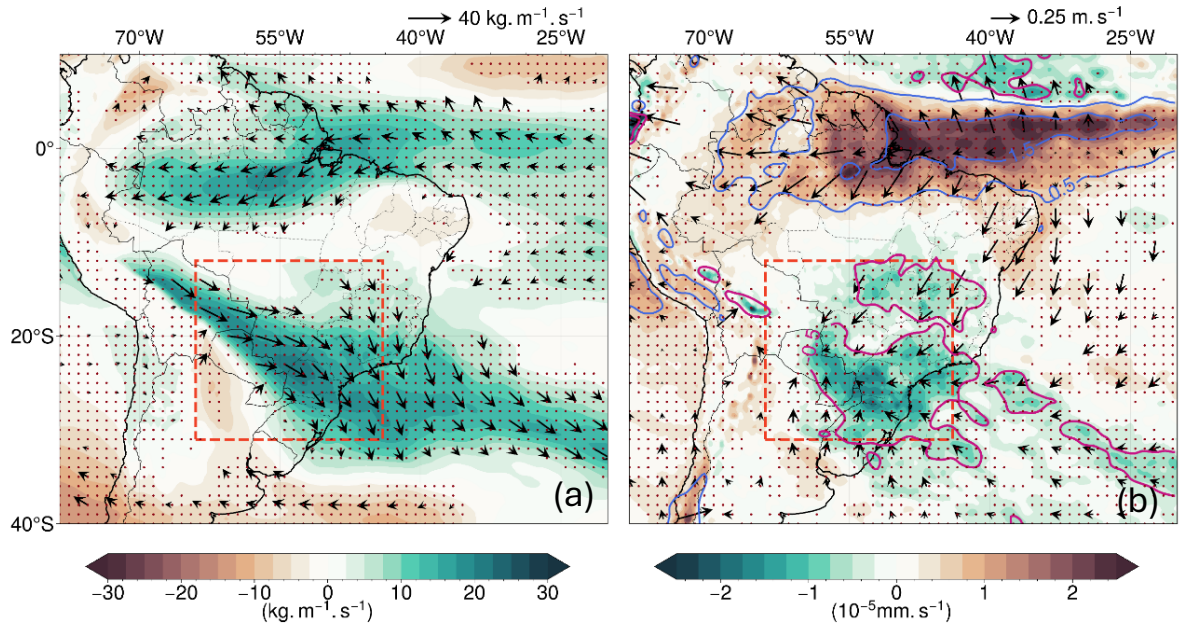

Figure S4.3 (**a**) Anomaly composites (regarding the 1981–2010 climatology) obtained considering the mean observed conditions during the wet years (1965, 1983, 1992, 1998, see Figure 4.2a) of the IVT intensity (color shading, $kg.m^{-1}.s^{-1}$) and direction (vector, only the statistically significant anomalies at a 5% level are shown). (**b**) Anomaly composites for the wet years of the Vertical Integral of divergence of moisture flux (color shading, $mm.s^{-1}$) and of the non-rotational (i.e., divergent) wind field at the 850hPa level (vectors, $m.s^{-1}$). Contours depict anomalies of the daily evaporation minus precipitation balance. Red dots in **b** and **c** mark the statistically significant anomalies at a 5% level. *p* values were computed using the student's two-tailed *t* test.

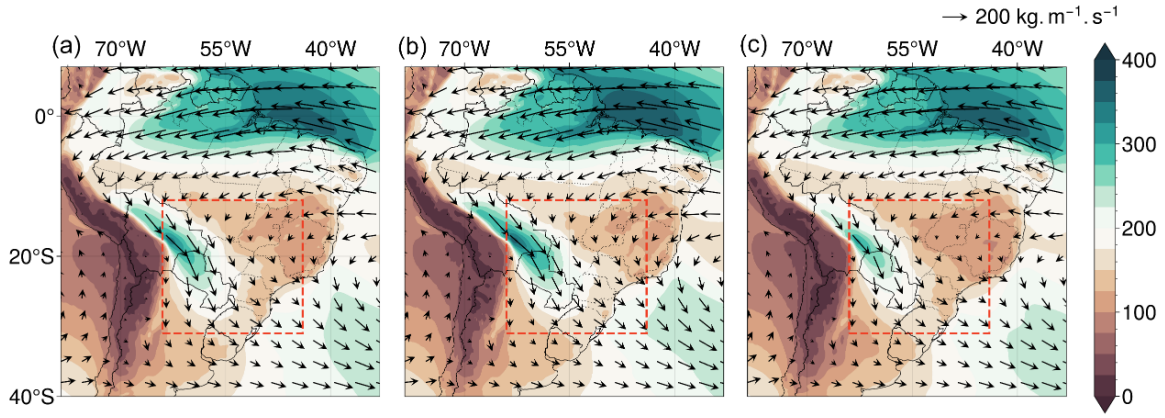

Figure S4.4 (**a**) Annual Climatological field (1981 -2010 base period) of the Vertically Integrated Water Vapor transport intensity (color shading, $kg.m^{-1}.s^{-1}$) and direction (vectors) over South America. (**b**) and (**c**) same in (**a**) but for the mean observed composites during the wet years of 1965, 1983, 1992 and 1998, and during the dry years of 2019, 2020, 2021 and 2022, respectively.

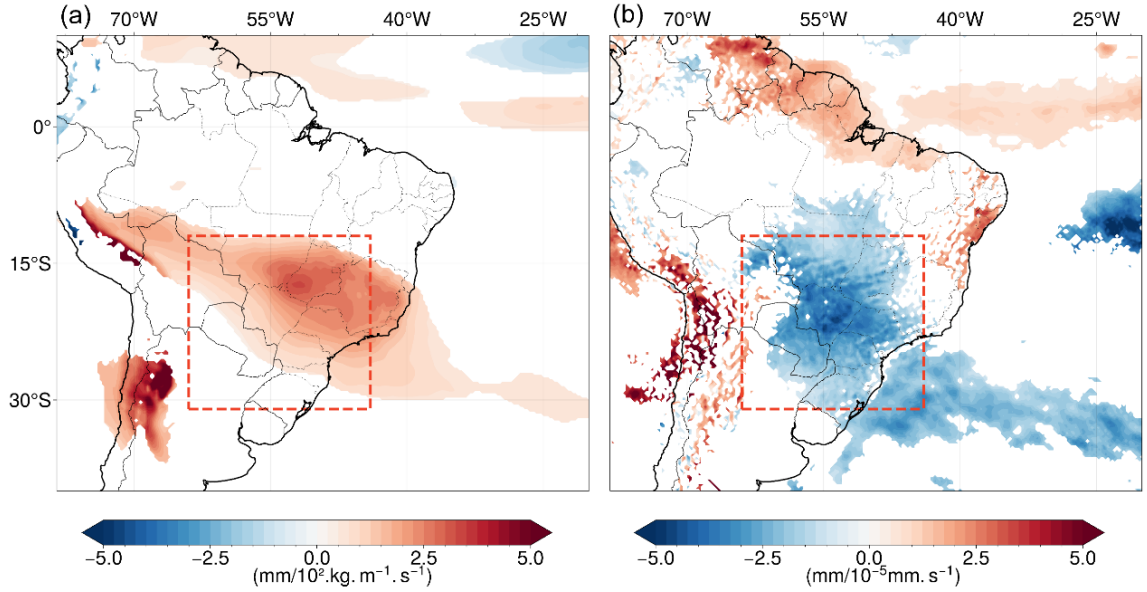

Figure S4.5 Regression maps of the IVT (**a**) and of vertically integrated divergence of moisture flux (**b**) against the CESA interannual time series of accumulated precipitation for the 1959-2022 period. Only the statistically significant regression coefficients at a 5% level are represented.

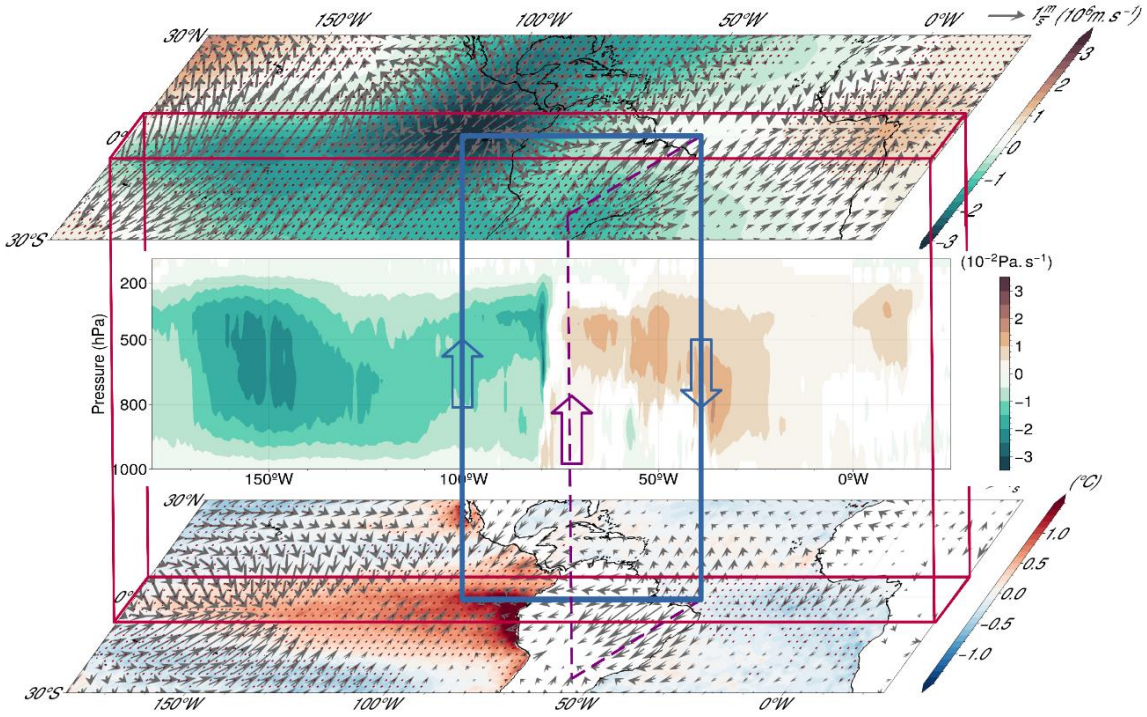

Figure S4.6 Three-dimensional **s**chematic framework of the oceanic and atmospheric mean anomalous conditions observed during the three wettest years (see Figure 4.2a). The lower panel highlights the SST anomalies (color shading, ºC) and the mean anomalous pattern of the low-tropospheric (850hPa) divergent wind field (vectors, $m.s^{-1}$). The middle panel shows a zonal-vertical circulation in a latitudinal band between 5ºN and 5ºS, with the color shading depicting the mean anomalies of vertical velocity ($10^{-2}Pa.s^{-1}$). Only the statistically significant anomalies ($p < 0.05$) are shown. The top panel illustrates the mean anomalous field of velocity potential (color shading, $10^{6}m.s^{-1}$) and of the 200hPa divergent wind (vectors, $m.s^{-1}$). The anomalies were filtered using a 31-day running mean filter. Red dots and vectors shown in the top and bottom panels mark the statistically significant anomalies. *p* values were computed using the student's two-tailed *t* test.

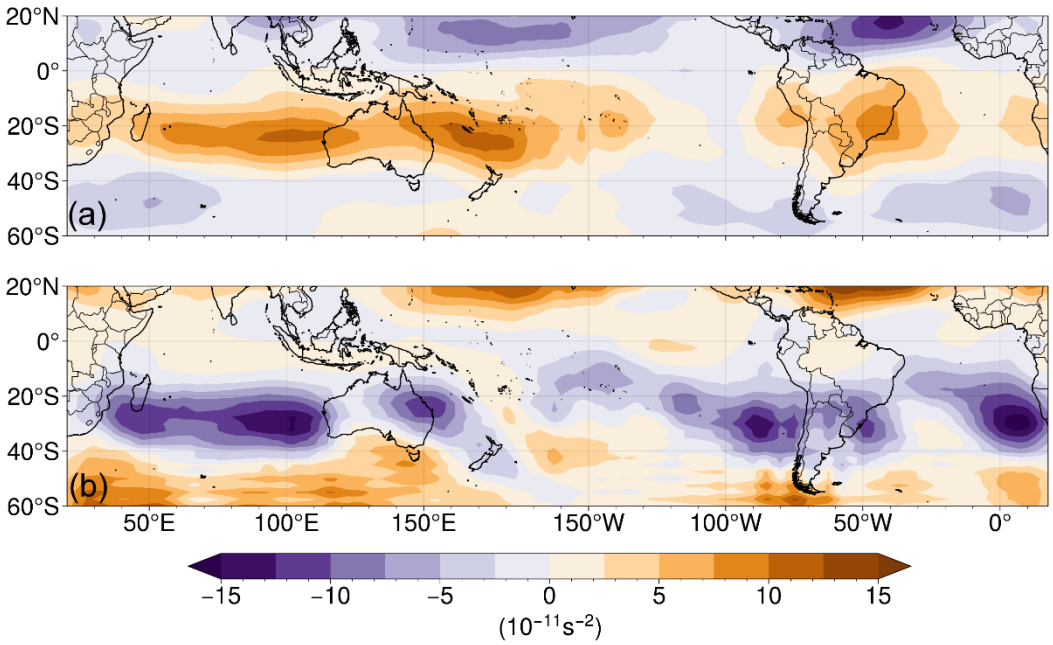

Figure S4.7 Spatial distribution of the mean observed Rossby wave source terms during the nine identified R-index peaks: the advection of absolute vorticity by the divergent flow (**a**) and the vortex stretching (**b**).

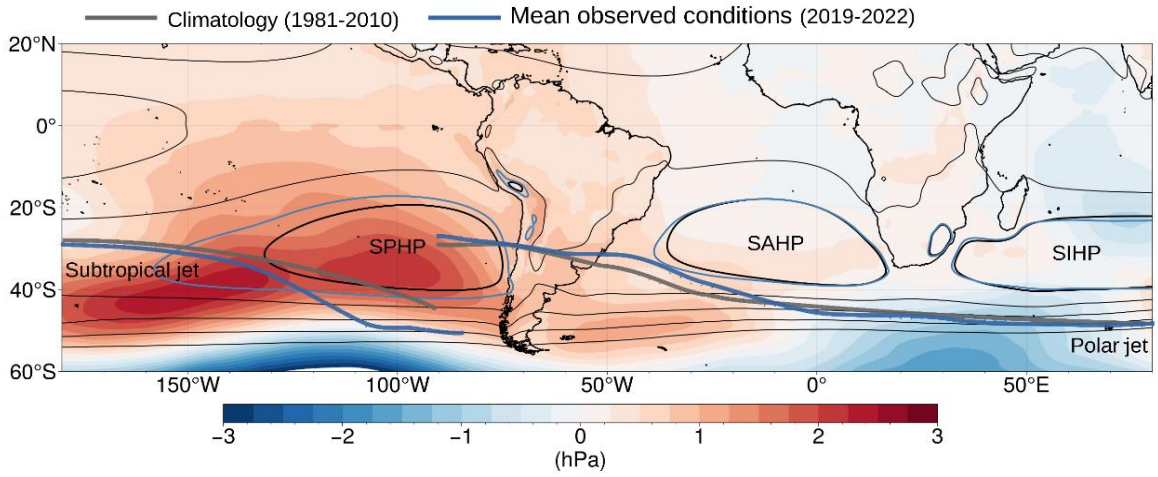

Figure S4.8 Climatology of the mean sea level pressure for the 1981-2010 period (black thin lines, 4 hPa interval) with the mean central position of the Southern Pacific high pressure (SPHP), Southern Atlantic high pressure (SAHP) and the Southern Indian high pressure (SIHP) and mean extension (considering the 1018 hPa isobar). The mean sea level pressure anomalies during the 2019-2022 drought period are also depicted (shaded areas). The mean position of the 250 hPa subtropical and polar jet-streams as well as the extension of the SPHP, the SAHP and the SIHP are marked by the thicker lines, with black and blue representing the climatological and mean observed condition during the 2019-2022 period, respectively.

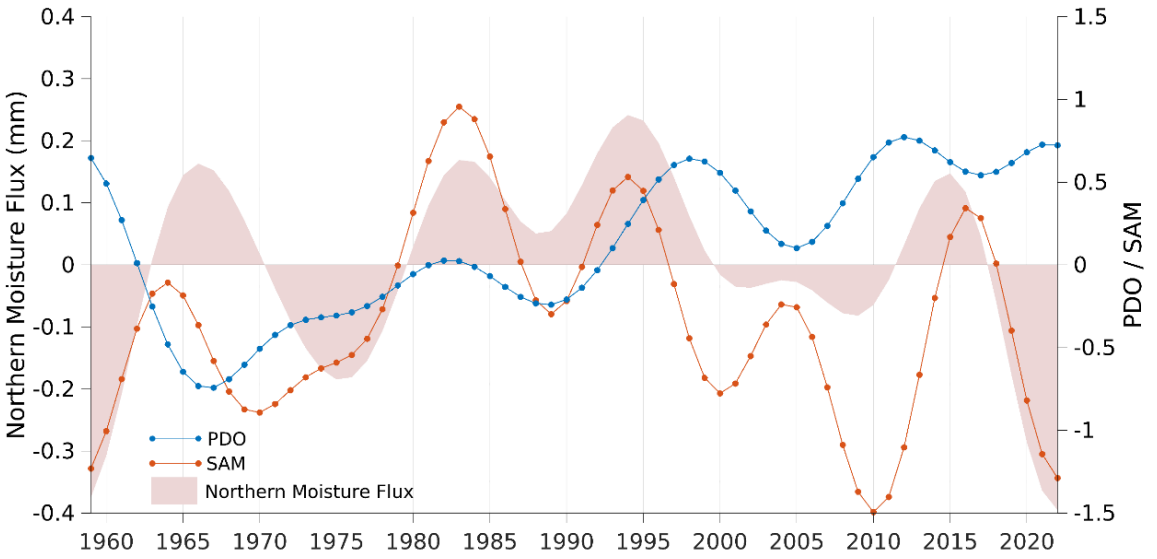

Figure S4.9 Time series from 1959 to 2022 of the mean annual anomaly levels of daily IVT across the northern border of CESA (shaded area; left y-axis), of the Pacific Decadal Mode - PDO (blue line; right y-axis) and of Southern Annular Mode - SAM (orange line; right y-axis) filtered by a 10-year low pass Lanczos filter.

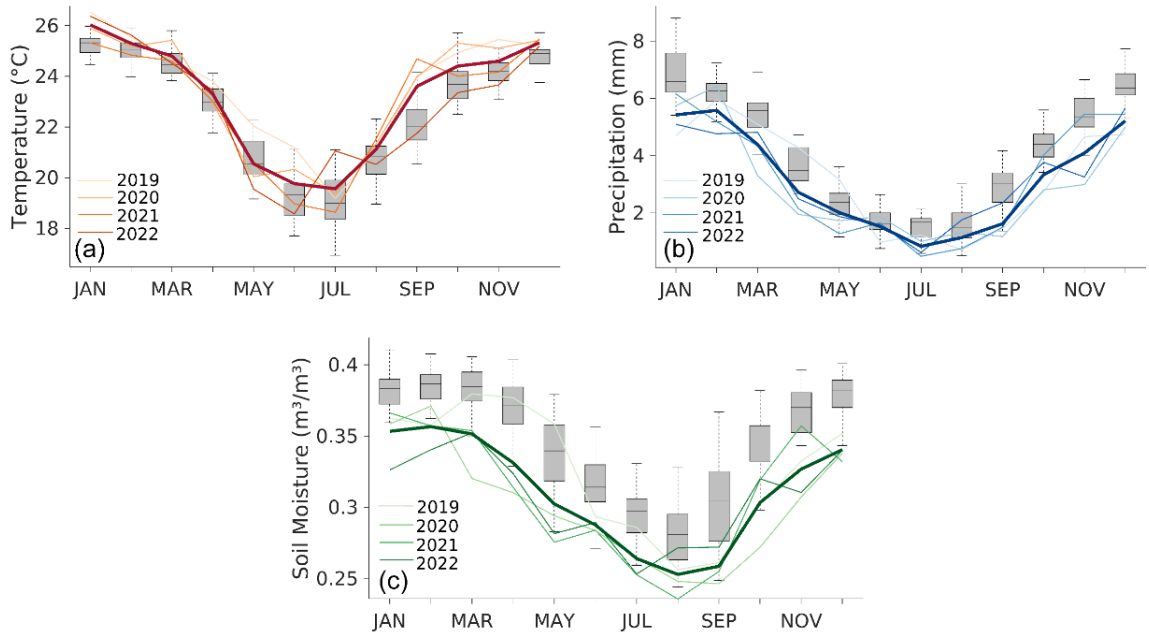

Figure S4.10 Intraseasonal variability for CESA of temperature (**a**), precipitation (**b**) and soil moisture (**c**) with boxplots showing the monthly climatologies (1981-2010 base period). The lines show the observed monthly values during each of the four considered years (see the bottom left legends). The corresponding means observed during the 2019-2022 drought years are depicted by the bold lines.

Table S4.1 Annual and monthly Spearman's correlation coefficients obtained between the two indexes (PDO and SAM) and the northern moisture transport over CESA for the 1959–2022 period. In bold are shown the statistically significant correlation coefficient at a 5% significant level, according to the student's two-tailed *t* test. The monthly correlations were obtained considering the non-filtered time series.

	***r* PDO**	***r* SAM**
JAN	-0.06	-0.13
FEB	0.05	**-0.34**
MAR	0.08	**-0.27**
APR	0.24	0.02
MAY	**0.37**	**-0.28**
JUN	0.18	0.06
JUL	**0.29**	0.06
AUG	0.18	-0.19
SEP	**0.29**	-0.11
OCT	0.03	-0.23
NOV	0.20	-0.18
DEC	0.22	-0.15
ANNUAL	**0.37**	0.13
ANNUAL (10-yr filtered)	**0.67**	**-0.25**

Chapter 5

The influence of soil moisture–temperature coupling on compound drought and heatwave conditions in South America: historical and future perspectives

Introductory Note

The analysis presented in this chapter sheds light on a relevant research topic, making use of a novel methodology and presenting important findings. The authors are engaged in concluding the work, aiming to prepare a manuscript for submission in a high impact journal.

Authors

João L. Geirinhas[1], Diego G. Miralles[2,] Ana Russo[1], Renata Libonati[3,1], Daniela C. A. Lima[1], Ricardo M. Trigo[1,3]

[1] *Universidade de Lisboa, Faculdade de Ciências, Instituto Dom Luiz (IDL), 1749-016 Lisboa, Portugal*

[2] *Hydro-Climate Extremes Lab (H-CEL), Ghent University, Ghent, Belgium.*

[3] *Departamento de Meteorologia, Universidade Federal do Rio de Janeiro, Rio de Janeiro, Brazil*

João Lucas Geirinhas contributions: *conceptualization of the study; preparation of the data; computation, analysis and interpretation of the results; production of all the figures and coordination of the writing process.*

Abstract

The global warming trends observed in the recent decades have been leading to an intensification of the Earth's water cycle and to widespread perturbations in both the thermodynamics and dynamics of the atmosphere. Hence, significant changes in temperature, precipitation and evaporation are foreseen, triggering a higher soil moisture variability and a stronger influence of land surface conditions in the portioning of surface energy and, ultimately, in temperature variability. Together, these changes are expected to promote an increase in the joint occurrence of extreme hot and dry episodes. This study aims to evaluate the degree to which future changes in the occurrence of CDHW episodes in SA, may be determined by perturbations in the coupling between soil moisture and temperature, using a robust multi-variable weighted ensemble based on CORDEX-CORE runs. Results show that an overall increment of these compound conditions is expected over most of the continent, even when the effect of the global warming trends is disregarded. A future strengthening of the soil moisture–temperature coupling stands as a valid candidate to explain such enhancement, particularly over the central SA, in an area shared by the southernmost parts of the Amazon basin and the Brazilian's Cerrado biome. Over other regions such as south SA, the future increase in the covariance between temperature and soil moisture will likely be explained by other pure atmospheric processes (e.g., strong temperature advection, enhanced shortwave radiative heating, lack of moisture advection and convergence). These results provide new important clues on how processes other than the increasing trends in temperature may affect CDHWs in SA, casting light into a relatively unexplored topic within the CDHW problematic.

5. The influence of soil moisture–temperature coupling on compound drought and heatwave conditions in South America: historical and future perspectives

5.1 Introduction

Anthropogenic forcing has been responsible for a global warming trend leading to surface temperatures 1.1ºC higher during the 2011–2020 period compared to the 1850–1900 period (IPCC 2023). This forcing has caused widespread and rapid changes in both the thermodynamics and dynamics of the atmosphere, leading to the intensification of Earth's water cycle (Allan et al. 2020; Chagas et al. 2022; Ficklin et al. 2022). Hence, climate extremes such as heatwaves and droughts have become more frequent, intense, longer-lasting and widespread, exhibiting a closer spatial and temporal relation with each other (Hao et al. 2018a; Geirinhas et al. 2021; Mukherjee and Mishra 2021). Recently, it has been demonstrated that compound drought and heatwave (CDHW) events, similarly to other compound extremes, lead to more devastating impacts when compared to single episodes (Zscheischler and Seneviratne 2017; Zscheischler et al. 2018).

In some regions, the increase in frequency and magnitude of CDHW extremes is explained by processes other than human-caused warming trends (Bevacqua et al. 2022; Zhang et al. 2022a). Additional physical processes that are also modulated by climate change and that are associated with local and large-scale atmospheric dynamics (Berg et al. 2015; King et al. 2018; Kornhuber et al. 2019; Schumacher et al. 2022a), as well as to other non-linear mechanisms such as land–atmosphere feedbacks (King 2019; Miralles et al. 2019; Dirmeyer et al. 2021; Schumacher et al. 2022b), may determine changes in the occurrence of hot and dry extremes. Some of these land–atmosphere processes involve the physical coupling between temperature and moisture, and, ultimately, influence the joint occurrence of hot and dry conditions, impacting terrestrial ecosystems, economy and society (Berg et al. 2015; Lesk et al. 2021). The intensification of the Earth's water cycle affects the land water balance, leading to a higher soil moisture variability and, therefore, a higher influence of land surface conditions in the partitioning of surface energy and temperature variability (Seneviratne et al. 2010; Miralles et

al. 2012). A limited soil moisture availability might suppress, on one hand, the energy used for evaporation, and, on the other, enhance the available energy for warming the atmosphere causing the mutual re-amplification of warm temperatures and of the previously established soil dryness (Seneviratne et al. 2010; Miralles et al. 2019). Such synergy between land surface and atmosphere occurs at local scales (Geirinhas et al. 2022; Lemus-Canovas et al. 2024) — often causing a progressive multi-day heat entrainment and accumulation in the atmospheric boundary layer (Miralles et al. 2014) — but it can lead to downwind influences through the advection of sensible heat, enabling the spatial propagation of CDHW conditions (Schumacher et al. 2019).

In recent years, the historical and future evolution of the frequency and magnitude of CDHW events has been broadly analyzed from a purely statistical perspective (e.g., Hao et al. 2018; Yu and Zhai 2020; Geirinhas et al. 2021; Mukherjee and Mishra 2021; Ridder et al. 2022; Raymond et al. 2022; Olmo et al. 2022; Hosseinzadehtalaei et al. 2024). However, the disentanglement of the impact promoted by the above-mentioned linear (i.e., warming trends) and nonlinear mechanisms (i.e., land-atmosphere feedbacks) to the historical and future occurrence of CDHW extremes has been understudied. This is particularly true for understudied regions such as South America (SA).

Therefore, the main goal is to evaluate the degree to which changes in soil moisture–temperature coupling may cause an increment in the occurrence of CDHW conditions in SA, using a robust multi-variable weighted ensemble based on CORDEX-CORE runs. In doing so, we aim to cast light into a relatively unexplored topic within the CDHW problematic, while providing new clues on how processes other than the increasing trends in temperature that may affect the joint occurrence of dry and hot events in SA, therefore, filling a crucial gap.

5.2 Data and Methods

5.2.1 Region of interest

The analysis was conducted for SA (Figure 5.1), focusing on its seven sub-regions proposed by the AR6 report from the Intergovernmental Panel on Climate Change (IPCC) (Castellanos et al. 2022). In addition, and considering that each one of these sub-regions incorporates a vast and diverse territory with different biomes, ecoregions and land covers (Olson et al. 2001) , we also categorized the regions into wet and non-wet domains based on the biomes defined by Olson et al. (2001). Accordingly, the wet domain (Figure 5.1) encompasses areas

with a moist hydroclimate that are typically associated with an energy-limited evaporation regime (McVicar et al. 2012) and a tropical and subtropical moist broadleaf forest (e.g., Amazonia rainforest and the Brazilian Atlantic Forest). The non-wet domain considers drier regions characterized by a higher seasonality on temperature and precipitation and by a land cover varying from tropical to subtropical grasslands, savannas and shrublands. It is typically associated with a water-limited evaporation regime and, thus, with favorable soil moisture–temperature coupling conditions (McVicar et al. 2012; Miralles et al. 2012).

5.2.2 Data

Daily data from surface mean and maximum temperature (T_{mean} and T_{max} respectively), precipitation (P), evaporation (E) and surface net radiation (R_n) was analyzed for two distinct periods: (1) historical, spanning from 1970 to 2005 and (2) future, spanning from 2006 to 2099. ERA5 reanalysis data (Hersbach et al. 2020) for the above-mentioned variables was obtained

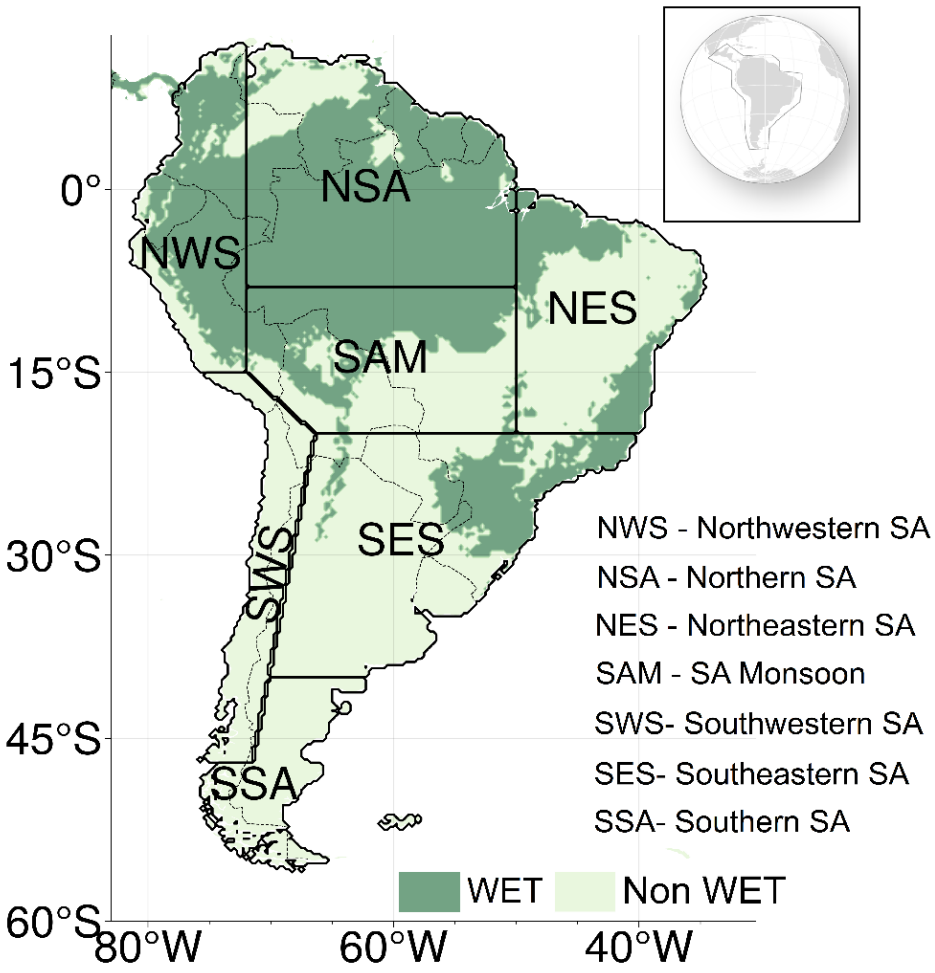

Figure 5.1 The South American domain with its sub-regions defined in Castellanos et al. (2022) and the wet and non-wet domains (Olson et al. 2001).

and computed for the historical period at a gridded 0.25×0.25° spatial resolution. Simulated fields of these variables for the historical period and the two Representative Concentration Pathways (RCPs) 2.6 and 8.5 were extracted from the Earth System Grid Federation (ESGF) data portal (Cinquini et al. 2014) and for the CORDEX-CORE runs on the South American domain, at a 0.22×0.22° spatial resolution (Giorgi et al. 2022). Accordingly, and as summarized in Table 5.1, this work relies on three realizations (Historical, RCP2.6 and RCP8.5) obtained from two Regional Climate Models (REMO2015, RegCM4-7), forced by three different Global Climate Models (HadGEM2-ES, MPI-ESM and NorESM1).

Each CORDEX model output was interpolated to a 0.25×0.25° grid and then evaluated at each grid-point in the historical period against ERA5 reanalysis, considering eight different error metrics. These metrics, namely the mean bias, mean absolute error, root mean square error, normalized standard deviation defined as the ration between the standard deviation of the modelled and the observed time-series, spatial correlation (Wilks 2011), Willmott-D Score (Willmott et al. 2012), Perkins skill score (Perkins et al. 2007) and Yule-Kendall skewness (Ferro et al. 2005), were chosen to guarantee different perspectives about each model skill and to measure the model's systematic errors. The Willmott-D Score is a combined measure of the differences in mean and standard deviation between model and observations, Perkins skill score quantifies the models' ability to reproduce the observed probability distribution functions (PDFs) while the Yule-Kendall skewness measures the matching between the skewness of the simulated and observed PDFs. A ranked average model weighted ensemble was built and used as the CORDEX future simulated data, following the approaches by Christensen et al. (2010) and Lima et al. (2023). According to this method, the multi-model ensemble p_{ENS} for a given variable *p,* is obtained by computing a weighted average over the *M* ensemble members as:

$$p_{ENS} = \frac{\sum_{m=1}^{M} w_m p_m}{\sum_{m=1}^{M} w_m} \qquad (5.1)$$

The variable-weights w_m were computed considering the individual performance of each model (ensemble member - *m*) in reproducing the variables against ERA5 reanalysis. Recently it has been demonstrated that ERA5 simulation of variables such as precipitation and temperature for SA, that are afterwards used to estimate other land-surface variables such as soil moisture, evaporation and other turbulent fluxes of sensible and latent heat, follow observations very closely when comparing to other known reanalysis (Coronato et al. 2020; Hassler and Lauer 2021; Balmaceda-Huarte et al. 2021). Five different weights are attributed

to each of the six ensemble members based on the previously described eight-error metrics. Although several approaches considering different combinations of variable-weights can be adopted, here, each ensemble member weight is obtained assuming the average of the weights of the five variables (precipitation, mean and maximum temperature, surface radiative balance and evaporation). These multi-weighted ensembles, considering multi-variable performances, are advantageous compared to the usual democratic multi-model ensemble (Eyring et al. 2019; Cos et al. 2022). More detailed information about the methodology can be found in Lima et al. (2023).

5.2.3 Methods

Before introducing and describing the methods, it is important to stress that, similarly to the approach adopted in Geirinhas et al. (2021), all the time series regarding the above-mentioned variables were first detrended, including the data regarding temperature. This was done to ensure that results reflect the effects of climate change beyond those imposed by the long-term trends in temperature and precipitation (IPCC 2023).

Definition of CDHW conditions

The CDHW conditions were assessed through the identification of summer (December–February) heatwave days occurring within a month under drought conditions (Geirinhas et al. 2021; Zhang et al. 2022a), hereafter referred as $CDHW_{days}$. Heatwaves were defined as periods of three or more consecutive days with daily T_{max} values above the respective climatological calendar day 90^{th} percentile (Perkins and Alexander 2013), while droughts were identified for the months with an associated 3-month Standardized Precipitation Index (SPI) lower than –1 (Svoboda et al. 2012).

Table 5.1 Details about the CORDEX-CORE runs considered in this study.

Model	Experiment	Time period	Forced by
ERA5	Historical	1970/01/01 – 2005/12/31	(-)
REMO2015	Historical	1970/01/01 – 2005/12/31	MOHC-HadGEM2-ES
	RCP2.6	2006/01/01 – 2099/12/31	MPI-M-MPI-ESM-LR
	RCP8.5	2006/01/01 – 2099/12/31	NCC-NorESM1-M
RegCM4-7	Historical	1970/01/01 – 2005/12/31	MOHC-HadGEM2-ES
	RCP2.6	2006/01/01 – 2099/12/31	MPI-M-MPI-ESM-MR
	RCP8.5	2006/01/01 – 2099/12/31	NCC-NorESM1-M

Soil moisture–temperature coupling

The soil moisture–temperature coupling metric (Π), defined in Miralles et al. (2012), was used to quantify land–atmosphere coupling and thus the influence of soil moisture on near surface temperature changes through anomalies in latent and sensible heat fluxes:

$$\Pi = \rho(R_n - \lambda E, T_{mean}) - \rho(R_n - \lambda E_p, T_{mean}) \quad (5.2)$$

where $R_n$is the surface net radiation, λE the surface latent heat flux, λE_p the potential latent heat flux, and T_{mean} the near-surface mean air temperature. The applicability of this metric relies on the availability of λE_p which is very sensitive to the method used to obtained it (Fisher et al. 2011; Gevaert et al. 2018) and it is not explicitly computed by the CORDEX models used in this study (table 5.1). According to Gevaert et al. (2018) and assuming that λE_p variability is mostly dictated by the variability in R_n (Priestley and Taylor 1972), equation (5.2) can be simplified as follows:

$$\Pi = \rho(R_n - \lambda E, T_{mean}) - \rho(R_n, T_{mean}) \quad (5.3)$$

Over very dry regions or conditions, soil moisture is often below wilting point, so evaporation is suppressed, thus the first and second correlation terms are nearly equal and Π approaches zero. In regions or conditions in which soil moisture is high and constantly above its critical level, λE tends to be a close function of R_n, thus both correlation terms are similar and Π approaches zero again. Moreover, in regions or conditions of high advection, temperature changes are largely independent from local land state, thus both correlation terms approach zero, and so does Π. Positive values of Π are expected when (i) soil moisture limits evaporation (water-limited regime), modulating sensible heat fluxes and therefore air temperature, and (ii) heat advection is not high enough to erase this influence of land conditions on air temperature. During drought conditions, the high evaporative demand promotes an early and pronounced soil dry-out. After a substantial soil moisture decrease, evaporation becomes gradually limited and sensible heat fluxes are enhanced, further increasing temperature and evaporative demand. This allows for a mutual re-amplification of drought and heatwaves and promotes the occurrence of CDHW events. In conclusion, when Π equals zero, changes in near-surface air temperature are independent from soil dryness, and the contribution of land–atmospheric feedbacks the occurrence of CDHW events is low. Under those conditions CDHW events are dominated by atmospheric forcing mechanisms, including enhanced radiative heating and

horizontal and/or vertical heat advection, which may nonetheless be affected by upwind land–atmosphere feedbacks (Schumacher et al., 2022).

Future strengthening or weakening of summer CDHW conditions and of soil moisture–temperature coupling

Changes in the statistical distribution of $CDHW_{days}$ and Π under two RCPs with respect to the historical period were analyzed in order to assess their strengthening or weakening in the future. The distributions were computed based on the values of $CDHW_{days}$ and Π for each grid-point located within the different sub-regions of SA. First, a strengthening or weakening requires that the distributions for the RCPs are significantly different from the one obtained for the historical period, at the 5% significance level, according to the non-parametric two-sample Kolmogorov-Smirnov test (Massey 1951). Second, a strengthening (weakening) is ensured only if the median and the 90th percentile of each distribution are higher (lower) for the RCPs compared to the historical simulation.

The impacts of the soil moisture–temperature coupling on summer CDHW conditions

To assess how the occurrence of CDHW conditions can be explained by a dependence on the soil moisture–temperature coupling (Π), linear regression models were computed as follows:

$$CDHW_{days} = \beta_0 + \beta_\Pi \Pi + \varepsilon \quad (8)$$

Where $CDHW_{days}$ is defined as the mean number of summer days under CDHW conditions per year, β_Π the regression coefficient that reflect the sensitivity of $CDHW_{days}$ to soil moisture–temperature coupling, β_0 is the intercept and ε the residual error. The regression models received as input the values for the above-mentioned variables obtained for each grid-point within SA. To the best of our knowledge, one attempt has been made to quantify, using the same methodology, a similar inter-link between the land–atmosphere feedbacks and crop production for the historical (Lesk et al. 2021). Regarding the future association between Π and CDHW conditions in SA, there's an absence of studies in the literature focusing on this research topic.

5.3 Results

5.3.1 Future occurrence of summer CDHW conditions over SA

Results for the summer CDHW conditions solely reflect the variability of temperature and precipitation, as well as the covariance between both variables (see Data and Methods), since all the time series were detrended. The hotspots of $CDHW_{days}$ for the historical period are mainly concentrated over the wet domain of NSA, and over the entire region of NES (Figure 5.2a). The lowest levels of $CDHW_{days}$ were found over NWS and the non-wet domains of SES, SWS and SSA. In general, under both RCPs, the distributions of $CDHW_{days}$ cover larger values resulting from a double effect promoted by an increase in the median and variance (Figure 5.2a). As expected, this becomes more evident under RCP8.5, excepting for SES, where a slight decrease in the future values of $CDHW_{days}$ is estimated. NSA is expected to witness the highest increase in summer CDHW conditions across all of SA, with a spatial median value higher 150% and almost 250% for RCP2.6 and RCP8.5, respectively, when compared to the historical (Figure 5.2c). A strong amplification is also expected for NWS and for the non-wet domains of SWS and SSA. Over the wet domain of SES, a decrease of almost 25% of the spatial median value is foreseen under RCP8.5, reflecting the overall weakening in summer CDHW conditions estimated for this climate change scenario and previously observed in Figure 5.2a.

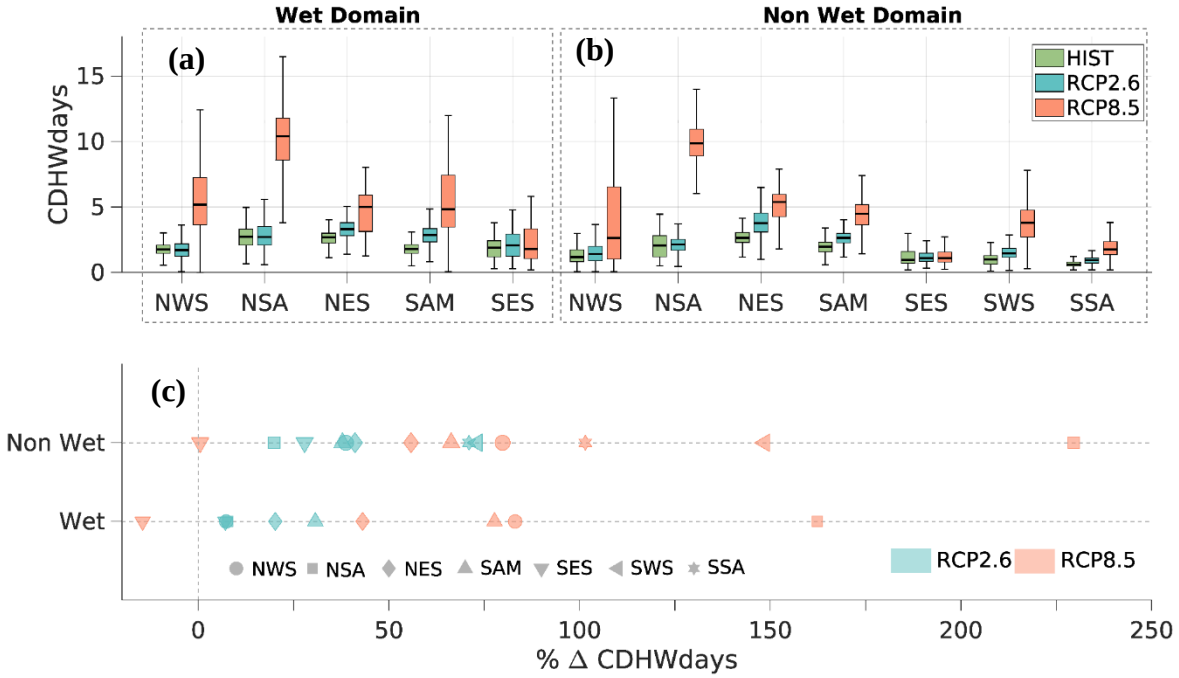

Figure 5.2 (**a, b**) Boxplots representing the distributions for the historical (green boxes), RCP2.6 (blue boxes) and RCP8.5 experiments (orange boxes), obtained by considering the values of $CDHW_{days}$, computed for all the grid-points within the wet (**a**) and non-wet (**b**) domains over each sub-region of SA. (**c**) Relative changes (in percentage) of the median value of $CDHW_{days}$ estimated for both RCPs comparing to the historical.

5.3.2 Future soil moisture–temperature coupling in SA

In this section we aim to analyze and compare over the three experiments (Historical, RCP2.6 and RCP8.5) the expected changes in the absolute values and in the spatial signature of the soil moisture–temperature coupling (Π) throughout SA. Furthermore, we also aim to establish a first link between $CDHW_{days}$ and an eventual future strengthening or weakening of Π. Under RCP2.6 a strengthening in Π is expected to occur mainly over the non-wet domains of SAM and NES (Figure 5.3e), in a region where an increment in $CDHW_{days}$ is also estimated to occur (Figure 5.3b). The northern part of NSA, characterized by the highest values of Π during the historical period (Figure 5.3d), is expected, under RCP2.6, to witness slight changes in this coupling dynamics and in $CDHW_{days}$ (Figure 5.3b, e). The overall increase of $CDHW_{days}$ expected for NSA under RCP8.5 is supported by an enhancement of these compound conditions throughout most of the region, except the southwestern section (Figure 5.3c). However, a spatial match with a strengthening of Π is only observed over specific areas located in the central and southeastern parts (Figure 5.3f). The coastal areas of NSA exhibiting a future amplification of $CDHW_{days}$ are either linked to a weakening or an absence of visible changes in Π. The land sections in SA showing the strongest future decreases in Π under RCP8.5 are located within the wet domain of NWS and the non-wet domain of NSA (Figure 5.3c). Over SAM region, there is a spatial correspondence between the future estimated increasing levels of $CDHW_{days}$ and a strengthening of the soil moisture–temperature coupling. A similar scenario is observed for the non-wet domain of NES. The overall reduction in the summer CDHW conditions for SES (Figure 5.2) is supported by a spatially homogenous pattern of decreasing levels of $CDHW_{days}$, associated with a very slight amplification of Π (Figure 5.3). Finally, although SWS and SSA are estimated to witness an enhancement of $CDHW_{days}$, a visible association with a weakening or a strengthening of Π is missing.

5.3.3 Influence of soil moisture–temperature coupling on the occurrence of summer CDHW conditions in SA

In the previous section we have shown how the absolute levels of $CDHW_{days}$ and Π are estimated to change in a future climate change scenario. Here, we aim to clarify the association of both variables. Table 5.2 assembles information, based on Figures S5.1–S5.6, Table S5.2 and other methods (see Data and Methods section), on how the statistical distributions, obtained by considering the values of Π and $CDHW_{days}$ recorded for all the grid-points located within each domain, are estimated to evolve under both RCPs, comparing to historical. The regions

covering the highest positive values in Π distributions are, in general, observed over the non-wet domains, particularly over the NSA region (Table S5.2 and Figures S5.1–S5.6). NSA is also characterized by high levels of $CDHW_{days}$, only surpassed by SAM and NES. With an opposite association stands NES, where pronounced summer CDHW conditions during the historical period have been associated with a relatively weak soil moisture–temperature coupling (Figure S5.3 and Table S5.2). However, this association corresponds to a spatial integrated overview that filters out particular spatial features of both variables. NES is a widespread region covering land sections associated with distinct dynamics as highlighted by Figure 5.3d. Under the historical experiment, the lowest values of Π are observed over the wet domains of SAM, despite the pronounced levels of $CDHW_{days}$ that define this region. This might indicate that compound dry and hot conditions in this central part of the continent are likely dictated by pure atmospheric forcing mechanism capable of imposing not just a strong variability in temperature and precipitation, but also a strong covariance between both variables.

Contrary to the changing patterns of $CDHW_{days}$ that are spatially coherent, the future evolution of Π distribution strongly depends on the region and the RCP considered (Figure 5.3 and Table 5.2). Even so, an overall spatial of this land–atmosphere coupling (e.g., wet domains

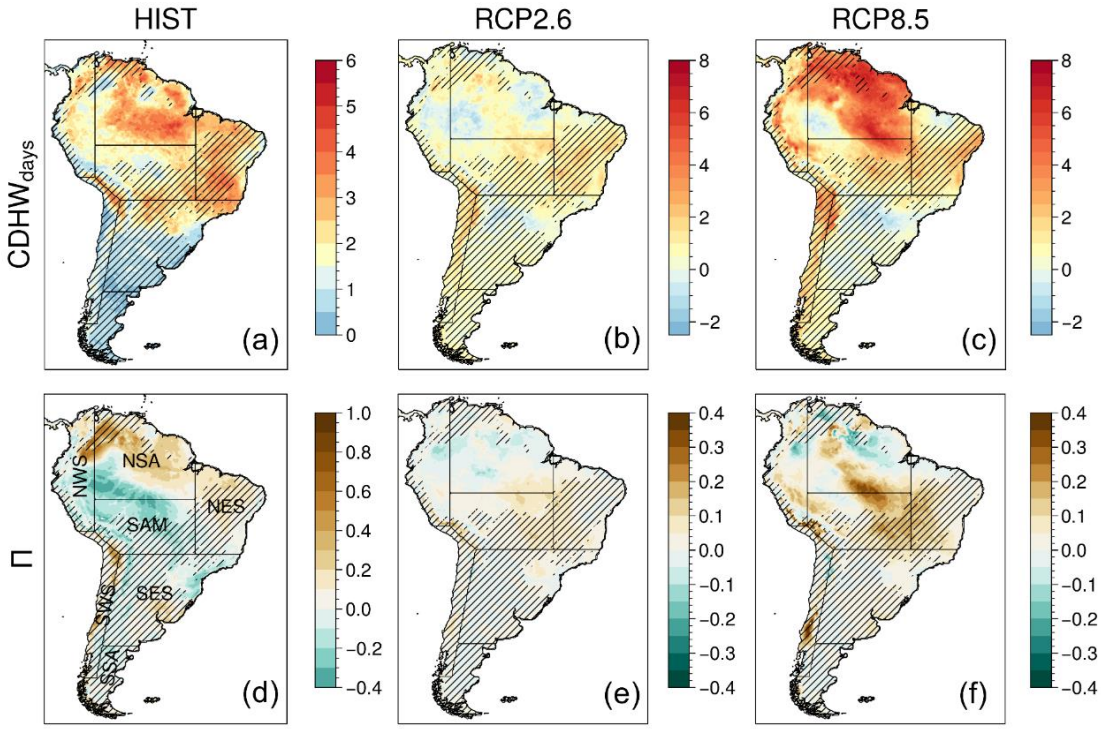

Figure 5.3 Spatial patterns of $CDHW_{days}$ (first row) and Π (second row) over South America and during the historical period (HIST - left column). The differences in respect to the historical period (HIST) recorded for the RCP2.6 and RCP8.5 experiments are shown by the panels included in the middle and right columns, respectively. The black hatches mark the non-wet domains.

over NWS and NSA). Finally, over the non-wet domain of SES, although we foresee an overall spatial amplification of the Π, the opposite is observed for the occurrence of summer CDHW conditions.

To quantify to which level the grid-points with the severest (minor) summer CDHW conditions are linked to the strongest (weakest) soil moisture–temperature coupling, linear regression models are computed using as input the values of $CDHW_{days}$, (response variable), and Π (predictor) recorded for all the grid-points in the twelve different sections of SA considered here (see Data and Methods). Tables S5.4 and S5.5 indicate the root mean square error (RMSE) and the explained variance (R^2) obtained from the several conducted modelling experiments considering the wet and non-wet domains, respectively. The explained variance and RMSE tend to increase from the historical to RCP8.5, particularly when considering the experiments conducted for the wet domains (Figure 5.4 and Table S5.4). This indicates that the spatial variability of summer CDHW conditions is more explained by the changes in Π as we consider the most extreme climate change scenario. Conversely, in terms of absolute values, there's a higher disparity between the "real" and the simulated values given by the regression curve.

Table 5.2 Changing patterns of $CDHW_{days}$ (left arrow) and Π distributions (right arrow) under the RCP2.6 and RCP8.5, comparing to the historical period. An orange arrow encodes a strengthening, indicating that the distributions of $CDHW_{days}$ and Π cover a higher range of values in future. A blue arrow indicates the opposite. A strengthening or weakening requires that the RCP and historical distributions are different according to the non-parametric two sample Kolmogorov-Smirnov test (at the 5% significance level). More details are provided in the Data and Methods chapter.

	Wet		**Non-Wet**	
	RCP2.6	RCP8.5	RCP2.6	RCP8.5
NWS	↑ ↓	↑ ↑	↑ -	↑ -
NSA	↑ -	↑ ↑	↑ ↑	↑ ↓
NES	↑ ↑	↑ ↑	↑ ↑	↑ ↑
SAM	↑ ↑	↑ ↑	↑ ↑	↑ ↑
SES	↑ ↑	↓ ↑	↑ -	↓ ↑
SWS	–	–	↑ -	↑ ↑
SSA	–	–	↑ -	↑ ↓

↑ **strengthening**

↓ **weakening**

\- **no change**

$CDHW_{days}$	Π

Figure 5.4 shows the obtained regression coefficients (bars) as well as the respective explained variance (vertical line) for all the conducted regression models. Although some exceptions (NES – wet domain; SAM – non wet domain; SSA), the regression coefficients are

expected to increase under both RCPs, meaning that in a future climate change scenario, the grid-points with enhanced values of $CDHW_{days}$ are estimated to be more closely linked to a strong soil moisture–temperature coupling and vice-versa. This is more evident under RCP8.5 and over NWS (both domains), NSA (both domains), SAM (wet domain), SES (wet domain) and SWS. Although Figure 5.3 proposes some level of association between increases in $CDHW_{days}$ and Π over eastern and southeastern NES, the regression models show a poor level of performance when an overall association for the whole region is conducted. This might be explained, on one hand, by the contrasting relation pattern found over the central and northeastern areas of the domain, where future increases in $CDHW_{days}$ are not followed by any robust modification in Π (Figure 5.3c and f), and on the other, by an erroneous assumption that the relation between both variables is linear. Over the non wet domain of SES, the modelling skill is also poor and so the level of association between the expected decreases in $CDHW_{days}$ and Π is negligible. A similar scenario is also expected for the non wet domains of SAM and SSA.

5.4 Discussion and Conclusions

The results highlight some variability among the future projections of summer CDHW episodes over SA. Nevertheless, an overall increment of these compound conditions is estimated over most of the continent, even when the effect of the global warming trends is disregarded. A future strengthening of the soil moisture–temperature coupling stands as a valid candidate to explain such enhancement, particularly over the central SA, in an area shared by the southernmost parts of the Amazon basin and the Brazilian's Cerrado biome. A similar link was not possible to unravel over several other regions of SA. This either indicates that the future increase in the covariance between temperature and soil moisture is explained by other pure atmospheric processes (e.g., strong temperature advection, enhanced shortwave radiative heating, lack of moisture advection and convergence), or the wrong assumption that the relation between both variables is linear is not valid.

Many regions located closer to the coastline of NSA and NES are expected to witness a weakening of this land–atmosphere coupling, particularly under RCP8.5. This decline might be the consequence of several changing patterns in land cover, atmospheric circulation (e.g. heat and moisture advection) and in precipitation regimes. For instance, an increase in precipitation may lead to soil moisture levels closer to saturation and to a more dominant energy limited soil moisture–evaporation regime. On the other hand, an intensification of precipitation deficits over

already dry regions, triggers more desert like conditions where soil moisture is below the wilting point and there is a suppression of evaporation (Seneviratne et al. 2010). The aridity levels throughout SA for the present climate, allows to conclude that this last scenario is more likely to occur over NSA, mainly over northern Venezuela and Guyana (Zomer et al. 2022). This agrees with the future projections of precipitation for the continent that highlight a dipole pattern marked by less precipitation over central and northern SA and more humid conditions over SES (IPCC 2021; Torres et al. 2022).

Results are marked by a relatively high spatial variability and disparity between the estimates given by two RCP experiments. We believe that this heterogeneity does not reflect any artifact associated with the datasets or the metrics used to perform the analysis. It is important to underline that the historical data was obtained from the state-of-the-art ERA5 reanalysis that shows a good performance for SA when comparing to other datasets (Coronato et al. 2020; Hassler and Lauer 2021; Balmaceda-Huarte et al. 2021). The future simulated data was retrieved from a set of regional climate models from the CORDEX experiment, while an effort was made to select those with the finest spatial resolution (Giorgi et al. 2022). The finer the resolution, the better the representation of topography, soil and vegetation dynamics, improving the estimates of surface runoff, evaporation and turbulent fluxes of sensible and latent heat (Wood et al. 2011; Benedict et al. 2019). Moreover, the results are based on a multi-weighted ensemble that was obtained after an exhaustive and rigorous statistical method of data selection and validation, proven to be advantageous compared to the commonly used

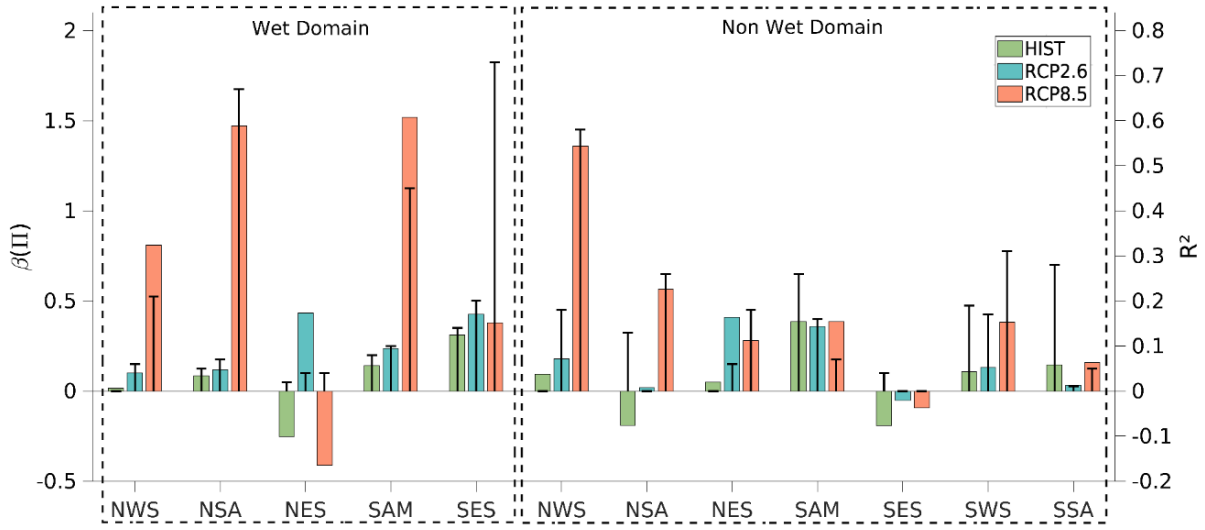

Figure 5.4 Regression coefficients (bars; left y-axis) and Explained Variance (vertical black lines; right y-axis) obtained from the regression models using Π as the explanatory variable and the $CDHW_{days}$ as the dependent variable (see Data and Methods chapter). The modelling experiments were conducted for the wet (left section of the panel) and non-wet domains (right section of the panel) within the seven sub-regions in SA and for the historical period (green bars), the RCP2.6 (blue bars) and RCP8.5 (orange bars).

democratic multi-model ensemble (see Data and Methods). Finally, heatwave and drought indexes, as well as metrics for the quantification of the soil moisture–temperature coupling were used (Miralles et al. 2012, 2014, 2019; Geirinhas et al. 2021, 2022; Wang et al. 2023; Yin et al. 2023; Lemus-Canovas et al. 2024). Nevertheless, we admit that the interpretation and comparison of the results between regions and experiments is wrapped by some complexity. To help on this, we present in the following sentences a short description of the main findings for each region. Regarding NWS and from a spatial integrated perspective, the levels of $CDHW_{days}$ are expected to increase over both domains and RCPs. Both RCPs point for a stronger association between CDHW conditions and Π, highlighting a potential higher role played soil moisture–temperature coupling in the occurrence of CDHW events. Similarly to NWS and from a spatially integrated perspective, the levels of $CDHW_{days}$ in NSA are expected to increase over both domains and RCPs. This is followed by a strengthening of Π for the wet domain, under RCP8.5, and for the non-wet domain, under RCP2.6. Regarding the wet domain, the association level between Π and $CDHW_{days}$ is expected to increase particularly under RCP8.5. For NES, an intensification of $CDHW_{days}$ is estimated for the whole region and for both RCPs. Under RCP8.5, a pronounced enhancement of Π is also foreseen especially over the interior of the non-wet domain. However, the strongest increases in $CDHW_{days}$ are expected over the coastal areas, where changes in Π are nearly zero. An overall association between the future changing pattern of Π and $CDHW_{days}$ throughout the region is estimated, particularly over the non wet domain. The SAM region will likely witness an increase in $CDHW_{days}$ under both RCPs. Over the non-wet domain and under RCP8.5, where these changes are estimated to be larger, an intense strengthening of Π is also foreseen. For this RCP, the increases in summer CDHW conditions are expected to be associated with stronger Π levels, pointing for a causal relation between both variables. SES this is the only region where a slight decrease in the levels of $CDHW_{days}$ is predicted, particularly for RCP8.5. This decline appears to be explained by a reduction in temperature and precipitation variability via other atmospheric dynamical processes as significant changes in Π are not expected. SWS is estimated to face a future escalation in $CDHW_{days}$ followed by an amplification in Π, particularly under RCP8.5 and over the southernmost sections. Finally, regarding SSA, an intensification in $CDHW_{days}$ is predicted for both RCPs. However, significant changes in Π are not expected and the level of influence of this coupling mechanism to the occurrence of summer CDHW conditions is expected to be deteriorated. The explanation for the amplification of these compound episodes might be related

to a higher short-term variability in temperature and precipitation, triggered by the dynamics of the atmosphere.

These results might have some limitations that are inevitably bound to the uncertainty that surrounds climate models and the limited number of model outputs for SA. Such uncertainty characterizes, particularly, the projections of hydrological variables such as precipitation and evaporation. Several studies have shown that climate models point for a dipole pattern of drier conditions centered in the Amazon basin and wetter conditions prevailing in the central-eastern parts of the continent (Reboita et al. 2014; Llopart et al. 2020; IPCC 2021). Our results are in line with these estimates. However, the recent observed trends over SA presented by Geirinhas et al. (2023), raise some questions about the confidence level of these projections. The mismatch between what climate models predicted years ago and what we have been actually observing since then, might be related to an already reported lack of skill from models in simulating internal variability, key atmospheric features associated with large-scale modes of variability and to errors in the parametrization of moist-convection processes (Fatichi et al. 2016; Peleg et al. 2019; Chen et al. 2021). Petrova et al. (2024) points for a large inter-model spread in the historical and future estimates of droughts conditions, across both CMIP5 and CMIP6 model ensembles. The same is also observed regarding heatwave projections within CORDEX-CORE runs for SA (Silva et al. 2022). In order to mitigate this uncertainty, a multi-variable weighted ensemble technique was applied to our climate data. When comparing the results from this multi-variable weighted ensemble with previous studies that used observational datasets, it is observed a good agreement throughout the majority of SA (Miralles et al. 2012; Lesk et al. 2021), providing a higher confidence level to our outcomes.

Until mid-century the differences in the outcomes between RCP2.6 and RCP8.5 are small. However, after this period, the climate system starts to slowly respond to the distinct anthropogenic changes in greenhouse gas concentration. Given the recent global CO_2 emissions, there's a chance that we might be considering two unrealistic scenarios. The 2023 estimate for the global CO_2 emissions is far from RCP2.6 and RCP8.5 trajectories and closer to the middle-of-the-road RCP4.5 (Rozenberg et al. 2015; Liu et al. 2024). Although the ideal would be to consider an intermediate scenario, RCP 2.6 and 8.5 are the only two climate change experiments provided by this set of climate models from CORDEX. To the best of our knowledge, few attempts have been made to highlight this problematic and to explore the impact of climate in the soil moisture–temperature coupling dynamics and, ultimately, in the occurrence of hot and dry extremes. Therefore, this study employs an exploratory approach that

has the potential to be refined and improved with further work. Namely, the application of other methods for causal inference between $CDHW_{days}$ and Π, would allow to determine to which point the poor association that was demonstrated here for some regions in SA might be explained by a wrong assumption that they are linearly correlated.

Despite all this, this study demonstrates how climate change may lead to more frequent and longer-lasting CDHW conditions through other less explored non-linear chain of processes. Thus, efforts must be made to improve the representation of these more complex land–atmosphere interactions in climate models, ensuring that all the meanders of climate change are understood and allowing for proper prediction and mitigation of natural and socio-economic impacts (Zscheischler et al. 2018; Tabari and Willems 2023). This is even more important for regions like SA that encompass a vast territory vulnerable to CDHW episodes (Libonati et al. 2022a, b). Despite countries in SA are only responsible for 8% of all greenhouse emissions globally (Watch 2024), their economies and population are strongly affected by climate hazards (Libonati et al. 2022b; Hartinger et al. 2023; dos Santos et al. 2024). In case this is ignored, the expected range of future climate variability, the magnitude of extreme weather events and the associated impacts, may exceed current estimates.

Supplementary Material

Table S5.1 Weights attributed to each member of the multi-variable weighed ensemble computed according to the method described in the Data and Methods chapter of the manuscript.

Ensemble Member		Weight
REMO2015	MOHC-HadGEM2-ES	0.222
	MPI-M-MPI-ESM-LR	0.151
	NCC-NorESM1-M	0.419
RegCM4-7	MOHC-HadGEM2-ES	0.094
	MPI-M-MPI-ESM-MR	0.068
	NCC-NorESM1-M	0.046

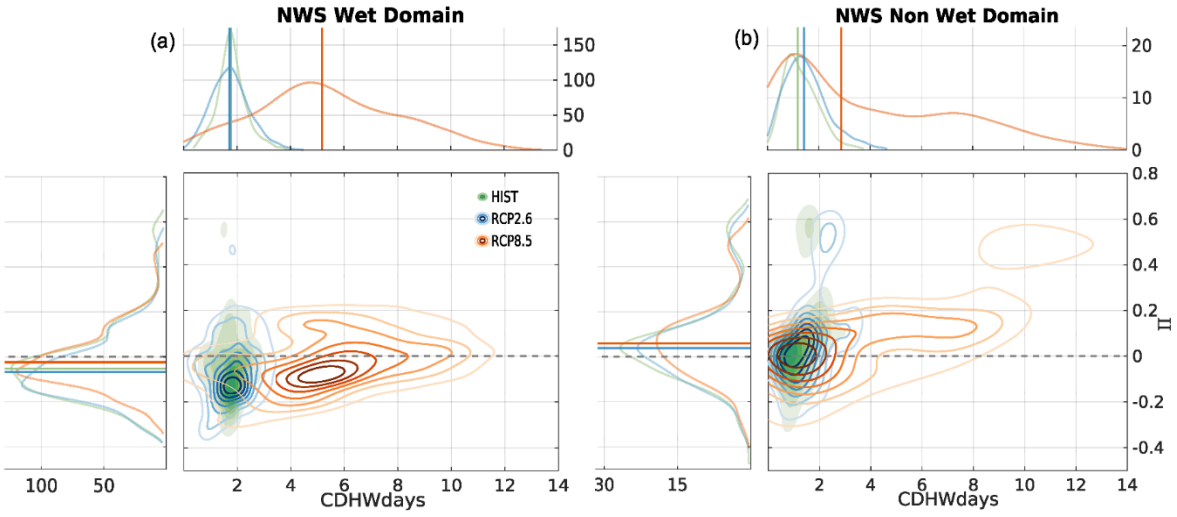

Figure S5.1 Bivariate Kernel distributions obtained from pairs of $CDHW_{days}$ (x-axis) and Π (y-axis) values recorded for each grid-point within the NWS wet (**a**) and the non wet domain (**b**), and considering the historical (green shades), RCP2.6 (blue contours) and RCP8.5 experiments (orange contours). The top and left-side panels show the univariate distribution of $CDHW_{days}$ and Π, respectively.

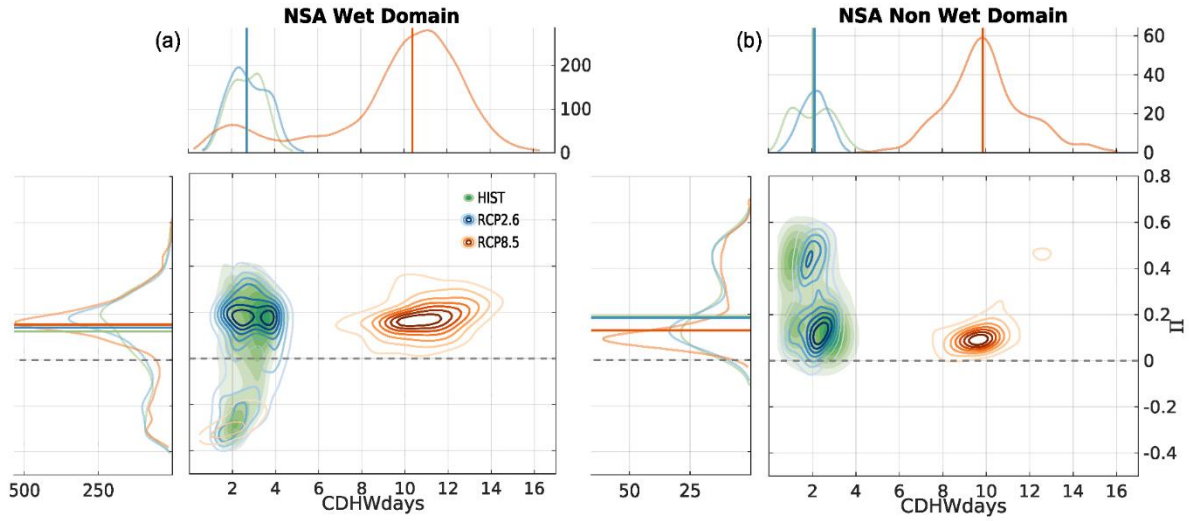

Figure S5.2 Same as Figure S5.1 but for the NSA region.

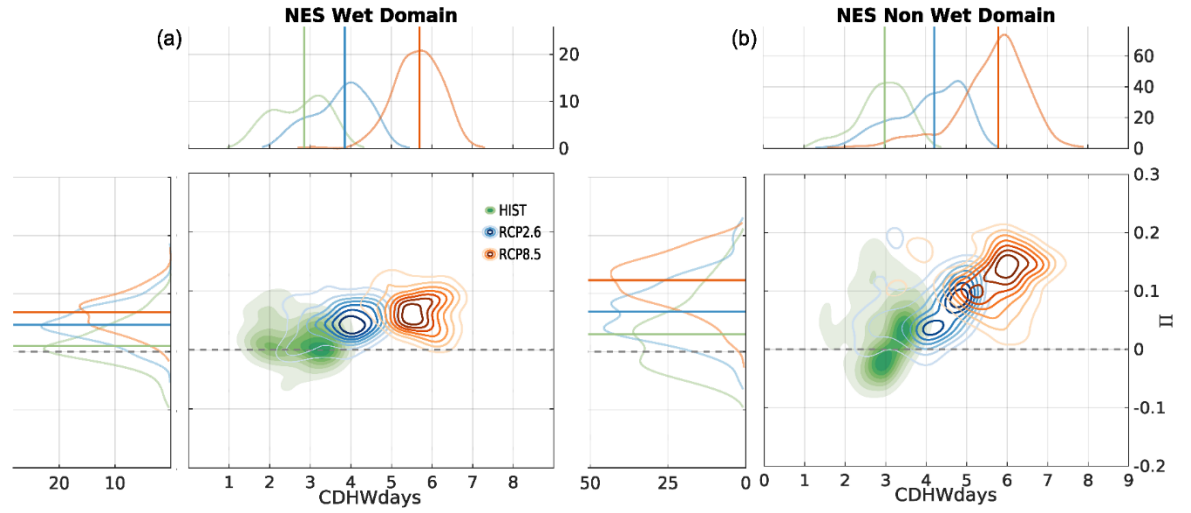

Figure S5.3 Same as Figure S5.1 but for the NES region

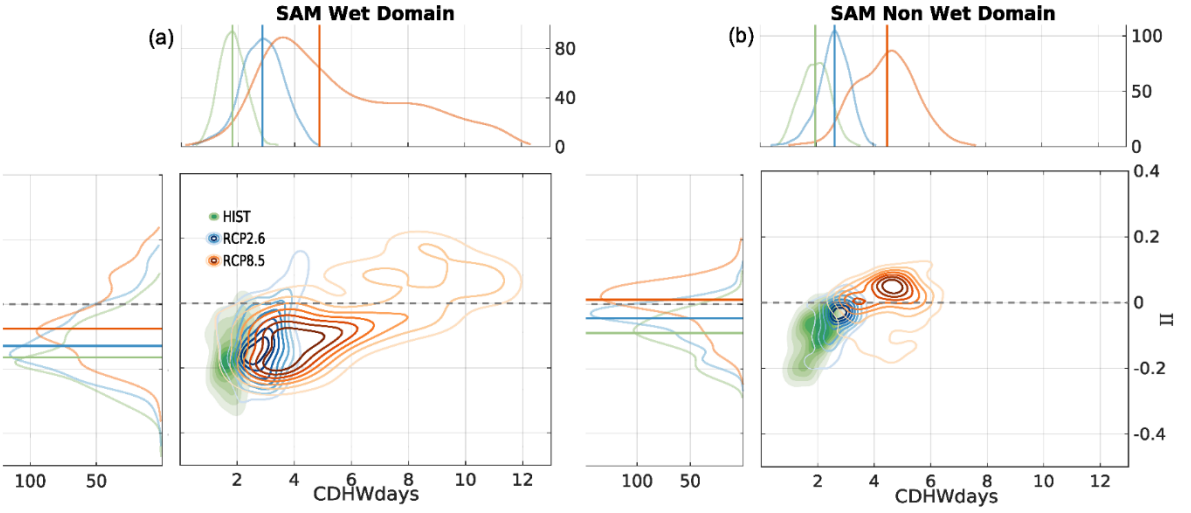

Figure S5.4 Same as Figure S5.1 but for the SAM region.

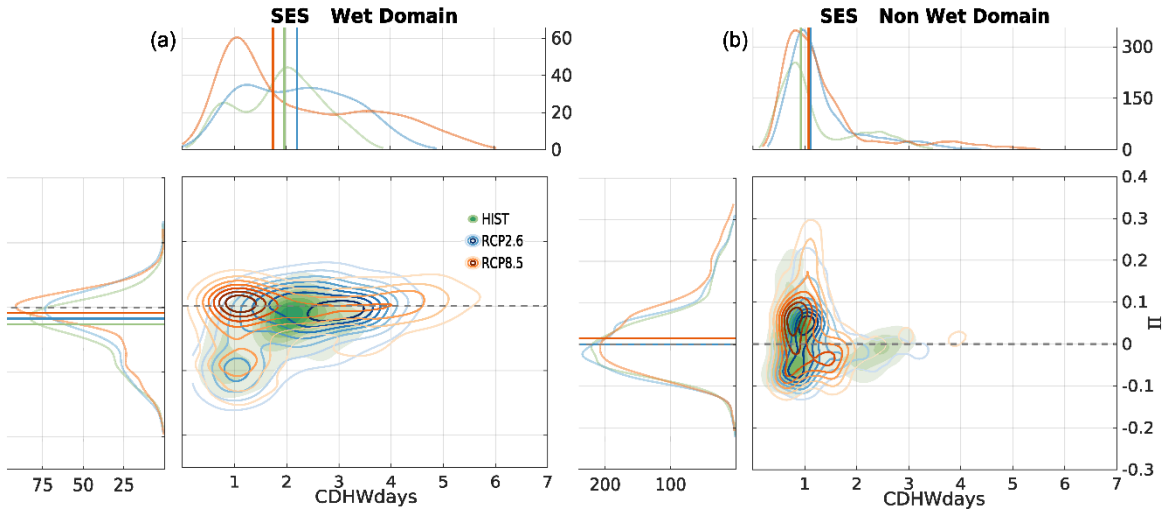

Figure S5.5 Same as Figure S5.1 but for the SES region.

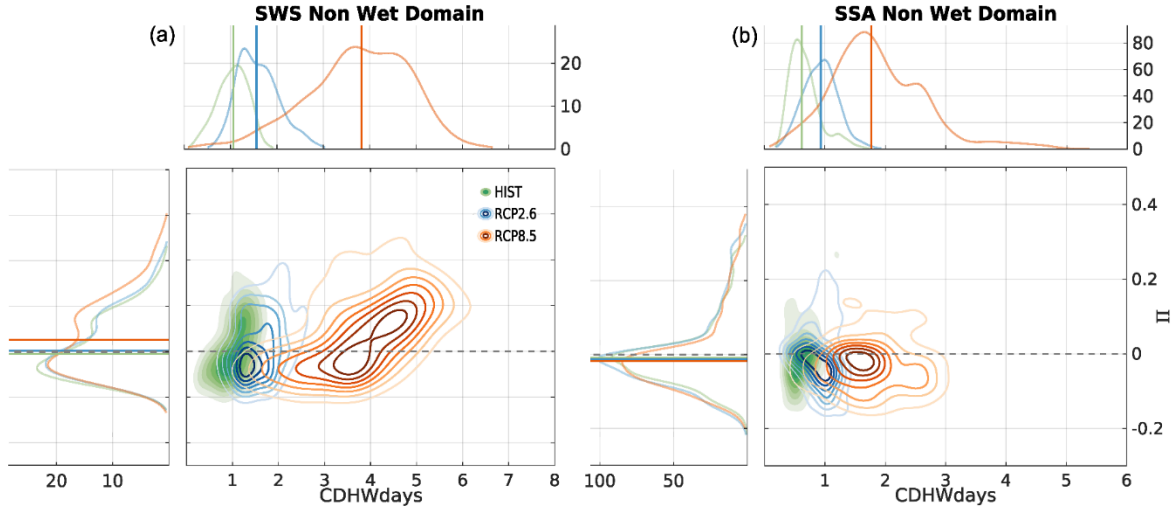

Figure S5.6 Same as Figure S5.1 but for the SWS (**a**) and SSA region (**b**).

Table S5.2 Statistical parameters (Median – Mdn; 90th percentile – P90) computed for the $CDHW_{days}$ and Π distributions obtained considering the values recorded for each grid-point within the wet domains of SA. In bold are marked the values corresponding to the distributions that are significantly different from the one obtained for the historical period, at a 5% significant level, according to the non-parametric two sample Kolmogorov-Smirnov test.

	$CDHW_{days}$			**Π**		
	HIST	RCP2.6	RCP8.5	HIST	RCP2.6	RCP8.5
Region	Mdn (P90)	Mdn (P90)	Mdn (P90)	Mdn (P90)	Mdn (P90)	Mdn (P90)
NWS	1.77(2.50)	**1.72(2.73)**	**5.18(9.13)**	-0.05(0.19)	**-0.07(0.17)**	**-0.02(0.18)**
NSA	2.73(3.72)	**2.71(4.02)**	**10.40(12.89)**	0.12(0.30)	**0.14(0.29)**	**0.16(0.30)**
NES	2.85(3.55)	**3.85(4.58)**	**5.70(6.38)**	0.01(0.06)	**0.05(0.08)**	**0.07(0.11)**
SAM	1.80(2.43)	**2.87(3.80)**	**4.87(9.42)**	-0.16(-0.03)	**-0.13(0.00)**	**-0.08(0.10)**
SES	1.96(2.92)	**2.20 (3.56)**	**1.74(4.38)**	-0.05(0.03)	**-0.03(0.06)**	**-0.02(0.06)**

Table S5.3 Same as Table S5.2 but for the non wet domains within the seven sub-regions in SA.

	$CDHW_{days}$			**Π**		
	HIST	RCP2.6	RCP8.5	HIST	RCP2.6	RCP8.5
Region	Mdn (P90)	Mdn (P90)	Mdn (P90)	Mdn (P90)	Mdn (P90)	Mdn (P90)
NWS	1.18(2.20)	**1.42(2.71)**	**2.87(9.05)**	0.04(0.47)	0.04(0.42)	0.06(-0.39)
NSA	2.06(3.23)	**2.13(2.93)**	**9.87(12.52)**	0.19(0.50)	-0.18(0.49)	**-0.13(0.48)**
NES	2.99(3.65)	**4.21(5.03)**	**5.79(6.61)**	0.03(0.12)	-0.07(0.13)	**0.12(0.18)**
SAM	1.96(2.60)	**2.64(3.28)**	**4.50(5.79)**	-0.09(-0.01)	-0.04(0.01)	**0.01(0.08)**
SES	0.92(2.48)	**1.10(2.41)**	**1.07(2.76)**	0.00(0.13)	0.00(0.22)	**0.05(0.28)**
SWS	1.06(1.47)	**1.56(2.20)**	**3.82(5.03)**	0.00(0.20)	0.00(0.22)	**0.05(0.28)**
SSA	0.62(1.03)	**0.93(1.28)**	**1.76(2.79)**	0.00(0.15)	-0.01(0.17)	**-0.02(0.18)**

Table S5.4 Error metrics (explained variance – R^2; Root Mean square error – RMSE) obtained from the several regression models computed for the wet domains of each of the seven sub-regions in SA and using $CDHW_{days}$ as response variable and *Π* as the explanatory variable (see Data and Methods for more details).

	R^2			**RMSE**		
	HIST	RCP2.6	RCP8.5	HIST	RCP2.6	RCP8.5
NWS	0	0.06	0.21	0.56	0.71	2.35
NSA	0.05	0.07	0.67	0.76	0.87	1.9
NES	0.02	0.04	0.04	0.65	0.67	0.60
SAM	0.08	0.1	0.45	0.45	0.72	1.91
SES	0.14	0.20	0.70	0.73	0.90	1.35

Table S5.5 Same as Table S5.4 but for the regression models computed for the non wet domains of each of the seven sub-regions in SA

	R^2			**RMSE**		
	HIST	RCP2.6	RCP8.5	HIST	RCP2.6	RCP8.5
NWS	0.09	0.18	0.58	0.64	0.77	2.16
NSA	0.13	0	0.26	0.85	0.61	1.57
NES	0	0.06	0.02	0.62	0.83	0.93
SAM	0.26	0.16	0.70	0.73	0.72	0.96
SES	0.04	0	0	0.73	0.72	0.96
SWS	0.19	0.17	0.31	0.3	0.41	0.91
SSA	0.28	0.01	0.04	0.22	0.28	0.78

Chapter 6
Conclusions

6. Conclusions

6.1 Outlook of the main results

The aim of this final chapter is to provide the general conclusions reached in this thesis, as well as future steps for continuing with the research topics presented here.

The main objective of this thesis was to contribute to advancing the state of the art, focusing on the occurrence of CDHWs on a particularly vulnerable region. A comprehensive framework was proposed, relying on a sound theoretical conceptualization of the research problem, on adequate *in situ* and modelling datasets, on classical and commonly used heatwave and drought indicators and on suitable statistical methods.

The outcomes of this thesis were aggregated into four main chapters (Chapter 2–5). To give an outlook of the overall thesis, the following paragraphs address the fundamental findings from each of these chapters and answer the target research questions (RQ) stated in Chapter 1. In addition, a summary of the main findings achieved in the annexed research work (Appendix A, B and C) is also addressed in this concluding chapter.

Chapter 2 – Recent increasing frequency of compound summer drought and heatwaves in Southeast Brazil

In Chapter 2, the first two research questions (RQ1 and RQ2) were explored, focusing on assessing the spatiotemporal evolution of CDHW conditions over the recent decades in SA and on understanding how soil moisture–temperature coupling has explained the occurrence, amplification and propagation of such co-occurring conditions. The physical mechanisms responsible for the triggering and amplification of CDHW events were explored, particularly concerning (i) the level to which heatwaves, as recurrent isolated events, could enhance already established drought conditions, (ii) the extent to which prolonged drought and subsequent surface sensible heat fluxes can amplify heatwaves, and (iii) the degree to which (i) and (ii) can concur.

This relationship between droughts and heatwaves, controlled by distinct soil moisture–temperature coupling regimes, was assessed for two summer periods (2013/2014 and 2014/2015) over Southeast Brazil. These two exceptional summer seasons occurred in a

historical context marked by significant increasing trends in the occurrence of CDHW events. An enhancement of non-linear mechanisms likely determined the escalation of these compound conditions, as the linear effect imposed by global warming in the temperature increase was disregarded in the analysis. During these summer periods, a weak soil moisture–temperature coupling (energy-limited) regime was replaced by strong coupling conditions (water-limited) due to the occurrence of persistent atmospheric blocking patterns over SEB, that induced, in a first stage, strong evaporation rates and soil moisture depletion, and, on a second stage, large fluxes of sensible heat linked to a reduction in the evaporative cooling.

Chapter 3 – The influence of soil dry-out on the record-breaking hot 2013/2014 summer in Southeast Brazil.

The work presented in Chapter 3 complements Chapter 2, addressing RQ1 and RQ2 with increased detail. Chapter 3 aimed to deeply explore the historical relevance of the CDHW conditions during the summer of 2013/2014 and investigate, over two large metropolitan areas of SEB, the inter-link between land–atmosphere feedbacks and mesoscale atmospheric circulation processes. It includes a detailed spatiotemporal analysis, where it was assessed, for the first time, the exceptional compound nature of the observed hot and dry conditions and of the physical processes (atmospheric and land–atmosphere) that leveraged record-breaking temperature levels.

During the outstanding 2013/2014 summer, the metropolitan regions of São Paulo and Curitiba faced the longest and most severe summer heatwave ever recorded at the time. It was found that such record-breaking heat stress conditions were followed by historically unprecedented levels of several other variables, namely VPD, precipitation deficits and strong soil moisture–temperature coupling. The harmful warm conditions were not explained by synoptic circulation anomalies alone and land–atmosphere feedbacks, coupled with mesoscale atmospheric processes, played a crucial role. This study has shown, at a regional scale and over the two above-mentioned metropolitan areas, how the whole summer season was marked by distinct levels of heat stress. Although dry conditions were present during the entire summer, the changes in surface temperature were dictated by a joint effect played by an intense soil moisture–temperature coupling, supported by an enhanced radiative heating and a suppression of the atmospheric cooling associated with sea breezes. Other periods within the summer season with distinct relation patterns between these land–atmosphere processes and the mesoscale atmospheric mechanisms, were also analyzed at a very fine spatial and temporal scale.

Chapter 4 – Combined large-scale tropical and subtropical forcing on the severe 2019–2022 drought in South America

Chapter 4 represents an important landmark for the thesis. The rationale surrounding the previous two chapters was focused on getting a purely statistical analysis of the historical evolution of CDHWs over SA and on assessing the role played by the land–atmosphere feedbacks in temperature escalation. In this chapter, an important step was given towards answering RQ3 and RQ4, and providing an in-depth spatiotemporal characterization of the recent severe 2019–2022 drought in SA. The specific goals included exploring the historical context of the event, the exceptionality of the soil moisture anomalies, the large-scale atmospheric forcing mechanisms from a daily to multiyear timescale and, finally, the joint role played by internal variability and climate change. Moreover, it was also aimed to investigate the influence of the observed soil desiccation on the occurrence and intensification of heatwaves, paving the way for extreme CDHW episodes and the occurrence of severe wildfires. This idea is enclosed by RQ3 and although it was not explored directly in Chapter 4, it ended up being addressed in Appendix A, whose analysis and results are strongly linked to this section (Figure 1.2).

It was found that the long-term and severe 2019–2022 drought occurred within a historical context marked by a prolonged drying trend observed over the past three decades in CESA, resulting from a joint contribution of natural variability, through large precipitation deficits, and climate change through the global warming trend. This long-term and slowly evolving drought was characterized by the occurrence of daily to weekly periods marked by a rapid intensification of the already established dry conditions. These short-term periods, known as flash droughts, led to an escalation of the fire danger levels and to the occurrence of devastating wildfires in CESA.

ENSO was responsible for the long-term dynamical forcing of this 4-year drought episode. A coupled tropical and subtropical forcing associated with pronounced changes in the normal Walker and Hadley cell circulation led to strong perturbations in the moisture transport and convergence over SA and, ultimately, to large precipitation deficits and enhanced evaporation in CESA. During the flash droughts episodes, when soil moisture reached record-breaking low levels, an anomalous subtropical dynamic, represented by a well-matured Rossby wave pattern extending from west south Pacific towards SA, reinforced the previously established circulation

anomaly associated with ENSO. This led to an amplification of the ideal meteorological conditions for soil desiccation and the occurrence of heatwaves.

These findings, merged with the results shown in Appendix A and B, allowed us to address RQ3 and RQ4 extensively. It became clear the interplay between different atmospheric mechanisms associated with climate change and variability in the occurrence of extreme CDHW conditions and catastrophic wildfires in the region.

Chapter 5 – The influence of soil moisture–temperature coupling on compound hot and dry conditions over South America: historical and future perspectives

The results and conclusions obtained in the previous chapters point to two major evidences: (i) the recent escalation of CDHW episodes over SA in recent decades and (ii) the synergy between dry and hot extremes through enhanced land–atmosphere feedbacks. Similar outcomes have been documented for other regions of the globe as many studies in recent years have focused their attention on this problem from a historical perspective. However, many questions remain unanswered when it comes to analyzing this research topic in a future climate change context. This was the main motivation behind the formulation of RQ5 and RQ6 and the analysis development included in Chapter 5.

Therefore, the main goal stated for Chapter 5 was to assess how the soil moisture–temperature coupling dynamics will evolve in a future climate change scenario, addressing to which point changes in this coupling mechanism will produce an increment in the occurrence of summer CDHWs. This was done using a multi-variable weighted ensemble based on CORDEX-CORE runs for SA, aiming to provide new evidences on how processes beyond the already expected increasing temperature trends may affect the future spatiotemporal dynamics of CDHW events. Furthermore, a link with Appendix C was established, addressing, once again, RQ3 (Figure 1.2). This supplementary section of the thesis presents an analysis conducted with the same CORDEX-CORE runs, forced with the same climate change scenarios (RCP2.6 and RCP8.5), and it points, similarly to Chapter 5, to a future increment of heatwaves over SA. As a result of this increase, it also extrapolates, using a statistical regression model, that favorable conditions for fire spread and consequent large burned areas are expected to occur more often in the future. Chapter 5 indicates that part of this escalation in the heatwave incidence may be explained by a strengthening of the soil moisture–temperature coupling.

A broad assessment throughout SA is provided, and overall, a future increase in summer CDHW episodes is expected over most of the continent, even when the effect of the global warming trends is disregarded. It was shown that a future strengthening of the soil moisture–temperature coupling, among other non-linear processes, will likely and partially explain the future increment of these compound conditions, particularly over central SA. On the other hand, it was concluded that over other regions of the continent, the future increase in the covariance between temperature and soil moisture is not followed by any significant change in this land–atmosphere feedback, unraveling a likely influence of other local and/or large-scale atmospheric processes driven by the dynamics of the climate system (e.g., strong temperature advection, enhanced shortwave radiative heating, lack of moisture advection and convergence). It is known that climate models often struggle to simulate these non-linear mechanisms. So, in this context, these outcomes underline the need to improve their representation in modeling experiments. With this, one can reasonably conclude that RQ5 and RQ6 were addressed in detail in Chapter 5 and that all the implicit challenges and queries found a solid and clear answer.

Appendix A – Assessing the role of compound drought and heatwave events on unprecedented 2020 wildfires in the Pantanal

In Appendix A, the main topic of this thesis, centered on the assessment of CDHW events over SA, was studied and discussed from an entirely different perspective. The idea was, from a cascading natural hazard approach, to estimate the contribution of CDHW episodes to the onset of extreme fire outbreaks in the Pantanal, with a particular focus on the dramatic 2020 fire season. Considering that this analysis used the same spatiotemporal window as the one adopted in Chapter 4 (i.e., Pantanal biome on CESA, during the 2019–2022 period) and that the case-study event under consideration was also the same (i.e., the historical 2019–2022 drought), there was a mutual complement between the two analysis that represented added value for the thesis (Figure 1.2).

The crucial influence of land–atmosphere feedbacks on the simultaneous occurrence of dry and hot spells and, ultimately, to the exacerbation of the fire risk in Pantanal was highlighted. These dry and hot spells found a match, in space and time, with the flash drought episodes addressed in Chapter 4 and that affected the region. These daily-to-weekly periods with maximum temperatures, on average, 6 °C above the normal, accounted for 55% of the total burned area recorded in the 2020 fire season. This was the most catastrophic fire season

observed over the last two decades in Pantanal, showing a correspondence in terms of severity, with the record-breaking 2019–2022 drought in CESA. Moreover, the vulnerability in the northern forested areas of Pantanal was higher than in the other areas, revealing a synergy effect between fuel availability and weather-hydrological conditions.

Appendix B – Drought–heatwave nexus in Brazil and related impacts on health and fires: A comprehensive review.

The rationale behind this Appendix section was to provide a review synthesis of the impacts associated with CDHW episodes, particularly on fire occurrence and public health in Brazil. To do this, this review relied on case-study events, methods and results similar to the ones shown in Chapters 2, 3 and 4. Therefore, and likewise Appendix A, this section stands as a supplement to the analysis conducted and presented in these three sections of the thesis, aiming to explore and address RQ3 more extensively (Figure 1.2).

In recent decades, Brazil has witnessed dramatic wildfire occurrences, partially fueled by a synergy between CDHW events and fire activity. The recent catastrophic 2020 fires in the Pantanal and the 2005, 2010 and 2015 wildfires in Amazon are clear examples of this link. It was also concluded that the outstanding and long-lasting heatwaves during the 2013/2014 and 2014/2015 warm summers were responsible for increasing mortality and preterm births in SEB. As shown in Chapters 2 and 3, these record-breaking hot spells were proven to be amplified by co-occurring conditions of extreme soil dry-out.

Appendix C – Heatwaves and fire in Pantanal: Historical and future perspectives from CORDEX-CORE

The main idea for this Appendix section was to characterize the relation between heatwaves and fire in Pantanal during the recent decades and assess future trends under a climate change scenario, exploring simultaneously RQ3, RQ5, and RQ6 (Figure 1.2). Thus, this study overlaps, on both the research topic and the spatiotemporal domain considered, the analysis shown in Chapter 5.

First, it was demonstrated for the historical period, that the occurrence of heatwave conditions was associated with an exacerbation of fires in Pantanal and to above normal levels of burned area. It was observed that heatwaves during the dry season explained 82% of the interannual variability of burned areas during the fire season. The second part of the work

highlights the future evolution of these variables under a climate change scenario (RCP2.6 and 8.5), applying the same datasets used in the analysis included in Chapter 5. It was concluded that under RCP2.6, a doubling in the Pantanal heatwave incidence during the dry season is expected by the second half of the 21st century, followed by a plateauing. Alternatively, under RCP8.5, it is estimated a steady increase in heatwave incidence until the end of the century, unraveling a dramatic scenario in which heatwave conditions would be observed nearly over all the Pantanal area and during practically all the days of the dry season.

Based on this projection, assuming the regression model's statistical robustness under future climate change conditions, stationarity on several aspects such as the land cover, heatwave and drought indicators, and that no mitigation measures are adopted, it was possible to extrapolate that the extreme fire incidence during the dramatic 2020 fire season will be the new normal by the end of the century.

6.2 Final Remarks

The thesis concludes that some regions of SA have been witnessing a significant increment in the frequency and magnitude of CDHW events over the recent decades. This is in line with the trends observed for other regions of the globe that have been broadly analyzed in recent years (Hao et al. 2018; Yu and Zhai 2020; Mukherjee and Mishra 2021). It was also demonstrated how this increasing trend is expected to be maintained or even further amplified by the end of the century, highlighting the effect of under-examined non-linear processes. In a global context, this corresponds to one of the few attempts made so far to explore the effect of land–atmosphere feedbacks on the historical and future changing patterns of droughts and heatwaves (e.g., Seo and Ha 2022). For SA and to the best of our knowledge, this is the first study exploring this link, emphasizing the novelty of the outcomes presented here.

In contrast to other regions of the globe (Miralles et al. 2014; Schumacher et al. 2019, 2022b; Lemus-Canovas et al. 2024), little was known for SA about the effect of land–atmosphere feedbacks on the re-amplification and self-propagation of hot and dry spells, and the occurrence of record-breaking heat stress conditions. Throughout this thesis, a particular focus was given to specific case-study CDHW events, allowing to conclude that densely populated urban settlements, with millions of inhabitants, are highly vulnerable to extreme heat exposure. Similarly to what Schumacher et al. (2022a) showed for the 2021 Pacific Northwest heatwave, Sousa et al. (2020) demonstrated for the 2019 European heatwaves and Miralles et

al. (2014) revealed for the 2003 European and 2010 Russian mega-heatwaves, here it was concluded that record-breaking heat stress conditions over megacities in SA result from a combination of several dynamical forcing mechanisms and land–atmosphere interactions. The thesis also concludes that other severe CDHW episodes with a larger spatial and temporal scale, linked to catastrophic wildfires and harmful public health impacts in SA, result from this complex network of physical processes with a distinct nature, source and spatiotemporal signature. It became clear the urge to better comprehend the multitude of processes involved in the development of CDHW conditions. Therefore, future work should strive to explore deeper this subject and to employ a broad analysis to account, as much as possible, for all the meanders of climate change. Otherwise, a misrepresentation of the causes and dynamics associated with CDHW events might occur, ultimately leading to an underestimation of the natural and socioeconomic impacts. Moreover, more attention should be given to regions such as SA, which have rich and unique ecosystems that play a key role in global climate regulation (Mitchard 2018). Currently, four-fifths of the population in SA live in urban areas of countries that have been showing a lack of planning for health adaptation and a failure in delivering adaptation measures in proportion with the rising risk that the population faces (Hartinger et al. 2023).

Finally, it is important to emphasize the relevance of all these outcomes. Such a conclusion arises not only from the fact that these findings represent a valuable contribution to the documentation of a subject that has been barely explored for SA, but also because they call attention to a potential under-examined positive feedback in the climate system (Figure 1.1). In line with this, some sections of the thesis have shown, on one hand, how land–atmosphere interactions are affected by climate change (Chapter 2 and 5), while others have demonstrated how the interplay between land-surface and atmosphere may also impact the climate itself through changes in the surface heat balance and the frequency and magnitude of hot and dry extremes (Chapter 3 and 4). With this, the thesis shows that an underestimation of the range of impacts caused by climate change might be real if we fail to account for non-linear warming processes like this one (Hsu and Dirmeyer 2023; Qiao et al. 2023). With all these conclusions, the thesis becomes wrapped up with a complete framework, providing a chronological answer to the following points: (i) What happened in the recent past and how did we get here? (ii) What explains from a scientifically based approach the near-present conditions? (iii) What should we expect in a future climate change scenario? Hopefully, this will help authorities and the scientific community to better understand climate extremes and to better predict and mitigate their occurrence.

6.3 Limitations

Even though the thesis presents novel and relevant outcomes, there are still some limitations surrounding the methods and the results. Hopefully, they could be used as inspiration and motivation to test new ideas and research lines, paving the way for future and complementary work. A point-by-point discussion is presented below:

- The assessment shown in Chapter 2 ended up being, spatially, a bit reductive, considering that it was conducted for a particular region of Brazil and thus for a small section of SA. At the time, due to a lack of studies focusing on this region, the analysis provided outcomes shrouded by a high level of novelty, representing an important starting point for more studies of this kind (Olmo et al. 2022; Collazo et al. 2023). However, compared to all the other assessments that have been published since then, and as mentioned previously, there´s an added value obtained from the alternative methodology adopted here, where other non-linear mechanisms driving CDHW trends are highlighted. Therefore, it would be of extreme relevance to expand this analysis to all the territory of SA and to a longer time period given that ERA5 reanalysis updated its product in the meantime and made available a new dataset from 1940 onwards.

- The case-study character of Chapter 3 has some inherent limitations due to the specificity, in space and time, of the analysis. A similar framework should be applied to other urban areas in SA and to more recent episodes in order to better understand, from a such detailed and wide perspective, the causes for harmful heat-stress conditions that affect human's well-being, particularly in vulnerable population groups, that in SA, represent a large majority of the inhabitants (dos Santos et al. 2024).

- Most of the results included in the thesis are supported by data from reanalysis and remote sensing-based models. Although they all correspond to state-of-the-art modelling experiments (Miralles et al. 2011; Hersbach et al. 2020; Muñoz-Sabater et al. 2021), some valid concerns about the fidelity of these products may rise, particularly for variables such as precipitation, evaporation and soil moisture (Beck et al. 2021; Lavers et al. 2022). However, for studies of this kind, covering such a wide area and time period, there is no other option but to use reanalysis models to ensure data with a minimum spatial and temporal consistency. This becomes even more evident when the region under consideration is SA,

where observational datasets have so often poor quality and are based in very sparce *in situ* stations (Dorigo et al. 2021). Nevertheless, it is important to emphasize that soil moisture data from ERA5, ERA5-Land and GLEAM show a good performance when compared to other products including satellites and other models with and without assimilation (Beck et al. 2021). In fact, ERA5 simulation of variables such as precipitation and temperature for SA, that are afterwards assimilated by ERA5-Land and GLEAM to estimate soil moisture, follow observations very closely when comparing to other known reanalysis (Coronato et al. 2020; Hassler and Lauer 2021; Balmaceda-Huarte et al. 2021). In conclusion, reanalysis models are not ideal, however, considering the even greater limitations surrounding other datasets, they are often the best option available to perform studies of this kind.

- Part of the results, particularly the ones included in Chapter 5, are inevitably bound to some level of uncertainty that surrounds climate models. This is more critical when it comes to simulating the future trajectory of hydrological variables such as precipitation and evaporation, that strongly depend on dynamical processes of the climate system as well as on other less-explored non-linear mechanisms (Zhang et al. 2021; Wood et al. 2021; Petrova et al. 2024). Recently, some divergence has been noted between what climate models predicted few years, in their future climate change scenarios, and what has been actually observed in the last decades over SA. Several studies, in line with this thesis' results, have been showing that climate models point for a dipole pattern of drier conditions centered in the Amazon basin and wetter conditions prevailing in the central-eastern parts of the continent (Reboita et al. 2014; Llopart et al. 2020; IPCC 2021). However, the recent observed drying trends over CESA, reported here in Chapter 4, raise some valid questions about the confidence level of these projections. The mismatch between what climate models predicted years ago and what we have been actually observing since then, might be related to an already reported lack of skill from models in simulating internal variability and key atmospheric features associated with large-scale modes of variability (Fatichi et al. 2016; Peleg et al. 2019). This was considered particularly in the analysis included in Chapter 5. Therefore, an effort was made to minimize this uncertainty by adopting a methodology that allowed to compute the results based on runs from the CORDEX experiment, from a multi-weighted ensemble that considers multi-variable performances. This approach contributed to increasing the level of robustness of the analysis as it has been proven to be advantageous when compared to the usual democratic multi-model ensemble (Eyring et al. 2019; Cos et al. 2022; Lima et al. 2023).

- Finally, and considering the recent global CO_2 emissions over the last years, there's a chance that we might have considered in Chapter 5 and in Appendix C, two unrealistic scenarios. The 2023 estimate for the global CO_2 emissions is closer to the middle-of-the-road RCP4.5 and far from RCP2.6 and RCP8.5 trajectories (Rozenberg et al. 2015; Liu et al. 2024). However, these RCPs are the only two climate change experiments provided by the set of regional climate models used here and that accommodate all the requirements needed to produce the analysis. This leaves an open door for further improvements and future work that could take advantage of the CMIP6 output for regional climate downscaling, that is expected to be fully available for the scientific community in the next couple of years (Gutowski Jr. et al. 2016).

6.4 Deliverables during the thesis

Three first-author (Chapters 2,3 and 4) and three second-author (Appendix A, B and C) peer-reviewed articles were published in the context of the PhD project. Chapter 5 includes a relevant analysis that, after some minor adjustments, is ready to be submitted and to be, potentially, published as a peer-reviewed article.

The results obtained during this 4-year period were presented at different national and international conferences as oral and poster communications (see Curriculum Vitae). The first two years of the PhD project were also marked by the presence in the Paper-Writing Workshop on Regional Climate Modeling organized by the CORDEX Central America and South America group (http://www.cima.fcen.uba.ar/cordex-2020/). This workshop was important to promote collaborative activities and networking focusing on regional climate phenomena. Thus, it allowed me to obtain, within the PhD framework, more know-how, expertise and working skills that were essential to address RQ5 and RQ6 and, therefore, to perform the analysis included in Chapter 5 and Appendix C. The presence in the Training School (Training School on Dynamical Modelling of Compound Events http://damocles.compoundevents.org/school.php?id=2) organized by the European COST Action DAMOCLES (CA17109), was also important for the project considering that it represented a chance to collaborate with colleagues that share the same working interests. The main outcome from this training school was the start of a project that aimed to perform a downward counterfactual analysis of compound tropical cyclone risk, and to get new perspectives and insights about the analysis of extreme climatic events from a compound event

framework. Throughout this period of four years there was also the chance to contribute as a co-supervisor to two Bachelor's degree final projects.

Finally, it is important to mention that several other collaborations with IDL researchers were established, particularly in the design and development of the FCT (Fundação para a Ciência e Tecnologia) funded project DHEFEUS (https://dhefeus.rd.ciencias.ulisboa.pt/). The project aims to contribute to the knowledge on compound or cascading weather/climate events, namely droughts and heatwaves, and further associate them to the occurrence of wildfires and pollution events in Europe and South America. Other minor collaborative projects were developed during the PhD project with colleagues from the Federal University of Rio de Janeiro and Ghent University, particularly during my stays in these two institutions (for more information, please see Curriculum Vitae).

6.5 Take home message

This thesis underscores a critical increase in CDHW events across SA. This upward path observed in the recent years will likely maintain its trajectory in the coming decades. As a result, SA faces heightened risks of unprecedented droughts, extreme temperatures, and destructive wildfires, threatening ecosystems and human well-being. These findings call for improved climate models capable to incorporate the complex feedback mechanisms highlighted here, aiding in the design of effective and informed mitigation strategies. This should draw the attention of scientific community and local authorities for the enormous challenge they currently face. In particular, it is crucial to gain a more profound understanding of what the future holds regarding the causal relation between land–atmosphere feedbacks and climate extremes. The impact of climate change via severe heat stress conditions and soil dryness will be determined by the nature and strength of this relation. Now that the theoretical background has been refined, it is time to move to practice and to build a more resilient future for the next generations.

Appendix A

Assessing the role of compound drought and heatwave events on unprecedented 2020 wildfires in the Pantanal

*Libonati R, **Geirinhas JL**, Silva PS, Russo A, Rodrigues JA, Belém LBC, Nogueira J, Roque FO, DaCamara CC, Nunes AMB, Marengo JA, Trigo RM. (2022) Assessing the role of compound drought and heatwave events on unprecedented 2020 wildfires in the Pantanal. Environ Res Lett 17:15005. https://doi.org/10.1088/1748-9326/ac462e*

João Lucas Geirinhas contributions: *conceptualization of the analysis, data management (download and curation), computation and analysis of the results, production of figures and manuscript writing.*

Abstract

The year 2020 had the most catastrophic fire season over the last two decades in the Pantanal, which led to outstanding environmental impacts. Indeed, much of the Pantanal has been affected by severe dry conditions since 2019, with evidence of the 2020's drought being the most extreme and widespread ever recorded in the last 70 years. Although it is unquestionable that this mega-drought contributed significantly to the increase of fire risk, so far, the 2020's fire season has been analyzed at the univariate level of a single climate event, not considering the co-occurrence of extreme and persistent temperatures with soil dryness conditions. Here, we show that similarly to other areas of the globe, the influence of land-atmosphere feedbacks contributed decisively to the simultaneous occurrence of dry and hot spells (HPs), exacerbating fire risk. The ideal synoptic conditions for strong atmospheric heating and large evaporation rates were present, in particular during the HPs, when the maximum temperature was, on average, 6 °C above the normal. The short span of the period during those compound drought-heatwave (CDHW) events accounted for 55% of the burned area of 2020. The vulnerability in the northern forested areas was higher than in the other areas, revealing a synergistic effect between fuel availability and weather-hydrological conditions. Accordingly, where fuel is not a limiting factor, fire activity tends to be more modelled by CDHW events. Our work advances beyond an isolated event-level basis towards a compound and cascading natural hazards approach, simultaneously estimating the contribution of drought and heatwaves to fueling extreme fire outbreaks in the Pantanal such as those in 2020. Thus, these findings are relevant within a broader context, as the driving mechanisms apply across other ecosystems, implying higher flammability conditions and further efforts for monitoring and predicting such extreme events.

A. Assessing the role of compound drought and heatwave events on unprecedented 2020 wildfires in the Pantanal

A.1 Introduction

In 2020, the world witnessed one-quarter of the Brazilian Pantanal, the largest continuous tropical wetland, on fire (Junk et al. 2011; Libonati et al. 2020). More than 3.9 million hectares were burned, an area four times larger than the long-term average observed between 2001 and 2019 (Damasceno-Junior et al. 2021; Garcia et al. 2021). The Pantanal 2020 fire (hereafter P20F) season may have directly affected 17 million native vertebrates (Tomas et al. 2021) and resulted in total national economic losses of ~USD 3.6 billion (Podlaha et al. 2020).

These extremely intense impacts inevitably raise the doubt: why was the P20F so exceptional? Evidence is mounting that the P20F resulted from a complex interplay of distinct contributing components, including human factors, landscape characteristics, and adverse meteorological conditions (Libonati et al. 2020; Marengo et al. 2021). Globally, the year 2020 tied with 2016 for the warmest year on record since record-keeping began in 1880 (NASA, 2021), with several record-breaking temperature (compounded) events taking place in different regions. The 2019/2020 mega-fires in Australia were tightly linked to record-breaking temperatures, both induced to a large extent, by widespread prolonged severe dryness (Boer et al. 2020; King et al. 2020; Collins et al. 2021). The 2020's catastrophic fires in California were enabled by long-lasting dry conditions across much of western U.S (Higuera and Abatzoglou 2021). Among the 2020´s unprecedented climate conditions favoring fire activity in Oceania, Euro-Asia and North America, South America (SA) was not an exception (Mishra et al. 2021). Extreme dry conditions were reported in countries across central-south SA, reaching Argentina, Brazil, Bolivia and Paraguay (Rivera et al. 2021; Thielen et al. 2021). Much of SA has been in drought since 2019, influenced by a warming trend in the sea surface temperature of Pacific and Atlantic Oceans (Thielen et al. 2020, 2021; Rivera et al. 2021).

The extremely dry conditions across central-south SA were accompanied by heatwave (HW) episodes throughout the austral spring which triggered record-breaking daily maximum temperatures (Marengo et al. 2022). In Brazil, between the end of September and early November, when anomalies were persistently above 5 °C in the central and southeastern

regions, including the Pantanal (WMO 2021; Marengo et al. 2022), several warnings of the HWs' risk were issued.

Previous studies suggest that the P20Fs were strongly influenced by the most extreme drought recorded in the region since 1950 (Libonati et al. 2020; Marengo et al. 2021, 2022) which was accompanied by the occurrence of several prolonged periods of extremely high temperatures. Compound drought-HW (CDHW) events usually cause more severe wildfires than single events of drought or HW alone (Sutanto et al. 2020) and are being routinely reported worldwide (Miralles et al. 2012, 2014; Schumacher et al. 2019; Sousa et al. 2020; Dirmeyer et al. 2021; Mukherjee and Mishra 2021), including in Brazil (Geirinhas et al. 2021). Although understanding the factors that influence the regional occurrence of a CDHW event is imperative, so far, its characterization and association with fire outbreaks have not been fully explored in wetlands such as the Pantanal. Thus, this study aims to assess, for the first time, the severe CDHW conditions and the land-atmosphere feedbacks associated with the P20Fs. A detailed analysis of the exceptional P20F season is provided together with the spatial and temporal analysis of surface conditions and the associated synoptic patterns. The present approach provides a more comprehensive understanding of the physical land-atmosphere coupling mechanisms associated with this extreme climate event, highlighting its dominant role in the observed record-breaking fires.

A.2 Data and methods

A.2.1 Datasets

Burned area (BA) was obtained from two main sources. Monthly values were obtained from the MCD64A1 collection 6 derived from the MODIS (moderate resolution imaging spectroradiometer) sensor at 500 m spatial resolution from 2001 to 2020 (Giglio et al. 2018). For improved accuracy on day-to-day variability of BA (Pinto et al. 2020), daily values for 2020 were obtained through the ALARMES dataset with a 500 m spatial resolution using images from the visible infrared imaging suite imager sensor (Pinto et al. 2020).

Meteorological parameters, including maximum temperature (*T*max), precipitation, surface net solar radiation, geopotential height and temperature at several levels of the atmosphere were extracted, at daily scale, from the European Centre of Medium-range Weather Forecast ERA-5 reanalysis dataset (Hersbach et al. 2020). Soil moisture, evaporation and

potential evaporation, at daily scale, were obtained from the Global Land Evaporation

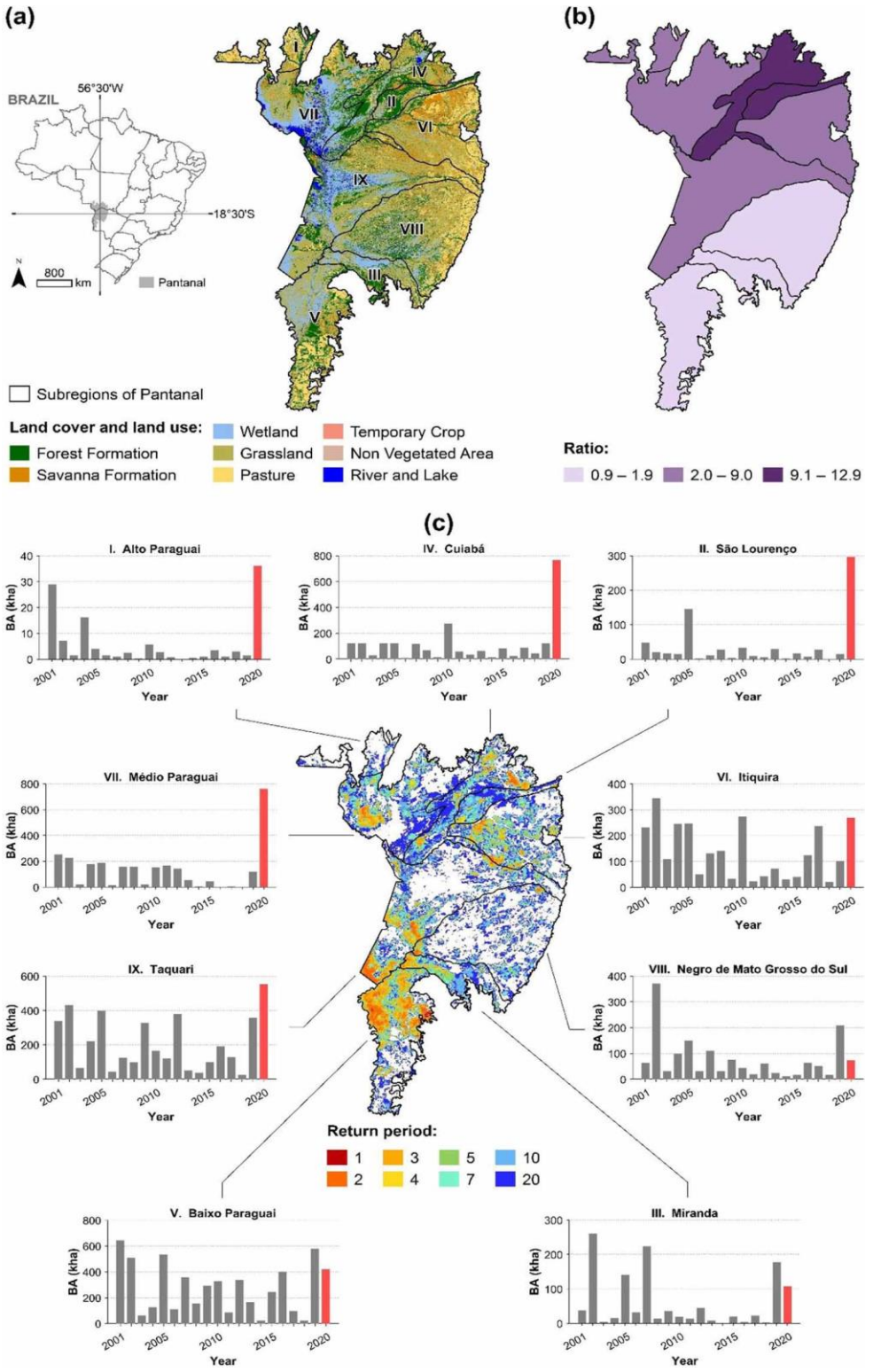

Figure A.1 (**a**) Location of Pantanal within Brazil (left) and the nine hydrological subregions with land cover and land use information from the MapBiomas Collection 5 (right). (**b**) Subregional ratio between the area burned in 2020 and the mean annual BA (2001–2019), colors represent: light purple for values ⩽ percentile 25, purple for value between percentiles 25 and 75 (included), and dark purple for values >percentile 75; (**c**) Return period (central map) and annual variability of BA in each subregion (2001–2020) (associated plots). Each subregion is labelled according to table S1, and values estimated using the MCD64A1 product.

Amsterdam Model (GLEAM v3.5a) (Miralles et al. 2011; Martens et al. 2017). All variables were retrieved at a gridded 0.25°×0.25° spatial resolution and the composite anomalies were computed with respect to the climatological seasonal cycle (1981–2010).

Surface meteorological fire danger conditions were evaluated using the fire weather index (FWI) , allowing summarizing the chances of a fire to ignite and propagate and to foresee hazardous fire conditions (Rodrigues et al. 2021). The FWI product is provided by the Copernicus Emergency Management Service (Vitolo et al. 2020), computed with meteorological fields from the ERA5 reanalysis (Hersbach et al. 2020). Daily values were obtained for the historical period (1980–2020) on a regular grid of 0.25° × 0.25° resolution (Di Giuseppe et al. 2016). All analyzes were carried out for the Brazilian sector of the Pantanal wetland.

A.2.2 Methodology

A2.2.1 Fire analysis

To assess the exceptionality of the P20Fs we considered the ratio between the total BA in 2020 and the respective mean BA for the 2001–2019 period. We also estimated the fire return period, defined as the ratio between the 20 years that encompass our study period (2001–2020) and the annual recurrence. Finally, we computed the 75th percentile (P75) of the 2001–2019 period and the percentage of the 2020 BA with no fire and low recurrence (1–2 years). The above-mentioned metrics were computed for each of the nine hydrological subregions of Pantanal, to evaluate regional discrepancies within the biome (Figure A.1a).

A2.2.2 Heat Wave identification

HW was defined as a period of three or more consecutive days with daily *T*max values above predefined climatological (1981–2010 base period) percentiles (80th, 90th and 95th) of *T*max for each calendar day (on a 15-day moving window). Based on this definition, a secondary metric was computed: the percentage of the Pantanal domain under HW conditions ($\%Pantanal_{HW}$). This method was already used in previous studies conducted for the USA (Mazdiyasni and AghaKouchak 2015) and Brazil (Geirinhas et al. 2021) and consists of determining the yearly percentage of the total Pantanal cells ($cellsPAN_{total}$) that experienced HW conditions:

$$\%Pantanal_{HW} = \frac{cellsPAN_{HW}}{cellsPAN_{total}} \times 100 \quad \text{(A. 1)}$$

Per year, the number of total cells ($cellsPAN_{total}$) is obtained by considering the total number of grid-points within the region ($cellsPAN_{region}$) and the hypothetical total number of days that could experience HW conditions ($cellsPAN_{time}$):

$$cellsPAN_{total} = cellsPAN_{region} \times cellsPAN_{time} \quad \text{(A. 2)}$$

In our particular case, the $cellsPAN_{time}$ corresponds to the total number of days of the fire season in the Pantanal (July to October) (Damasceno-Junior et al. 2021). For instance, for a particular year, a percentage of 100% indicates that all the Pantanal experienced HW conditions during all the fire season days.

A2.2.3 Drought conditions

Drought conditions were assessed by analyzing soil moisture anomaly composites and monthly standardized precipitation index (SPI) values (Svoboda et al. 2012) from 1980 to 2020, using a 6 month accumulation timescale (SPI-6) and precipitation from ERA5 reanalysis as input data. SPI is widely used to characterize drought conditions using a purely meteorological perspective: it indicates the number of standard deviations by which the observed precipitation anomaly deviates from the long-term mean in a particular location. To better assess the long-term tendencies (quantified by applying a 1st-degree polynomial regression) and interannual variability, we further analyze the temporal evolution of key average meteorological parameters over the fire seasons between 1980 and 2020.

A2.2.4 Relating fires with the heatwave/drought conditions

We first identified the temporal evolution of each hazard (fire, HW and drought) at the daily scale for the entire Pantanal allowing the identification of concurrent behavior, i.e., co-occurrence of two or even three of these hazards. Since the Brazilian Pantanal is quite large, we also analyzed the co-occurrence of the multiple hazards for each one of the nine hydrological subregions. During the fire season, we calculated, at the subregional level, the percentage of the BA during the identified hot periods (HPs), defined here as consecutive HWs separated by days with a short heat-stress relief and under drought conditions.

A.3 Results

A.3.1 The 2020 fire season in perspective

The P20Fs show an increase in BA for almost all subregions ranging from ~60% to 1190% of the historical mean value (Figure A.1b). Higher ratios are found in the northern subregions, namely São Lourenço (II) and Cuiabá (IV), which burned ~65% and 55% of their area in 2020 (Table SA.1 available online at stacks.iop.org/ERL/17/015005/mmedia), respectively. These values were absolute outliers within the historical series (Figure A.1c), as so far these subregions had burned a yearly average of ~5.1% and 5.8% (Table SA.1), respectively. In the P20Fs only one subregion burned less than its annual average over the 2001–2019 period: Negro de Mato Grosso do Sul (VIII); which, along with Miranda (III) and Baixo Paraguai (V), obtained the lowest ratios to historical mean values (Figure A.1b). Historically, the northern regions are characterized by lower return periods, whereas the southern regions burn more regularly (Figure A.1c). However, this historical tendency was reversed in 2020, when most of the BA was in forested areas of northern Pantanal. Conversely, southern and south-eastern subregions, characterized by large extents of pasture and grasslands (Fig. A.1a), burned considerably in 2020 but did not reach record levels. Nevertheless, with the exception of Negro de Mato Grosso do Sul (VIII), the BA from the P20Fs went above P75 of the historical time series for all southern subregions (Table SA.1).

Most subregions in the Pantanal burn within a 4-month period from July to October (Figure SA.1) and, in this regard, 2020 kept as expected: a steady BA increase from July to September is seen in Pantanal, with a peak on 12 September (116 605 ha) and a secondary observed on 27 September (95 478 ha; Figure SA.1). Médio Paraguai (VII) and Taquari (IX) showed the earliest signs of burning in July, while the remaining subregions burned over August to October, and solely Baixo Paraguai (V) and Médio Paraguai (VII) showed considerable BA in the earlier weeks of November. The latter subregion burned consistently over a period of 5 months, severely contrasting with its historical series where BAs mainly occur in September and October. It is also worth noting how Médio Paraguai (VII) burned very little in previous years (2016–2018; Figure A1c).

Around a third of the BAs in the P20Fs had been undisturbed since 2001, and another 31% burned only once or twice over the entire study period (Table SA.1). Of the entire P20Fs, 64% of BAs were areas not accustomed to regular and systematic burning. Noteworthy are the cases

of Cuiabá (IV) and Médio Paraguai (VII) with ~18% and 19%, respectively, of areas that had not or barely burned within the last 19 years.

A.3.2 Compound drought and heatwaves

Results show unprecedented extreme heat conditions, with *T*max anomalies for the last two fire seasons over the Pantanal (2019 and 2020) positioned in the high-end tail of the empirical distribution of average *T*max anomalies (Figure A.2a). By contrast, the years 1992,

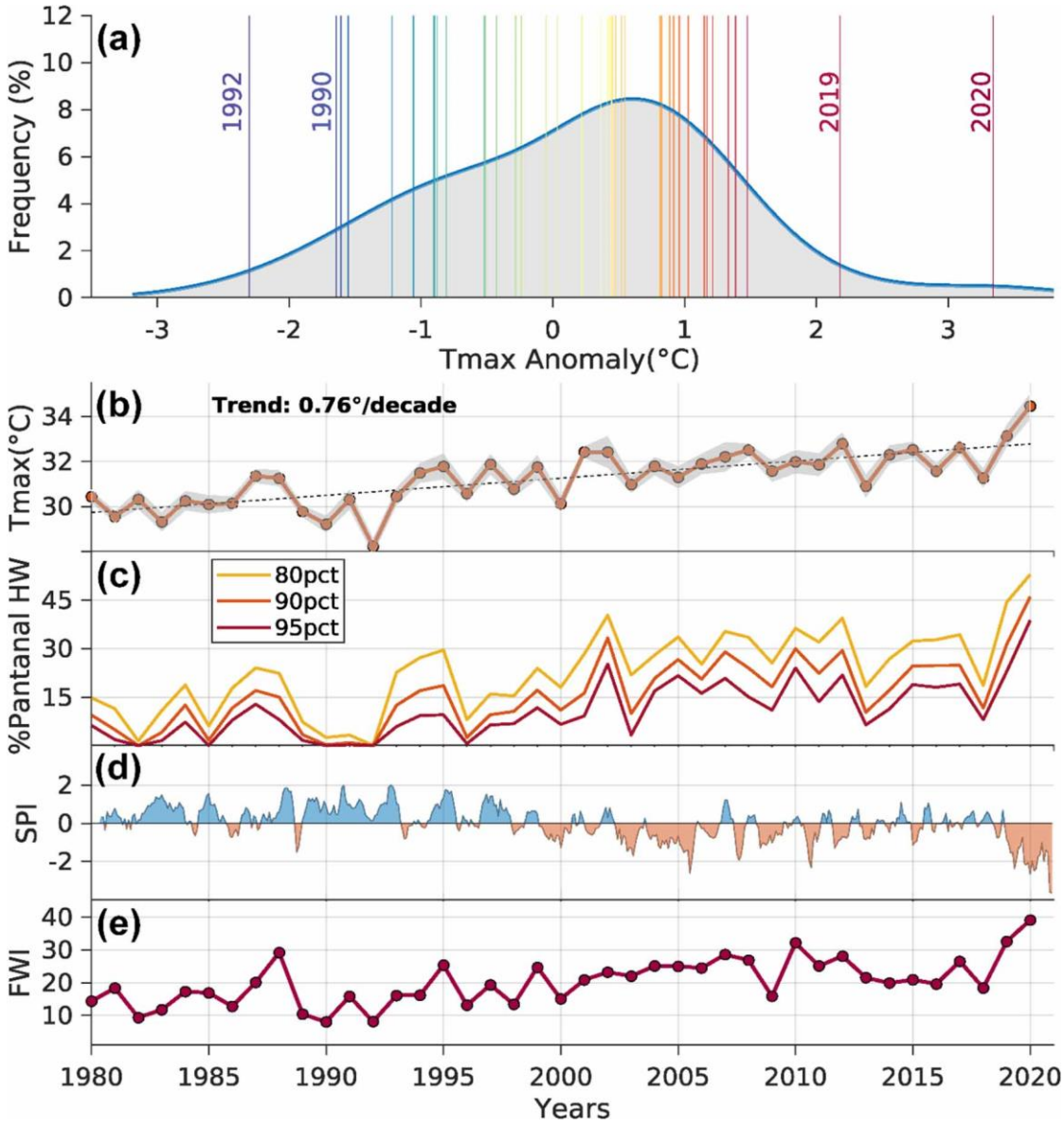

Figure A.2 (**a**) The grey shading shows the fit of a Kernel distribution function for the averaged Tmax anomaly values over the Pantanal (fire seasons between 1980 and 2020). Vertical colored lines indicate mean Tmax anomaly values during the fire seasons for specific years. (**b**) Temporal evolution from 1980 to 2020 of the Tmax average values for the Pantanal and during the fire season (orange line). The grey shading shows the Tmax variability by highlighting the area delimited by **mean (*Tmax*) + 2 std (*Tmax*)**. (**c**) Temporal evolution from 1980 to 2020 of the percentage of Pantanal in HW conditions: $\%Pantanal_{HW}$. (**d**) Temporal evolution from 1980 to 2020 of the SPI-6 and (**e**) fire season averaged FWI average values for the Pantanal.

1990, 1984 are in the low-end tail, as in general, the years within the first half of the analysis period. The time series of *T*max (Figure A.2b) is characterized by a pronounced and statistically significant positive trend of 0.76 °C per decade, responsible for warming throughout the last four decades of ~3 °C. Accordingly, the spatially averaged *T*max level during the P20F season was 34 °C, roughly 4 °C higher than the average for the first decade in the 1980s. The percentage of the Pantanal under HW conditions (Figure A.2c) followed, closely, the *T*max evolution (Figure A.2b). Because of this sharp warming trend, the spatial and temporal signature of HWs had marked increase, with unprecedented extreme heat conditions in 2020 as well. Analyzing the monthly SPI-6 values from 1980 and 2020 (Figure A.2d), one concludes that during the 21st century most of the fire seasons were preceded by the occurrence of precipitation deficits. As previously described, this period also marks a sharp increase in the Pantanal under HW conditions (Figure A.2b), indicating that after the turn of the century the CDHW conditions became more frequent, in particular for 2020. Accordingly, 2020 was also marked by record fire danger (Figure A.2e): fire season averaged FWI reached values above 30 for the second year in a row. Previously, 2010 held the highest value, consistent with widespread drought conditions in neighboring biomes (Panisset et al. 2018; Ribeiro et al. 2018). Higher fire danger values over the last two decades strongly contrast with those of the 20th century, with a significant positive trend over the last 40 years.

In general, 2020 was marked by the occurrence of numerous HW episodes over the Pantanal when the daily area-averaged *T*max values were considerably above the expected levels for several periods of three or more consecutive days (Figure A.3a and Figure SA.2). Thus, several HPs were also observed, particularly during the fire season. The first HP occurred from 26 August to 1 September, the second from 5 to 20 September and the third from 25 September to 15 October (red boxes in Figure A.3a).

Throughout 2020, a temporal match between the occurrence of HPs and increasing values of BA (Figure A.3a and Figure SA.2) was observed. However, it was during the austral winter and the three considered HPs that this temporal correspondence was more pronounced, indicating a close relationship between the induced atmospheric heat-stress conditions and the occurrence of fires. On average, the *T*max value for the three HPs was 38.5 °C, representing a staggering temperature anomaly of about 5.8 °C. In fact, on 1 October (the 6th day of the third HP) the mean *T*max value reached 41 °C, establishing a new record-breaking level for the region. A very similar value was observed nine days later on 10 October, defining this as a

period of outstanding extreme heat stress conditions. During this HP of 21 d, the *T*max values were on average 6.5 °C higher than the expected mean levels and a total of 983 900 ha burned, a value that accounts for 25% of the total BA recorded during 2020 in Pantanal. The BA recorded over the entire Pantanal during these three massive HPs accounted for 55% (60%) of the total 2020 (fire season) BA. In all subregions, with the exception of Baixo Paraguai, the BA observed during the three HPs accounted for more than 50% of the amount from the fire season. Moreover, in six of the nine subregions, this BA amount corresponds to more than two-thirds of the fire season, reaching 95% in Miranda (Figure SA.2).

The months preceding the 2020 fire season were marked by large deficits in precipitation (Figure A.2d), within the drought period. During the P20F season, precipitation levels were lower than expected, reaching zero or near-zero values for most of the days (Figure A.3b). Thus, the drought pattern and soil desiccation that initiated during the first months due to a drier wet season substantially amplified throughout the following months, leading to extreme negative anomalies of accumulated soil moisture (Figure A.3c). These precipitation deficits combined

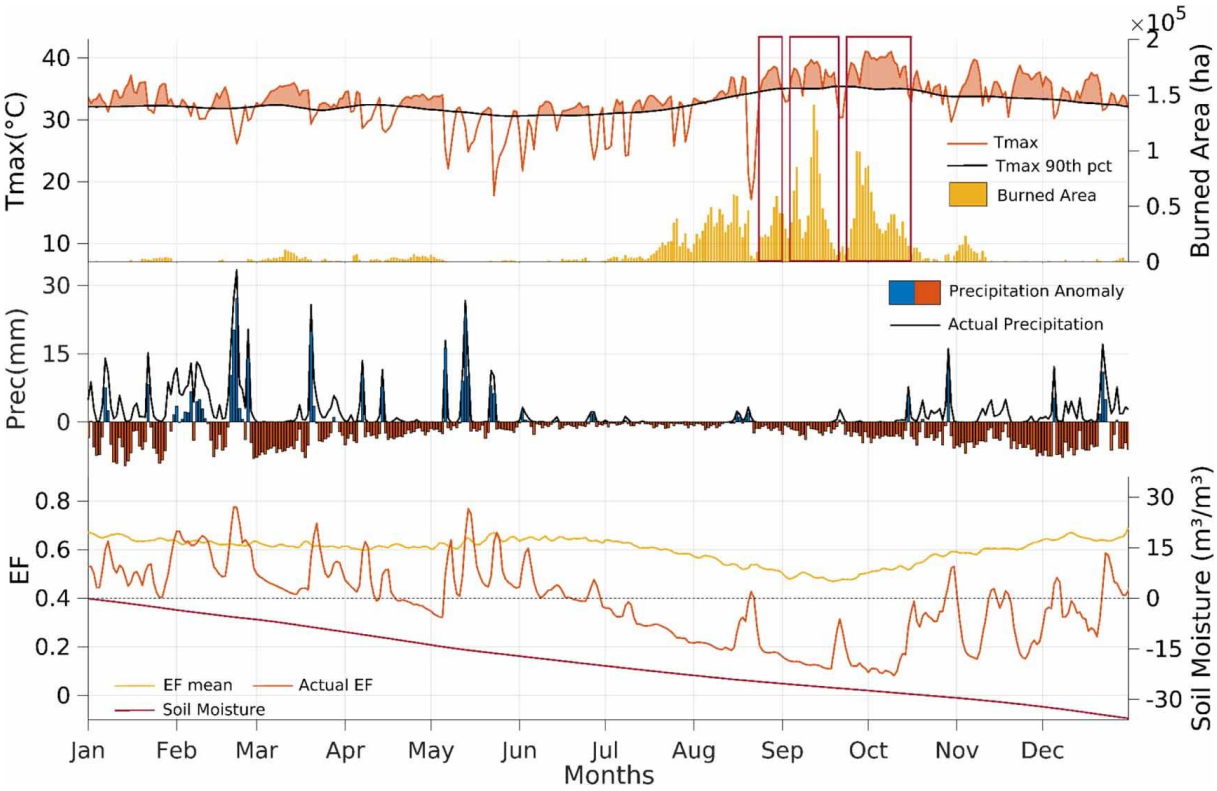

Figure A.3 (**a**) Time series from January to December 2020 of daily area-averaged Tmax values for the Pantanal (orange line) and the respective calendar day climatological (1981–2010 base period) 90th percentile (black line). Yellow bars indicate the daily total BA recorded (using the ALARMES product). (**b**) Time series of daily area-averaged precipitation levels (black line) and the respective anomalies (bars) regarding climatology (1981–2010 base period). (**c**) Time series of the observed and expected daily area-averaged evaporative fraction values (orange and yellow line, respectively). The red line indicates the daily accumulated area-averaged soil moisture anomaly values during 2020. HPs are highlighted in red rectangles in panel (**a**).

with clear sky conditions that were linked to large amounts of incoming shortwave radiative energy at the surface and enhanced diabatic processes (Figure A.3a), induced large evaporation rates from the surface to satisfy the high atmospheric demand for water. This combined process was crucial for the establishment of the pronounced soil moisture deficits and evaporative stress observed during the P20F season.

Concurring warm and dry conditions controlled the partitioning of water and energy fluxes at the surface. The evaporative fraction observed during 2020 followed very closely the precipitation and temperature regimes (Figure A.3c and Figure SA.2). Several periods marked by a sharp decrease in the evaporative fraction values were clearly paired with dry episodes combined with extremely hot conditions. Thus, negative anomalies of the evaporative fraction were a constant presence during 2020 (Figure A.3c and Figure SA.2). However, it was during the fire season that the values reached their minima indicating the presence of a strong soil moisture-temperature coupling regime (water-limited) in which disproportional surface losses in the incoming shortwave radiation through upward sensible heat flux allowed a re-amplification of the near-surface (air) temperatures. The atmospheric cooling through latent heat flux was then suppressed as well as the capacity of the surface to mitigate the low atmospheric humidity levels.

Finally, we evaluate the synoptic conditions that triggered the development of such CDHW events (Figure A.4). The spatial pattern of the 500 hPa geopotential height anomaly field indicates the presence of concentric positive anomalies during the second and third HPs over the Pantanal (Figure A.4b and c). During the first HP, positive anomalies were also observed. However, they resulted from a northwest extension of the high-pressure system located over the South Atlantic Ocean (Figure A.4a). Exceptional low-tropospheric heating was also recorded as it can be observed by analyzing the 850 hPa temperature anomaly field. These conditions represent an enhanced anomalous anticyclonic circulation pattern over the Pantanal. This continental high-pressure anomaly was widespread and responsible for the air subsidence, causing pronounced adiabatic heating at the surface, through air compression, as well as the persistent clear sky conditions that promoted enhanced diabatic heating at surface (Figure A.S3), low levels of humidity and the absence of precipitation episodes. Therefore, the ideal synoptic conditions for strong atmospheric heating and large evaporation rates were present throughout the P20F season, in particular during the third HP, when the *T*max values were, on average, 6 °C above the expected levels (Figure A.4f). Changes in the low tropospheric wind

configuration were also observed, showing the signature, close to the surface, of this anticyclonic circulation pattern. During the two first HPs, it can be observed that the wind pattern presented a higher-than-normal northeast–southwest orientation (Figure A.4d and e). This anomalous wind pattern was marked by a confluence throughout a north-south oriented asymptote towards south Paraguay (during the first HP), and throughout a northwest-southeast oriented asymptote towards southeastern Brazil (during the second HP). In fact, by analyzing the mean of the observed wind configuration recorded during these two periods (Figure SA.3a and b) one may conclude that air masses predominantly from the northeastern regions moved towards the Pantanal. During the third HP the 925 hPa wind pattern was substantially different (Figure A.4f and Figure. SA.3), showing an anomalous northwest-southeast orientation over the Pantanal. Nevertheless, a pronounced confluence similar to the one observed during the second HP was present. In fact, the asymptotes marking these regions of strong confluence were, for all the analyzed HP's, oriented towards the regions where the anomalies of *T*max were higher. This could indicate that the intense daytime heating in the low troposphere over these regions caused the lifting of air, imposing pronounced changes in the normal near-surface wind configuration.

Therefore, during three HPs, the ideal synoptic conditions, triggering high rates of potential evaporation from the occurrence of clear sky conditions linked to atmospheric subsidence (Figure SA.3), were observed over central SA, particularly in the Pantanal. However, due to the desiccated soil already observed at the time (Figure A.3b), the surface could not meet such atmospheric water demand. This led to low rates of actual evaporation and, consequently, to pronounced evaporative stress in the region (Figure A.3c) when extreme low levels of evaporative fraction were observed during these periods. The spatial pattern of the SPI-6 values, computed from the months when these HPs occurred, confirms severe meteorological drought conditions (Figure A.4g, h and i). An approximately northwest-southeast oriented broad region extending from northern Bolivia to southeastern Brazil, with Pantanal in its center, endured pronounced negative SPI-6 levels from August to October (ranging from −1 to −4). The soil moisture deficits during the three HPs (Figure A.4g, h and i) confirm this situation and are spatially consistent with the analysis of Figure SA.2 by showing the high potential of soil desiccation in inducing low levels of evaporative fraction. A similar situation was also observed southwards, particularly over southern Paraguay and over northern Argentina. It is noteworthy the spatial match between the regions with strong positive *T*max

anomalies and areas with negative soil moisture anomalies, emphasizing CDHW conditions, unequivocally associated with the land-atmosphere feedbacks over these SA regions and particularly over all subregions of the Pantanal (Figure SA.2).

A.4 Discussion and conclusions

Previous studies for several regions in the globe, markedly Europe, the Mediterranean, the USA and Australia, highlighted the key role played by land-atmosphere feedbacks in the amplification of fire episodes (Gouveia et al. 2016; Ruffault et al. 2020; Schiermeier 2021; Sharples et al. 2021). However, to the best of our knowledge, the inter-links played by CDHW

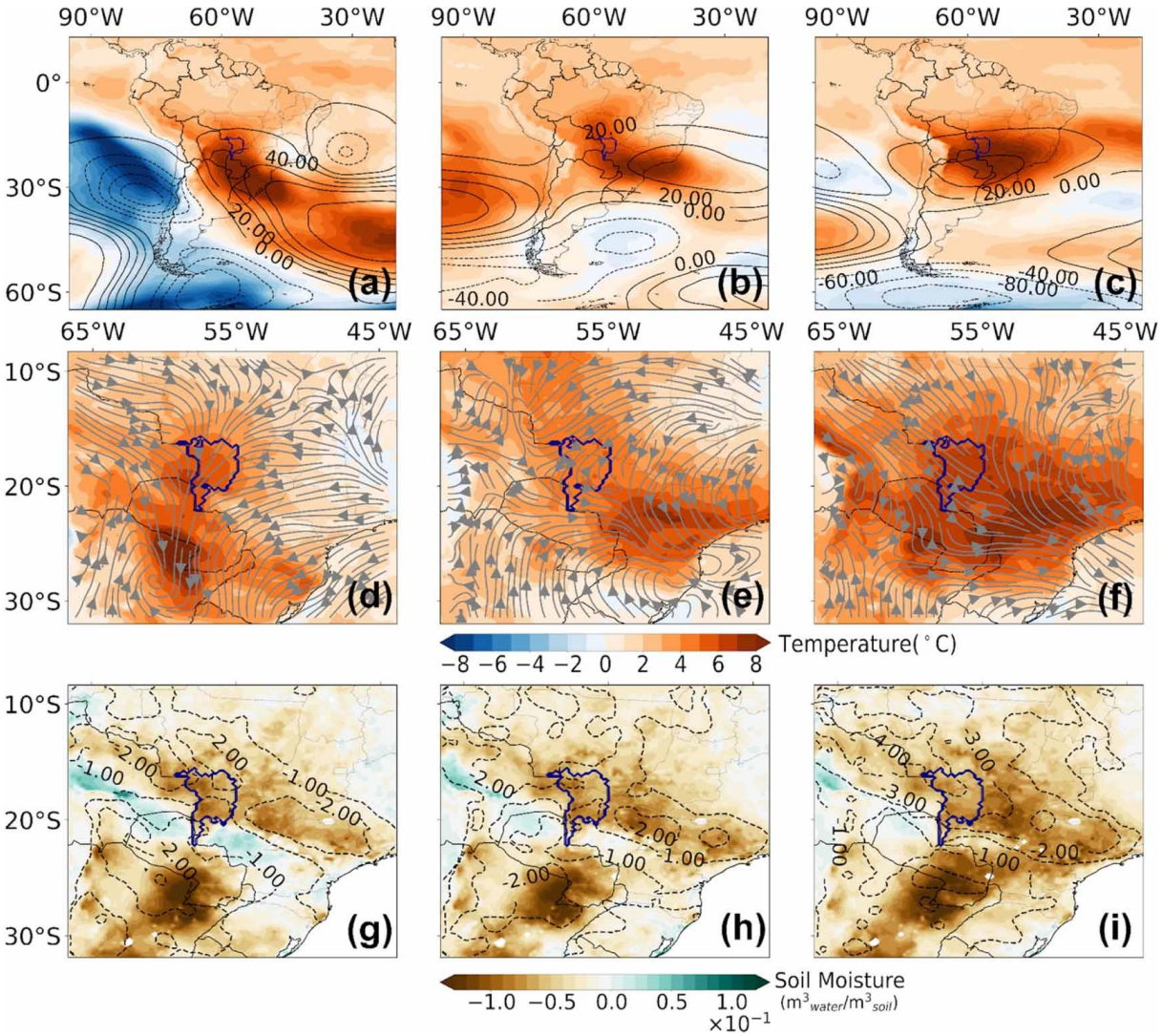

Figure A.4 (**a, b** and **c**) Spatial patterns of the 850 hPa temperature (°C, shading) and of the 500 hPa geopotential height (gpm, contours) anomaly composites for the (**a**) 1st HP (26 August to 1 September), the (**b**) the 2nd HP (5 to 20 September) and **c** the 3rd HP (25 September to 10 October). (**d**, **e** and **f**) Spatial patterns of the Tmax (°C, shading) and of the 925 hPa atmospheric circulation (streamlines) anomaly composites during the three previously considered HP (following the same panel order as in the first row). (**g**, **h** and **i**) Spatial patterns of the soil moisture (m^3_{water}/m^3_{soil}) average anomalies during the three previously considered HP (following the same panel order as in the first and second rows). Contours show the spatial patterns of the SPI-6 values for August (**g**), September (**h**) and October (**i**) 2020.

and fires in Brazil remained practically unknown, particularly in wetlands. Here, we provide evidence that the unprecedented P20Fs were favored by the joint effect of the observed drought and hot conditions. In fact, most of the P20Fs occurred simultaneously to CDHW episodes, which have fueled fires through two distinct mechanisms, in a cascading effect. First, long-term precipitation deficits and large evaporation rates were essential to dry out the soil and vegetation and to reduce the flood pulse, providing unusual amounts of fuel to fires. In parallel, soil desiccation also played a key role in boosting the concurrence of extremely hot conditions through the establishment of a water-limited regime and an increase in the sensible heat flux between the surface and the atmosphere, increasing flammability thresholds.

High-pressure systems are known to favor CDHW conditions (Cai et al. 2020), particularly in the Pantanal (Marengo et al. 2022) and also over surrounding regions such as Southeast Brazil (Geirinhas et al. 2021). These high-pressure (anticyclonic) anomalies are linked to large-scale teleconnections induced by perturbations of inter-tropical oceanic modes such as the Madden–Julian oscillation (Sharples et al. 2021) and the El Niño-Southern oscillation (Cai et al. 2020). In the analyzed CDHW events, positive anomalies of the 500 hPa geopotential heights associated with higher surface pressure over Central SA contributed to pronounced diabatic heating rates at the surface and strong atmospheric subsidence, allowing the escalation of temperatures and leveraging high evaporation rates until the soil dry out.

The occurrence of concurrent hazards (CDHW-fires) is widespread over Pantanal, showing however a great spatial variability in the amount of area affected by fire in each subregion. The P20F occurred mainly in forested zones (in the north) and areas that experienced no flooding and, consequently, had a huge amount of biomass as fuel, mainly as histosols (Damasceno-Junior et al. 2021), while the fires during the 2001–2019 fire seasons tended to occur in savanna environments (mainly in the south). This fact reinforces the relative contribution of climate and fuel as drivers of fire activity (Pausas and Ribeiro 2013; Gouveia et al. 2016). Accordingly, in regions where fuel was not a limiting factor, fire activity tended to be more vulnerable to CDHW, increasing flammability and the probability of high fire spread.

Previous studies have shown that differences in hydrology modulate nexus between large-scale climatic or geomorphic drivers and vegetation (fuel availability) in the Pantanal (Ivory et al. 2019). Therefore, it is fundamental to consider the hydrological variability to understand fire dynamics, through the influence of the seasonal north-to-south flood-pulse wave of the

Paraguay River, as noted before for Amazonia floodplains (Schöngart et al. 2017). In general, summer rainfall in surrounding areas of the Pantanal results in a slow-moving flood pulse from north to south. Due to complex processes of water retention and flow through floodplain, inundation of the central and southern Pantanal may occur several months after the rainfall peaks (Cai et al. 2020). Under these circumstances, areas in the northern Pantanal and areas away from floodplains, vegetation biomass respond synchronically to rainfall (Ivory et al. 2019). Moreover, as we showed here these areas have spatial matches between strong positive *T*max and negative soil moisture anomalies, particularly in some hydrological regions in the north. On the other hand, in flooded areas, rainfall and vegetation productivity are not clearly correlated (Ivory et al. 2019). This dynamic suggests that land-atmosphere physical mechanisms responsible for triggering the amplification of fires as we showed here seem to operate more strongly in the years without large floods, as in 2019 and 2020. It is likely that these mechanisms do not have the same importance and synchronicity across the different regions of the Pantanal, nor during years of large floods.

Climate change scenarios from state-of-the-art models, project significant warming in the Pantanal, and although changes in the precipitation pattern are less clear cut than those expected for temperature (Marengo et al. 2016a; Llopart et al. 2020), projected changes in SA monsoon have shown a reduction in the length of the rainy season by the end of the century (Gomes et al. 2022). Indeed, our results highlight that the current trend in the Pantanal temperature since 1980 is approximately four times greater than the average global warming (NASA, 2021). The fact that CDHW events are expected to become more frequent and intense worldwide under future climate scenarios (Zscheischler et al. 2018) may reinforce the occurrence of large fires as also shown for other regions (Gouveia et al. 2016; Ribeiro et al. 2018; Turco et al. 2019; Ruffault et al. 2020; Sutanto et al. 2020; Xi et al. 2021). We are confident that our findings are relevant for other regions of the world, as some of the driving physical mechanisms described here, namely those responsible for the CDHWs, also apply across other ecosystems, implying higher flammability conditions and further efforts for monitoring and predicting such events.

It is worth mentioning that fire is also influenced by drivers beyond those directly associated with weather conditions, namely fuel availability and socio-economic factors. As stated by previous authors (Libonati et al. 2020; Garcia et al. 2021; Leal Filho et al. 2021), the P20F outbreak is not attributable to just a single factor, but rather results from a complex interplay among several contributing factors, including weather conditions, availability of fuel

(vegetation), and human ignition sources (both accidental and intended) (Libonati et al. 2020). A recent study showed that human-caused fires exacerbated drought effects on natural ecosystem during the P20F season, with more BAs primarily over natural areas (Kumar et al. 2022).

Accordingly, any strategy to mitigate the effects of wildfires in the Pantanal needs to consider a combination of these factors and the different characteristics of each one. Accordingly, integrative fire strategies should require adaptive and social transformative perspectives (McWethy et al. 2019; Garcia et al. 2021). Thus, our results may improve the assessment of potential high-impact hazards, like the P20F, helping stakeholders to act upon these complex events.

Supplementary Material

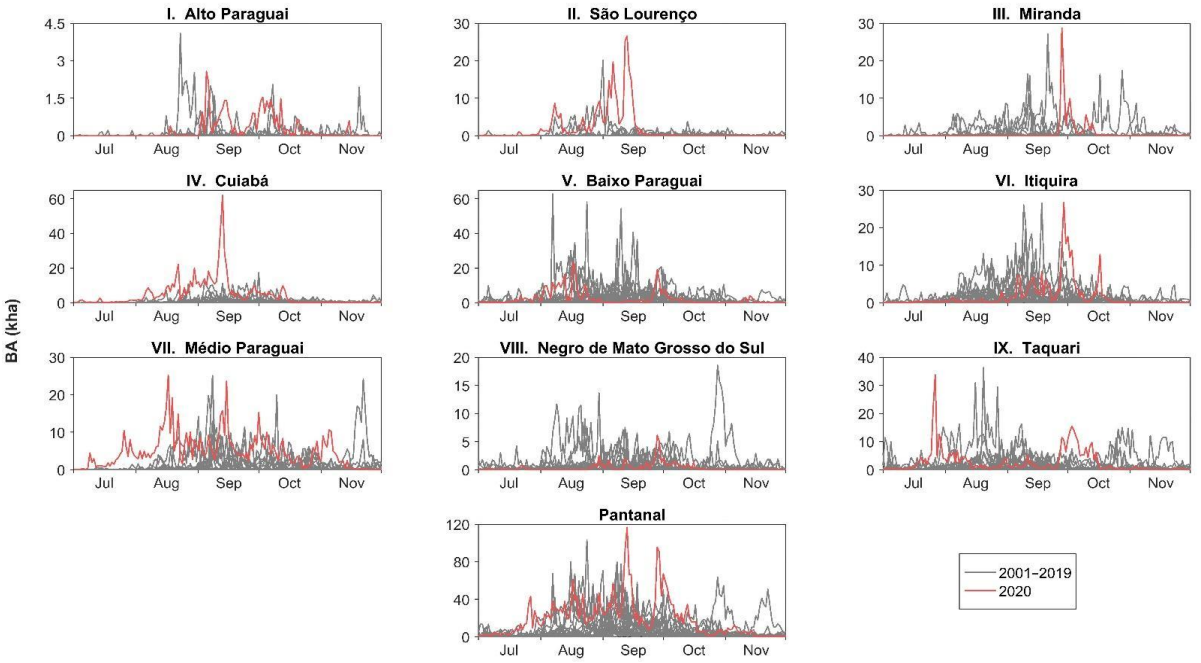

Figure SA.1 Daily values of BA (estimated using the MCD64A1 product) from July to November in Pantanal and within its 9 hydrological subregions. The red curve represents BA values for the P20Fs, and grey curves represent historical BA values (2001–2019).

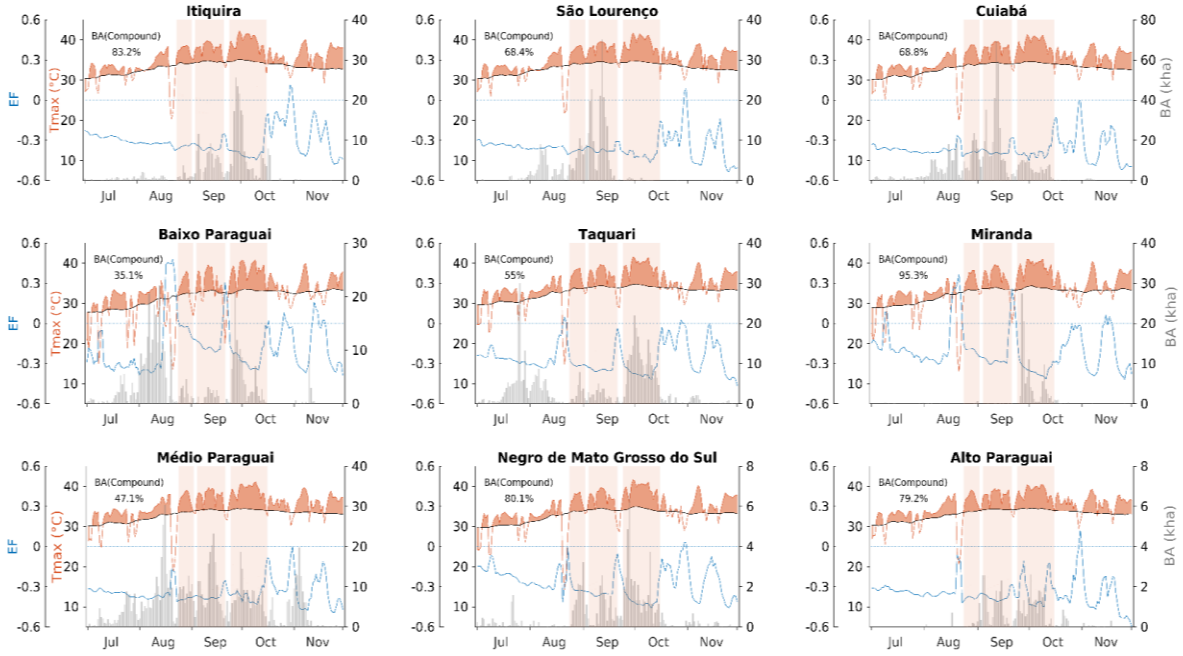

Figure SA.2 Time series from July to November 2020 of daily area-averaged Tmax values for each one of the 9 subregions (orange lines) and the respective calendar day climatological (1981–2010 base period) 90th percentile (black lines). Grey bars indicate the daily total BA recorded (using the ALARMES product). Time series of the observed daily area-averaged anomalies of evaporative fraction are depicted in blue lines. Hot periods (HPs) are highlighted in orange rectangles. The percentage of burned area during the three HPs regarding the total burned area in the fire season (July to November) is shown in the top left corner.

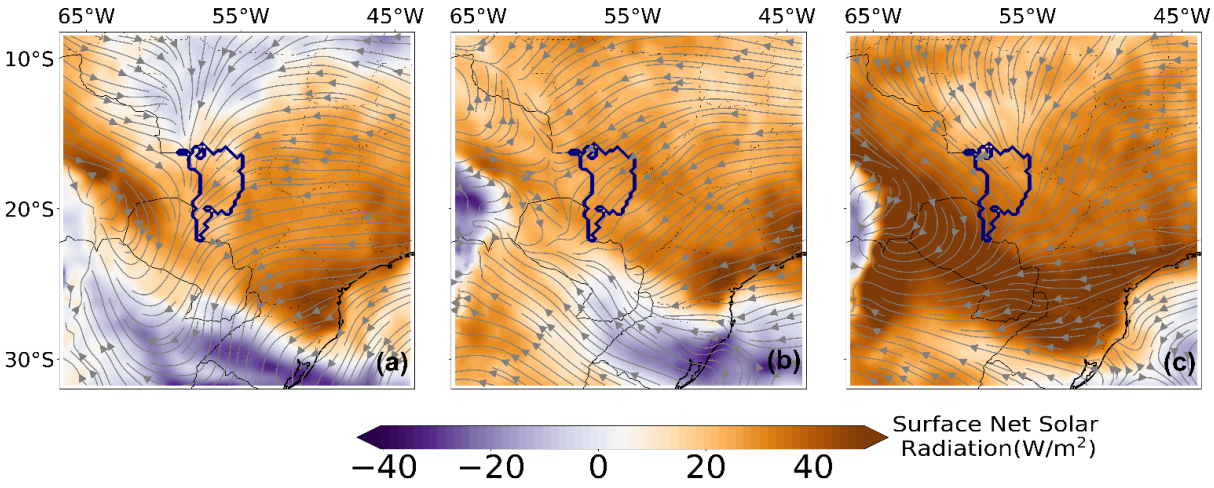

Figure SA.3 (**a, b** and **c**) Spatial patterns of the surface net solar radiation average anomalies ($W.m^{-2}$, shading) of the mean observed 925-hPa atmospheric circulation (streamlines) during the (**a**) 1st HP (August 26th to September 1st), the (**b**) the 2nd HP (September 5th to 20th) and (**c**) the 3rd HP (September 25th to October 10th).

Table SA.1 The main characteristics of BA as estimated using the MCD64A1 product, for the 9 hydrological subregions of Pantanal shown in Figure A.1: Area, Average BA (2001–2019), 2020 BA, 75th percentile of the BA historical time series (2001–2019), 2020 BA with low recurrence (1–2 years), and 2020 BA with no fire in the previous 19 years.

Id	Subregion	Area [kha]	Average BA [kha] (proportional area [%])	2020 BA [kha] (proportional area [%])	Historical BA 75th percentile [kha]	2020 BA with low recurrence (1–2 years) [%]	2020 BA with no fire since 2001 [%]
I	Alto Paraguai	341	4 (1.2)	36 (10.6)	3.8	0.5	0.6
II	São Lourenço	454	23 (5.1)	297 (65.4)	27.7	4.2	3.7
III	Miranda	717	57 (7.9)	107 (14.9)	41.6	0.9	0.3
IV	Cuiabá	1,407	81 (5.8)	768 (54.6)	121.4	7.8	10.1
V	Baixo Paraguai	1,851	267 (14.4)	419 (22.6)	378.8	1.7	0.4
VI	Itiquira	1,952	132 (6.8)	270 (13.8)	235.4	2.6	2.0
VII	Médio Paraguai	2,454	101 (4.1)	761 (31.0)	162.5	7.6	11.4
VIII	Negro de Mato Grosso do Sul	2,848	78 (2.7)	74 (2.6)	87.2	0.8	0.7
IX	Taquari	3,064	190 (6.2)	552 (18.0)	333.2	5.0	3.9
Total (Pantanal)		15,088	933 (6.2)	3283 (21.8)	1266.9	31.0	33.0

Appendix B

Drought–heatwave nexus in Brazil and related impacts on health and fires: A comprehensive review

*Libonati R, **Geirinhas JL**, Silva PS, Monteiro dos Santos DM, Rodrigues JA, Russo A, et al. (2022) Drought–heatwave nexus in Brazil and related impacts on health and fires: A comprehensive review. Ann N Y Acad Sci 1517:44–62. https://doi.org/https://doi.org/10.1111/nyas.14887*

João Lucas Geirinhas contributions: *conceptualization of the analysis, data management (download and curation), computation and analysis of the results, production of figures and manuscript writing.*

Abstract

Climate change is drastically altering the frequency, duration, and severity of compound drought-heatwave (CDHW) episodes, which present a new challenge in environmental and socioeconomic sectors. These threats are of particular importance in low-income regions with growing populations, fragile infrastructure, and threatened ecosystems. This review synthesizes emerging progress in the understanding of CDHW patterns in Brazil while providing insights about the impacts on fire occurrence and public health. Evidence is mounting that heatwaves are becoming increasingly linked with droughts in northeastern and southeastern Brazil, the Amazonia, and the Pantanal. In those regions, recent studies have begun to build a better understanding of the physical mechanisms behind CDHW events, such as the soil moisture–atmosphere coupling, promoted by exceptional atmospheric blocking conditions. Results hint at a synergy between CDHW events and high fire activity in the country over the last decades, with the most recent example being the catastrophic 2020 fires in the Pantanal. Moreover, we show that HWs were responsible for increasing mortality and preterm births during record-breaking droughts in southeastern Brazil. This work paves the way for a more in-depth understanding on CDHW events and their impacts, which is crucial to enhance the adaptive capacity of different Brazilian sectors.

B. Drought–heatwave nexus in Brazil and related impacts on health and fires: A comprehensive review

B.1 Introduction

Heatwave (HW) events are typically defined as prolonged periods where temperatures are substantially hotter than a specific climatological threshold (Perkins and Alexander 2013). The frequency, duration, and severity of such extreme climate events have substantially risen since the middle of the 20th century due to the observed global warming (Perkins-Kirkpatrick and Lewis 2020). The intensity of heat-related extremes significantly increased during the last four decades globally, with the fastest rates being observed in the tropical and polar zones (Zhang et al. 2022b). Prolonged periods of excessive heat pose a serious challenge for public health (Chambers 2020; Vicedo-Cabrera et al. 2021), the economy (García-León et al. 2021), and terrestrial and marine ecosystems (Wohlfahrt et al. 2018; Sen Gupta et al. 2020). Studies show evidence of the impact of temperature on health, especially in hospitalizations and mortality (Rey et al. 2009; Merte 2017; Cheng et al. 2018; Guo et al. 2018; Sousa et al. 2022; Yan et al. 2022). The effects on society may vary according to the vulnerability of individuals or social groups due to factors, such as the social, economic, and political scenario, in addition to age, gender, and pre-existing diseases (Wang et al. 2017a). Recent HW episodes have affected billions of people worldwide, particularly in densely populated urban settlements located in both tropical and mid-latitude regions (Papalexiou and Aghakouchak 2014; Herold et al. 2017). Excessive heat can impact the human body, leading to death (Gasparrini et al. 2015; Hertig et al. 2020), with more vulnerable people, such as the elderly, the poorest, and those suffering from additional comorbidity factors, such as cardiovascular, respiratory, or diabetic diseases (Patz et al. 2005; Péres et al. 2020) at higher risk. Even low-intensity HW episodes may increase mortality, particularly in regions with hot and humid summers (Strathearn et al. 2022). In addition to deaths, extreme heat is known to influence human cognitive performance (Hancock and Vasmatzidis 2003), mental health and suicide rates (Florido Ngu et al. 2021), work-related injuries and illnesses (Varghese et al. 2019), the normal gestational period (Kuehn and McCormick 2017), and the number of premature births (Barreca and Schaller 2020). Recent evidence also links HW episodes with the dynamics of dengue mosquito outbreaks in tropical regions (Jia et al. 2019; Cheng et al. 2020) and with the intensification of urban heat islands

(He et al. 2021). HWs are often associated with a lack of rainfall and large evaporation rates, which can increase vegetation flammability and favor the occurrence of vegetation fires (Trigo et al. 2006; Ruffault et al. 2020; Libonati et al. 2022a). A large amount of particulate matter and gases released into the atmosphere during vegetation fires increases the levels of air pollution which, in turn, contributes to an increase in mortality and hospitalizations due to respiratory diseases (Shaposhnikov et al. 2014; Machado-Silva et al. 2020), evidencing a cascade effect of HW episodes on human health. There are several other heat-related effects on terrestrial and marine ecosystems, such as long-lasting changes in forest productivity (Salomón et al. 2022) and increases in harmful algal blooms (Jöhnk et al. 2008) and coral bleaching (Leggat et al. 2019). Economic heat-related impacts include increases in electricity demand (Larcom et al. 2019), vulnerability of electricity supply (van Vliet et al. 2012), crop losses (Ribeiro et al. 2020a; Brás et al. 2021), weakening of the tourism sector (Rosselló et al. 2020), and water scarcity (Larbey and Weitkamp 2020).

Evidence is mounting that HWs are becoming increasingly linked with drought episodes in many parts of the world, particularly in transition zones between wet and dry climates (Schumacher et al. 2019; Feng et al. 2020; Shi et al. 2021; Wang et al. 2021; He et al. 2022a; Wouters et al. 2022). Independently of their temporal and spatial scales, the occurrence of both events in a compound manner is usually linked to local land−atmospheric interactions triggered by large-scale atmospheric circulation anomalies responsible for persistent clear sky conditions and strong subsidence and advection of warm air (Miralles et al. 2014, 2019; Schumacher et al. 2022b). Recent results point out that over the last two decades, many regions in Europe and the Americas had over 2/3 of their areas under increased susceptibility to HWs during drought episodes (Mukherjee et al. 2022). In accordance with the Intergovernmental Panel on Climate Change (IPCC), which considers compound events as "the combination of multiple drivers and/or hazards that contribute to societal or environmental risk (IPCC 2022)," the periods characterized by simultaneous extreme hot and dry conditions were defined here as compound drought-heatwave (CDHW) events. Those CDHW events are shown to cause considerably more impacts than those related to the occurrence of an isolated event (Zscheischler and Seneviratne 2017). The last IPCC report (IPCC 2022) states that CDHW episodes have been more frequent over the last century and that there is high confidence that this trend will persist with higher global warming. Several studies also reveal the enhanced impacts of CDHW events on vegetation productivity (Zhou et al. 2019; Wu and Jiang 2022), tree mortality (Gazol and

Camarero 2022), food and water supply (He et al. 2022b), health (Ebi et al. 2021), vegetation fires, and air pollution (Richardson et al. 2022), among others. Compound extremes and their associated impacts occur in a complex chain of interactions shaped not only by physical and environmental drivers, but also dependent on population exposure, governance, and infrastructure (Raymond et al. 2020). In contrast to single-hazard analyzes, the investigation of multiple hazards poses additional challenges due to the diversity of processes and spatial-temporal scales involved (Kappes et al. 2012; Zscheischler and Seneviratne 2017). Given the complexity of the such interplay between events, a multidisciplinary approach is required, involving the understanding of societal or environmental impacts, climate-related hazards, drivers of these hazards, and, finally, the modulators of the drivers (Zscheischler and Seneviratne 2017; Bevacqua et al. 2021).

Over the course of the last two decades, evidence of CDHW events has been well documented regionally, mainly for the northern hemisphere, and their impacts on vegetation, vegetation fires, and human health have been studied extensively in North America (Mazdiyasni and AghaKouchak 2015; Alizadeh et al. 2020; Khorshidi et al. 2020; Tavakol et al. 2020; Haqiqi et al. 2021), Asia (Sharma and Mujumdar 2017; Flach et al. 2018; Kong et al. 2020; Wu et al. 2020; Yu and Zhai 2020), and Europe (Rammig et al. 2015; Sedlmeier et al. 2018; Manning et al. 2019; Russo et al. 2019; Ribeiro et al. 2020b; Sutanto et al. 2020; Vogel et al. 2021; Orth et al. 2022). Although CDHW occurrences have been amplified considerably during the 21st century in both hemispheres (Mukherjee and Mishra 2021; Mukherjee et al. 2022), compound events analysis in the southern hemisphere is still underexplored and poorly understood, despite the recent efforts conducted for Australia (Reddy et al. 2022) and some sectors of Brazil (Geirinhas et al. 2021, 2022; Libonati et al. 2022a). Accordingly, few studies have been devoted to the characterization, modeling, and impact evaluation of these compound events over South America (SA), despite its size (i.e., larger than Europe or Australia) and a large number of densely populated regions. Nevertheless, in the past decade, the number of studies focusing on individual extreme climate events of high temperature and low precipitation in different regions of Brazil has increased notably. For instance, studies have analyzed the observed changes in both the temperature and precipitation extremes over Brazil, although employing a single and separate hazard perspective (de los Milagros Skansi et al. 2013; Regoto et al. 2021).

Among them, drought studies are generally the main topic considered. For instance, in the last two decades, droughts over Amazonia (Marengo and Espinoza 2016; Jimenez et al. 2018; Panisset et al. 2018), Northeast (Marengo et al. 2017; Jimenez et al. 2021) and Southeast Brazil (Coelho et al. 2016a, b; Getirana et al. 2021), and the Pantanal (Marengo et al. 2021; Thielen et al. 2021) have been thoroughly analyzed from an individual perspective of drivers and impacts. More recently, a number of studies regarding drought-related events have also reported direct and indirect harmful impacts on the environment, economy, and society. For example, fires in the Brazilian Amazonia increased dramatically during the strong drought years of 2005, 2007, and 2010 (Cano-Crespo et al. 2021; Libonati et al. 2021), as well as in the Pantanal during 2020 (Libonati et al. 2020; Garcia et al. 2021). Reduction in tree growth and forest productivity are connected with recurrent drought episodes in Amazonia, leading to the reduction in biomass carbon uptake (Feldpausch et al. 2016; Machado-Silva et al. 2021). From a health impact perspective, drought is considered as one of the most far-reaching natural disasters that threaten the Brazilian population, mainly linked to food and water scarcity, vector-borne infectious diseases, and respiratory health effects (Sena et al. 2018; Menezes et al. 2021). From 2001 to 2016, there was an increase of 27% in hospital admissions for respiratory diseases affecting children and the elderly related to drought and fire in southern Amazonia (Machado-Silva et al. 2020). Fire smoke is also associated with birth defects, including cleft lip/cleft palate and congenital anomalies of both respiratory and nervous systems (Requia et al. 2022b, a). In addition, adverse birth outcomes were recently related to dry periods in the Amazonia (Chacón-Montalván et al. 2021), and a positive association between drought exposure and mortality was evidenced in the population of the main Brazilian metropolitan regions between 2000 and 2019 (Salvador et al. 2022). Recent studies show that crop production from the Amazonia-Cerrado region, which is one of the largest agricultural regions in the world, is highly vulnerable to droughts (Costa et al. 2019; Rattis et al. 2021). The recurrent, intense, and severe drought events during the last decade have also critically impacted hydroelectricity generation in almost all Brazilian regions (Cuartas et al. 2022).

Compared to drought events, relatively few studies in Brazil have focused on HW modeling and interpretation, with the majority of these published since 2011 (Cerne and Vera 2011; Rusticucci 2012; Ceccherini et al. 2016; Geirinhas et al. 2018b, 2019b; Feron et al. 2019). By contrast, most of the HW-related studies in Brazil mainly focus on public health impacts (Bell et al. 2008; Son et al. 2016; Guo et al. 2017; Zhao et al. 2019b, a; Geirinhas et al. 2019,

2020; Xu et al. 2019; Diniz et al. 2020; Péres et al. 2020; Prosdocimi and Klima 2020; Costa et al. 2021; Moraes et al. 2022). Besides health-related studies in the country, a few studies show HW impacts on agriculture (Gusso et al. 2014), food production (Vale et al. 2010), and fires (Libonati et al. 2022a). The overwhelming majority of health-related assessments address HWs and excess deaths, although the results are mainly limited to the southeastern Brazilian states of São Paulo and Rio de Janeiro. Regardless of the HW definition used, all those studies suggest an excess of deaths due to extreme heat in both cities, highlighting the elderly and the least educated as the most vulnerable groups. The highest mortality rates during HW events are mainly linked to circulatory illnesses and diabetes (Xu et al. 2019; Geirinhas et al. 2020). Rural and urban populations also show different susceptibility to high-temperature events in those regions, suggesting the role of the heat-island effect in exacerbating HW impacts (Peres et al. 2018). Comprehensive country-level analyzes showed that the risk of hospitalization during HW events is mainly for children, the elderly, and pregnant women (Zhao et al. 2019a). It has also been shown that the effects on mortality risk last for almost 3–4 days after the end of an HW event (Guo et al. 2017). By the end of this century, Brazil will experience a more than doubling of heat-related health stress, due to the increased severity of natural hazards and ongoing population growth (Sun et al. 2019).

Although the response of compound weather and climate events to climate change is challenging, recent studies point out that the entire globe will experience increased occurrences of CDHW episodes (Ridder et al. 2022), mainly driven by regional precipitation trends (Bevacqua et al. 2022). Globally, the future frequency of such events is estimated to increase by 37%, with an increase in warming from 1.5 to 2◦C (Meng et al. 2022). By the end of this century, between 1/3 and half of the global land area, depending on the mitigation scenario, is estimated to be exposed to deadly temperatures and drought conditions for more than 20 days per year, exposing around half to two-thirds of the world's human population (Mora et al. 2017). Depending on the rates of warming and population growth over the coming 50 years, around 1–3 billion people are expected to find themselves in areas outside the range of climatic conditions acceptable for humans (Xu et al. 2020). By mid-century, CDHW impacts on the economy may increase drastically, compared to current estimates (García-León et al. 2021). However, these future changes may be underestimated in tropical and subtropical regions (Freychet et al. 2021; Ridder et al. 2022), suggesting that the risk for developing tropical countries, like Brazil, will likely be worse than previously assessed. Due to the strong impacts

of drought and heat extremes, the lack of adaptive capacity will become critical in regions where growing population, poor infrastructure, fragile public health systems, and threatened natural ecosystems are extensively exposed to extreme events (Perkins-Kirkpatrick and Lewis 2020), particularly the extreme heat ones (Mora et al. 2017). Therefore, improving knowledge about the joint occurrence of drought and HW events in tropical regions, particular in SA and specifically in Brazil, is an important prerequisite for the development and maintenance of strong strategies to predict and mitigate the associated impacts.

By recognizing and addressing current knowledge gaps, here we provide a comprehensive compilation of the most recent assessments of CDHW events in Brazil. On the one hand, we pinpoint the most vulnerable areas within this very large country and its wide range of ecosystems; additionally, we contribute to the assessment and quantification of the impacts on public health and on vegetation fires of record-breaking CDHW events around the country. Fire outbreaks triggered by 21st-century CDHW episodes are highlighted in three main ecosystems: the Amazonia rainforest, the Pantanal wetlands, and the Cerrado savannas. The impact of recent persistent CDHW conditions on human mortality and premature births is analyzed for the most populated region, southeastern Brazil.

B.2 Emerging evidence and physical mechanisms of CDHW events in Brazil

In this section, we first analyze studies that highlight Brazil in their global analysis regarding the occurrence of CDHW events. Then, we present and discuss the available recent few regional studies which have begun to look at the physical mechanisms connecting the occurrence of hot and dry conditions in different regions of Brazil.

Emerging global studies highlight SA, including Brazil, as a potential hotspot for the occurrence of compound events, particularly those linked to droughts and HWs (Mukherjee and Mishra 2021; Raymond et al. 2022). For instance, two recent global assessments on the impact of anthropogenic warming and natural climate variability in the occurrence of CDHWs concluded that northeastern and southeastern Brazil and central Amazonia were some of the regions with an increase in the frequency, duration, and magnitude of CDHW events per year since 2000 (Feng et al. 2020; Mukherjee et al. 2022). Another global survey revealed a strong relationship between the occurrence of CDHW conditions and the phase of the El Niño–

Southern Oscillation (ENSO), particularly during the warm season in the northern region of Brazil (Hao et al. 2018b). Agricultural regions, namely those dominated by rice, maize, and soybean production in Brazil, have been increasingly exposed to CDHW events (He et al. 2022b; Raymond et al. 2022). Regional increases in the frequency of CDHW conditions from the present to the time when mean global temperature increases by 1.5 °C (2 °C) above the preindustrial levels are projected to span between 140% and 200% in many parts of SA, including Brazil (Meng et al. 2022). As projected for other parts of the globe, continuous warming of the South American continent will inflict dire impacts on the well-being of the populations. Global warming between 1.5 and 3 °C is estimated to imply an increment in the population exposure to CDHW events over southeastern SA (2–6 million people), the Amazonia (1–5 million people), northeastern Brazil (1–5 million people), and over the west coast of SA (1–4 million people) (Liu et al. 2021). Bevacqua et al. (2022) suggested that improving the representation of the physical processes controlling the mean precipitation trends over the Amazonia rainforest is essential for enhancing the robustness of risk estimates of future

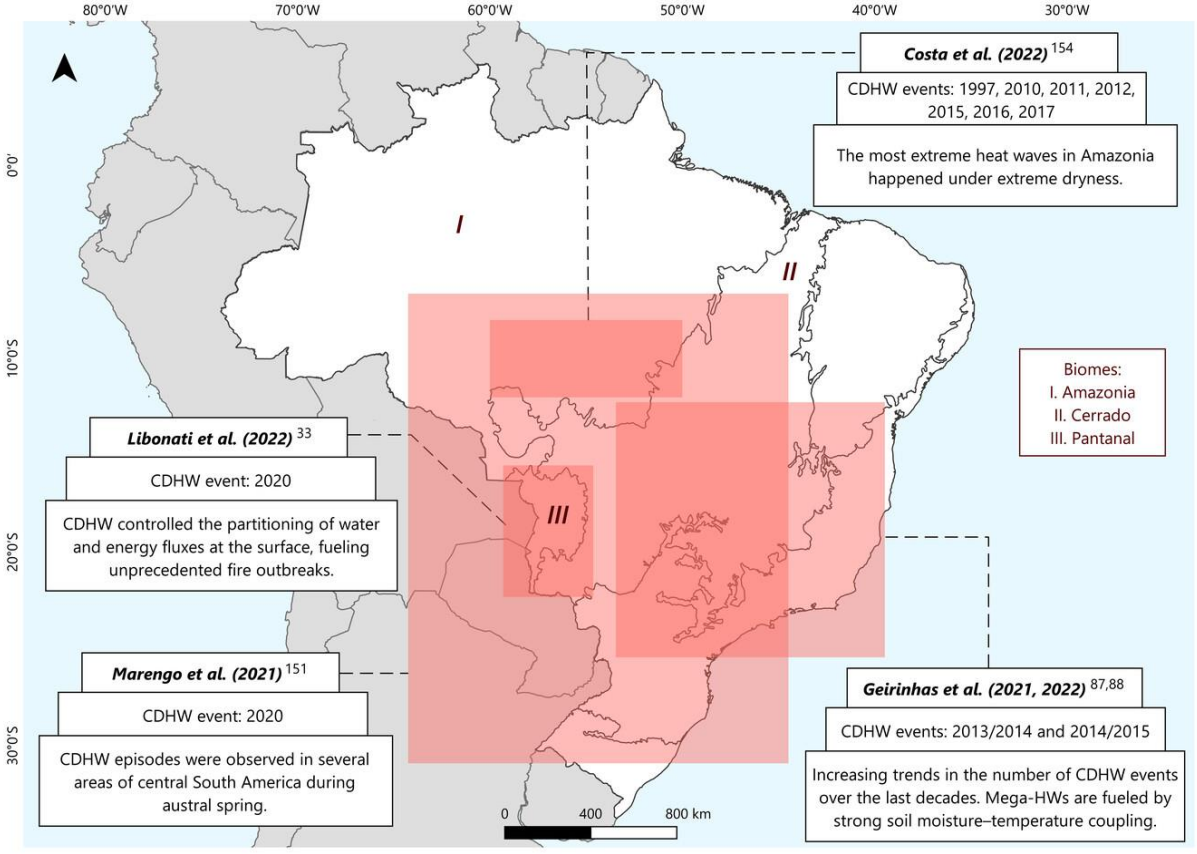

Figure B.1 Main regions targeted (red squares) by the first emerging studies of the patterns, trends, and physical mechanisms triggering the occurrence of CDHW events in different regions of Brazil over the last decade. The main biomes used here to illustrate the impacts on vegetation fires are depicted in the figure.

CDHW events. These authors estimate that the frequency of compound events will increase between 20% and 42%, according to wet and dry future scenarios for the region, respectively.

Regional efforts by the Brazilian academic community to understand extreme CDHW events are slowly refocusing toward a compound perspective, aiming to help to close the gap between climate science and risk assessment (Figure B.1). This joint effort has been encapsulated in a recent editorial in the journal "Nature," where more than 95 national and international water and climate scientists cosigned a letter regarding the 2021 Brazilian water crisis, recommending, among other points, that compound event studies should be a research priority in the country to best inform policymakers and managers (Getirana et al. 2021). Here, we introduce existing literature on understanding the general patterns and physical mechanisms associated with multivariate climate extreme episodes consisting of drought and HW events co-occurring in space and time, in distinct regions of Brazil.

B.2.1 Southeastern Brazil

The first effort to evaluate changes in the occurrence of CDHW events in Brazil was undertaken by Geirinhas et al. (2021). They found that during the last two decades the number of summer CDHW events has increased substantially over parts of southeastern Brazil, namely, the central section of the state of Minas Gerais, the state of Rio de Janeiro, and the eastern and northeastern parts of the state of São Paulo. For these particular regions, increasing levels ranged from 50% to 100% during the second half of the analysis period (2000–2018), when compared with the first half (1980–1999). The period that contributed the most to these positive changes were the two consecutive summers of 2013/2014 and 2014/2015 when southeastern Brazil witnessed severe CDHW conditions. During 2013/2014 summer, the incidence of compound conditions was more noticeable over the state of São Paulo, while during 2014/2015 summer, the states of Minas Gerais and Rio de Janeiro recorded the severest concurrence incidence. This study also explored the atmospheric and surface conditions that triggered such a high incidence of CDHW episodes in the region. Geirinhas et al. (2021) found that surface dryness and hot temperature anomalies were promoted by a higher-than-normal number of summer days defined by atmospheric blocking conditions affecting southeastern Brazil (Silva et al. 2015). These quasi-stationary anticyclonic patterns were embedded in a large-scale Rossby wave train that spanned from the western South Pacific to the South Atlantic and offered the ideal conditions for the occurrence of persistent precipitation deficits throughout the

2013/2014 and 2014/2015 summer seasons (Coelho et al. 2016a, b). At a synoptic time-scale, large diabatic heating rates and strong subsidence conditions enhanced temperature escalation and the occurrence of high evaporation rates, triggering the development of HW episodes and the reamplification of the already established drought conditions. The maintenance of these atmospheric conditions throughout both summer seasons promoted a steady soil moisture decrease into exceptionally low levels. Consequently, a strong soil moisture–atmosphere coupling (water-limited) regime was leveraged and the surface lost its capability to meet the atmospheric water demand, starting to disproportionately dissipate the extra incoming shortwave radiative energy back to the atmosphere as sensible heat, allowing a reamplification of HW episodes. This study unraveled for the first time the relationship between CDHW extremes over southeastern Brazil, demonstrating that, at the first stage, HWs are important for soil desiccation, while during the second stage, under a strong soil moisture imbalance, drought conditions can play a crucial role in temperature escalation and HW amplification through the establishment of strong soil moisture–atmosphere coupling regimes.

Several studies have provided an analysis of the atmospheric causes for the drought event recorded over southeastern Brazil and during the abovementioned two summer periods (Seth et al. 2015; Coelho et al. 2016a, b; Rodrigues et al. 2019; Finke et al. 2020). However, the assessment and quantification of the simultaneous hot temperature anomalies and land–atmosphere interactions have been receiving much less attention. Accordingly, Geirinhas et al. (2022) proposed to fill this gap by presenting at several temporal (from yearly to daily) and spatial (from large to mesoscale) scales a detailed analysis of the extreme temperature anomalies induced during 2013/2014 summer over southeast Brazil, with a special focus on the metropolitan regions of São Paulo and Curitiba. This study shows the exceptionality of the hot conditions that were observed, particularly over the state of São Paulo, where the surface temperature anomalies reached values of 8°C, exceeding the mean by four standard deviations. These massive temperature extremes led to record-breaking temperature levels corresponding, in some cases, to values 5°C higher than the previous record. Another signature of this severe hot summer season was the occurrence of several hot spells over the two metropolitan regions of São Paulo and Curitiba. In fact, the 2013/2014 season witnessed the highest ever recorded number of summer days under HW conditions in both cities, with the occurrence of an unprecedented mega-HW episode (Geirinhas et al. 2022) that lasted for around 20 days. Some of these hot spells, including this mega-HW, were fueled by a combined effect of strong diabatic

heating, low entrainment of cooler air masses caused by a suppression of mesoscale sea-breeze circulation mechanisms, and the establishment of strong soil moisture–temperature coupling that resulted in enhanced sensible heat fluxes from the surface to the atmosphere. In fact, the authors found a close parallel in what concerns the magnitude and spatial extent of this exceptional HW episode and also the major role played by the land–atmosphere interactions in temperature escalation with the remarkable and well-known 2003 European and 2010 Russian mega-HWs (Miralles et al. 2014). This clearly underlines the massive amplitude and persistence of temperature extremes throughout 2013/2014 summer, showing that such temperature escalation was not explained by atmospheric circulation anomalies alone and that the combined effect of soil dryness with atmospheric heating due to radiative processes and other mesoscale temperature advection processes was crucial.

B.2.2 The Pantanal wetlands

Recently, Libonati et al. (2022a) and Marengo et al. (2021a) identified the occurrence of outstanding CDHW conditions in central SA during 2020. Several countries, including Brazil, Argentina, Peru, Paraguay, and Bolivia, have recorded a large number of HW events, with record-breaking temperatures reaching up to 10°C above the 1981–2010 climatology. Those HWs occurred in the middle of an unprecedented drought that affected that region since 2018 linked to the warming trends in sea surface temperature of the Pacific and Atlantic Oceans (Thielen et al. 2020, 2021; Marengo et al. 2021). On the other hand, the persistent atmospheric blocking conditions in the region fueled by a stationary Rossby wave train in the middle and upper atmosphere coming from the Indian Ocean region (Marengo et al. 2021) were crucial for temperature escalation and large evaporation rates that resulted in pronounced soil moisture deficit during these HW episodes. This drought-HW configuration was supported by enhanced land–atmosphere interactions, thus influencing the persistence of more warm and dry days. CDHW conditions in 2020 were particularly widespread over the Pantanal, located in central-southern Brazil (Libonati et al. 2022a). The 2020 dry season (July–November) was hotter and drier than any other corresponding dry season period in the Pantanal, since at least 1980 (Libonati et al. 2020). During these exceptional CDHW conditions, a pronounced decrease in the evaporative fraction values was observed, indicating the establishment of a strong soil moisture−temperature coupling regime (water-limited) characterized by a near-zero evaporative cooling and a large flux of sensible heat from the surface to the atmosphere (Libonati et al. 2022a).

B.2.3 The Amazon rainforest

During the dry season, the southern part of the Amazonia rainforest faced a warming trend of 0.49°C/decade over the 1979–2012 period, with a sharper trend of 1.12°C/decade since the year 2000 (Jimenez et al. 2021). In addition, this region has been recording an increasing frequency in the number of hot days since 1961 (Regoto et al. 2021) as well as in the number of HW events (Geirinhas et al. 2018a). The synoptic conditions associated with HWs in this region are linked to the northward displacement of the Intertropical Convergence Zone (Geirinhas et al. 2018a) and to the intensification of the northerly South Atlantic Anticyclone, which reduces the influx of moisture to southeast Amazonia linked to the South American Low-Level Jet (Costa et al. 2022). Concurrent with this warming, the region has experienced three major droughts in the short span of 10 years, namely, in 2005, 2010, and 2015. These extreme drought episodes were triggered by large-scale teleconnections patterns forced by warm anomalies in the sea surface temperatures of both the Pacific and Atlantic oceans (Coelho et al. 2012; Marengo and Espinoza 2016; Andreoli et al. 2017). Recent studies have pointed out that the hottest years in the biome were coincident with those extreme droughts (Jiménez-Muñoz et al. 2013; Machado-Silva et al. 2021). The area stricken by precipitation deficits (high temperatures) has increased from 37.9% (10.3%) in 2005 to 42.9% (42%) in 2010, reaching 80.1% (90%) of the Amazonia basin in 2015 (Panisset et al. 2018). In particular, long-term records suggest that 2015 was likely the hottest and driest year over the region in a century (Jiménez-Muñoz et al. 2016). Recently, it was shown that drought conditions over the southeast of Amazonia have a critical impact on the amplification of surface temperature, with the most extreme HW episodes co-occurring during extreme dry years (Costa et al. 2022). During these drought events, warm temperature anomalies were concurrent with anomalously high amounts of incoming solar radiation (Panisset et al. 2018), reduction in cloud cover (Jimenez et al. 2018), and soil moisture deficits (Garcia et al. 2018). These compound conditions probably led to enhanced land–atmosphere feedbacks that caused a reamplification of the already established conditions of soil dryness and extreme hot temperatures (Miralles et al. 2014, 2019; Coronato et al. 2020; Benson and Dirmeyer 2021; Geirinhas et al. 2022).

B.3 Impacts of CDHW events on the environment and society: early evidence

In the above sections, we highlighted current knowledge regarding individual hot and dry extremes in Brazil and their associated impacts, as well as the emerging evidence about the occurrence and physical processes associated with CDHW episodes, based on global and regional studies over the last decades. Although each individual type of extreme (hot or dry) is known to trigger severe impacts over the affected region, the implications of the co-occurrence of both extremes over the country are still not well understood. Taking into account the increasing role played by the abovementioned CDHW events in the region, we present a first overview of the associated impacts at a country level. The focus is to evaluate the associated impacts on human health and fire occurrence, in a top-down approach. Using early published case studies representative of main CDHW events that affected diverse areas of the country (Figure B.1), we present a first-hand interpretation of potential impacts. In each of the following two subsections, we first introduce some aspects associated with general research available on the topic and then identify the individual case study from the second main section, and then the analysis of the impacts is carried out separately for threats to human health and vegetation fires. The aim is not to exhaustively analyze the results but instead to introduce research questions and methods to be further explored in the future. The key databases and methods used to formally address the impacts are described in the Supplementary Material.

B.3.1 Threats to public health

The understanding of the potential impacts of CDHW events on public health in Brazil is still far from satisfactory, despite the widespread efforts to quantify the impacts of droughts (Sena et al. 2018; Machado-Silva et al. 2020; Menezes et al. 2021; Salvador et al. 2022) and HWs (Bell et al. 2008; Son et al. 2016; Guo et al. 2017; Zhao et al. 2019b, a; Geirinhas et al. 2019; Xu et al. 2019; Diniz et al. 2020; Péres et al. 2020; Prosdocimi and Klima 2020; Costa et al. 2021; Moraes et al. 2022) from the perspective of a single climate extreme.

To first address this knowledge gap, here we analyze the impacts of the CDHW events during the 2013/2014 and 2014/2015 summer seasons (Geirinhas et al. 2021, 2022) on human mortality and preterm births in southeastern Brazil. We follow the methods used in previous work on the region (Geirinhas et al. 2019, 2020), to analyze daily mortality for all-natural death

causes (nonaccidental or nonviolent) and total births/preterm births (<37 gestational weeks) for the metropolitan region of Rio de Janeiro (MRRJ), based on the Brazilian Health System database (DATASUS) for 2000–2018 and 2011–2017, respectively (see Supplementary Material). With around 12 million inhabitants, the MRRJ is one of the most densely populated urban areas in SA, and the second most populated metropolitan region in Brazil, surpassed only by the metropolitan region of São Paulo.

B3.1.1 Human Mortality

The existing literature has investigated the impacts of HW events on human mortality across the entire country over the last decades. Particularly for the MRRJ, according to Geirinhas et al. (2019) during an intense HW that took place in February 2010, 737 excess deaths occurred, with a greater impact on women (44% higher than expected) than on men (21% higher than expected). In terms of age, the elderlies were the most affected, with a higher excess of deaths for elderly women (56% higher than expected). Geirinhas et al. (2020) expanded the previous analysis to four major HW events, highlighting an excess of 1748 fatalities regarding the expected mortality, with women and the elderly being the most affected. The effects of different levels of drought severity on mortality rates were analyzed by Salvador et al. (2022) from 2000 to 2019 for the main metropolitan regions of Brazil, including MRRJ. Evidence of positive association was found, mainly for females, children, and the elderly, and the effects were exacerbated as the drought severity increased. Furthermore, this study found that the excess mortality risk due to extreme drought exposure was greater than that observed due to heat stress in Brazil.

To illustrate the joint impacts of both hot and dry events on excess mortality, we analyzed the 2013/2014 and 2014/2015 summer compound conditions recorded in Rio de Janeiro (Geirinhas et al. 2021, 2022). Over these two record-breaking dry summer periods, the excess heat factor (EHF) (Nairn and Fawcett 2014) allowed identifying several HW events. The EHF quantifies the heat stress levels considering not only the actual hot conditions but also taking into account the previous 30 days, thus considering, to some extent, the human body's acclimatization (Nairn and Fawcett 2014). Therefore, this index is recommended to describe the impacts of HW events on human mortality and morbidity (Scalley et al. 2015). A total of four and six HW events occurred during the 2013/2014 and 2014/2015 summer compound conditions, respectively (Table B.1). From all CDHW events, seven presented excess mortality

(O/E > 1), five of them statistically significant (*p*-value < 0.05) (Table B.1). The highest increase in the observed number of deaths was 33% (O/E = 1.33, CI: 1.21–1.45), which corresponds to an estimated 269 excess deaths during the event of January 3, 2014. Since this event occurred shortly after the previous one (December 29, 2013), with an O/E = 1.18 (CI: 1.09–1.28) and excess mortality estimated at 195 deaths, their combined effect on mortality (464 excess deaths) can be interpreted as a single and longer HW. During the largest HW (26 days during January 2015), with an O/E of 1.08 (CI: 1.04–1.11), 567 excess deaths were estimated.

Considering only the CDHW conditions in which O/E ratio was statistically significant and higher than unity, the estimate of the total excess mortality during 2013/2014 and 2014/2015 reaches 828 and 759 deaths, respectively. Several factors, such as gender, age, social inequalities, and pre-existing diseases, influence the population vulnerability to CDHWs (Ellena et al. 2020), which need to be better investigated in the MRRJ and other Brazilian metropolitan regions. Future population aging is expected to amplify climate-related excess deaths, thus representing a particular challenge for Brazil, in a scenario where population aging has been rapid and marked by socioeconomic and regional disparities (Tramujas Vasconcellos Neumann and Albert 2018).

Table B.1 Heatwaves identified during the 2013/2014 and 2014/2015 summer CDHW conditions in MRRJ. Start, duration, and intensity of heatwaves were derived from EHF. Observed to expected (O/E) ratio for total number of deaths during the CDHW is also presented, including the 95% confidence interval.

Summer Season	Start of HW	HW duration (days)	O/E (95% CI) for total number of deaths
2013/2014	2013-12-29	4	1.18 (1.09–1.29)
	2014-01-03	3	1.33 (1.21–1.45)
	2014-01-23	3	1.07 (0.98–1.18)
	2014-02-06	5	1.25 (1.17–1.34)
2014/2015	2014-12-20	4	1.04 (0.96–1.13)
	2014-12-28	8	1.09 (1.03–1.16)
	2015-01-07	26	1.08 (1.04–1.11)
	2015-02-09	7	0.97 (0.91-1.04)
	2015-02-17	6	1.00 (0.93–1.07)
	2015-02-25	4	1.00 (0.92–1.08)

B3.1.2 Gestational health effects under CDHW conditions

Studies have shown that temperature extremes can affect gestational health and promote an increase in preterm births (Kuehn and McCormick 2017; Barreca and Schaller 2020; Huang et al. 2021). For instance, maternal exposure to extreme temperatures was linked to an increased risk of preterm birth in Australia (Strand et al. 2012), Europe (Schifano et al. 2016), the United States (Basu et al. 2010), and China (Li et al. 2021). Although most preterm babies survive, maternal exposure to extreme temperature has been pointed out as a leading cause of child mortality, long-term neurological disabilities, and increased risk of respiratory and gastrointestinal complications (Goldenberg et al. 2008; Villar et al. 2018). Consequently, the occurrence of premature births also leads to an increase in the demand for long-term care, which puts pressure on the public health system (WHO 2015).

Drought can affect pregnancy health by limiting water and food availability, disrupting infrastructures, and facilitating the dissemination of water-related diseases (Roos et al. 2021). Studies about the direct impact of extreme droughts on human pregnancy are still limited worldwide (Ha 2022). Nevertheless, Gitau et al. (2005) showed that the Southern African drought of 2001–2002 led to the increase in food prices and consequently to poor maternal nutrition status, culminating in decreased infant length. These results indicate that drought can have long-term effects on the population and public health services (Ebi and Bowen 2016). In Brazil, the studies of health risks of droughts highlight that social and economic vulnerabilities aggravate the associated health impacts (Sena et al. 2018; Salvador et al. 2022).

Despite evidence in the literature about the impacts of isolated HW and drought events, little is known about the magnitude of the association between CDHW episodes and preterm birth in Brazil, and the factors that influence this relationship, mainly due to regional differences. Here, we evaluated the impact of CDHW conditions on gestational health by analyzing the increase in total births and preterm births during the already discussed 2013/2014 and 2014/2015 summers (Table B.1). For this purpose, some HW events from Table B.1, consecutive and in close proximity, were concatenated, resulting in five longer periods (Table B.2).

Table B.2 Classification of periods composed of sequential CDHWs. The duration of each period was calculated by adding the duration of each sequential HW from Table B.1**.**

Summer Season	Period label	Start of period	Period duration (days)	Number of sequential HW induced in this period (from Table b.1)
2013/2014	P1	2013-12-29	8	2
	P2	2014-01-23	3	1
	P3	2014-02-06	5	1
2014/2015	P4	2014-12-20	44	3
	P5	2015-02-09	20	3

For both the 2013/2014 and 2014/2015 summer seasons, a statistically significant increase (O/E > 1) in total and preterm births was observed in all CDHW events (Fig. B.2). For preterm births, CDHW conditions were associated with an increase varying from 10% (O/E = 1.10, CI: 1.01–1.19) to 23% (O/E = 1.23, CI: 1.09–1.39). The increase in the O/E ratio obtained here is within the same range reported by Chersich et al. (2020) in their systematic review of 70 studies in 27 countries (1.16; 95% CI: 1.10–1.23). Overall, a small increment of the O/E ratio was observed for total births, with an increase observed from 5% (O/E = 1.05; CI: 1.01–1.09) to 13% (O/E = 1.13; CI: 1.08–1.19). No clear links between the HW duration and intensity and birth rates were observed here, despite previous studies suggesting that such factors can be positively associated with an increase in early-term births (Huang et al. 2021). A possible explanation for this is the fact that the Brazilian birth certificates record the gestational time in weeks. This could be a confounder for the daily analysis of HW events conducted here, which motivates further long-term analysis in Brazil.

B.4 Vegetation fire response to the simultaneous occurrence of hot and dry events

The link between fire activity and climate has been extensively covered worldwide, with the IPCC defining fire weather as "weather conditions favorable to fire activity, which generally includes temperature, soil moisture, humidity, and wind" (Jolly et al. 2015; IPCC 2022). In general, fire activity is linked to concurrent high temperatures, low relative humidity and precipitation, and windy conditions, although meteorological conditions during the growing

season also play a major role in modulating both vegetation and fuel levels (Bowman et al. 2020; Jain et al. 2022). In the case of Brazil, there are several studies evaluating the relationship between fire and meteorological parameters; however, due to the extent of the country and the variety of ecosystems, these relationships differ among biomes and even at a regional scale. Moreover, regarding the impact of CDHW events in Brazilian biomes, there is very little research. In fact, to the best of our knowledge, the only explicit joint assessment on the present-day impact of CDHW events on vegetation fires was a recent study for the 2020 fire season in the Pantanal region (Libonati et al. 2022a). In addition, future fire danger forced by dry and hot conditions under climate change scenarios was only recently evaluated for two Brazilian regions, namely the Xingu Basin and the Pantanal (Ribeiro et al. 2022). Here, we attempt to go a few steps further, summarizing the efforts developed by the academic research community to describe these fire–CDHW relationships over the Pantanal wetlands, the Amazonia rainforest, and the Cerrado savannas. We further provide novel results covering both the Amazonia rainforest and the savannas of Cerrado, where we followed the methods used in (Libonati et al. 2022a) based on well-consolidated satellite-derived active fire and burned area datasets. More information on these datasets and the methods employed here may be found in the Supplementary Material.

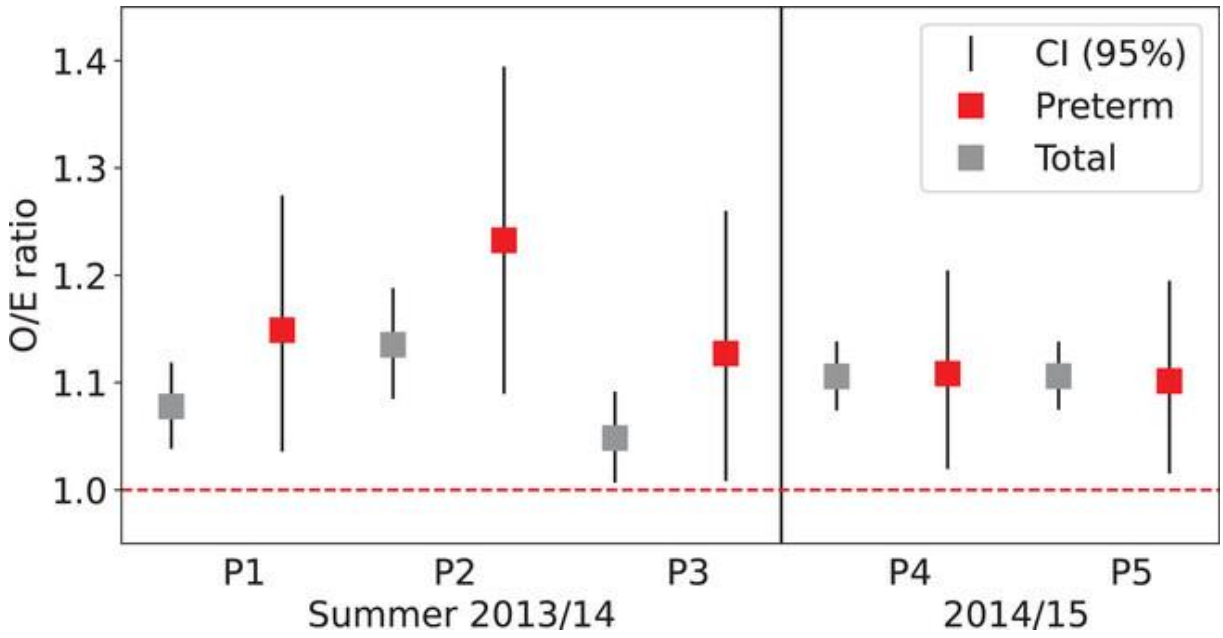

Figure B.2 Observed to expected (O/E) ratio for total (gray squares) and preterm births (red squares) in the metropolitan area of Rio de Janeiro during CDHW periods in the summers of 2013/2014 and 2014/2015. Error bars indicate the 95% confidence intervals (CIs). Values greater than unity (red dotted line) represent a statistically significant increase in birth rates during compound events. The vertical line visually separates the 2013/2014 and 2014/2015 periods.

B.4.1 The Pantanal wetlands

Up until the catastrophic 2020 wildfire event, there was very little literature on vegetation fires over Pantanal and their connection to meteorological conditions and climate change. When roughly 4 million hectares (1/3 of the biome) burned down in 2020 (Libonati et al. 2020), including long stretches of wetlands and forest formations (Kumar et al. 2022), and around 17 million vertebrates were killed (Tomas et al. 2021), attention shifted to understanding why and how this fire-sensitive biome was burning. The 2020 fire season in Pantanal was marked by anomalous meteorological conditions associated with unprecedented meteorological danger (Libonati et al. 2020) and severe drought (Thielen et al. 2021). Libonati et al. (2022a) developed this analysis further, linking CDHW conditions to daily variations of the burned area within Pantanal and its hydrological subregions. Most burned areas occurred within a 4-month period from July to October (henceforth the Pantanal's fire season), with record values of hot and dry conditions. The percentage of Pantanal under CDHW conditions ($\%Pantanal_{CDHW}$), a single metric that illustrates the temporal and spatial occurrence of CDHW conditions during the fire season (Geirinhas et al. 2021), reached its maximum during 2020 (Figure B.3). From August 26th to October 15th, three consecutive CDHW events were recorded (see orange shaded areas in Figure B.3), where maximum temperatures rose almost 6°C above the climatological mean, reaching a staggering 41°C on the third CDHW event that lasted more than 20 consecutive days. Long-term precipitation deficits coupled with a large evaporative demand leveraged by the occurrence of several hot spells since the beginning of 2020 promoted a steady and sharp decrease of soil moisture values during the Pantanal's wet season, culminating in pronounced soil desiccation during the fire season. Accordingly, the HW conditions triggered during the Pantanal's fire season concurred with a near-zero evaporative cooling evidenced by the sharp decreases observed in the evaporative fraction values (see blue lines in Figure B.3). This highlights the establishment of strong soil moisture–temperature coupling regime (water-limited) in which the surface started to disproportionately dissipate the incoming radiation as sensible heat, instead of latent heat (evaporation), allowing a reamplification of the HW episodes and thus fostering the ideal conditions for fire propagation. In fact, the highest levels of vegetation flammability thresholds ever recorded over the last 4 decades were observed during 2020. Although the number of days during the three abovementioned CDHW periods represented circa 37% of the total fire season days, they accounted disproportionately for 71% of the total burned area of that period. Contrary to

previous years (Correa et al. 2022), most of these fires were located over northern Pantanal in forested areas (Libonati et al. 2022a). These regions, where fuel is not a limiting factor, are more vulnerable to CDHW events and their effects are greater in years that experience less flooding, as is the case of 2019 and 2020. They also found that, in the Pantanal, conditions for the occurrence of CDHW episodes are becoming more frequent, with temperatures rising at a rate four times that of the global average, and negative precipitation anomalies occurring more frequently since the turn of the 21st century. Although models do not fully agree on future precipitation trends, state-of-the-art projections agree on a warmer future for the biome (Marengo et al. 2016a). A recent study highlights that limiting global warming to 1.5°C instead of 3°C is likely to reduce the expected increase in CDHW-related fire danger by 11.4% in the Pantanal (Ribeiro et al. 2022).

It is worth mentioning that intense fire seasons in the Pantanal, like in most other regions around the globe, result from the interplay of the appropriate conditions for fire triggering and maintenance, that is, availability of fuels, appropriate extreme meteorological conditions, and

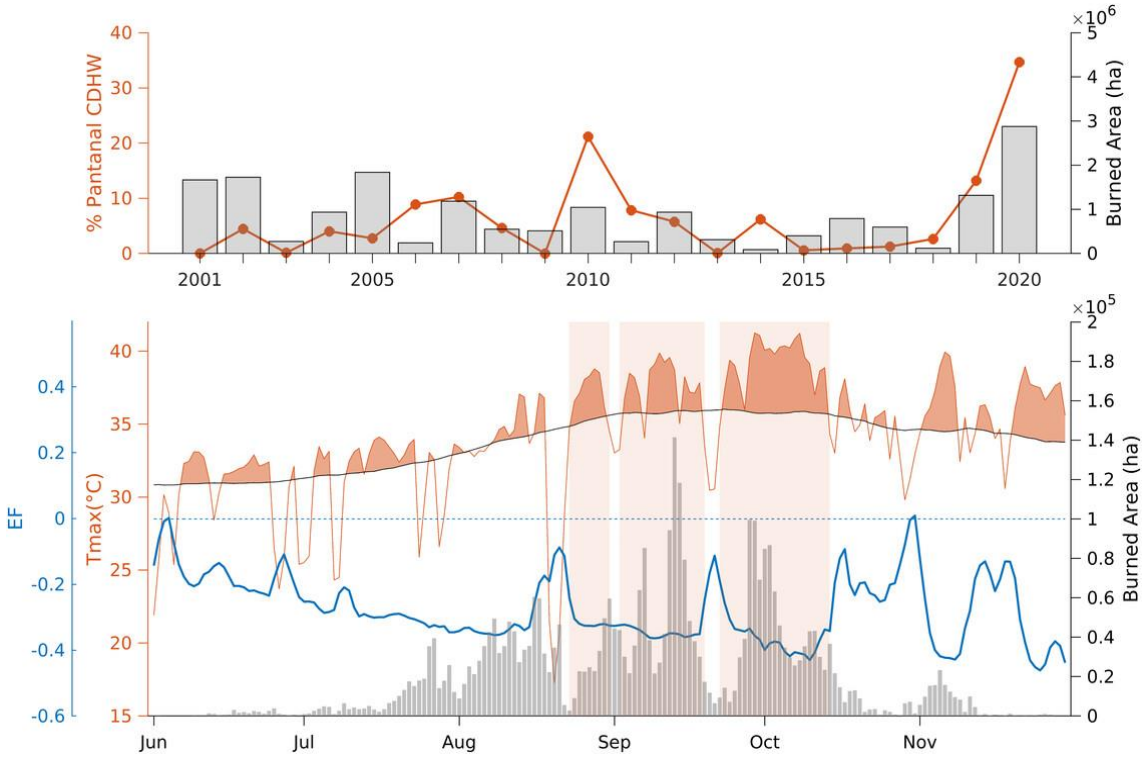

Figure B.3 Vegetation fire response to the simultaneous occurrence of hot and dry events during the Pantanal fire crisis in 2020. Top panel: Interannual variability from 2001 to 2020 of the percentage of Pantanal under CDHW conditions (orange line, left y-axis) and of total annual burned area (gray bars, right y-axis) computed for the Pantanal's fire season period (July–October). Bottom panel: Time series from June to November 2020 (bottom panel) of daily area-averaged values of maximum temperatures (T_{max}, orange line, left y-axis), the respective calendar day climatological (1981–2010 base period) 90th percentile (black line), and of evaporative fraction anomalies over Pantanal (EF, blue line, left y-axis); gray bars indicate daily total burned area recorded over Pantanal (right y-axis); the orange shaded rectangles highlight periods marked by the occurrence of consecutive HW episodes followed by a pronounced decrease in the EF values.

frequency of ignitions. Therefore, the existence of intense drought and HW conditions such as the ones that took place in 2010 (Figure B.3) represents a necessary (but not sufficient) condition, to ensure a higher-than-usual fire season. The condition of the fuels, and particularly the number of ignitions (natural or anthropogenic), also play a critical role. In the case of the Pantanal, human activities are the main source of vegetation fire ignitions, accounting for 84% of the annual burned area (Menezes et al. 2022).

B.4.2 The Amazon rainforest

Over the past few decades, human activities and climate variability contributed to periodic spikes in forest fire activity in the Amazonia rainforest (Cano-Crespo et al. 2021). Since natural fires are uncommon in Amazonia, the fire regime is mainly shaped by anthropogenic activities. Nevertheless, the role of climate has to be considered, especially during extreme droughts, which have been shown to exacerbate fire incidence, intensity, and severity in the region (Chen et al. 2017). From 2000 to 2015, drought frequency in Amazonia was almost three times higher than the decadal incidence of the last century (Panisset et al. 2018), which represents a major threat to the forest ecosystem (Machado-Silva et al. 2021). During the drought event of 1997–1998, which was related to one of the most intense episodes of the ENSO ever recorded, 1/3 of the Amazonia became susceptible to fire, and approximately 40,000 km^2 burned (Nepstad et al. 2004). In 2005, the lack of precipitation induced by the warming tropical North Atlantic Ocean affected mainly the western Amazonia, promoting an extended and extreme fire season in this region (Jolly et al. 2015). In 2010, the co-occurrence of positive phases of both the ENSO and the Atlantic Multidecadal Oscillation (AMO) led to record drought and fire activity over western and southern Amazonia (Chen et al. 2017). In the face of the observed extreme values of temperature and precipitation that were exacerbated by the strong El Niño event of 2015 (Jiménez-Muñoz et al. 2016), new record-breaking drought conditions occurred in the rainforest during that year but resulted in a relatively low level of fire activity due to decreasing levels of deforestation (Cano-Crespo et al. 2021; Libonati et al. 2021). Climate anomalies triggered by ENSO and AMO-related activity are expected to continue impacting Amazonia through a higher frequency of extreme droughts (Duffy et al. 2015). Such an increase in hydroclimatic extremes, coupled with anthropogenic land cover changes, are expected to further promote fire activity in this region (Richardson et al. 2022). In addition, the observed warming trends (Geirinhas et al. 2018a; Regoto et al. 2021) may increase evapotranspiration,

leading to a decrease in soil moisture (Choat et al. 2012), thus enhancing vegetation flammability.

The ongoing intensification of the hydrological cycle is linked to the amplification of surface temperature (Jimenez et al. 2018), with the most extreme HW episodes co-occurring during extreme dry years (Costa et al. 2022), and presents a showcase to explore the responses of Amazonia fires under CDHW conditions. Here, we show preliminary results on the synergy between fire activity and CDHW events that further confirm that these hot and dry conditions favor the occurrence of fire. Figure B.4 shows the spatial distribution of CDHW conditions (see Supplementary Material) in Amazonia over 2005 (June–August), 2010 (June–August), and 2015 (October–December), along with active fire anomalies and deforestation patterns. CDHW conditions increased in duration and extent over the considered periods, and in 2015, almost the entire Amazonia was affected. In comparison, the periods of 2005 and 2010 experienced fewer days under CDHW conditions, and these occurred mainly in the western and southern parts of the biome. Fire anomalies, on the other hand, seem to have decreased from 2005 onward and show fewer regional fire hotspots. At first glance, there appears to be no spatial concurrence of CDHW conditions and increased active fire anomalies. However, as pointed out before, the anthropogenic disturbance has a preponderant role in fire activity over the Amazonia. The period considered for 2005 saw more than double the extent of deforestation compared to both 2010 and 2015 (Libonati et al. 2021). In 2005 and 2010, higher fire anomalies were found in areas that experienced increased CDHW conditions and high deforestation, whereas in 2015, despite extreme hot and dry conditions, the biome saw lower deforestation and consequently, less fire activity. These preliminary results demonstrate that, given anthropogenic ignitions, CDHW conditions exacerbate fire activity in Amazonia.

Other factors can also influence fire activity and may contribute to some of the variability that is not explained by climate extremes, for instance, anthropogenic factors, including political and economic drivers (Rochedo et al. 2018), but also natural factors, such as soil moisture content (Nepstad et al. 2004), and positive fire–climate and deforestation–climate (Lejeune et al. 2015) feedbacks. In particular, the influence of deforestation-induced feedback on the occurrence, intensity, and frequency of CDHW events should be further investigated, given the observed influence of Amazonia land cover changes on surface temperature, the energy budget, and the hydrological cycle (Jiang et al. 2021). Additionally, the direct impacts of hot and dry compound events on the forest ecosystem are not yet documented over the region,

although studies have reported changes in Amazonia forest productivity related to drought frequencies and warming trends (Nepstad et al. 2004; Feldpausch et al. 2016; Machado-Silva et al. 2021).

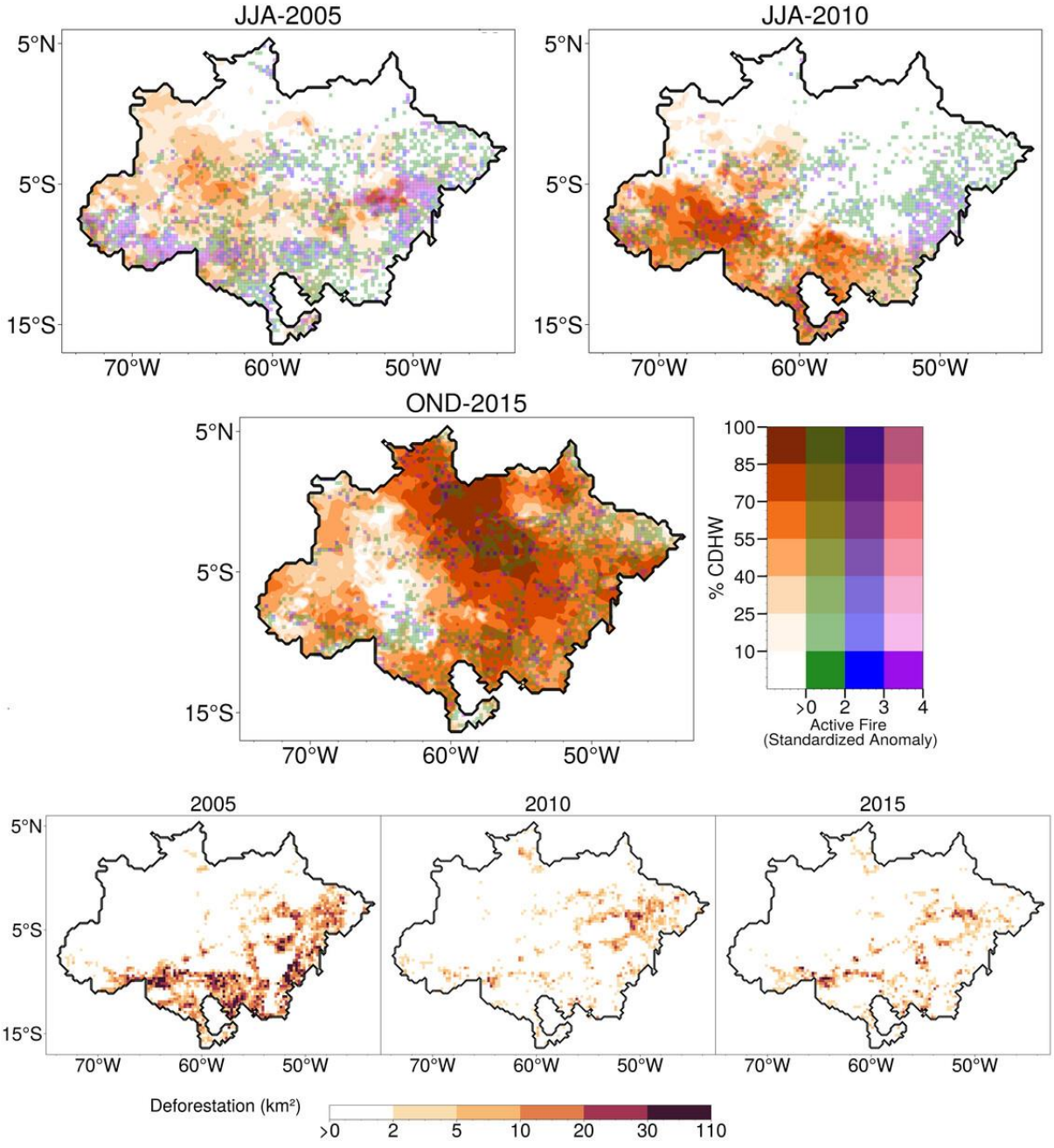

Figure B.4 The spatial distribution of CDHW conditions in the Amazonia in 2005, 2010, and 2015, along with active fire anomalies and deforestation patterns. Top panels: Spatial distribution over Amazon of the percentage of days affected by CDHW conditions (%, top color bar) and of active fire standardized anomalies (bottom color bar) during the periods of June–August 2005 (left panel), June–August 2010 (right panel), and October–December 2015 (bottom panel).

B.4.3 The Cerrado savannas

By contrast to the other biomes referred to in this section, the Cerrado is no stranger to fire. This fire-prone biome sees high fire activity every year as the largest contributor to Brazil's annual burned area and a major fire hotspot worldwide (United Nation 2022). Fires in Cerrado have been shown to be linked with meteorological conditions, in particular rainfall and temperature (Nogueira et al. 2017; Li et al. 2022). For instance, the Daily Severity Rating (DSR in short, an extension of the Canadian Forest Fire Weather Index System) explains 71% of the interannual variability of burned area in Cerrado (Silva et al. 2021). Here, we show further evidence for the Cerrado's fire seasons (defined here as August–October) from 2001 to 2019 of a link between CDHW conditions with fire activity over four Cerrado ecoregions (Figure B.5): Bico do Papagaio, Araguaia Tocantins, Bananal, and Alto Parnaíba. These ecoregions (Sano et al. 2019) are located in the central and northern Cerrado and are the highest annual contributors to the total burned area in the biome, burning more than 8% of their respective areas every year, on average (Silva et al. 2021). Indeed, there seems to be a link between CDHW conditions and fire as, for all ecoregions, the top three years with higher burned areas fall into the lower right quadrant of Figure B.5, except for the year 2010 for Alto Parnaíba. The years of 2007 and 2010 are associated with La Niña events that, as usual, induced widespread drought conditions over the Cerrado (Andreoli et al. 2017), confirmed by low soil moisture values and associated with a $\%Cerrado_{HW}$ incidence - a single metric that illustrates the temporal and spatial occurrence of HW conditions during the fire season above the historical series 75th percentile (Geirinhas et al. 2021; Libonati et al. 2022a). These two years witnessed the most severe fire seasons within the Cerrado over the last two decades, with all four ecoregions showing positive burned area anomalies (Silva et al. 2021). The year of 2012 saw moderate to severe drought over Alto Parnaíba and Araguaia Tocantins (Cunha et al. 2019), and are here associated with a high percentage of HW incidence in both ecoregions. Noteworthy is the case of Bananal in 2017, and to a lesser extent, Bico do Papagaio, with the highest ever-recorded value of HW incidence in the region and corresponding peak in burned area values. These results hint at a possible synergy between CDHW events and fire activity in the Cerrado, but additional research is needed to properly characterize these relationships and explain the associated physical mechanisms. Nevertheless, fire activity in this biome is linked to meteorological conditions and the Cerrado seems to be heading for a hotter and drier future (Feron et al. 2019; Silva et al. 2019) where CDHW events are bound to occur more often.

B.5 Future perspectives and recommendations

Extreme climate events, such as intense, prolonged, and frequent CDHW episodes, present a new challenge for human health, the economy, and ecosystems around the world. These threats are of particular importance in low-income regions with limited public health resources, low environmental protection investments, and a growing urban population, such as Brazil (Alizadeh et al. 2022). Therefore, it is crucial that the country acknowledges this multiple hazard framework and becomes more engaged internationally as part of a global network of research on CDHW events. This is particularly relevant for Brazilian public agencies, with oversight attributions in different socioeconomic sectors (e.g., agriculture, energy, or health), that aim to provide rigorous and useful information for decision-makers to mitigate the impacts of current and future extreme climatic episodes linked to HW and drought. As described in this

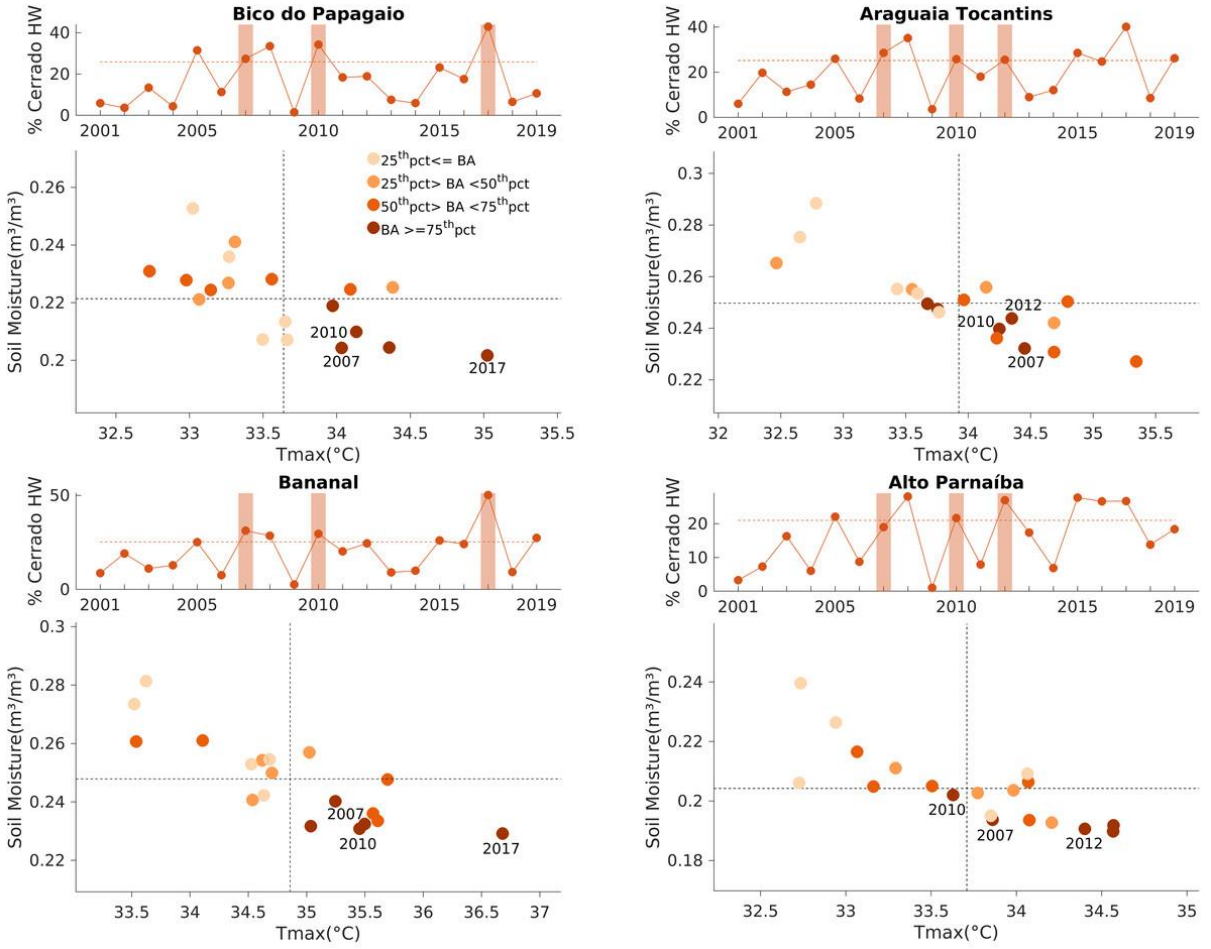

Figure B.5 The impact of soil moisture deficits and HW events during the Cerrado fire season (August–October) on burned areas in distinct ecoregions of the Cerrado. The upper panels represent the year-to-year variability of the percentage of HW incidence over each ecoregion; the dashed line is the 75th percentile over the time series (2001–2019) and the years highlighted in orange are the top three years with higher burned areas. The bottom panels show the yearly average of maximum temperature T_{max} (°C) and soil moisture (m^3/m^3): dot colors represent the burned area in a given year; finally, dashed lines indicate the medians of T_{max} and soil moisture during 2001–2019.

work, some studies have begun to build a better understanding of the physical mechanisms connecting the occurrence of persistent hot and dry conditions in Brazil. However, to the best of our knowledge, and with the exception of the recent works of Libonati et al. (2022a) and Ribeiro et al. (2022) there is a clear gap in the identification and quantification of the spatial pattern and temporal evolution of impacts associated with CDHW in the country. We are confident that obtaining a better understanding of the coupled phenomena of HWs and droughts in the country is crucial to enhance the adaptive capacity of different sectors, such as public health, civil defense, agriculture, tourism, and public policy management. In this context, we would like to highlight below some recommendations for the development of this research field in Brazil:

- **Disentangling the physical mechanisms and atmospheric patterns associated with CDHW events**. Given the complexity involved, accurately forecasting CDHW events is a major challenge for climate scientists. It requires a deep understanding of the various physical processes involved, including the associated soil–atmosphere feedback. If the research community aims to improve the CDHW forecasting field, it is mandatory to have a better understanding of the large-scale meteorological conditions that trigger hot and dry conditions observed in past events and how remote forcing factors, such as sea surface temperature anomalies, influence these patterns. With this information in hand, researchers can then develop monitoring systems and even early warning systems that can predict the evolution of these events. To this end, it is urgent to guarantee high-quality and long-term *in situ* observational datasets around the country as well as refined satellite-derived information covering land-related, meteorological, and hydrological variables, an area where Brazil suffers serious deficiencies (Coelho et al. 2016b). Moreover, the enhancement of regional physical models as climate and hydrological modeling is also crucial for studying the current and future dynamics of such compound events. For instance, a recent study pointed out that, for the Amazonia rainforest, improving the representation of the processes driving precipitation trends, such as forest productivity response to global warming and shifts in the Atlantic meridional overturning circulation, is crucial for better estimates of future compound risk (Bevacqua et al. 2022). In this context, the exploitation of new techniques, such as machine learning, aiming to circumvent current uncertainties and missing processes in Earth system models is a promising field of research.

- **Quantitative mapping of high-intensity and high-frequency CDHW areas**. As more information is gathered across different Brazilian regions, the understanding of spatial and temporal patterns (duration, frequency, and intensity) and trends of CDHW events will move beyond a general approach and toward a region-specific one based on the intrinsic characteristics of each ecosystem (e.g., geographical, climatic, urbanization, and degree of degradation). This would allow the identification of still-unknown important climatic and anthropogenic drivers of CDHW events in hotspot areas (Feng et al. 2020; Mukherjee et al. 2022). Such an approach may serve to determine the effects of these extreme events on different environmental and socioeconomic sectors, allowing the adoption of more local strategies for better management and prediction. Besides, regionalized climate projections can be applied in the assessment of CDHW events in such vulnerable areas to identify changes between the present and future regime and assess the impacts of regional climate changes (Bevacqua et al. 2021).

- **Quantification of the impacts and identification of regions/populations with the highest vulnerability**. The continuous exposure of the country to CDHW episodes provides strong motivation to explore adaptation strategies to increase societal and environmental resilience. In this context, multidisciplinary scientific research is essential to provide robust knowledge about the impacts of CDHW events. Accordingly, impacts can be correlated with auxiliary economic or demographic data, such as population density, average income, land cover and land use changes, social conditions, and other factors that reflect the conditions of human life and natural ecosystems. In this way, and considering the likely increase in frequency and amplitude of CDHWs in Brazil (Mukherjee and Mishra 2021; Raymond et al. 2022), there is a strong need for work that provides clear guidelines for public health and environmental policies related to CDHW events, contributing to change the purely reactive response of historical basis and avoiding the escalation of socioeconomic inequalities. As we have outlined above, most of the current impact analysis on the country relies on isolated droughts and HWs events. Accordingly, progress in impact analysis may be accelerated if these extreme events are considered combined instead of separately.

Supplementary Material

Here we describe in depth the key databases and methods used in section 3 to address the impacts of compound drought and heatwave (CDHW) events on human health and vegetation fires.

Data

Dataset used in section 3.1 Threats to public health

The impact of CDHW events on public health was investigated, including effects on human mortality and preterm births. Daily mortality data from the Brazilian Health Informatics Department (DATASUS) was provided by the Brazil Mortality Information System (SIM). All-natural deaths for the 2000–2018 period, considering all municipalities within the Metropolitan Region of Rio de Janeiro (MRRJ) were considered, except deaths related to external causes, such as accidents or murders.

Live birth certificates from the DATASUS were provided by the Brazilian Information System on Live Births (SINASC) for the 2011–2017 period in the MRRJ, including total births and preterm births (< 37 gestational weeks) from hospital births (excluding home births or others).

Dataset used in section 3.2 Vegetation fire response to the simultaneous occurrence of hot and dry events

Fire data was obtained from different sources, depending on the biome. For the Pantanal and Cerrado biomes, we used monthly burned area values from the MCD64A1 collection 6 derived from the MODIS (Moderate Resolution Imaging Spectroradiometer) sensor at 500 m spatial resolution from 2001 to 2019 (Giglio et al. 2018) .In the case of Pantanal, we further employed daily burned area values for 2020 from the ALARMES dataset (https://alarmes.lasa.ufrj.br/login) with a 500 m spatial resolution based on images from the Visible Infrared Imaging Suite Imager (VIIRS) sensor (Pinto et al. 2020), following the approach of Libonati et al. (2022a). Due to the low accuracy of satellite-derived burned area products over the Amazonia[4], for this biome, we opted to use daily Active fire information at 1

km resolution from collection 6 AQUA MODIS active fire detection product (Giglio et al. 2018) for the 2003–2019 period.

Annual Deforestation rates for the Amazon were provided by the Program for Deforestation Assessment in the Brazilian Amazonia (PRODES - http://www.obt.inpe.br/OBT/assuntos/programas/amazonia/prodes) for the drought years of 2005, 2010 and 2015.

Daily fields of maximum 2m temperature (Tmax), surface net radiation and hourly data of total precipitation was extracted from the European Centre of Medium-range Weather Forecast ERA5 reanalysis dataset (Hersbach et al. 2020). Daily estimates of soil moisture and evaporation were also obtained from the Global Land Evaporation Amsterdam Model (GLEAM v3.5a) (Martens et al. 2017).

All variables were analyzed at a gridded 0.25° × 0.25° spatial resolution.

Methods

The methodology used in section 3.1 Threats to public health

To investigate the impacts of CDHW events on public health we analyzed excess mortality and births during HWs over the 2013/2014 and 2014/2015 summer compound conditions period recorded in the MRRJ according to Geirinhas et al. (2022). Then, over these two record-breaking dry summer periods, we identify HW events using the excess heat factor (EHF) (Nairn and Fawcett 2014). The EHF has been shown as an adequate index for HW-related epidemiologic studies (Nairn and Fawcett 2014). The EHF is composed of two indices: the significance index (EHI_{sig}) and the acclimatization index (EHI_{accl}), as follows:

$$EHI_{sig} = (T_i + T_{i+1} + T_{i+2})/3 - T_{95} \quad (1)$$

$$EHI_{accl} = (T_i + T_{i+1} + T_{i+2})/3 - (T_{i-1} + \ \dots \ + T_{i-30})/30 \quad (2)$$

The EHI_{sig} is the difference between the three-day-averaged daily mean temperature and the 95_{th} percentile of daily mean temperature across the 1981–2010 period (T95). The EHI_{accl} is calculated as the difference between the same three-day-averaged daily mean temperature

and the average daily mean temperature over the recent past (previous 30 days). So, the EHF is calculated as:

$$EHF = EHI_{sig} \times \max(1,\ EHI_{accl}) \quad (3)$$

Thus, if the EHF is positive, all the days within the three-day period are considered heatwave days.

Once CDHW events have been identified, the effects on human health were evaluated by calculating the observed-to-expected ratio (O/E) for daily mortality and total/preterm births. For each CDHW period, the expected number of deaths/births was calculated as the average during a reference period, i. e., the same period of the event in the previous and subsequent years. The confidence interval (95% I.C.) for O/E ratio was estimated as proposed by Hoshiko et al. (2009).

Methodology used in section 3.2 Vegetation fire response to the simultaneous occurrence of hot and dry events

Heatwave definition and indexes:

Similarly to previous studies (Perkins and Alexander 2013; Geirinhas et al. 2018a), a heatwave (HW) event was defined as a period of three or more consecutive days marked by daily Tmax levels above the climatological (1981–2010 base period) 90th percentile of Tmax for each calendar day (computed on a 15-day moving window). Based on this HW definition, a single one dimensional parameter that allows to quantify the time and spatial incidence of HW conditions over four Cerrado ecoregions (Bico de Papagaio, Araguaia Tocantins, Bananal and Alto de Paraíba) was defined and used to obtain the results presented in Figure B.5: the percentage of Cerrado ecoregion under HW conditions (%Cerrado$_{HW}$):

$$\%Cerrado_{HW} = \frac{cellsCER_{HW}}{cellsCER_{total}} \times 100 \quad (4)$$

This metric consists in determining the percentage of the total cells (both in space and time $cellsCER_{total}$) within each Cerrado ecoregion that is under HW conditions ($cellsCER_{HW}$). The $cellsCER_{total}$ index is obtained by multiplying the total number of grid-points within each one

of the considered Cerrado ecoregions ($cellsCER_{region}$) and the total number of days of the Cerrado's fire season (August to October - $cellsCER_{time}$) as in Eq. (4):

$$cellsCER_{total} = cellsCER_{region\ x}\ cellsCER_{time} \quad (5)$$

In parallel, the $cellsCER_{HW}$ parameter is computed in the same way as $cellsCER_{total}$ by considering only the number of days and grid-points within the Cerrado ecoregion domain that are under HW conditions. For example, a $\%Cerrado_{HW}$ value of 100% indicates that all the area of the considered Cerrado ecoregion experienced HW conditions for every day of the fire season ($cellsCER_{HW}$equals $cellsCER_{total}$).

Compound drought and heatwave definitions and indexes:

A CDHW episode was simply defined as an HW event (as defined earlier in this section) occurring in a region also experiencing drought conditions. Throughout the manuscript, drought conditions were characterized and quantified using different approaches: by computing and analyzing (i) soil moisture anomalies composites; (ii) evaporative fraction anomalies composites and (iii) standardized precipitation index (SPI) values obtained for a 6-month timescale (SPI-6).

Based on all these criteria, a metric similar to $\%Cerrado_{HW}$ described previously, was defined in order to quantify in space and time the incidence of CDHW condition over Pantanal ($\%Pantanal_{CDHW}$ - Figure B.3). The definition of this metric is similar to the one used to compute $\%Cerrado_{HW}$ with the exception that it considers not only the space and time incidence HW conditions but of compound drought and HW conditions.

For the analysis of the link between CDHW episodes and fires over Pantanal, each Pantanal grid-point was considered to be under the influence of CDHW conditions everytime that the corresponding daily SPI-6 level was equal to or lower than -1 and HW conditions were simultaneously witnessed according to the HW definition presented at the beginning of this section.

Regarding the manuscript section where the link between CDHW episodes and fires is analyzed for the Amazonia biome (Figure B.4), the percentage of days during a predefined period affected by CDHW conditions (June–August 2005; June–August 2010 and October–

December 2015) was computed and evaluated for each grid-point within the Amazon biome. In this section, the CDHW conditions were defined in the exact same way as they were defined for the analysis of the link between CDHW events and fires in Pantanal.

Fire analysis:

For the interannual variability of the burned area within the Pantanal biome, burned area totals were computed from July to October over the 2001–2019 period. In the case of Cerrado, annual burned area totals per ecoregion were estimated for the same 19-year period.

Regarding Figure B.4, active fire datasets from June–August 2005, June–August 2010 and October–December 2015 were standardized by subtracting 2003–2019 mean from total fire counts in that period at each grid point and then dividing by the standard deviation for the same period.

Appendix C

Heatwaves and fire in Pantanal: Historical and future perspectives from CORDEX-CORE

*Silva PS, **Geirinhas JL**, Lapere R, Laura W, Cassain D, Alegría A, Campbell J. (2022) Heatwaves and fire in Pantanal: Historical and future perspectives from CORDEX-CORE. J Environ Manage 323:116193. https://doi.org/https://doi.org/10.1016/j.jenvman.2022.116193*

João Lucas Geirinhas contributions: *conceptualization of the analysis, data management (download and curation), computation and analysis of the results and manuscript writing.*

Abstract

The Pantanal biome, at the confluence of Brazil, Bolivia and Paraguay, is the largest continental wetland on the planet and an invaluable reserve of biodiversity. The exceptional 2020 fire season in Pantanal drew particular attention due to the severe wildfires and the catastrophic natural and socio-economic impacts witnessed within the biome. So far, little progress has been made in order to better understand the influence of climate extremes on fire occurrence in Pantanal. Here, we evaluate how extreme hot conditions, through heatwave events, are related to the occurrence and the exacerbation of fires in this region. A historical analysis using a statistical regression model found that heatwaves during the dry season explained 82% of the interannual variability of burned area during the fire season. In a future perspective, an ensemble of CORDEX-CORE simulations assuming different Representative Concentration Pathways (RCP2.6 and RCP8.5), reveal a significant increasing trend in heatwave occurrence over Pantanal. Compared to historical levels, the RCP2.6 scenario leads to more than a doubling in the Pantanal heatwave incidence during the dry season by the second half of the 21st century, followed by a plateauing. Alternatively, RCP8.5 projects a steady increase of heatwave incidence until the end of the century, pointing to a very severe scenario in which heatwave conditions would be observed nearly over all the Pantanal area and during practically all the days of the dry season. Accordingly, favorable conditions for fire spread and consequent large burned areas are expected to occur more often in the future, posing a dramatic short-term threat to the ecosystem if no preservation action is undertaken.

C. Heatwaves and fire in Pantanal: Historical and future perspectives from CORDEX-CORE

C.1 Introduction

The Pantanal biome is the largest continental wetland in the world, extending over parts of Brazil (Bergier and Assine 2016). This World Heritage Site (UNESCO 2022) is home to a wide variety of plants (Pott et al. 2011) and animals (Alho 2008), including several endangered species (Tomas et al. 2019). In 2020, Pantanal faced the most devastating fires in the last two decades. Satellite-derived estimates showed that around a third of the Brazilian section of Pantanal was affected (Libonati et al. 2020), including several indigenous territories and conservation units being completely burnt.

Fire activity and climate have been shown to be closely linked (Mariani et al. 2018; Abatzoglou et al. 2019; Ruffault et al. 2020; Sutanto et al. 2020) and the 2020 Pantanal fires resulted from an interplay between extreme hot and dry conditions (Libonati et al. 2022a) associated with the negligent use of fire (Mataveli et al. 2021). Leading up to the 2020 fire season, Pantanal had been under severe drought conditions since 2019 (Marengo et al. 2021), which severely impacted vegetation flammability. Soil desiccation conditions concurred with several heatwave episodes, leading to the establishment of strong soil moisture–temperature coupling regimes (water-limited) that triggered a temperature escalation through enhanced sensible heat fluxes from the surface to the atmosphere (Libonati et al. 2022a). As a result of this, the compound dry and hot conditions observed during 2020 over Pantanal, essentially drove fire danger to levels not seen since 1980 (Libonati et al. 2020).

The future dynamics and intensity of global fires is uncertain under climate change scenarios, and highly depends on the climate zone and local human drivers (Moritz et al. 2012; Williams and Abatzoglou 2016). For South America however, an increasing trend in fire risk and extent is projected under a range of likely scenarios (Cochrane and Barber 2009; Liu et al. 2010; Silva et al. 2019; de Oliveira-Júnior et al. 2021; Burton et al. 2022; Oliveira et al. 2022). In parallel, the number of heatwaves associated with record-breaking temperatures have been increasing over Pantanal (Marengo et al. 2021; Libonati et al. 2022a). Such a growing trend in the number of extreme hot spells is expected to continue in most regions including South America (Dosio 2017; Baker et al. 2018; Feron et al. 2019; Di Luca et al. 2020; Molina

et al. 2020; Coppola et al. 2021). Feron et al. (2019) found for South America that the magnitude of this increase would not be spatially homogeneous, although by 2050, the tropical areas, including Pantanal, would witness extremely warm temperatures during at least half the days of the year. By the end of the century, annual average temperatures in Pantanal can increase by up to 7 °C relative to the 1961–1990 period (Marengo et al. 2015; Llopart et al. 2020). Additionally, daily maximum temperature in Pantanal will likely increase by several degrees over the period 2050–2080 under different scenarios (Reboita et al. 2022). Although the effects of climate change on Pantanal remain by far uncertain and are probably outweighed by human development and wetland destruction (Junk 2013), the possible trends can induce changes in the dynamics and properties of the fire season, possibly jeopardizing even more of Pantanal's ecosystems.

This work aims to evaluate the connection between heatwaves and fire in the Pantanal biome during the 2002–2020 period, and assess future trends under two climate change scenarios. Historical COordinated Regional Climate Downscaling EXperiment-COmmon Regional Experiment (CORDEX-CORE) simulations are then evaluated and compared to reanalysis data, evidencing the need for bias-correction. Accordingly, we compute bias-corrected future projections of heatwaves using the CORDEX-CORE ensemble and interpret the results in light of future climate change and what it might mean for fires in Pantanal.

C.2 Data and Methods

C.2.1 Data

The region of interest is the Pantanal biome as defined by the Terrestrial Ecoregions of the World (Olson et al. 2001). Burned area was derived from the Moderate Resolution Imaging Spectroradiometer (MODIS) MCD64A1 Collection 6 product (Giglio et al. 2018), developed by the National Atmospheric Space Agency (NASA). Derived from the MODIS sensors aboard Terra and Aqua satellites, MCD64A1 is a monthly burned area product at a 500 m spatial resolution from 2001 to 2020. Re-projected GeoTIFF data for South America was obtained from the University of Maryland's fuoco SFTP Server (fuoco.geog.umd.edu). Burned area totals were computed for the Pantanal and 2001 was dropped as it only includes data from the MODIS sensor aboard Terra.

Daily maximum surface air temperature (Tmax) values from 1980 to present were obtained for Pantanal by computing the daily maximum of hourly surface temperatures retrieved from the European Centre of Medium-range Weather Forecast (ECMWF) ERA5 reanalysis dataset (Hersbach et al. 2020), at a gridded 0.25° × 0.25° spatial resolution.

Using data available from the ESGF platform (Cinquini et al. 2014), simulated daily maximum temperature for the historical period (spanning 1981 to 2005) and Representative Concentration Pathways (RCP) 2.6 and 8.5 were extracted from CORDEX-CORE runs on the South American domain at a 0.22° spatial resolution (Gutowski Jr. et al. 2016; Giorgi et al. 2022). This work relies on three realizations (historical, RCP2.6 and RCP8.5) from two Regional Climate Models - RCMs (REMO2015, RegCM4-7), each one forced by three different Global Climate Models — GCMs (HadGEM2-ES, MPI-ESM, NorESM1) as described in Table C.1. RCPs represent possible trajectories of future greenhouse gas and air pollutants emissions: the low-emission RCP2.6 scenario limits additional radiative forcing to 2.6 W/m2 by 2100 (van Vuuren et al. 2011) whereas the high-emission RCP8.5 scenario corresponds to a 8.5 W/m2 radiative forcing (Riahi et al. 2011).

C.2.2 Heatwave definition

Using a relative threshold index (Perkins and Alexander 2013; Geirinhas et al. 2021) heatwaves were defined as periods of three or more consecutive days featuring Tmax values above the climatological (1981–2010 in the case of data computation with ERA5, and 1981–2005 with the historical CORDEX-CORE simulations) calendar day 90th percentile (P90) of Tmax (centered on a 15-day window). Based on this definition, a single one dimensional variable accounting for the time and spatial incidence of heatwaves over Pantanal was defined: the percentage of the total Pantanal domain under heatwave conditions ($\%Pantanal_{HW}$). This metric was already used in previous studies conducted for regions within the USA (Mazdiyasni and AghaKouchak 2015) and Brazil (Geirinhas et al. 2021), and consists in determining the percentage of the total Pantanal cells (in space and time - $cellsPAN_{total}$) that experience heatwave conditions ($cellsPAN_{HW}$), as expressed in Eq. (C.1).

Table C.1 Regional climate models (RCM) considered in this study: runs for the South American domain at 0.22° × 0.22° spatial resolution (SAM-22) available within the COordinated Regional Climate Downscaling EXperiment-COmmon Regional Experiment (CORDEX-CORE; (Giorgi et al. 2022)).

Model	Experiment	Time period	Forced by
ERA5	Historical	1970/01/01 – 2005/12/31	(-)
REMO2015	Historical	1970/01/01 – 2005/12/31	MOHC-HadGEM2-ES
	RCP2.6	2006/01/01 – 2099/12/31	MPI-M-MPI-ESM-LR
	RCP8.5	2006/01/01 – 2099/12/31	NCC-NorESM1-M
RegCM4-7	Historical	1970/01/01 – 2005/12/31	MOHC-HadGEM2-ES
	RCP2.6	2006/01/01 – 2099/12/31	MPI-M-MPI-ESM-MR
	RCP8.5	2006/01/01 – 2099/12/31	NCC-NorESM1-M

$$\%Pantanal_{HW} = \frac{cellsPAN_{HW}}{cellsPANtotal} \times 100 \quad \text{(C. 1)}$$

The number of total Pantanal cells ($cellsPAN_{total}$) is obtained by considering the total number of grid-points within the Pantanal region ($cellsPAN_{region}$) and the total number of days of the dry season (April through October - Figure C.1b - $cellsPAN_{time}$) as in Eq. (C.2).

$$cellsPAN_{total} = cellsPAN_{region} \times cellsPAN_{time} \quad \text{(C. 2)}$$

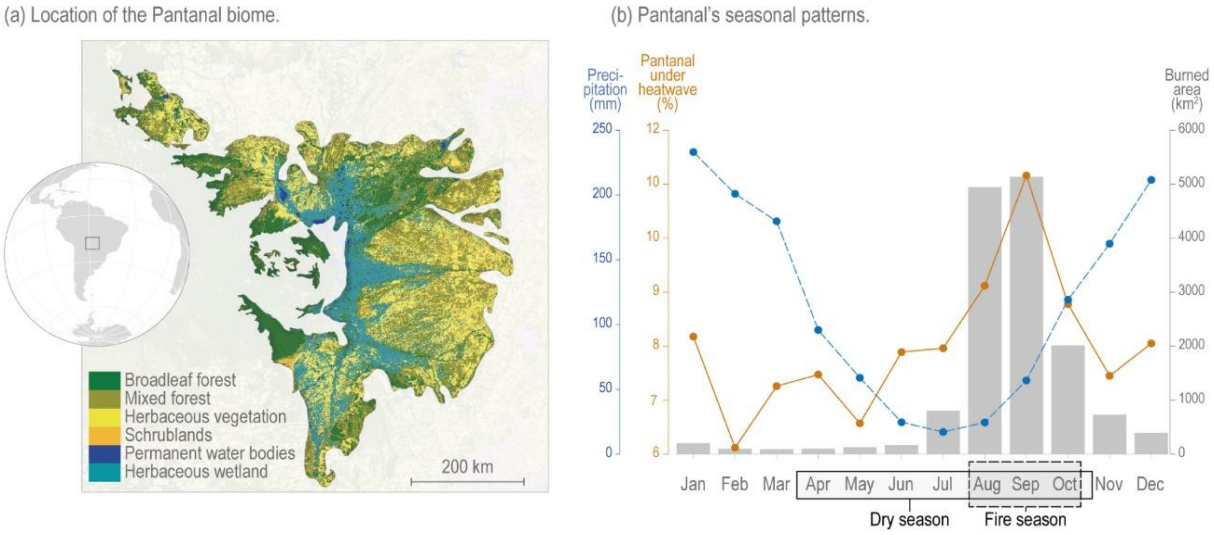

Figure C.1 (**a**) The Pantanal biome with land cover information for 2019 from the Copernicus Global Land Service (Buchhorn et al., 2020). (**b**) Pantanal's monthly averages of burned area (gray bars) as estimated by the MCD64A1 Collection 6 product over 2002–2020, and seasonal precipitation (blue line) and heatwave incidence (orange line) patterns in ERA5 reanalysis for the period 1981–2020. (For interpretation of the references to color in this figure legend, the reader is referred to the web version of this article.)

The number of total Pantanal cells under heatwave ($cellsPAN_{HW}$) is computed in the exact same way as $cellsPAN_{total}$, however it only considers the number of days and grid-points that are under heatwave conditions (as defined earlier in this section). As an example of application, a percentage of 100% indicates that every single grid point in the Pantanal domain witnessed heatwave conditions for every day of the dry season, and so, $cellsPAN_{HW}$ equals $cellsPAN_{total}$.

C.2.3 Heatwave definition

The statistical relationship between burned area and heatwaves was evaluated using a simple linear regression model. Interannual variations of burned area (predictand, BA) were correlated with variations of the percentage of the total Pantanal domain under heatwave conditions (predictor, $\%Pantanal_{HW}$) as in Eq. (C.3).

$$BA = m \times \%Pantanal_{HW} + b \quad \text{(C. 3)}$$

where m and b are the slope and intercept of the model, respectively. The goodness of fit was analyzed and assessed through the resulting coefficient of determination and p-value. To further test the robustness of the statistical model, and given the short length of the time series, a leave-one-out cross-validation scheme was performed (Wilks 2011) and the Spearman's rank correlation coefficient computed.

Throughout this work, monotonic trends were estimated using the non-parametric Mann–Kendall two-tailed test (Mann 1945; Kendall 1948; Gilbert 1987), and the Theil–Sen slope (Theil 1950; Sen 1968).

C.2.4 Bias correction

Bias correction was performed using a Quantile Delta Mapping (QDM) approach, in order to match Tmax distribution in the RCM realizations to that of ERA5, despite the discrepancies initially observed. The correction is applied both to historical and future scenario runs. QDM is known to perform well when it comes to preserving raw signals, trends and extremes (Cannon et al. 2015; Casanueva et al. 2020). QDM relies on the computation of the cumulative distribution functions (CDF) of the variable of interest, in the dataset of reference (here ERA5), and in the model to be adjusted on the historical and future periods (here CORDEX-CORE historical and RCPs). Based on these statistical distributions, the transformation applied can be summarized in Eq. (C.4). Using this approach, the bias corrected Tmax obtained with Eq. (C.4),

referred to as $Tmax_{FUT_{QDM}}$, will incorporate the climate change signals present in the original CORDEX-CORE RCP runs.

$$Tmax_{FUT_{QDM}} = Tmax_{FUT} \times \frac{CDF_{ERA5}^{-1}(CDF_{FUT}(Tmax_{FUT}))}{CDF_{HIST}^{-1}(CDF_{FUT}(Tmax_{FUT}))} \quad (C.4)$$

QDM can be performed either in a parametric or empirical approach to compute the CDF. Here, the choice of a parametric (thus continuous) rather than empirical (thus discrete) approach is made so as to be able to capture future extreme values that may not be reached in the historical period distribution. For well-chosen parametric distribution forms, the performance is similar for parametric and empirical approaches (Enayati et al. 2021). Further details on QDM and its suitability and performance for our purpose can be found in Supplementary Material, Figures SC.1 and SC.2.

C.3 Results

C.3.1 Fire-Heatwave connection

Pantanal burns quite frequently and mostly during the period from August to October, henceforth referred to as the fire season (Figure C.1b; Damasceno-Junior et al. 2021). These months account, on average, for 79% of the annual burned area over the study period and coincide with low rainfall levels. Heatwaves also occur more often and over larger areas during these three months, with the maximum value of $\%Pantanal_{HW}$ in September concurrent with the yearly peak in burned area. Heatwaves taking place in the austral summer (December, January, February) and during the transition from wet to dry season (March–April) are not associated with high burned areas as the vegetation is growing and moisture levels are high, which constrains the spread and extent of fires (Ivory et al. 2019). Accordingly, in the upcoming analysis we evaluate heatwave conditions over the months from April to October, considered here as the biome's dry season (Figure C.1b; de Oliveira et al. (2014) and Ivory et al. (2019)), to account for the effects of heatwaves on fuel moisture levels prior to the fire season.

The biome averages 14,439 ± 9649 km^2 burned area (8.5 ± 5.7% of Pantanal's area) per year over the 2002–2020 time series, with high interannual variability (Figure C.2a). The years

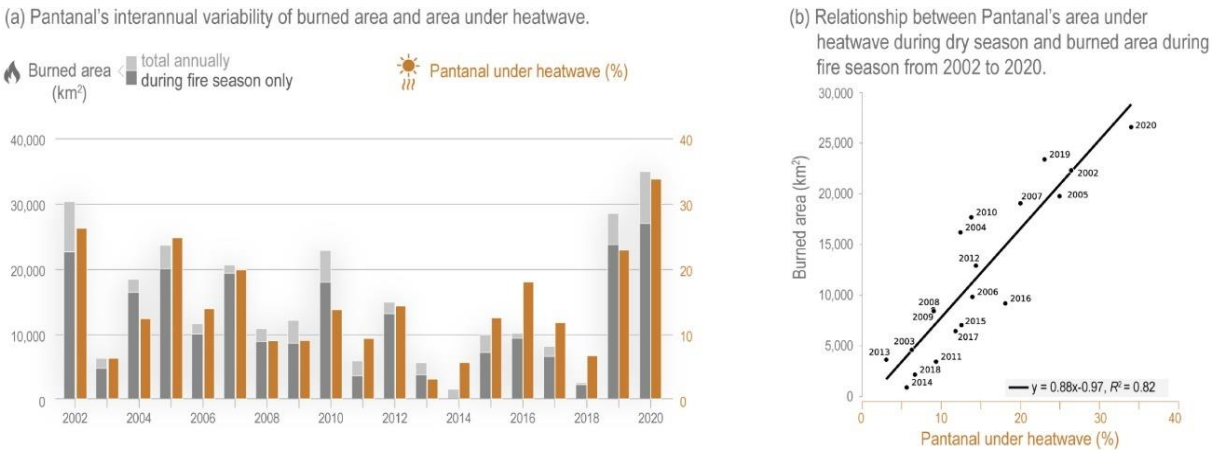

Figure C.2 (**a**) Interannual variability of annual burned area (light gray bars) and fire season burned area (August to October; dark gray bars), using the MODIS MCD64A1 product, and the percentage of Pantanal under heatwave (%$Pantanal_{HW}$) over the dry season (April to October; orange bars), from 2002 to 2020. (**b**) Relationship between %$PantanalHW$ over the dry season and the fire season burned area, estimated using ERA5 reanalysis, from 2002 to 2020, evaluated using simple linear regression model. Black line indicates the resulting regression line and on the bottom right corner is the corresponding equation. (For interpretation of the references to color in this figure legend, the reader is referred to the web version of this article.)

of 2002, 2019 and 2020, stand out as the most dramatic, with the latter burning a record-shattering amount unseen in Pantanal over the last two decades.

The interannual variability of burned area over the fire season seems to be closely related to the percentage of Pantanal that is under heatwave over the dry season (Figure C.2a). Years with the highest (lowest) burned area correspond with higher (lower) percentages of heatwave incidence over Pantanal (%$Pantanal_{HW}$), with the exception of 2007, when the %$Pantanal_{HW}$ reached its maximum value over the 2002–2019 period while burned area values were below the time series 75th percentile.

A simple linear regression model between annual values of these two variables obtained a Pearson coefficient of 0.90 (p-value < 0.001). Hence, the linear model described in Eq. (C.5) based on %$Pantanal_{HW}$ significantly explains 82% of the variance of burned area over the 2002–2020 period (Figure C.2b). It is worth noting here that causality is not assumed in this relationship. It only constitutes a purely statistical conception that holds for values of %$Pantanal_{HW}$ varying between approximately 3% to 34%, which is the historically observed range.

$$BurnedArea = 0.88 \times \%Pantanal_{HW} - 0.97 \quad (C.5)$$

with burned area in 1000 km^2 and %$Pantanal_{HW}$ in percentage.

The leave-one-out cross-validation scheme (Supplementary Material, Figure SC.3) resulted in a coefficient of determination of 0.78 between the observed and the predicted burned area values, and a Spearman's correlation ρ of 0.90 (p-value < 0.001), which confirms that the linear model is robust and indeed the best approach to correlate these variables.

C.3.2 Model evaluation

There is a large variability in the outcomes of each of the six members of the CORDEX-CORE ensemble considered. The comparison of Tmax between the six historical runs and the ERA5 reanalysis, for the Pantanal region, during the dry season and for the period 1981–2005, shows correlations on the time series of monthly averages of daily Tmax ranging from 0.42 to 0.67, and correlations on monthly P90 of Tmax between 0.60 and 0.84 (Figure C.3a). Mean biases on these variables are between 0.4 °C to 5.3 °C and 0.28 °C to 4.4 °C, for monthly averages and P90, respectively. REMO2015 forced by HadGEM2-ES shows the best agreement with ERA5, contrary to RegCM4-7 forced by NorESM1 that features the largest discrepancies with the ERA5 reanalysis. The remaining models show intermediate values and, for all models, lower mean biases and higher correlations are found when looking at the monthly P90. This large inter-model spread is commonly observed in multi-model analyzes of RCMs, in particular in the CORDEX framework for South America (e.g. Feron et al. 2019). The ensemble is also shown to have a mean bias of 2.72 °C and 3.76 °C, and a Pearson correlation coefficient of 0.68 and 0.79, for the mean and P90 of Tmax, respectively. For impact studies, the ensemble mean is usually able to properly reproduce the main climatological features of the region,

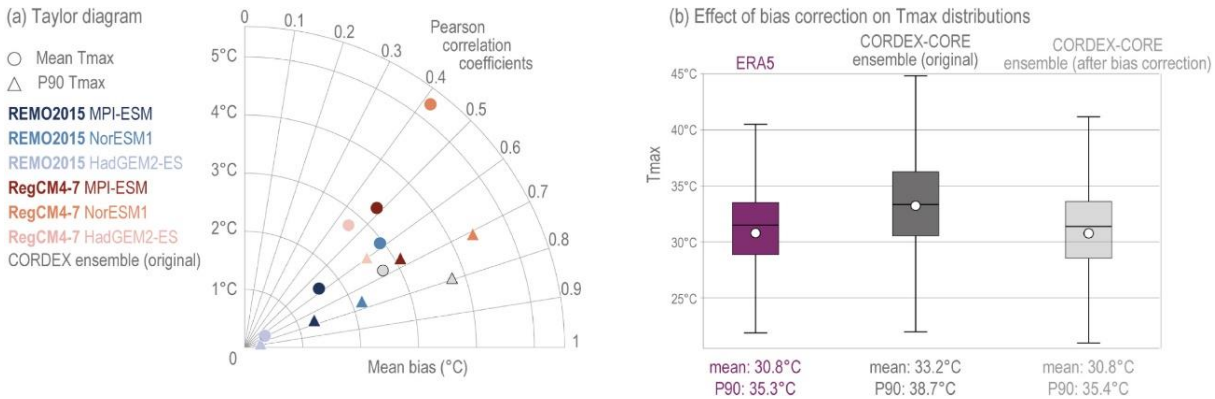

Figure C.3 (**a**) Taylor diagram of raw CORDEX-CORE historical simulations compared to ERA5. Tmax monthly mean (circles) and monthly P90 (triangles) during dry season months (April–October) over Pantanal for the period 1981–2005, for each simulation (color range) and for the ensemble mean (gray). All Pearson correlation coefficients presented here are statistically significant at the 99.9% level. (**b**) Tmax distribution over Pantanal for dry season months of the historical period in ERA5 (purple), CORDEX-CORE original (gray) and CORDEX-CORE after bias correction (light gray).

notwithstanding the large variability across individual members (Coppola et al. 2021; Teichmann et al. 2021).

Considering this inter-model variability and discrepancies compared to ERA5, Tmax datasets from the CORDEX-CORE runs were bias-corrected towards the distribution of Tmax in ERA5. Figure SC.1 shows the time series for Tmax of raw CORDEX-CORE historical data and both RCP runs over the 1981–2099 period, and the result after bias-correction. A clear shift is observed towards ERA5 values after bias correction, while keeping the trends intact. The performance of the bias correction is also illustrated in Figure C.3b, which shows that the bias between CORDEX-CORE and ERA5 ensemble mean (P90) Tmax goes from 2.4 °C (3.4 °C) before correction to less than 0.1 °C after. QDM therefore seems to be successful in approximating the CORDEX-CORE ensemble mean distribution to that of ERA5, as also evidenced in Figure SC.2. The bias-corrected results are now in the same range as those of the reanalysis: the historical mean of Tmax is now equal for CORDEX-CORE after QDM and the ERA5 reanalysis, at 30.8 °C (Figure C.3b). Moreover, Figure SC.1 confirms the above-mentioned large inter-model variability, with large shaded areas representing the maximum and minimum values simulated by CORDEX-CORE runs after bias-correction.

Figures C.4 and C.5 further highlight this inter-model variability, which is found also in future projections. Under RCP8.5 scenario (Figure C.4), for the near future period (2026–2050, top line in the Figure), Tmax during the dry season increases on average between 0 to 2 °C approximately, depending on the considered GCM/RCM combination. For the mid-term

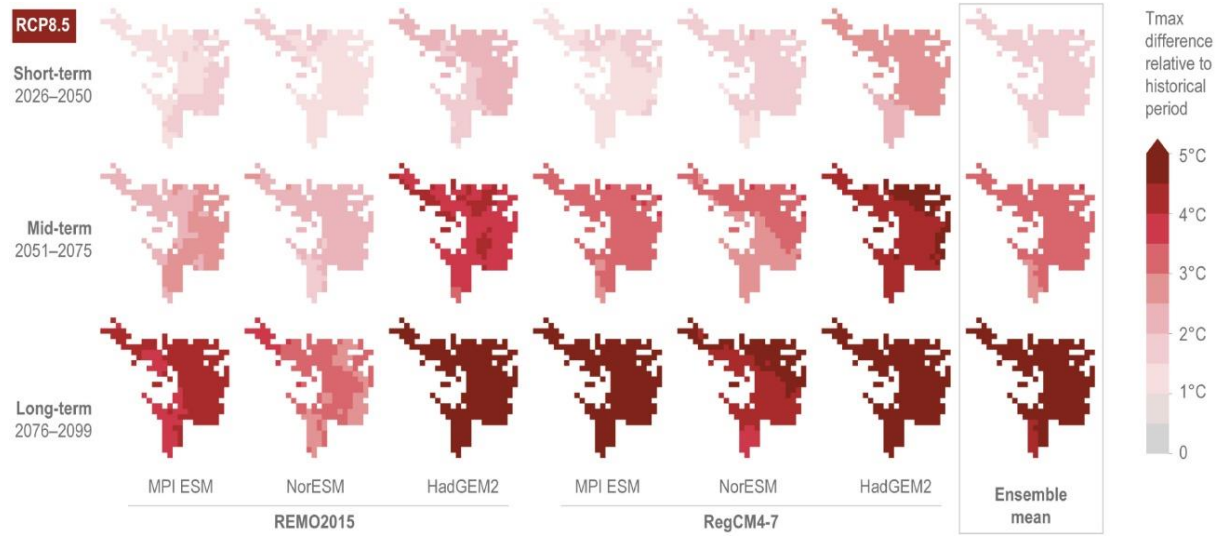

Figure C.4 Average difference on Tmax over the Pantanal region for April to October between the historical period and three projected RCP8.5 periods (2026–2050 as short term; 2051–2075 as mid term; and 2076–2099 as long term), for the six CORDEX-CORE simulations considered and the ensemble mean (rightmost panel). All data is from the bias-corrected simulations.

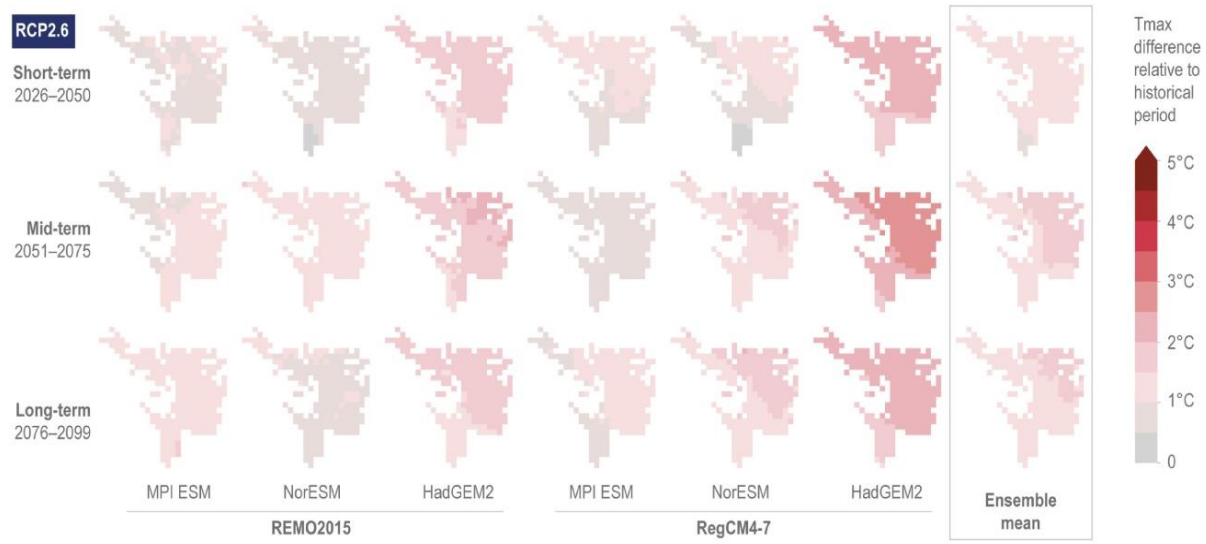

Figure C.5 Same as Figure C.4 for RCP2.6.

(2051–2075) and long-term (2076–2099) periods, the spread increases, with Tmax warming between 1.5 to 5 °C and 3 to 9 °C, respectively. The trajectory under RCP2.6 assumptions suggests a lesser warming of Pantanal, along with a smaller inter-model spread, in absolute value, as compared with RCP8.5 (Figure C.5). For that scenario, all runs feature an increase in Tmax between 0 to 4 °C without a clear temporal evolution, with Tmax departure from its historical values in the short-term being similar to the mid- and long-term periods ones. In both scenarios, the expected warming is spatially quite homogeneous over the Pantanal region, except for its southernmost part, which seems to be slightly less affected in most runs, as opposed to the northeastern part that might suffer from even warmer conditions by up to 1 °C according to several runs.

C.3.3 Future trends in heatwaves

We analyzed the simulated evolution of heatwaves over Pantanal from 1981 to the end of the 21st century, under scenarios RCP2.6 and RCP8.5, using CORDEX-CORE bias-corrected ensemble mean. Under both scenarios, the $\%Pantanal_{HW}$ is expected to increase by 2100 (Figure C.6), albeit with distinct growing patterns. Considering the optimistic emission scenario RCP2.6, the average $\%PantanalHW$ is expected to increase up to 36.4% over the mid-term period, followed by a decrease to 35.2% in the long-term period (Table C.2). When compared to the historical average (12.5%), this represents a relative increase of 191% and 182% of the $\%Pantanal_{HW}$ for mid and long-term, respectively. Extremes, evaluated by the P90, reach 43.4% over mid-term and more than double the historical value with relative increases above 140% in all three time periods. However, no significant trend was found in either period,

consistent with RCP2.6 assumptions of peaking emissions mid-century followed by a steady decrease afterwards (van Vuuren et al. 2011).

Table C.2 Future evolution of heatwave index (%Pantanal$_{HW}$) under RCP2.6 and RCP8.5 scenarios for three time periods: short-term from 2006 to 2050; mid-term from 2051to 2075; and long-term from 2076 to 2099. For comparison, we further show values for the historical runs from 1981 to 2005. Average values are calculated as ensemble means from all RCM realizations. Std corresponds to the standard deviation, over time, of the ensemble mean for the considered period. Values between parentheses indicate relative change compared to the historical value. The presence of a trend is evaluated through the Mann-Kendall test at a 5% significance level. Upwards arrows indicate a significant positive trend. The average inter-model spread corresponds to the average, over each period, of the difference between the highest and lowest individual member value every year.

		Average	Std	P90	Trend	Inter-model spread
Historical		12.5	4.5	17.4	-	23.2
RCP2.6	Short-term	32.9 (163%)	6.6	41.8 (140%)	-	35.1
	Mid-term	36.4 (191%)	6.4	43.4 (149%)	-	32.8
	Long-term	35.2 (182%)	5.4	42.5 (144%)	-	33.9
RCP8.5	Short-term	39.9 (219%)	8.3	51 (193%)	↗	30.6
	Mid-term	58.5 (368%)	7.6	67.3 (287%)	↗	31.5
	Long-term	73.3 (486%)	4.6	7804 (351%)	↗	24.1

Alternatively, under the high-emission scenario RCP8.5 there is a statistically significant monotonic increase, clearly departing from the RCP2.6 scenario after the mid-term period, leading to a $\%Pantanal_{HW}$ level of 80% by the end of the 21st century (Fig. C.6). Average (and P90) values of $\%Pantanal_{HW}$ differ considerably over the three time periods (Table C.2): from 39.9% (51%) in the short-term period, slightly above the corresponding values in RCP2.6, to 73.3% (78.4%) in the long-term period. In this scenario, departures from the mean (and P90) historical values are dramatic, with relative increases of 219% (193%), 368% (287%) and 486% (351%), for the short, mid and long-term periods, respectively.

Nevertheless, in both scenarios, inter-model variability is relatively large (Table C.2). In particular, the spread of $\%Pantanal_{HW}$ between the minimum and maximum individual members from the ensemble for each projection year is around 32%, on average. In RCP2.6 scenario, this inter-model spread remains relatively stable, from 35% in the short-term period to 34% in the long-term, pointing to a moderate climate signal in Pantanal in that scenario. Contrarily, RCP8.5 leads to a decrease in the spread between models, from 31% in the short-term down to 24% in the last 25 years of the century. This indicates that under the stronger climate forcing of the RCP8.5 scenario, models tend to agree more on the long-term pathway

as all of them foresee extreme heatwave conditions in Pantanal at the end of the century. For the RCP2.6 scenario, although the mean is clearly higher than historical values, the ensemble member with the lowest warming projection is indistinguishable from the historical envelope for all the time periods considered. On the other hand, the lowest warming projection for RCP8.5 is well above the maximum of the historical envelope despite a relatively large inter-model spread. In the first half of the century, individual simulations from both RCPs overlap (shaded areas in Figure C.6), however, after 2050 there is a clear distinction between the maximum and minimum simulated values obtained for each RCP (Figure C.6). By the end of the century, although the maximum simulated value of $\%Pantanal_{HW}$ under RCP2.6 is higher than that of the historical run, the historical simulations that achieved the highest $\%Pantanal_{HW}$ are in the same range of values as RCP2.6 $\%Pantanal_{HW}$ ensemble means. This is not the case with RCP8.5, where, by 2100, the minimum value of simulated $\%Pantanal_{HW}$ far exceeds the maximum value obtained in any historical simulation, highlighting how RCP8.5 is a much more severe scenario.

For both RCPs, inter-model variability seems to decrease over the 21st century, with model predictions converging towards the end of the simulation period. This is particularly sharp in RCP8.5 where there is a decrease in inter-model spread and standard deviations (Table C.2), due to a threshold effect on the heatwave index computation, which is based on a comparison between Tmax and the fixed historical P90 of Tmax (see Section C2.2). In the case of RCP8.5 the significant increase in Tmax is such that, even though the inter-model variability in Tmax is large, all individual members are mostly above the historical heatwave threshold.

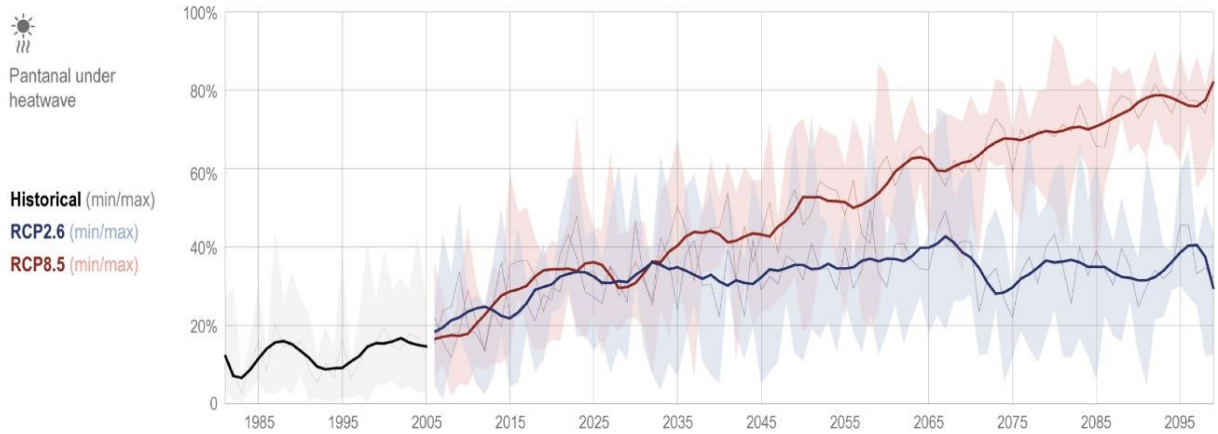

Figure C.6 Percentage of Pantanal under heatwave from 1981 to 2099. Evolution for historical (black line), RCP2.6 (blue line), and RCP8.5 (red line) bias-corrected CORDEX-CORE runs. The gray, blue and red shaded regions show the maximum range between individual model runs. Solid lines represent the ensemble mean and those that are thicker show a smoothed time series for better visualization. The smoothing is performed by applying a Savitzky–Golay filter with a window length of 19 years and a polynomial order 5.

Consequently, even the member with the lowest warming trajectory still generates a high heatwave index value, thereby dampening the variability observed in $\%Pantanal_{HW}$.

C.4 Discussion

The linear regression model developed in this study showed that 82% of the annual variance in Pantanal's burned area is related to annual variations in heatwave incidence. This strong connection between fire events and heatwaves is in agreement with previous analyzes conducted worldwide (Chuvieco et al. 2021) and for Pantanal in particular (Viganó et al. 2018; Libonati et al. 2022a). The occurrence of heatwaves over the dry season triggers large evaporation rates and thus soil desiccation that, ultimately, may influence the level of vegetation dryness and increase flammability. On the other hand, during the fire season heatwaves promote favorable conditions for larger burned areas if an ignition source is provided (which in the case of Pantanal is mostly human; Menezes et al. (2022)). Recent heatwave episodes in this region have been associated with the establishment of quasi-stationary anticyclonic circulation anomalies over central South America as a response of large-scale Rossby wave patterns forced by remote warm sea surface temperatures in Indian and Pacific oceans (e.g. ENSO, MJO, IOD) (Taschetto and Ambrizzi 2012; Reboita et al. 2021; Cuartas et al. 2022; Marengo et al. 2022; Libonati et al. 2022a). These mid-atmospheric high pressure systems are responsible for strong subsidence and large amounts of incoming shortwave radiative energy at surface (Geirinhas et al. 2022; Marengo et al. 2022; Libonati et al. 2022a). On the other hand, they can induce large disturbances in the South Atlantic Convergence Zone (Nielsen et al. 2019) and/or in the South American Low-Level Jet (Montini et al. 2019) suppressing the passage of frontal systems and promoting the occurrence of large deficits in the water vapor transport from the Amazon basin towards Pantanal. A long-term shortage of moisture being advected from the Amazon basin coupled with a lower than normal atmospheric convergence in the region leverages large precipitation deficits and evaporation rates that, ultimately, promote a sharp decrease in soil moisture levels. In fact, Libonati et al. (2022) showed that during the 2020 fire season due to pronounced drought conditions over Pantanal, a strong soil moisture–temperature coupling (water-limited) was established allowing a re-amplification of the already established surface hot temperature anomalies during several heatwave episodes (Coronato et al. 2020; Geirinhas et al. 2022). As such, fire activity in Pantanal is also inevitably linked to drought and flood (Libonati et al. 2021; Marengo et al. 2021; Mataveli et al. 2021). However, precipitation estimates show large inter-model

discrepancies over South America (Solman et al. 2013; Falco et al. 2019; Solman and Blázquez 2019) due to the commonly acknowledged shortcoming of RCMs when it comes to capturing precipitation. Accordingly, here the focus was made exclusively on the heatwave–fire connection.

Still, large biases were found in temperature estimates by the RCMs and, in order to legitimate the analysis of future heatwaves, the bias observed in CORDEX-CORE historical Tmax data with respect to ERA5 was corrected through QDM. Such an adjustment is required in order to obtain more plausible climate change projections, especially when it comes to extreme temperature-related phenomena (Iturbide et al. 2022). Although in this work the bias correction showed a good performance as evidenced in Table S1 and Figure S1, such approaches to adjust simulation data towards a better match with observations have known limitations and shortcomings. In particular, they can be considered statistical artifacts that do not provide clues on the credibility of the physical processes represented in the model (Maraun 2016; Maraun et al. 2017). However, Maraun et al. (2017) recognize that for reasonably well captured physical processes, such as the ones driving the spatio-temporal variability of Tmax, usual bias correction methods work adequately. This is arguably the case here since the distribution of Tmax from ERA5 and from all the CORDEX-CORE models could be successfully fitted to the same class of theoretical distribution. These elements indicate that the underlying physical processes are consistently represented in the reanalysis and in the RCMs demonstrating that bias correction can be applied confidently. The choice of the bias correction technique is also known to condition the results obtained. Casanueva et al. (2020) and Iturbide et al. (2022) show that there are differences in the outputs of bias corrected models when different methods are applied to the same data, including Tmax in CMIP or CORDEX simulations, resulting in slightly different future projection scenarios. Nevertheless, the QDM applied here shows good performance to steer CORDEX-CORE data towards ERA5 values, and consistency in the climate signal between original and adjusted time series (Figure SC.1), which gives confidence in the conclusions of this study.

In particular, the climate change signal displaying increasing heatwave importance, and comparatively larger increase in RCP8.5 than in other scenarios, is consistent with previous studies investigating future trends in hot extremes. Despite differences in the projections, RCP4.5 and RCP8.5 scenarios are both known to lead to an increase in extreme temperature events, with larger changes over lower latitudes (Russo et al. 2014; Perkins-Kirkpatrick and

Gibson 2017; Feron et al. 2019). They also evidence, consistent with our findings, that heatwave future trends and levels are much worse under RCP8.5 scenario, across all of South America. Global warming will likely impose in Pantanal the occurrence of more intense and prolonged heatwaves due to linear increases of the mean surface temperature and non-linear feedbacks triggered by deep changes in precipitation, evaporation and radiative regimes (Donat et al. 2017; King 2019). This raises new challenges not just for the ecosystems but also for human health and for other socio-economic sectors (e.g. agriculture and energy production). These threats are expected to be particularly relevant in low-income developing countries such as the ones that share the Pantanal biome (Brazil, Paraguay and Bolivia), where the public health services are fragile and where there is still a lack of investment in environmental protection policies. The heatwave projections highlighted here for Pantanal suggest that the heat-stress levels witnessed by the population of Pantanal will increase, leveraging the number of heat-related deaths to dramatic levels (Gasparrini et al. 2015; Guo et al. 2018).

Our results also suggest that such an increase in heatwave conditions could lead to higher burned areas, as favorable conditions for fire occurrence will occur more frequently and widespread over the region (Libonati et al. 2022a). This could also trigger other cascading impacts of heatwaves in public health through the occurrence of more and widespread fires: a higher exposure to wildfire smoke is likely to lead to an increase in the number of respiratory illnesses and in birth defects not just for the living population of Pantanal but also for the inhabitants of downwind regions (Aguilera et al. 2021; Requia et al. 2022b).

Nevertheless, such an increase in the heatwave index over the 21st century, and thus fire activity, would inevitably translate to changes in vegetation cover and climate–vegetation dynamics. Studies have found that fire influences the forest-savanna threshold (Hoffmann et al. 2012; de L. Dantas et al. 2013), which means that such dramatic changes in fire activity could put several areas of Pantanal at risk of biome transition. As a result, these climate-fire-vegetation dynamics could change entirely the shape of the correlation between $\%Pantanal_{HW}$ and burned area for more intense heatwaves, which are not taken into account here as RCMs consider a static vegetation cover. For both scenarios, in addition, nonlinear vegetation-atmosphere and/or land–atmosphere feedback induced by climate change could also corrupt the climate assumptions on which our statistical regression model is based. Considering that the model assumes a climate stationarity, in that case the relation between heatwaves and fires would need to be adjusted and the model would need to be calibrated according to new climate conditions.

C.5 Conclusions

This study aimed at evaluating and modeling the connection between fire and heatwaves in Pantanal, and employed, for the first time, the CORDEX-CORE regional climate simulations at 0.22° spatial resolution, to project future heatwave estimates over the Pantanal biome. A robust connection was found between a heatwave index and burned area. A simple linear model based on $\%Pantanal_{HW}$ significantly explains 82% of the variance of burned area over the 2002–2020 period.

When looking at bias-corrected future projections of heatwaves by CORDEX-CORE model runs, we find that results differ considerably between scenarios, with RCP2.6, the low-emission scenario, reaching close to 40% of Pantanal under heatwave by mid-century to then stabilize to around 35% in 2100, whereas RCP8.5, the most severe scenario, shows a steady increase up to 80% by the end of the century.

The aforementioned ensemble means are associated with a large inter-model spread and therefore uncertainty. This spread is much smaller in RCP8.5 scenario indicating a stronger shift in heatwaves, with a significantly increasing trend. The lesser inter-model variability in heatwaves observed in the long-term in RCP8.5 compared to RCP2.6 reveals how extreme the former scenario is. In this trajectory, every model predicts maximum temperature occurrence and therefore heatwave frequency well above past values, thereby saturating the historical thresholds. Possible changes in climate mechanisms and dynamics in the future (e.g. surface–atmosphere feedbacks) prevent the application of the statistical link between heatwaves and burned area that was evidenced in this study. However, this model can serve as a basis for educated guesses and qualitative assessments on possible future burned area, and suggests that under any scenario, even the more optimistic RCP2.6, burned area will likely increase, and the exceptional 2020 fire season in Pantanal could possibly compare as moderate with events in the near future.

Both fire (Alho et al. 2019) and climate change (Thielen et al. 2021) are major threats to the Pantanal biome, and the 2020 fire events were illustrative of the severe consequences it can have in biodiversity (Tomas et al. 2021), economy, and human health (Machado-Silva et al. 2020). The increased frequency of these fires is among the most visible results of human-induced climate change, posing a serious threat to biodiversity conservation, as the cumulative

impact of widespread burning would be catastrophic if the situation of 2020 becomes common in the coming decades. Climate change may considerably alter the ecological properties of the Pantanal (de Oliveira Aparecido et al. 2021) which, associated with changes in land use and cover (Miranda et al. 2018; Colman et al. 2019; Marques et al. 2021), further contribute to a disturbed landscape and pave the way to increased fire activity (Kumar et al. 2022). Fire and land management are thus imperative within the Pantanal wetlands, to avoid further degradation to this unique ecosystem (Berlinck et al. 2021; Garcia et al. 2021).

As to the authors' knowledge this is the first study evaluating fire and heatwaves over the Pantanal biome, employing a set of regional climate simulations of relatively-high spatial resolution to project future trends. Very little research has been done in climate extremes over this region and more so is needed to properly understand the physical mechanisms associated with the found heatwave–fire relationship. These results provide useful information for fire activity in the biome in light of future climate change, and may also assist with regional information of the connection between fire and heatwaves in Pantanal to improve statistical or physical models.

Supplementary Material

Bias Correction

The parametric Quantile Delta Mapping (QDM) bias correction method applied in this work uses Mielke beta-kappa distribution function for the description of CORDEX-CORE and ERA5 Tmax distributions. The formula of the associated cumulative distribution function is given in Equation (SC.1), where parameters κ and θ are optimized through a least squares regression to best fit the models' empirical distributions.

$$CDF(x;k;\theta) = \frac{x^k}{(1+x^\theta)^{k/\theta}} \qquad \text{(SC. 1)}$$

The adequacy of the choice of this theoretical form is assessed in Table SC.1 where a Kolmogorov-Smirnov (KS) test for goodness of fit is performed for each dataset. These tests reveal that we cannot reject the hypothesis that the samples fit a Mielke beta-kappa distribution at least at the 25% level for all the historical models and ERA5. Although not shown here, Tmax in RCP future scenarios also complies with a KS test against Mielke beta-kappa distribution, at

the 5% level, despite a decreasing goodness of fit for periods farther in the future.

Table SC.1 Kolmogorov-Smirnov test p-values against Mielke beta-kappa distribution for Tmax in ERA5 and the historical CORDEX-CORE simulations, for months from April to October during the period 1981-2005.

Model	**ERA5**	**REMO2015**			**RegCM4-7**		
		HADGEM	MPI	NCC	HADGEM	MPI	NCC
***p*-value**	0.36	0.37	0.36	0.33	0.28	0.44	0.41

For the sake of consistency, QDM was applied on future Tmax values separately for different time windows, with a duration similar to the historical period. Namely, QDM was performed independently for the future periods 2006–2025, 2026–2050, 2051–2075 and 2076–2099. The bias corrected time series of yearly mean and P90 Tmax is shown in Figure SC.1, along with the original data and ERA5 time series for the historical period. The effect of the bias correction can also be observed in the shift in distributions before and after correction shown in Figure SC.2

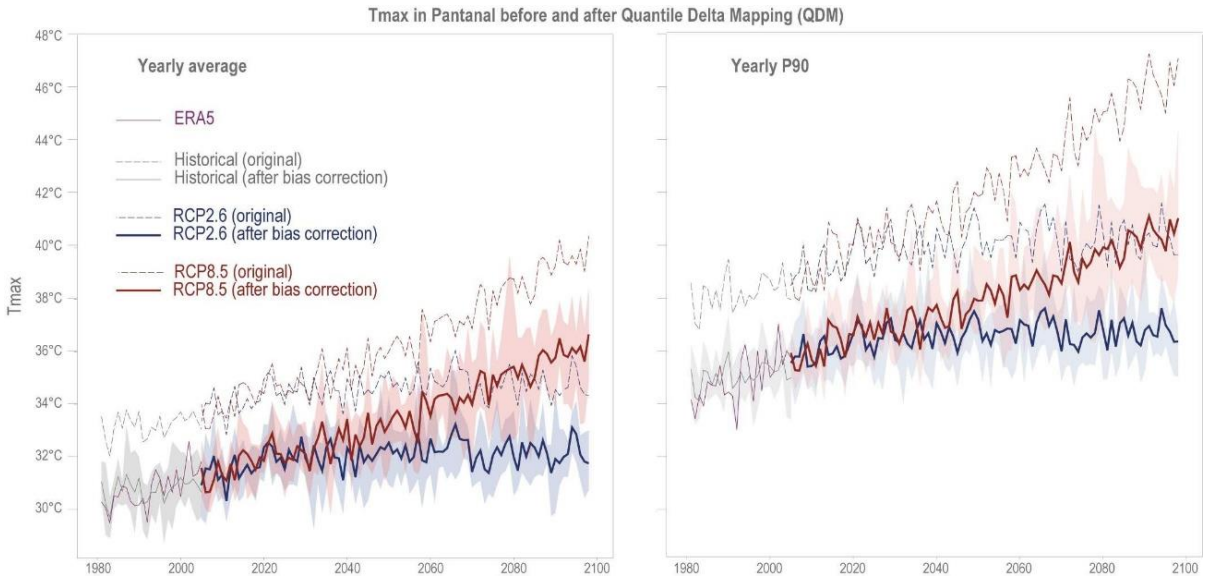

Figure SC.1 Yearly average of Tmax (left) and P90 Tmax (right) over Pantanal during the 1981–2099 period,in ERA5 (solid purple line), and for CORDEX-CORE RCP scenarios ensemble means before (dashed blue and red lines) and after (solid blue and red lines) bias correction. For CORDEX-CORE corrected, ensemblemeans are shown in solid lines, and the minimum and maximum of each single realization is shown in shades for the bias corrected time series.

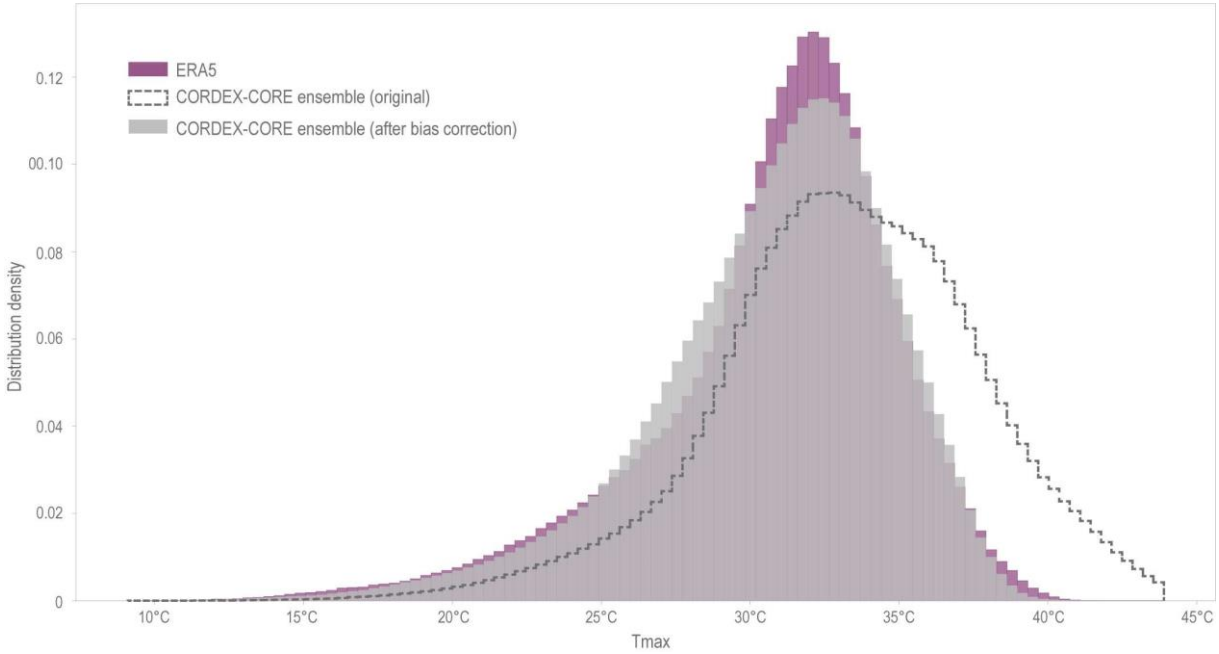

Figure SC.2 Distribution of hourly Tmax in ERA5 (purple bars) and in the ensemble of CORDEX-CORE historical runs before (black line) and after (gray bars) bias correction. Period 1981–2005.

Cross-Correlation

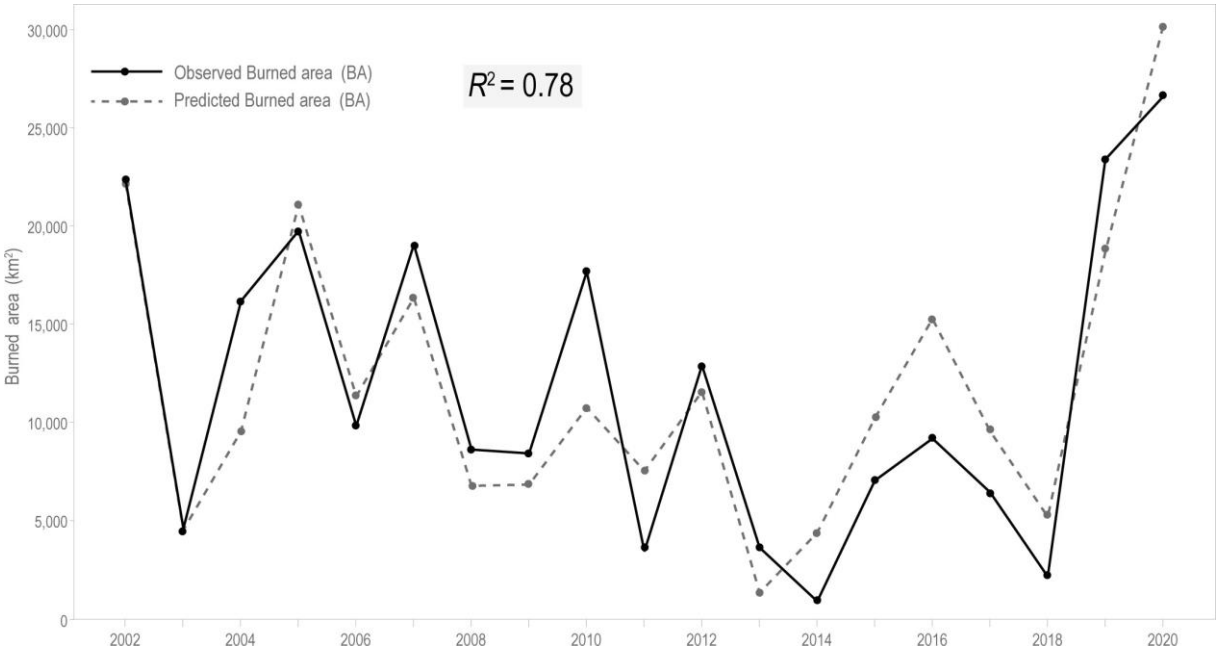

Figure SC.3 Leave-One-Out Cross-Validation (LOOCV) scheme performed from 2002 to 2020: observed burned area values (from MODIS MCD64A1) are shown in a solid black line, whereas the LOOCV predicted values for burned area are shown in a dashed black line. The resulting coefficient of determination from the observed and the predicted burned area values is also shown in red.

References

Abatzoglou JT, Williams AP, Barbero R (2019) Global Emergence of Anthropogenic Climate Change in Fire Weather Indices. Geophys Res Lett 46:326–336. https://doi.org/10.1029/2018GL080959

Aguilera R, Corringham T, Gershunov A, Benmarhnia T (2021) Wildfire smoke impacts respiratory health more than fine particles from other sources: observational evidence from Southern California. Nat Commun 12:1493. https://doi.org/10.1038/s41467-021-21708-0

Alho CJR (2008) Biodiversity of the Pantanal: response to seasonal flooding regime and to environmental degradation. Brazilian J Biol 68:957–966. https://doi.org/10.1590/S1519-69842008000500005

Alho CJR, Mamede SB, Benites M, et al (2019) Threats to the biodiversity of the Brazilian Pantanal due to land use and occupation. Ambient Soc 22:e01891. https://doi.org/10.1590/1809-4422asoc201701891vu2019L3AO

Alizadeh MR, Abatzoglou JT, Adamowski JF, et al (2022) Increasing Heat-Stress Inequality in a Warming Climate. Earth's Futur 10:e2021EF002488. https://doi.org/10.1029/2021EF002488

Alizadeh MR, Adamowski J, Nikoo MR, et al (2020) A century of observations reveals increasing likelihood of continental-scale compound dry-hot extremes. Sci Adv 6:eaaz4571. https://doi.org/10.1126/sciadv.aaz4571

Allan RP, Barlow M, Byrne MP, et al (2020) Advances in understanding large-scale responses of the water cycle to climate change. Ann N Y Acad Sci 1472:49–75. https://doi.org/10.1111/nyas.14337

Almazroui M, Ashfaq M, Islam MN, et al (2021) Assessment of CMIP6 Performance and Projected Temperature and Precipitation Changes Over South America. Earth Syst Environ 5:155–183. https://doi.org/10.1007/s41748-021-00233-6

Alvarez MS, Vera CS, Kiladis GN, Liebmann B (2016) Influence of the Madden Julian Oscillation on precipitation and surface air temperature in South America. Clim Dyn 46:245–262. https://doi.org/10.1007/s00382-015-2581-6

Andreoli RV, de Oliveira SS, Kayano MT, et al (2017) The influence of different El Niño types on the South American rainfall. Int J Climatol 37:1374–1390. https://doi.org/10.1002/joc.4783

Anthony Barnston (2015) Why are these so many ENSO indexes, instead of just one? https://www.climate.gov/news-features/blogs/enso/why-are-there-so-many-enso-indexes-instead-just-one

Baker HS, Millar RJ, Karoly DJ, et al (2018) Higher CO2 concentrations increase extreme event risk in a 1.5 °C world. Nat Clim Chang 8:604–608. https://doi.org/10.1038/s41558-018-0190-1

Baker JCA, de Souza DC, Kubota PY, et al (2021) An Assessment of Land–Atmosphere Interactions over South America Using Satellites, Reanalysis, and Two Global Climate Models. J Hydrometeorol 22:905–922. https://doi.org/10.1175/JHM-D-20-0132.1

Ballester J, Quijal-Zamorano M, Méndez Turrubiates RF, et al (2023) Heat-related mortality in Europe during the summer of 2022. Nat Med 29:1857–1866. https://doi.org/10.1038/s41591-023-02419-z

Balmaceda-Huarte R, Olmo ME, Bettolli ML, Poggi MM (2021) Evaluation of multiple reanalyzes in reproducing the spatio-temporal variability of temperature and precipitation indices over southern South America. Int J Climatol 41:5572–5595. https://doi.org/10.1002/joc.7142

Bamston AG, Chelliah M, Goldenberg SB (1997) Documentation of a highly ENSO-related sst region in the equatorial pacific: Research note. Atmosphere-Ocean 35:367–383. https://doi.org/10.1080/07055900.1997.9649597

Barkhordarian A, Saatchi SS, Behrangi A, et al (2019) A Recent Systematic Increase in Vapor Pressure Deficit over Tropical South America. Sci Rep 9:15331. https://doi.org/10.1038/s41598-019-51857-8

Barreca A, Schaller J (2020) The impact of high ambient temperatures on delivery timing and gestational lengths. Nat Clim Chang 10:77–82. https://doi.org/10.1038/s41558-019-0632-4

Barreiro M, Tippmann A (2008) Atlantic modulation of El Niño influence on summertime

rainfall over southeastern South America. Geophys Res Lett 35:. https://doi.org/10.1029/2008GL035019

Barriopedro D, Fischer EM, Luterbacher J, et al (2011) The hot summer of 2010: Redrawing the temperature record map of Europe. Science 332:220–224. https://doi.org/10.1126/science.1201224

Bastos A, Gouveia CM, Trigo RM, Running SW (2014) Analyzing the spatio-temporal impacts of the 2003 and 2010 extreme heatwaves on plant productivity in Europe. Biogeosciences 11:3421–3435. https://doi.org/10.5194/bg-11-3421-2014

Basu R, Malig B, Ostro B (2010) High ambient temperature and the risk of preterm delivery. Am J Epidemiol 172:1108–1117. https://doi.org/10.1093/aje/kwq170

BBC (2015) Brazil faces surge in number of dengue fever cases. https://www.bbc.com/news/world-latin-america-32589268

Beck HE, Pan M, Miralles DG, et al (2021) Evaluation of 18 satellite- and model-based soil moisture products using in situ measurements from 826 sensors. Hydrol Earth Syst Sci 25:17–40. https://doi.org/10.5194/hess-25-17-2021

Bell ML, O'Neill MS, Ranjit N, et al (2008) Vulnerability to heat-related mortality in Latin America: A case-crossover study in São Paulo, Brazil, Santiago, Chile and Mexico City, Mexico. Int J Epidemiol 37:796–804. https://doi.org/10.1093/ije/dyn094

Benedict I, van Heerwaarden CC, Weerts AH, Hazeleger W (2019) The benefits of spatial resolution increase in global simulations of the hydrological cycle evaluated for the Rhine and Mississippi basins. Hydrol Earth Syst Sci 23:1779–1800. https://doi.org/10.5194/hess-23-1779-2019

Benson DO, Dirmeyer PA (2021) Characterizing the Relationship between Temperature and Soil Moisture Extremes and Their Role in the Exacerbation of Heat Waves over the Contiguous United States. J Clim 34:2175–2187. https://doi.org/10.1175/JCLI-D-20-0440.1

Berg A, Lintner BR, Findell K, et al (2015) Interannual Coupling between Summertime Surface Temperature and Precipitation over Land: Processes and Implications for Climate Change. J Clim 28:1308–1328. https://doi.org/10.1175/JCLI-D-14-00324.1

Bergier I, Assine ML (2016) Dynamics of the Pantanal wetland in South America. Springer - Book Series. 10.1007/978-3-319-18735-8. https://doi.org/10.1007/978-3-319-18735-8

Berlinck CN, Lima LHA, Pereira AMM, et al (2021) The Pantanal is on fire and only a sustainable agenda can save the largest wetland in the world. Brazilian J Biol 82:e244200. https://doi.org/10.1590/1519-6984.244200

Bevacqua E, De Michele C, Manning C, et al (2021) Guidelines for Studying Diverse Types of Compound Weather and Climate Events. Earth's Futur 9:e2021EF002340. https://doi.org/10.1029/2021EF002340

Bevacqua E, Zappa G, Lehner F, Zscheischler J (2022) Precipitation trends determine future occurrences of compound hot–dry events. Nat Clim Chang 12:350–355. https://doi.org/10.1038/s41558-022-01309-5

Bieri CA, Dominguez F, Lawrence DM (2021) Impacts of Large-Scale Soil Moisture Anomalies on the Hydroclimate of Southeastern South America. J Hydrometeorol 22:657–669. https://doi.org/10.1175/JHM-D-20-0116.1

Boer MM, Resco de Dios V, Bradstock RA (2020) Unprecedented burn area of Australian mega forest fires. Nat Clim Chang 10:171–172. https://doi.org/10.1038/s41558-020-0716-1

Boers N, Marwan N, Barbosa HMJ, Kurths J (2017) A deforestation-induced tipping point for the South American monsoon system. Sci Rep 7:41489. https://doi.org/10.1038/srep41489

Bowman DMJS, Kolden CA, Abatzoglou JT, et al (2020) Vegetation fires in the Anthropocene. Nat Rev Earth Environ 1:500–515. https://doi.org/10.1038/s43017-020-0085-3

Brando PM, Balch JK, Nepstad DC, et al (2014) Abrupt increases in Amazonian tree mortality due to drought–fire interactions. Proc Natl Acad Sci 111:6347–6352. https://doi.org/10.1073/pnas.1305499111

Brás TA, Seixas J, Carvalhais N, Jägermeyr J (2021) Severity of drought and heatwave crop losses tripled over the last five decades in Europe. Environ Res Lett 16:65012. https://doi.org/10.1088/1748-9326/abf004

Brown L, Medlock J, Murray V (2014) Impact of drought on vector-borne diseases--how does one manage the risk? Public Health 128:29–37. https://doi.org/10.1016/j.puhe.2013.09.006

Buckley TN (2019) How do stomata respond to water status? New Phytol 224:21–36. https://doi.org/10.1111/nph.15899

Burton C, Kelley DI, Jones CD, et al (2022) South American fires and their impacts on ecosystems increase with continued emissions. Clim Resil Sustain 1:e8. https://doi.org/10.1002/cli2.8

Cai W, McPhaden MJ, Grimm AM, et al (2020) Climate impacts of the El Niño–Southern Oscillation on South America. Nat Rev Earth Environ 1:215–231. https://doi.org/10.1038/s43017-020-0040-3

Cannon AJ, Sobie SR, Murdock TQ (2015) Bias correction of GCM precipitation by quantile mapping: how well do methods preserve changes in quantiles and extremes? J Clim 28:6938–6959. https://doi.org/10.1175/JCLI-D-14-00754.1

Cano-Crespo A, Traxl D, Thonicke K (2021) Spatio-temporal patterns of extreme fires in Amazonian forests. Eur Phys J Spec Top 230:3033–3044. https://doi.org/10.1140/epjs/s11734-021-00164-3

Casanueva A, Herrera S, Iturbide M, et al (2020) Testing bias adjustment methods for regional climate change applications under observational uncertainty and resolution mismatch. Atmos Sci Lett 21:e978. https://doi.org/10.1002/asl.978

Castellanos E, Lemos MF, Astigarraga L, et al (2022) Central and South America. In: Pörtner HO, Roberts DC, Tignor M, et al. (eds) Climate Change 2022: Impacts, Adaptation and Vulnerability. Contribution of Working Group II to the Sixth Assessment Report of the Intergovernmental Panel on Climate Change. Cambridge University Press, Cambridge, UK and New York, USA, pp 1689–1816

Ceccherini G, Russo S, Ameztoy I, et al (2016) Magnitude and frequency of heat and cold waves in recent decades: the case of South America. Nat Hazards Earth Syst Sci 16:821–831. https://doi.org/10.5194/nhess-16-821-2016

Cerne SB, Vera CS (2011) Influence of the intraseasonal variability on heat waves in subtropical South America. Clim Dyn 36:2265–2277. https://doi.org/10.1007/s00382-010-0812-4

Chacón-Montalván EA, Taylor BM, Cunha MG, et al (2021) Rainfall variability and adverse

birth outcomes in Amazonia. Nat Sustain 4:583–594. https://doi.org/10.1038/s41893-021-00684-9

Chagas VBP, Chaffe PLB, Blöschl G (2022) Climate and land management accelerate the Brazilian water cycle. Nat Commun 13:5136. https://doi.org/10.1038/s41467-022-32580-x

Chambers J (2020) Global and cross-country analysis of exposure of vulnerable populations to heatwaves from 1980 to 2018. Clim Change 163:539–558. https://doi.org/10.1007/s10584-020-02884-2

Chen D, Dai A, Hall A (2021) The Convective-To-Total Precipitation Ratio and the "Drizzling" Bias in Climate Models. J Geophys Res Atmos 126:e2020JD034198. https://doi.org/10.1029/2020JD034198

Chen Y, Morton DC, Andela N, et al (2017) A pan-tropical cascade of fire driven by El Niño/Southern Oscillation. Nat Clim Chang 7:906–911. https://doi.org/10.1038/s41558-017-0014-8

Cheng J, Bambrick H, Yakob L, et al (2020) Heatwaves and dengue outbreaks in Hanoi, Vietnam: New evidence on early warning. PLoS Negl Trop Dis 14:e0007997. https://doi.org/10.1371/journal.pntd.0007997

Cheng J, Xu Z, Bambrick H, et al (2018) Heatwave and elderly mortality: An evaluation of death burden and health costs considering short-term mortality displacement. Environ Int 115:334–342. https://doi.org/10.1016/j.envint.2018.03.041

Chersich MF, Pham MD, Areal A, et al (2020) Associations between high temperatures in pregnancy and risk of preterm birth, low birth weight, and stillbirths: systematic review and meta-analysis. BMJ 371:m3811. https://doi.org/10.1136/bmj.m3811

Choat B, Jansen S, Brodribb TJ, et al (2012) Global convergence in the vulnerability of forests to drought. Nature 491:752–755. https://doi.org/10.1038/nature11688

Christensen J, Kjellström E, Giorgi F, et al (2010) Weight assignment in regional climate models. Clim Res 44:179–194. https://dx.doi.org/10.3354/cr00916

Christian JI, Basara JB, Hunt ED, et al (2020) Flash drought development and cascading impacts associated with the 2010 Russian heatwave. Environ Res Lett 15:94078.

https://doi.org/10.1088/1748-9326/ab9faf

Christidis N, Jones GS, Stott PA (2015) Dramatically increasing chance of extremely hot summers since the 2003 European heatwave. Nat Clim Chang 5:46–50. https://doi.org/10.1038/nclimate2468

Chug D, Dominguez F, Yang Z (2022) The Amazon and La Plata River Basins as Moisture Sources of South America: Climatology and Intraseasonal Variability. J Geophys Res Atmos 127:1–19. https://doi.org/10.1029/2021JD035455

Chuvieco E, Pettinari ML, Koutsias N, et al (2021) Human and climate drivers of global biomass burning variability. Sci Total Environ 779:146361. https://doi.org/10.1016/j.scitotenv.2021.146361

Cinquini L, Crichton D, Mattmann C, et al (2014) The Earth System Grid Federation: An open infrastructure for access to distributed geospatial data. Futur Gener Comput Syst 36:400–417. https://doi.org/10.1016/j.future.2013.07.002

Cochrane MA, Barber CP (2009) Climate change, human land use and future fires in the Amazon. Glob Chang Biol 15:601–612. https://doi.org/10.1111/j.1365-2486.2008.01786.x

Coelho CAS, Cardoso DHF, Firpo MAF (2016a) Precipitation diagnostics of an exceptionally dry event in São Paulo, Brazil. Theor Appl Climatol 125:769–784. https://doi.org/10.1007/s00704-015-1540-9

Coelho CAS, de Oliveira CP, Ambrizzi T, et al (2016b) The 2014 southeast Brazil austral summer drought: regional scale mechanisms and teleconnections. Clim Dyn 46:3737–3752. https://doi.org/10.1007/s00382-015-2800-1

Coelho CAS, Cavalcanti IAF, Costa SMS, et al (2012) Climate diagnostics of three major drought events in the Amazon and illustrations of their seasonal precipitation predictions. Meteorol Appl 19:237–255. https://doi.org/10.1002/met.1324

Coffel ED, Keith B, Lesk C, et al (2019) Future Hot and Dry Years Worsen Nile Basin Water Scarcity Despite Projected Precipitation Increases. Earth's Futur 7:967–977. https://doi.org/10.1029/2019EF001247

Cole R, Hajat S, Murage P, et al (2023) The contribution of demographic changes to future

heat-related health burdens under climate change scenarios. Environ Int 173:107836. https://doi.org/10.1016/j.envint.2023.107836

Collazo S, Suli S, Zaninelli PG, et al (2024) Influence of large-scale circulation and local feedbacks on extreme summer heat in Argentina in 2022/23. Commun Earth Environ 5:231. https://doi.org/10.1038/s43247-024-01386-8

Collins L, Bradstock RA, Clarke H, et al (2021) The 2019/2020 mega-fires exposed Australian ecosystems to an unprecedented extent of high-severity fire. Environ Res Lett 16:44029. https://doi.org/10.1088/1748-9326/abeb9e

Colman CB, Oliveira PTS, Almagro A, et al (2019) Effects of climate and land-cover changes on soil erosion in Brazilian Pantanal. Sustainability 11:7053. https://doi.org/10.3390/su11247053

Coppola E, Raffaele F, Giorgi F, et al (2021) Climate hazard indices projections based on CORDEX-CORE, CMIP5 and CMIP6 ensemble. Clim Dyn 57:1293–1383. https://doi.org/10.1007/s00382-021-05640-z

Coronato T, Carril AF, Zaninelli PG, et al (2020) The impact of soil moisture–atmosphere coupling on daily maximum surface temperatures in Southeastern South America. Clim Dyn 55:2543–2556. https://doi.org/10.1007/s00382-020-05399-9

Correa DB, Alcântara E, Libonati R, et al (2022) Increased burned area in the Pantanal over the past two decades. Sci Total Environ 835:155386. https://doi.org/10.1016/j.scitotenv.2022.155386

Cos J, Doblas-Reyes F, Jury M, et al (2022) The Mediterranean climate change hotspot in the CMIP5 and CMIP6 projections. Earth Syst Dyn 13:321–340. https://doi.org/10.5194/esd-13-321-2022

Costa DF, Gomes HB, Silva MCL, Zhou L (2022) The most extreme heat waves in Amazonia happened under extreme dryness. Clim Dyn 59:281–295. https://doi.org/10.1007/s00382-021-06134-8

Costa IT, Wollmann CA, Gobo JPA, et al (2021) Extreme Weather Conditions and Cardiovascular Hospitalizations in Southern Brazil. Sustainability 13:12194. https://doi.org/10.3390/su132112194

Costa MH, Fleck LC, Cohn AS, et al (2019) Climate risks to Amazon agriculture suggest a rationale to conserve local ecosystems. Front Ecol Environ 17:584–590. https://doi.org/10.1002/fee.2124

Cuartas LA, Cunha APM do A, Alves JA, et al (2022) Recent Hydrological Droughts in Brazil and Their Impact on Hydropower Generation. Water 14(4), 601. https://doi.org/10.3390/w14040601

Cui Y, Yin M, Cheng X, et al (2024) Towards cool cities and communities: Preparing for an increasingly hot future by the development of heat-resilient infrastructure and urban heat management plan. Environ Technol Innov 34:103568. https://doi.org/10.1016/j.eti.2024.103568

Cunha APMA, Zeri M, Leal KD, et al (2019) Extreme drought events over Brazil from 2011 to 2019. Atmosphere (Basel) 10(11), 642. https://doi.org/10.3390/atmos10110642

Damasceno-Junior GA, de Oliveira Roque F, Garcia LC, et al (2021) Lessons to be learned from the wildfire catastrophe of 2020 in the Pantanal wetland. https://doi.org/10.1672/UCRT083-212

de Abreu RC, Tett SFB, Schurer A, Rocha HR (2019) Attribution of Detected Temperature Trends in Southeast Brazil. Geophys Res Lett 46:8407–8414. https://doi.org/10.1029/2019GL083003

de Barros Soares D, Lee H, Loikith PC, et al (2017) Can significant trends be detected in surface air temperature and precipitation over South America in recent decades? Int J Climatol 37:1483–1493. https://doi.org/10.1002/joc.4792

de Carvalho LMV, Cavalcanti IFA (2016) The South American Monsoon System (SAMS). In: de Carvalho LMV, Jones C (eds) The Monsoons and Climate Change: Observations and Modeling. Springer International Publishing, Cham, pp 121–148

de L. Dantas V, Batalha MA, Pausas JG (2013) Fire drives functional thresholds on the savanna–forest transition. Ecology 94:2454–2463. https://doi.org/10.1890/12-1629.1

de los Milagros Skansi M, Brunet M, Sigró J, et al (2013) Warming and wetting signals emerging from analysis of changes in climate extreme indices over South America. Glob Planet Change 100:295–307. https://doi.org/10.1016/j.gloplacha.2012.11.004

de Oliveira-Júnior JF, Mendes D, Correia Filho WLF, et al (2021) Fire foci in South America: Impact and causes, fire hazard and future scenarios. J South Am Earth Sci 112:103623. https://doi.org/10.1016/j.jsames.2021.103623

de Oliveira Aparecido LE, Lorençone PA, Lorençone JA, et al (2021) Climate changes and their influences in water balance of Pantanal biome. Theor Appl Climatol 143:659–674. https://doi.org/10.1007/s00704-020-03445-4

de Oliveira MT, Damasceno-Junior GA, Pott A, et al (2014) Regeneration of riparian forests of the Brazilian Pantanal under flood and fire influence. For Ecol Manage 331:256–263. https://doi.org/10.1016/j.foreco.2014.08.011

Deng L, Li T (2016) Relative Roles of Background Moisture and Vertical Shear in Regulating Interannual Variability of Boreal Summer Intraseasonal Oscillations. J Clim 29:7009–7025. https://doi.org/10.1175/JCLI-D-15-0498.1

Di Giuseppe F, Pappenberger F, Wetterhall F, et al (2016) The potential predictability of fire danger provided by numerical weather prediction. J Appl Meteorol Climatol 55:2469–2491. https://doi.org/10.1175/JAMC-D-15-0297.1

Di Luca A, de Elía R, Bador M, Argüeso D (2020) Contribution of mean climate to hot temperature extremes for present and future climates. Weather Clim Extrem 28:100255. https://doi.org/10.1016/j.wace.2020.100255

Diniz FR, Gonçalves FLT, Sheridan S (2020) Heat wave and elderly mortality: Historical analysis and future projection for metropolitan region of Sao Paulo, Brazil. Atmosphere (Basel) 11(9), 933. https://doi.org/10.3390/atmos11090933

Dirmeyer PA, Balsamo G, Blyth EM, et al (2021) Land-Atmosphere Interactions Exacerbated the Drought and Heatwave Over Northern Europe During Summer 2018. AGU Adv 2:1–16. https://doi.org/10.1029/2020av000283

Dirmeyer PA, Wang Z, Mbuh MJ, Norton HE (2014) Intensified land surface control on boundary layer growth in a changing climate. Geophys Res Lett 41:1290–1294. https://doi.org/10.1002/2013GL058826

Donat MG, Lowry AL, Alexander L V, et al (2016) More extreme precipitation in the world's dry and wet regions. Nat Clim Chang 6:508–513. https://doi.org/10.1038/nclimate2941

Donat MG, Pitman AJ, Seneviratne SI (2017) Regional warming of hot extremes accelerated by surface energy fluxes. Geophys Res Lett 44:7011–7019. https://doi.org/10.1002/2017GL073733

Donges JF, Schleussner C-F, Siegmund JF, Donner R V (2016) Event coincidence analysis for quantifying statistical interrelationships between event time series. Eur Phys J Spec Top 225:471–487. https://doi.org/10.1140/epjst/e2015-50233-y

dos Santos DM, Libonati R, Garcia BN, et al (2024) Twenty-first-century demographic and social inequalities of heat-related deaths in Brazilian urban areas. PLoS One 19:1–30. https://doi.org/10.1371/journal.pone.0295766

Dosio A (2017) Projection of temperature and heat waves for Africa with an ensemble of CORDEX Regional Climate Models. Clim Dyn 49:493–519. https://doi.org/10.1007/s00382-016-3355-5

Dosio A, Mentaschi L, Fischer EM, Wyser K (2018) Extreme heat waves under 1.5 °C and 2 °C global warming. Environ Res Lett 13:54006. https://doi.org/10.1088/1748-9326/aab827

Douville H, Ribes A, Decharme B, et al (2013) Anthropogenic influence on multidecadal changes in reconstructed global evapotranspiration. Nat Clim Chang 3:59–62. https://doi.org/10.1038/nclimate1632

Drumond A, Marengo J, Ambrizzi T, et al (2014) The role of the Amazon Basin moisture in the atmospheric branch of the hydrological cycle: a Lagrangian analysis. Hydrol Earth Syst Sci 18:2577–2598. https://doi.org/10.5194/hess-18-2577-2014

Duffy PB, Brando P, Asner GP, Field CB (2015) Projections of future meteorological drought and wet periods in the Amazon. Proc Natl Acad Sci 112:13172–13177. https://doi.org/10.1073/pnas.1421010112

Ebi KL, Bowen K (2016) Extreme events as sources of health vulnerability: Drought as an example. Weather Clim Extrem 11:95–102. https://doi.org/10.1016/j.wace.2015.10.001

Ebi KL, Vanos J, Baldwin JW, et al (2021) Extreme Weather and Climate Change: Population Health and Health System Implications. Annu Rev Public Health 42:293–315. https://doi.org/10.1146/annurev-publhealth-012420-105026

Eiras-Barca J, Dominguez F, Yang Z, et al (2020) Changes in South American hydroclimate under projected Amazonian deforestation. Ann N Y Acad Sci 1472:104–122. https://doi.org/10.1111/nyas.14364

Ellena M, Ballester J, Mercogliano P, et al (2020) Social inequalities in heat-attributable mortality in the city of Turin, northwest of Italy: a time series analysis from 1982 to 2018. Environ Heal 19:116. https://doi.org/10.1186/s12940-020-00667-x

Enayati M, Bozorg-Haddad O, Bazrafshan J, et al (2021) Bias correction capabilities of quantile mapping methods for rainfall and temperature variables. J Water Clim Chang 12:401–419. https://doi.org/10.2166/wcc.2020.261

Eyring V, Cox PM, Flato GM, et al (2019) Taking climate model evaluation to the next level. Nat Clim Chang 9:102–110. https://doi.org/10.1038/s41558-018-0355-y

Falco M, Carril AF, Menéndez CG, et al (2019) Assessment of CORDEX simulations over South America: added value on seasonal climatology and resolution considerations. Clim Dyn 52:4771–4786. https://doi.org/10.1007/s00382-018-4412-z

Fatichi S, Ivanov VY, Paschalis A, et al (2016) Uncertainty partition challenges the predictability of vital details of climate change. Earth's Futur 4:240–251. https://doi.org/10.1002/2015EF000336

Feldpausch TR, Phillips OL, Brienen RJW, et al (2016) Amazon forest response to repeated droughts. Global Biogeochem Cycles 30:964–982. https://doi.org/10.1002/2015GB005133

Feng S, Wu X, Hao Z, et al (2020) A database for characteristics and variations of global compound dry and hot events. Weather Clim Extrem 30:100299. https://doi.org/10.1016/j.wace.2020.100299

Fernandes LG, Grimm AM (2023) ENSO Modulation of Global MJO and Its Impacts on South America. J Clim 36:7715–7738. https://doi.org/10.1175/JCLI-D-22-0781.1

Feron S, Cordero RR, Damiani A, et al (2019) Observations and Projections of Heat Waves in South America. Sci Rep 9:1–15. https://doi.org/10.1038/s41598-019-44614-4

Ferro CAT, Hannachi A, Stephenson DB (2005) Simple nonparametric techniques for exploring changing probability distributions of weather. J Clim 18:4344–4354.

https://doi.org/10.1175/JCLI3518.1

Ficklin DL, Null SE, Abatzoglou JT, et al (2022) Hydrological Intensification Will Increase the Complexity of Water Resource Management. Earth's Futur 10:e2021EF002487. https://doi.org/10.1029/2021EF002487

Finke K, Jiménez-Esteve B, Taschetto AS, et al (2020) Revisiting remote drivers of the 2014 drought in South-Eastern Brazil. Clim Dyn 55:3197–3211. https://doi.org/10.1007/s00382-020-05442-9

Fischer EM, Seneviratne SI, Vidale PL, et al (2007) Soil moisture-atmosphere interactions during the 2003 European summer heat wave. J Clim 20:5081–5099. https://doi.org/10.1175/JCLI4288.1

Fisher JB, Whittaker RJ, Malhi Y (2011) ET come home: potential evapotranspiration in geographical ecology. Glob Ecol Biogeogr 20:1–18. https://doi.org/10.1111/j.1466-8238.2010.00578.x

Flach M, Sippel S, Gans F, et al (2018) Contrasting biosphere responses to hydrometeorological extremes: revisiting the 2010 western Russian heatwave. Biogeosciences 15:6067–6085. https://doi.org/10.5194/bg-15-6067-2018

Florido Ngu F, Kelman I, Chambers J, Ayeb-Karlsson S (2021) Correlating heatwaves and relative humidity with suicide (fatal intentional self-harm). Sci Rep 11:22175. https://doi.org/10.1038/s41598-021-01448-3

Ford TW, Dirmeyer PA, Benson DO (2018) Evaluation of heat wave forecasts seamlessly across subseasonal timescales. npj Clim Atmos Sci 1:20. https://doi.org/10.1038/s41612-018-0027-7

Freychet N, Hegerl G, Mitchell D, Collins M (2021) Future changes in the frequency of temperature extremes may be underestimated in tropical and subtropical regions. Commun Earth Environ 2:28. https://doi.org/10.1038/s43247-021-00094-x

García-León D, Casanueva A, Standardi G, et al (2021) Current and projected regional economic impacts of heatwaves in Europe. Nat Commun 12:5807. https://doi.org/10.1038/s41467-021-26050-z

Garcia BN, Libonati R, Nunes AMB (2018) Extreme Drought Events over the Amazon Basin:

The Perspective from the Reconstruction of South American Hydroclimate. Water 10:. https://doi.org/10.3390/w10111594

Garcia LC, Szabo JK, de Oliveira Roque F, et al (2021) Record-breaking wildfires in the world's largest continuous tropical wetland: Integrative fire management is urgently needed for both biodiversity and humans. J Environ Manage 293:112870. https://doi.org/10.1016/j.jenvman.2021.112870

Gasparrini A, Guo Y, Hashizume M, et al (2015) Mortality risk attributable to high and low ambient temperature : a multicountry observational study. 369–375. https://doi.org/10.1016/S0140-6736(14)62114-0

Gasparrini A, Guo Y, Sera F, et al (2017) Projections of temperature-related excess mortality under climate change scenarios. Lancet Planet Heal 1:e360–e367. https://doi.org/10.1016/S2542-5196(17)30156-0

Gatti L V, Basso LS, Miller JB, et al (2021) Amazonia as a carbon source linked to deforestation and climate change. Nature 595:388–393. https://doi.org/10.1038/s41586-021-03629-6

Gazol A, Camarero JJ (2022) Compound climate events increase tree drought mortality across European forests. Sci Total Environ 816:151604. https://doi.org/10.1016/j.scitotenv.2021.151604

Geirinhas JL, Trigo RM, Libonati R, et al (2018a) Climatic and synoptic characterization of heat waves in Brazil. Int J Climatol 38:1760-1776. https://doi.org/10.1002/joc.5294

Geirinhas JL, Trigo RM, Libonati R, Peres L de F (2018b) Climatic characterization of heat waves in Brazil. Anu do Inst Geociencias 41:333–350. https://doi.org/10.11137/2018_3_333_350

Geirinhas JL, Trigo RM, Libonati R, et al (2019) Characterizing the atmospheric conditions during the 2010 heatwave in Rio de Janeiro marked by excessive mortality rates. Sci Total Environ 650:796–808. https://doi.org/10.1016/j.scitotenv.2018.09.060

Geirinhas JL, Russo A, Libonati R, et al (2020) Heat-related mortality at the beginning of the twenty-first century in Rio de Janeiro, Brazil. Int J Biometeorol 64:1319–1332. https://doi.org/10.1007/s00484-020-01908-x

Geirinhas JL, Russo A, Libonati R, et al (2021) Recent increasing frequency of compound

summer drought and heatwaves in Southeast Brazil. Environ Res Lett 16:. https://doi.org/10.1088/1748-9326/abe0eb

Geirinhas JL, Russo AC, Libonati R, et al (2022) The influence of soil dry-out on the record-breaking hot 2013/2014 summer in Southeast Brazil. Sci Rep 12:5836. https://doi.org/10.1038/s41598-022-09515-z

Geirinhas JL, Russo AC, Libonati R, et al (2023) Combined large-scale tropical and subtropical forcing on the severe 2019–2022 drought in South America. npj Clim Atmos Sci 6:185. https://doi.org/10.1038/s41612-023-00510-3

Gelbrecht M, Boers N, Kurths J (2023) Phase coherence between precipitation in South America and Rossby waves. Sci Adv 4:eaau3191. https://doi.org/10.1126/sciadv.aau3191

Getirana A, Libonati R, Cataldi M (2021) Brazil is in water crisis-it needs a drought plan. Nature 600:218–220. https://doi.org/10.1038/d41586-021-03625-w

Gevaert AI, Miralles DG, de Jeu RAM, et al (2018) Soil Moisture-Temperature Coupling in a Set of Land Surface Models. J Geophys Res Atmos 123:1481–1498. https://doi.org/10.1002/2017JD027346

Giglio L, Boschetti L, Roy DP, et al (2018) The Collection 6 MODIS burned area mapping algorithm and product. Remote Sens Environ 217:72–85. https://doi.org/10.1016/j.rse.2018.08.005

Gilbert RO (1987) Sen's nonparametric estimator of slope. In *Statistical Methods for Environmental Pollution Monitoring*. Van Nostrand Reinhold Company Inc: New York, 217–219. ISBN: 0-442-23050-8.

Giorgi F, Coppola E, Jacob D, et al (2022) The CORDEX-CORE EXP-I Initiative: Description and Highlight Results from the Initial analysis. Bull Am Meteorol Soc 103:E293–E310. https://doi.org/10.1175/BAMS-D-21-0119.1

Gitau R, Makasa M, Kasonka L, et al (2005) Maternal micronutrient status and decreased growth of Zambian infants born during and after the maize price increases resulting from the southern African drought of 2001-2002. Public Health Nutr 8:837–843. https://doi.org/10.1079/phn2005746

Global Forest Watch (2024) World forest map & tree cover change data.

https://www.globalforestwatch.org/map/?map=eyJjZW50ZXIiOnsibGF0IjotMTMuNDc1NTUxMjUyMDE0NDIzLCJsbmciOi0zMC41MzkwNjI0OTk5OTk3MjN9fQ%3D%3D&mapPrompts=eyJvcGVuIjp0cnVlLCJzdGVwc0tleSI6InN1YnNjcmliZVRvQXJlYSJ9

Goldenberg RL, Culhane JF, Iams JD, Romero R (2008) Epidemiology and causes of preterm birth. Lancet (London, England) 371:75–84. https://doi.org/10.1016/S0140-6736(08)60074-4

Gomes GD, Nunes AMB, Libonati R, Ambrizzi T (2022) Projections of subcontinental changes in seasonal precipitation over the two major river basins in South America under an extreme climate scenario. Clim Dyn 58:1147–1169. https://doi.org/10.1007/s00382-021-05955-x

Gomes MS, Cavalcanti IF de A, Müller G V. (2021) 2019/2020 drought impacts on South America and atmospheric and oceanic influences. Weather Clim Extrem 34:100404. https://doi.org/10.1016/j.wace.2021.100404

Gouveia CM, Bistinas I, Liberato MLR, et al (2016) The outstanding synergy between drought, heatwaves and fuel on the 2007 Southern Greece exceptional fire season. Agric For Meteorol 218–219:135–145. https://doi.org/10.1016/j.agrformet.2015.11.023

Gozzo LF, Palma DS, Custodio MS, Machado JP (2019) Climatology and trend of severe drought events in the state of Sao Paulo, Brazil, during the 20th century. Atmosphere (Basel) 10:1–16. https://doi.org/10.3390/ATMOS10040190

Grimm AM (2019) Madden–Julian Oscillation impacts on South American summer monsoon season: precipitation anomalies, extreme events, teleconnections, and role in the MJO cycle. Clim Dyn 53:907–932. https://doi.org/10.1007/s00382-019-04622-6

Grynszpan D (2003) Lessons from the French heatwave. Lancet (London, England) 362:1169–70. https://doi.org/10.1016/S0140-6736(03)14555-2

Guo Y, Gasparrini A, Armstrong BG, et al (2017) Heat Wave and Mortality: A Multicountry, Multicommunity Study. Environ Health Perspect 125:87006. https://doi.org/10.1289/EHP1026

Guo Y, Gasparrini A, Li S, et al (2018) Quantifying excess deaths related to heatwaves under climate change scenarios: A multicountry time series modelling study. PLoS Med 15:1–

17. https://doi.org/10.1371/journal.pmed.1002629

Gusso A, Ducati JR, Veronez MR, et al (2014) Monitoring the vulnerability of soybean to heat waves and their impacts in Mato Grosso state, Brazil. In: 2014 IEEE Geoscience and Remote Sensing Symposium. pp 859–862

Gutowski Jr. WJ, Giorgi F, Timbal B, et al (2016) WCRP COordinated Regional Downscaling EXperiment (CORDEX): a diagnostic MIP for CMIP6. Geosci Model Dev 9:4087–4095. https://doi.org/10.5194/gmd-9-4087-2016

Ha S (2022) The Changing Climate and Pregnancy Health. Curr Environ Heal reports 9:263–275. https://doi.org/10.1007/s40572-022-00345-9

Haddeland I, Heinke J, Biemans H, et al (2014) Global water resources affected by human interventions and climate change. Proc Natl Acad Sci 111:3251–3256. https://doi.org/10.1073/pnas.1222475110

Hajat S, Kosatky T (2010) Heat-related mortality: A review and exploration of heterogeneity. J Epidemiol Community Health 64:753–760. https://doi.org/10.1136/jech.2009.087999

Hancock PA, Vasmatzidis I (2003) Effects of heat stress on cognitive performance: the current state of knowledge. Int J Hyperth Off J Eur Soc Hyperthermic Oncol North Am Hyperth Gr 19:355–372. https://doi.org/10.1080/0265673021000054630

Hao Z, Hao F, Singh VP, Zhang X (2018a) Changes in the severity of compound drought and hot extremes over global land areas. Environ Res Lett 13:124022. https://doi.org/10.1088/1748-9326/aaee96

Hao Z, Hao F, Singh VP, Zhang X (2018b) Quantifying the relationship between compound dry and hot events and El Niño–southern Oscillation (ENSO) at the global scale. J Hydrol 567:332–338. https://doi.org/10.1016/j.jhydrol.2018.10.022

Haqiqi I, Grogan DS, Hertel TW, Schlenker W (2021) Quantifying the impacts of compound extremes on agriculture. Hydrol Earth Syst Sci 25:551–564. https://doi.org/10.5194/hess-25-551-2021

Hart RE, Grumm RH (2001) Using Normalized Climatological Anomalies to Rank Synoptic-Scale Events Objectively. Mon Weather Rev 129:2426–2442. https://doi.org/10.1175/1520-0493(2001)129<2426:UNCATR>2.0.CO;2

Hartinger SM, Yglesias-González M, Blanco-Villafuerte L, et al (2023) The 2022 South America report of The Lancet Countdown on health and climate change: trust the science. Now that we know, we must act. Lancet Reg Heal Am 20:100470. https://doi.org/10.1016/j.lana.2023.100470

Hassler B, Lauer A (2021) Comparison of Reanalysis and Observational Precipitation Datasets Including ERA5 and WFDE5. Atmosphere (Basel) 12(11):1462. https://doi.org/10.3390/atmos12111462

He B-J, Wang J, Liu H, Ulpiani G (2021) Localized synergies between heat waves and urban heat islands: Implications on human thermal comfort and urban heat management. Environ Res 193:110584. https://doi.org/10.1016/j.envres.2020.110584

He B-J, Wang J, Zhu J, Qi J (2022a) Beating the urban heat: Situation, background, impacts and the way forward in China. Renew Sustain Energy Rev 161:112350. https://doi.org/10.1016/j.rser.2022.112350

He Y, Hu X, Xu W, et al (2022b) Increased probability and severity of compound dry and hot growing seasons over world's major croplands. Sci Total Environ 824:153885. https://doi.org/10.1016/j.scitotenv.2022.153885

Herold N, Alexander L, Green D, Donat M (2017) Greater increases in temperature extremes in low versus high income countries. Environ Res Lett 12:034007. https://doi.org/10.1088/1748-9326/aa5c43

Herold N, Kala J, Alexander L V. (2016) The influence of soil moisture deficits on Australian heatwaves. Environ Res Lett 11:064003. https://doi.org/10.1088/1748-9326/11/6/064003

Hersbach H, Bell B, Berrisford P, et al (2020) The ERA5 global reanalysis. Q J R Meteorol Soc 146:1999–2049. https://doi.org/10.1002/qj.3803

Hertig E, Russo A, Trigo RM (2020) Heat and Ozone Pollution Waves in Central and South Europe—Characteristics, Weather Types, and Association with Mortality. Atmosphere (Basel) 11(12):1271. https://doi.org/10.3390/atmos11121271

Higuera PE, Abatzoglou JT (2021) Record-setting climate enabled the extraordinary 2020 fire season in the western United States. Glob Chang Biol 27:1–2. https://doi.org/10.1111/gcb.15388

Hoffmann WA, Geiger EL, Gotsch SG, et al (2012) Ecological thresholds at the savanna-forest boundary: how plant traits, resources and fire govern the distribution of tropical biomes. Ecol Lett 15:759–768. https://doi.org/10.1111/j.1461-0248.2012.01789.x

Hollander M, Wolfe A. D, Chicken E (2015) Nonparametric Statistical Methods, 3rd Edition. Wiley. https://doi.org/10.1002/9781119196037

Holton JR, Hakim GJ (2012) An introduction to dynamic meteorology: Fifth edition. 978-0-12-384866-6. https://doi.org/10.1016/C2009-0-63394-8

Huang M, Strickland MJ, Richards M, et al (2021) Acute associations between heatwaves and preterm and early-term birth in 50 US metropolitan areas: a matched case-control study. Environ Health 20:47. https://doi.org/10.1186/s12940-021-00733-y

IBGE (2018) Resident population estimate by federation and municipality in 2018

IPCC (2014) Climate Change 2014: Synthesis Report. Contribution of Working Groups I, II, III to the fifth Assessment Report of the Intergovernmental Panel on Climate Change. Geneva, Switzerland

IPCC (2021) Climate Change 2021: The Physical Science Basis. Contribution of Working Group I to the Sixth Assessment Report of the Intergovernmental Panel on Climate Change. Cambridge University Press, Cambridge, United Kingdom and New York, NY, USA

IPCC (2022) Climate Change 2022: Impacts, Adaptation and Vulnerability. Cambridge University Press, Cambridge, UK and New York, USA

IPCC (2023) Climate Change 2023: Synthesis Report. Contribution of Working Groups I, II and III to the Sixth Assessment Report of the Intergovernmental Panel on Climate Change. Geneva, Switzerland

Iturbide M, Casanueva A, Bedia J, et al (2022) On the need of bias adjustment for more plausible climate change projections of extreme heat. Atmos Sci Lett 23:e1072. https://doi.org/10.1002/asl.1072

Ivory SJ, McGlue MM, Spera S, et al (2019) Vegetation, rainfall, and pulsing hydrology in the Pantanal, the world's largest tropical wetland. Environ Res Lett 14:124017.

https://doi.org/10.1088/1748-9326/ab4ffe

Jain P, Castellanos-Acuna D, Coogan SCP, et al (2022) Observed increases in extreme fire weather driven by atmospheric humidity and temperature. Nat Clim Chang 12:63–70. https://doi.org/10.1038/s41558-021-01224-1

Jia P, Liang L, Tan X, et al (2019) Potential effects of heat waves on the population dynamics of the dengue mosquito Aedes albopictus. PLoS Negl Trop Dis 13:e0007528. https://doi.org/10.1371/journal.pntd.0007528

Jiang Y, Wang G, Liu W, et al (2021) Modeled Response of South American Climate to Three Decades of Deforestation. J Clim 34:2189–2203. https://doi.org/10.1175/JCLI-D-20-0380.1

Jiménez-Muñoz JC, Mattar C, Barichivich J, et al (2016) Record-breaking warming and extreme drought in the Amazon rainforest during the course of El Niño 2015–2016. Sci Rep 6:33130. https://doi.org/10.1038/srep33130

Jiménez-Muñoz JC, Sobrino JA, Mattar C, Malhi Y (2013) Spatial and temporal patterns of the recent warming of the Amazon forest. J Geophys Res Atmos 118:5204–5215. https://doi.org/10.1002/jgrd.50456

Jimenez JC, Libonati R, Peres LF (2018) Droughts Over Amazonia in 2005, 2010, and 2015: A Cloud Cover Perspective. Front Earth Sci 6:227. https://doi.org/10.3389/feart.2018.00227

Jimenez JC, Marengo JA, Alves LM, et al (2021) The role of ENSO flavours and TNA on recent droughts over Amazon forests and the Northeast Brazil region. Int J Climatol 41:3761–3780. https://doi.org/10.1002/joc.6453

Jöhnk KD, Huisman JEF, Sharples J, et al (2008) Summer heatwaves promote blooms of harmful cyanobacteria. Glob Chang Biol 14:495–512. https://doi.org/10.1111/j.1365-2486.2007.01510.x

Jolly WM, Cochrane MA, Freeborn PH, et al (2015) Climate-induced variations in global wildfire danger from 1979 to 2013. Nat Commun 6:7537. https://doi.org/10.1038/ncomms8537

Jung M, Reichstein M, Ciais P, et al (2010) Recent decline in the global land evapotranspiration

trend due to limited moisture supply. Nature 467:951–954. https://doi.org/10.1038/nature09396

Junk WJ (2013) Current state of knowledge regarding South America wetlands and their future under global climate change. Aquat Sci 75:113–131. https://doi.org/10.1007/s00027-012-0253-8

Junk WJ, da Silva CJ, Nunes da Cunha C (2011) The Pantanal: Ecology, biodiversity and sustainable management of a large neotropical seasonal wetland. Pensoft Publishers

Kappes MS, Keiler M, von Elverfeldt K, Glade T (2012) Challenges of analyzing multi-hazard risk: a review. Nat Hazards 64:1925–1958. https://doi.org/10.1007/s11069-012-0294-2

Kayano MT, Andreoli R V (2007) Relations of South American summer rainfall interannual variations with the Pacific Decadal Oscillation. Int J Climatol 27:531–540. https://doi.org/10.1002/joc.1417

Kendall MG (1948) Rank correlation methods. Oxford University Press, New York, NY, USA.

Khorshidi MS, Dennison PE, Nikoo MR, et al (2020) Increasing concurrence of wildfire drivers tripled megafire critical danger days in Southern California between1982 and 2018. Environ Res Lett 15:104002. https://doi.org/10.1088/1748-9326/abae9e

King AD (2019) The drivers of nonlinear local temperature change under global warming. Environ Res Lett 14:64005. https://doi.org/10.1088/1748-9326/ab1976

King AD, Knutti R, Uhe P, et al (2018) On the Linearity of Local and Regional Temperature Changes from 1.5°C to 2°C of Global Warming. J Clim 31:7495–7514. https://doi.org/10.1175/JCLI-D-17-0649.1

King AD, Pitman AJ, Henley BJ, et al (2020) The role of climate variability in Australian drought. Nat Clim Chang 10:177–179. https://doi.org/10.1038/s41558-020-0718-z

Konapala G, Mishra AK, Wada Y, Mann ME (2020) Climate change will affect global water availability through compounding changes in seasonal precipitation and evaporation. Nat Commun 11:1–10. https://doi.org/10.1038/s41467-020-16757-w

Kong Q, Guerreiro SB, Blenkinsop S, et al (2020) Increases in summertime concurrent drought and heatwave in Eastern China. Weather Clim Extrem 28:100242.

https://doi.org/10.1016/j.wace.2019.100242

Kornhuber K, Osprey S, Coumou D, et al (2019) Extreme weather events in early summer 2018 connected by a recurrent hemispheric wave-7 pattern. Environ Res Lett 14:54002. https://doi.org/10.1088/1748-9326/ab13bf

Kuehn L, McCormick S (2017) Heat Exposure and Maternal Health in the Face of Climate Change. Int J Environ Res Public Health 14(8):853. https://doi.org/10.3390/ijerph14080853

Kumar S, Getirana A, Libonati R, et al (2022) Changes in land use enhance the sensitivity of tropical ecosystems to fire-climate extremes. Sci Rep 12:964. https://doi.org/10.1038/s41598-022-05130-0

Kumar S, Lawrence DM, Dirmeyer PA, Sheffield J (2014) Less reliable water availability in the 21st century climate projections. Earth's Futur 2:152–160. https://doi.org/10.1002/2013ef000159

Larbey R, Weitkamp E (2020) Water Scarcity Communication in the UK: Learning From Water Company Communications Following the 2018 Heatwave. Front Environ Sci 8:578423. https://doi.org/10.3389/fenvs.2020.578423

Larcom S, She P-W, van Gevelt T (2019) The UK summer heatwave of 2018 and public concern over energy security. Nat Clim Chang 9:370–373. https://doi.org/10.1038/s41558-019-0460-6

Leal Filho W, Azeiteiro UM, Salvia AL, et al (2021) Fire in Paradise: Why the Pantanal is burning. Environ Sci Policy 123:31–34. https://doi.org/10.1016/j.envsci.2021.05.005

Lee S, L'Heureux M, Wittenberg AT, et al (2022) On the future zonal contrasts of equatorial Pacific climate: Perspectives from Observations, Simulations, and Theories. npj Clim Atmos Sci 5:82. https://doi.org/10.1038/s41612-022-00301-2

Leggat WP, Camp EF, Suggett DJ, et al (2019) Rapid Coral Decay Is Associated with Marine Heatwave Mortality Events on Reefs. Curr Biol 29:2723-2730.e4. https://doi.org/10.1016/j.cub.2019.06.077

Lejeune Q, Davin EL, Guillod BP, Seneviratne SI (2015) Influence of Amazonian deforestation on the future evolution of regional surface fluxes, circulation, surface temperature and

precipitation. Clim Dyn 44:2769–2786. https://doi.org/10.1007/s00382-014-2203-8

Lemus-Canovas M, Insua-Costa D, Trigo RM, Miralles DG (2024) Record-shattering 2023 Spring heatwave in western Mediterranean amplified by long-term drought. npj Clim Atmos Sci 7:25. https://doi.org/10.1038/s41612-024-00569-6

Lesk C, Coffel E, Winter J, et al (2021) Stronger temperature–moisture couplings exacerbate the impact of climate warming on global crop yields. Nat Food 2:683–691. https://doi.org/10.1038/s43016-021-00341-6

Lesk C, Rowhani P, Ramankutty N (2016) Influence of extreme weather disasters on global crop production. Nature 529:84–87. https://doi.org/10.1038/nature16467

Li C, Bloom MS, Lin S, et al (2021) Temperature variation and preterm birth among live singleton deliveries in Shenzhen, China: A time-to-event analysis. Environ Res 195:110834. https://doi.org/10.1016/j.envres.2021.110834

Li H, Keune J, Smessaert F, et al (2023) Land–atmosphere feedbacks contribute to crop failure in global rainfed breadbaskets. npj Clim Atmos Sci 6:51. https://doi.org/10.1038/s41612-023-00375-6

Li S, Rifai S, Anderson LO, Sparrow S (2022) Identifying local-scale meteorological conditions favorable to large fires in Brazil. Clim Resil Sustain 1:e11. https://doi.org/10.1002/cli2.11

Liberato MLR, Montero I, Gouveia C, et al (2021) Rankings of extreme and widespread dry and wet events in the Iberian Peninsula between 1901 and 2016. Earth Syst Dyn 12:197–210. https://doi.org/10.5194/esd-12-197-2021

Libonati R, Dacamara CC, Peres LF, et al (2020) Rescue Brazil's burning Pantanal wetlands. Nature 588:217–219. https://doi.org/10.1038/d41586-020-03464-1

Libonati R, Pereira JMC, Da Camara CC, et al (2021) Twenty-first century droughts have not increasingly exacerbated fire season severity in the Brazilian Amazon. Sci Rep 11:4400. https://doi.org/10.1038/s41598-021-82158-8

Libonati R, Geirinhas JL, Silva PS, et al (2022a) Assessing the role of compound drought and heatwave events on unprecedented 2020 wildfires in the Pantanal. Environ Res Lett 17:15005. https://doi.org/10.1088/1748-9326/ac462e

Libonati R, Geirinhas JL, Silva PS, et al (2022b) Drought–heatwave nexus in Brazil and related impacts on health and fires: A comprehensive review. Ann N Y Acad Sci 1517:44–62. https://doi.org/10.1111/nyas.14887

Lima DCA, Lemos G, Bento VA, et al (2023) A multi-variable constrained ensemble of regional climate projections under multi-scenarios for Portugal – Part I: An overview of impacts on means and extremes. Clim Serv 30:100351. https://doi.org/10.1016/j.cliser.2023.100351

Liu W, Sun F, Feng Y, et al (2021) Increasing population exposure to global warm-season concurrent dry and hot extremes under different warming levels. Environ Res Lett 16:94002. https://doi.org/10.1088/1748-9326/ac188f

Liu Y, Pan Z, Zhuang Q, et al (2015) Agriculture intensifies soil moisture decline in Northern China. Sci Rep 5:11261. https://doi.org/10.1038/srep11261

Liu Y, Stanturf J, Goodrick S (2010) Trends in global wildfire potential in a changing climate. For Ecol Manage 259:685–697. https://doi.org/10.1016/j.foreco.2009.09.002

Liu Z, Deng Z, Davis SJ, Ciais P (2024) Global carbon emissions in 2023. Nat Rev Earth Environ 5:253–254. https://doi.org/10.1038/s43017-024-00532-2

Llopart M, Simões Reboita M, Porfírio da Rocha R (2020) Assessment of multi-model climate projections of water resources over South America CORDEX domain. Clim Dyn 54:99–116. https://doi.org/10.1007/s00382-019-04990-z

Lopes dos Santos G, Pereira MG, Delgado RC, et al (2021) Degradation of the Brazilian Cerrado: Interactions with human disturbance and environmental variables. For Ecol Manage 482:118875. https://doi.org/10.1016/j.foreco.2020.118875

Lu Y, Hu H, Li C, Tian F (2018) Increasing compound events of extreme hot and dry days during growing seasons of wheat and maize in China. Sci Rep 8:16700. https://doi.org/10.1038/s41598-018-34215-y

Machado-Silva F, Libonati R, Melo de Lima TF, et al (2020) Drought and fires influence the respiratory diseases hospitalizations in the Amazon. Ecol Indic 109:105817. https://doi.org/10.1016/j.ecolind.2019.105817

Machado-Silva F, Peres LF, Gouveia CM, et al (2021) Drought Resilience Debt Drives NPP

Decline in the Amazon Forest. Global Biogeochem Cycles 35:e2021GB007004. https://doi.org/10.1029/2021GB007004

Mann HB (1945) Nonparametric tests against trend. Econometrica 13(3):245–259. https://doi.org/10.2307/1907187

Mann ME, Rahmstorf S, Kornhuber K, et al (2017) Influence of Anthropogenic Climate Change on Planetary Wave Resonance and Extreme Weather Events. Sci Rep 7:45242. https://doi.org/10.1038/srep45242

Mann ME, Rahmstorf S, Kornhuber K, et al (2018) Projected changes in persistent extreme summer weather events: The role of quasi-resonant amplification. Sci Adv 4:eaat3272. https://doi.org/10.1126/sciadv.aat3272

Manning C, Widmann M, Bevacqua E, et al (2019) Increased probability of compound long-duration dry and hot events in Europe during summer (1950–2013). Environ Res Lett 14:94006. https://doi.org/10.1088/1748-9326/ab23bf

Mantua NJ, Hare SR, Zhang Y, et al (1997) A Pacific Interdecadal Climate Oscillation with Impacts on Salmon Production*. Bull Am Meteorol Soc 78:1069–1080. https://doi.org/10.1175/1520-0477(1997)078<1069:APICOW>2.0.CO;2

Maraun D (2016) Bias correcting climate change simulations-a critical review. Curr Clim Chang Reports 2:211–220. https://doi.org/10.1007/s40641-016-0050-x

Maraun D, Shepherd TG, Widmann M, et al (2017) Towards process-informed bias correction of climate change simulations. Nat Clim Chang 7:764–773. https://doi.org/10.1038/nclimate3418

Marengo JA, Douglas MW, Silva Dias PL (2002) The South American low-level jet east of the Andes during the 1999 LBA-TRMM and LBA-WET AMC campaign. J Geophys Res Atmos 107:LBA 47-1-LBA 47-11. https://doi.org/10.1029/2001JD001188

Marengo JA, Oliveira GS, Alves LM (2015) Climate change scenarios in the Pantanal. Dyn Pantanal Wetl South Am. The Handbook of Environmental Chemistry 37. Springer. https://doi.org/10.1007/698_2015_357

Marengo JA, Alves LM, Torres RR (2016a) Regional climate change scenarios in the Brazilian Pantanal watershed. Clim Res 68:201–213. https://doi.org/10.3354/cr01324

Marengo JA, Espinoza JC (2016b) Extreme seasonal droughts and floods in Amazonia: Causes, trends and impacts. Int J Climatol 36:1033–1050. https://doi.org/10.1002/joc.4420

Marengo JA, Torres RR, Alves LM (2017) Drought in Northeast Brazil—past, present, and future. Theor Appl Climatol 129:1189–1200. https://doi.org/10.1007/s00704-016-1840-8

Marengo JA, Cunha AP, Cuartas LA, et al (2021) Extreme Drought in the Brazilian Pantanal in 2019–2020: Characterization, Causes, and Impacts. Front Water 3:639204. https://doi.org/10.3389/frwa.2021.639204

Marengo JA, Ambrizzi T, Barreto N, et al (2022) The heat wave of October 2020 in central South America. Int J Climatol 42:2281–2298. https://doi.org/10.1002/joc.7365

Mariani M, Holz A, Veblen TT, et al (2018) Climate Change Amplifications of Climate-Fire Teleconnections in the Southern Hemisphere. Geophys Res Lett 45:5071–5081. https://doi.org/10.1029/2018GL078294

Marques JF, Alves MB, Silveira CF, et al (2021) Fires dynamics in the Pantanal: Impacts of anthropogenic activities and climate change. J Environ Manage 299:113586. https://doi.org/10.1016/j.jenvman.2021.113586

Marshall GJ (2003) Trends in the Southern Annular Mode from Observations and Reanalyzes. J Clim 16:4134–4143. https://doi.org/10.1175/1520-0442(2003)016<4134:TITSAM>2.0.CO;2

Martens B, Miralles DG, Lievens H, et al (2017) GLEAM v3: Satellite-based land evaporation and root-zone soil moisture. Geosci Model Dev 10:1903–1925. https://doi.org/10.5194/gmd-10-1903-2017

Massey FJ (1951) The Kolmogorov-Smirnov Test for Goodness of Fit. J Am Stat Assoc 46:68–78. https://doi.org/10.2307/2280095

Mataveli GA V, Pereira G, de Oliveira G, et al (2021) 2020 Pantanal's widespread fire: short- and long-term implications for biodiversity and conservation. Biodivers Conserv 30:3299–3303. https://doi.org/10.1007/s10531-021-02243-2

Matricardi EAT, Skole DL, Costa OB, et al (2020) Long-term forest degradation surpasses deforestation in the Brazilian Amazon. Science 369:1378–1382. https://doi.org/10.1126/science.abb3021

Mazdiyasni O, AghaKouchak A (2015) Substantial increase in concurrent droughts and heatwaves in the United States. Proc Natl Acad Sci U S A 112:11484–11489. https://doi.org/10.1073/pnas.1422945112

McVicar TR, Roderick ML, Donohue RJ, et al (2012) Global review and synthesis of trends in observed terrestrial near-surface wind speeds: Implications for evaporation. J Hydrol 416–417:182–205. https://doi.org/10.1016/j.jhydrol.2011.10.024

McWethy DB, Schoennagel T, Higuera PE, et al (2019) Rethinking resilience to wildfire. Nat Sustain 2:797–804. https://doi.org/10.1038/s41893-019-0353-8

Meehl GA, Tebaldi C (2004) More Intense, More Frequent, and Longer Lasting Heat Waves in the 21st Century. Science 305:994–997. https://doi.org/10.1126/science.1098704

Mendes MCD, Cavalcanti IFA, Herdies DL (2012) Southern Hemisphere atmospheric blocking diagnostic by ECMWF and NCEP/NCAR data. Rev Bras Meteorol 27:263–271. https://doi.org/10.1590/s0102-77862012000300001

Menezes JA, Madureira AP, Santos RB Dos, et al (2021) Analyzing Spatial Patterns of Health Vulnerability to Drought in the Brazilian Semiarid Region. Int J Environ Res Public Health 18(12):6262. https://doi.org/10.3390/ijerph18126262

Menezes LS, de Oliveira AM, Santos FLM, et al (2022) Lightning patterns in the Pantanal: Untangling natural and anthropogenic-induced wildfires. Sci Total Environ 820:153021. https://doi.org/10.1016/j.scitotenv.2022.153021

Meng Y, Hao Z, Feng S, et al (2022) Increase in compound dry-warm and wet-warm events under global warming in CMIP6 models. Glob Planet Change 210:103773. https://doi.org/10.1016/j.gloplacha.2022.103773

Merte S (2017) Estimating heat wave-related mortality in Europe using singular spectrum analysis. Clim Change 142:321–330. https://doi.org/10.1007/s10584-017-1937-9

Miralles DG, Holmes TRH, De Jeu RAM, et al (2011) Global land-surface evaporation estimated from satellite-based observations. Hydrol Earth Syst Sci 15:453–469. https://doi.org/10.5194/hess-15-453-2011

Miralles DG, Van Den Berg MJ, Teuling AJ, De Jeu RAM (2012) Soil moisture-temperature coupling: A multiscale observational analysis. Geophys Res Lett 39:2–7.

https://doi.org/10.1029/2012GL053703

Miralles DG, Teuling AJ, Van Heerwaarden CC, De Arellano JVG (2014) Mega-heatwave temperatures due to combined soil desiccation and atmospheric heat accumulation. Nat Geosci 7:345–349. https://doi.org/10.1038/ngeo2141

Miralles DG, Nieto R, McDowell NG, et al (2016) Contribution of water-limited ecoregions to their own supply of rainfall. Environ Res Lett 11:124007. https://doi.org/10.1088/1748-9326/11/12/124007

Miralles DG, Gentine P, Seneviratne SI, Teuling AJ (2019) Land–atmospheric feedbacks during droughts and heatwaves: state of the science and current challenges. Ann N Y Acad Sci 1436:19–35. https://doi.org/10.1111/nyas.13912

Miranda C de S, Paranho Filho AC, Pott A (2018) Changes in vegetation cover of the Pantanal wetland detected by Vegetation Index: a strategy for conservation. Biota Neotrop 18:e20160297. https://doi.org/10.1590/1676-0611-BN-2016-0297

Mishra A, Bruno E, Zilberman D (2021) Compound natural and human disasters: Managing drought and COVID-19 to sustain global agriculture and food sectors. Sci Total Environ 754:142210. https://doi.org/10.1016/j.scitotenv.2020.142210

Molina MO, Sánchez E, Gutiérrez C (2020) Future heat waves over the Mediterranean from an Euro-CORDEX regional climate model ensemble. Sci Rep 10:1–10. https://doi.org/10.1038/s41598-020-65663-0

Montini TL, Jones C, Carvalho LM V (2019) The South American Low-Level Jet: A New Climatology, Variability, and Changes. J Geophys Res Atmos 124:1200–1218. https://doi.org/10.1029/2018JD029634

Mora C, Dousset B, Caldwell IR, et al (2017) Global risk of deadly heat. Nat Clim Chang 7:501–506. https://doi.org/10.1038/nclimate3322

Moraes SL de, Almendra R, Barrozo LV (2022) Impact of heat waves and cold spells on cause-specific mortality in the city of São Paulo, Brazil. Int J Hyg Environ Health 239:113861. https://doi.org/10.1016/j.ijheh.2021.113861

Moritz MA, Parisien M-A, Batllori E, et al (2012) Climate change and disruptions to global fire activity. Ecosphere 3:art49. https://doi.org/10.1890/ES11-00345.1

Muggeo VMR (2003) Estimating regression models with unknown break-points. Stat Med 22:3055–3071. https://doi.org/10.1002/sim.1545

Muggeo VMR (2016) Testing with a nuisance parameter present only under the alternative: a score-based approach with application to segmented modelling. J Stat Comput Simul 86:3059–3067. https://doi.org/10.1080/00949655.2016.1149855

Muggeo VMR (2017) Interval estimation for the breakpoint in segmented regression: a smoothed score-based approach. Aust \& New Zeal J Stat 59:311–322. https://doi.org/10.1111/anzs.12200

Mukherjee S, Ashfaq M, Mishra AK (2020) Compound Drought and Heatwaves at a Global Scale: The Role of Natural Climate Variability-Associated Synoptic Patterns and Land-Surface Energy Budget Anomalies. J Geophys Res Atmos 125:e2019JD031943. https://doi.org/10.1029/2019JD031943

Mukherjee S, Mishra AK (2021) Increase in Compound Drought and Heatwaves in a Warming World. Geophys Res Lett 48:e2020GL090617. https://doi.org/10.1029/2020GL090617

Mukherjee S, Mishra AK, Ashfaq M, Kao S-C (2022) Relative effect of anthropogenic warming and natural climate variability to changes in Compound drought and heatwaves. J Hydrol 605:127396. https://doi.org/10.1016/j.jhydrol.2021.127396

Mukherjee S, Mishra AK, Zscheischler J, Entekhabi D (2023) Interaction between dry and hot extremes at a global scale using a cascade modeling framework. Nat Commun 14:277. https://doi.org/10.1038/s41467-022-35748-7

Muñoz-Sabater J, Dutra E, Agust\'\i-Panareda A, et al (2021) ERA5-Land: a state-of-the-art global reanalysis dataset for land applications. Earth Syst Sci Data 13:4349–4383. https://doi.org/10.5194/essd-13-4349-2021

Nairn JR, Fawcett RJB (2014) The excess heat factor: a metric for heatwave intensity and its use in classifying heatwave severity. Int J Environ Res Public Health 12:227–253. https://doi.org/10.3390/ijerph120100227

NASA (2022) La Niña times three. https://earthobservatory.nasa.gov/images/150691/la-nina-times-three

NASA NASA's Jet Propulsion Laboratory 2021 Global temperature | vital signs—climate

change: vital signs of the planet. https://climate.nasa.gov/vital-signs/global-temperature/. Accessed 5 Aug 2021

Nepstad D, Lefebvre P, da Silva U, et al (2004) Amazon drought and its implications for forest flammability and tree growth: a basin-wide analysis. Glob Chang Biol 10:704–717. https://doi.org/10.1111/j.1529-8817.2003.00772.x

Nielsen DM, Belém AL, Marton E, Cataldi M (2019) Dynamics-based regression models for the South Atlantic Convergence Zone. Clim Dyn 52:5527–5553. https://doi.org/10.1007/s00382-018-4460-4

Nnamchi HC, Li J, Kucharski F, et al (2015) Thermodynamic controls of the Atlantic Niño. Nat Commun 6:8895. https://doi.org/10.1038/ncomms9895

Nobre CA, Marengo JA, Seluchi ME, et al (2016) Some Characteristics and Impacts of the Drought and Water Crisis in Southeastern Brazil during 2014 and 2015. J Water Resour Prot 08:252–262. https://doi.org/10.4236/jwarp.2016.82022

Nogueira JMP, Rambal S, Barbosa JPRAD, Mouillot F (2017) Spatial Pattern of the Seasonal Drought/Burned Area Relationship across Brazilian Biomes: Sensitivity to Drought Metrics and Global Remote-Sensing Fire Products. Climate 5:42. https://doi.org/10.3390/cli5020042

Oliveira MI, Nascimento EL, Kannenberg C (2018) A New Look at the Identification of Low-Level Jets in South America. Mon Weather Rev 146:2315–2334. https://doi.org/10.1175/MWR-D-17-0237.1

Oliveira U, Soares-Filho B, Bustamante M, et al (2022) Determinants of Fire Impact in the Brazilian Biomes. Front For Glob Chang 5:735017. https://doi.org/10.3389/ffgc.2022.735017

Olmo ME, Weber T, Teichmann C, Bettolli ML (2022) Compound Events in South America Using the CORDEX-CORE Ensemble: Current Climate Conditions and Future Projections in a Global Warming Scenario. J Geophys Res Atmos 127:e2022JD037708. https://doi.org/10.1029/2022JD037708

Olson DM, Dinerstein E, Wikramanayake ED, et al (2001) Terrestrial Ecoregions of the World: A New Map of Life on Earth: A new global map of terrestrial ecoregions provides an

innovative tool for conserving biodiversity. Bioscience 51:933–938. https://doi.org/10.1641/0006-3568(2001)051[0933:TEOTWA]2.0.CO;2

Orth R, O S, Zscheischler J, et al (2022) Contrasting biophysical and societal impacts of hydro-meteorological extremes. Environ Res Lett 17:14044. https://doi.org/10.1088/1748-9326/ac4139

Otkin JA, Svoboda M, Hunt ED, et al (2018) Flash Droughts: A Review and Assessment of the Challenges Imposed by Rapid-Onset Droughts in the United States. Bull Am Meteorol Soc 99:911–919. https://doi.org/10.1175/BAMS-D-17-0149.1

Panisset JS, Libonati R, Gouveia CMP, et al (2018) Contrasting patterns of the extreme drought episodes of 2005, 2010 and 2015 in the Amazon Basin. Int J Climatol 38:1096–1104. https://doi.org/10.1002/joc.5224

Papalexiou SM, Aghakouchak A (2014) Earth ' s Future Special Section : Global , Regional , and Megacity Trends in the Highest Temperature of the Year : Diagnostics and Evidence for Accelerating Trends Earth ' s Future. 1–9. https://doi.org/10.1002/eft2.278

Park Williams A, Allen CD, Macalady AK, et al (2013) Temperature as a potent driver of regional forest drought stress and tree mortality. Nat Clim Chang 3:292–297. https://doi.org/10.1038/nclimate1693

Patz JA, Campbell-Lendrum D, Holloway T, Foley JA (2005) Impact of regional climate change on human health. Nature 438:310–317. https://doi.org/10.1038/nature04188

Pausas JG, Ribeiro E (2013) The global fire–productivity relationship. Glob Ecol Biogeogr 22:728–736. https://doi.org/10.1111/geb.12043

Pechan A, Eisenack K (2014) The impact of heat waves on electricity spot markets. Energy Econ 43:63–71. https://doi.org/10.1016/j.eneco.2014.02.006

Peixoto JP (1973) Atmospheric vapor flux computations for hydrological purposes. WMO Publ. No. 357, World Meteorol. Org., Geneva, 83 pp.

Peixoto JP, Oort AH (1992) Physics of Climate. American Institute of Physics: New York, NY, USA 520 pp.

Peleg N, Molnar P, Burlando P, Fatichi S (2019) Exploring stochastic climate uncertainty in

space and time using a gridded hourly weather generator. J Hydrol 571:627–641. https://doi.org/10.1016/j.jhydrol.2019.02.010

Pendergrass AG, Meehl GA, Pulwarty R, et al (2020) Flash droughts present a new challenge for subseasonal-to-seasonal prediction. Nat Clim Chang 10:191–199. https://doi.org/10.1038/s41558-020-0709-0

Peres L de F, Lucena AJ de, Rotunno Filho OC, França JR de A (2018) The urban heat island in Rio de Janeiro, Brazil, in the last 30 years using remote sensing data. Int J Appl Earth Obs Geoinf 64:104–116. https://doi.org/10.1016/j.jag.2017.08.012

Péres WE, Ribeiro AFS, Russo A, Nunes B (2020) The Association between Air Temperature and Mortality in Two Brazilian Health Regions. Climate 8:. https://doi.org/10.3390/cli8010016

Perkins-Kirkpatrick SE, Gibson PB (2017) Changes in regional heatwave characteristics as a function of increasing global temperature. Sci Rep 7:1–13. https://doi.org/10.1038/s41598-017-12520-2

Perkins-Kirkpatrick SE, Lewis SC (2020) Increasing trends in regional heatwaves. Nat Commun 11:3357. https://doi.org/10.1038/s41467-020-16970-7

Perkins SE, Alexander L V. (2013) On the measurement of heat waves. J Clim 26:4500–4517. https://doi.org/10.1175/JCLI-D-12-00383.1

Perkins SE, Pitman AJ, Holbrook NjmJ, McAneney J (2007) Evaluation of the AR4 climate models' simulated daily maximum temperature, minimum temperature, and precipitation over Australia using probability density functions. J Clim 20:4356–4376. https://doi.org/10.1175/JCLI4253.1

Petrova IY, Miralles DG, Brient F, et al (2024) Observation-constrained projections reveal longer-than-expected dry spells. Nature 633:594–600. https://doi.org/10.1038/s41586-024-07887-y

Pinto MM, Libonati R, Trigo RM, et al (2020) A deep learning approach for mapping and dating burned areas using temporal sequences of satellite images. ISPRS J Photogramm Remote Sens 160:260–274. https://doi.org/10.1016/j.isprsjprs.2019.12.014

Podlaha A, Lorinc M, Srivastava G, et al (2020) Weather, Climate & Catastrophe Insight: 2020

Annual Report. Technical Report

Pott A, Oliveira AKM, Damasceno-Junior GA, Silva JS V (2011) Plant diversity of the Pantanal wetland. Brazilian J Biol 71:265–273. https://doi.org/10.1590/S1519-69842011000200005

Priestley CHB, Taylor RJ (1972) On the Assessment of Surface Heat Flux and Evaporation Using Large-Scale Parameters. Mon Weather Rev 100:81–92. https://doi.org/10.1175/1520-0493(1972)100<0081:otaosh>2.3.co;2

Prosdocimi D, Klima K (2020) Health effects of heat vulnerability in Rio de Janeiro: a validation model for policy applications. SN Appl Sci 2:1948. https://doi.org/10.1007/s42452-020-03750-7

Qiao L, Zuo Z, Zhang R, et al (2023) Soil moisture–atmosphere coupling accelerates global warming. Nat Commun 14:4908. https://doi.org/10.1038/s41467-023-40641-y

Qing Y, Wang S, Ancell BC, Yang Z-L (2022) Accelerating flash droughts induced by the joint influence of soil moisture depletion and atmospheric aridity. Nat Commun 13:1139. https://doi.org/10.1038/s41467-022-28752-4

Rahmstorf S, Coumou D (2011) Increase of extreme events in a warming world. Proc Natl Acad Sci 108:17905–17909. https://doi.org/10.1073/pnas.1101766108

Rammig A, Wiedermann M, Donges JF, et al (2015) Coincidences of climate extremes and anomalous vegetation responses: comparing tree ring patterns to simulated productivity. Biogeosciences 12:373–385. https://doi.org/10.5194/bg-12-373-2015

Ramos AM, Trigo RM, Liberato MLR (2014) A ranking of high-resolution daily precipitation extreme events for the Iberian Peninsula. Atmos Sci Lett 15:328–334. https://doi.org/10.1002/asl2.507

Rasmijn LM, van der Schrier G, Bintanja R, et al (2018) Future equivalent of 2010 Russian heatwave intensified by weakening soil moisture constraints. Nat Clim Chang 8:381–385. https://doi.org/10.1038/s41558-018-0114-0

Rattis L, Brando PM, Macedo MN, et al (2021) Climatic limit for agriculture in Brazil. Nat Clim Chang 11:1098–1104. https://doi.org/10.1038/s41558-021-01214-3

Raymond C, Horton RM, Zscheischler J, et al (2020) Understanding and managing connected extreme events. Nat Clim Chang 10:611–621. https://doi.org/10.1038/s41558-020-0790-4

Raymond C, Suarez-Gutierrez L, Kornhuber K, et al (2022) Increasing spatiotemporal proximity of heat and precipitation extremes in a warming world quantified by a large model ensemble. Environ Res Lett 17:35005. https://doi.org/10.1088/1748-9326/ac5712

Reboita MS, Ambrizzi T, Crespo NM, et al (2021) Impacts of teleconnection patterns on South America climate. Ann N Y Acad Sci 1504:116–153. https://doi.org/10.1111/nyas.14592

Reboita MS, Da Rocha RP, Dias CG, Ynoue RY (2014) Climate projections for South America: RegCM3 driven by HadCM3 and ECHAM5. Adv Meteorol 376738. https://doi.org/10.1155/2014/376738

Reboita MS, Kuki CAC, Marrafon VH, et al (2022) South America climate change revealed through climate indices projected by GCMs and Eta-RCM ensembles. Clim Dyn 58:459–485. https://doi.org/10.1007/s00382-021-05918-2

Reddy PJ, Perkins-Kirkpatrick SE, Ridder NN, Sharples JJ (2022) Combined role of ENSO and IOD on compound drought and heatwaves in Australia using two CMIP6 large ensembles. Weather Clim Extrem 37:100469. https://doi.org/10.1016/j.wace.2022.100469

Regoto P, Dereczynski C, Chou SC, Bazzanela AC (2021) Observed changes in air temperature and precipitation extremes over Brazil. Int J Climatol 41:5125–5142. https://doi.org/10.1002/joc.7119

Requia WJ, Kill E, Papatheodorou S, et al (2022a) Prenatal exposure to wildfire-related air pollution and birth defects in Brazil. J Expo Sci Environ Epidemiol 32:596–603. https://doi.org/10.1038/s41370-021-00380-y

Requia WJ, Papatheodorou S, Koutrakis P, et al (2022b) Increased preterm birth following maternal wildfire smoke exposure in Brazil. Int J Hyg Environ Health 240:113901. https://doi.org/10.1016/j.ijheh.2021.113901

Rey G, Fouillet A, Bessemoulin P, et al (2009) Heat exposure and socio-economic vulnerability as synergistic factors in heat-wave-related mortality. Eur J Epidemiol 24:495–502. https://doi.org/10.1007/s10654-009-9374-3

Riahi K, Rao S, Krey V, et al (2011) RCP 8.5—A scenario of comparatively high greenhouse

gas emissions. Clim Change 109:33. https://doi.org/10.1007/s10584-011-0149-y

Ribeiro AFS, Brando PM, Santos L, et al (2022) A compound event-oriented framework to tropical fire risk assessment in a changing climate. Environ Res Lett 17:65015. https://doi.org/10.1088/1748-9326/ac7342

Ribeiro AFS, Russo A, Gouveia CM, et al (2020a) Risk of crop failure due to compound dry and hot extremes estimated with nested copulas. Biogeosciences 17:4815–4830. https://doi.org/10.5194/bg-17-4815-2020

Ribeiro AFS, Russo A, Gouveia CM, Pires CAL (2020b) Drought-related hot summers: A joint probability analysis in the Iberian Peninsula. Weather Clim Extrem 30:100279. https://doi.org/10.1016/j.wace.2020.100279

Ribeiro IO, Andreoli RV, Kayano MT, et al (2018) Biomass burning and carbon monoxide patterns in Brazil during the extreme drought years of 2005, 2010, and 2015. Environ Pollut 243:1008–1014. https://doi.org/10.1016/j.envpol.2018.09.022

Richardson D, Black AS, Irving D, et al (2022) Global increase in wildfire potential from compound fire weather and drought. npj Clim Atmos Sci 5:23. https://doi.org/10.1038/s41612-022-00248-4

Ridder NN, Ukkola AM, Pitman AJ, Perkins-Kirkpatrick SE (2022) Increased occurrence of high impact compound events under climate change. npj Clim Atmos Sci 5:3. https://doi.org/10.1038/s41612-021-00224-4

Rivera JA, Otta S, Lauro C, Zazulie N (2021) A decade of hydrological drought in Central-Western Argentina. Front Water 3:640544. https://doi.org/10.3389/frwa.2021.640544

Rochedo PRR, Soares-Filho B, Schaeffer R, et al (2018) The threat of political bargaining to climate mitigation in Brazil. Nat Clim Chang 8:695–698. https://doi.org/10.1038/s41558-018-0213-y

Rodrigues JA, Libonati R, Peres LDF, Setzer A (2018) Mapeamento de Áreas Queimadas em Unidades de Conservação da Região Serrana do Rio de Janeiro Utilizando o Satélite Landsat-8 Durante a Seca de 2014. Anuário do Inst Geociências - UFRJ 41:318–327. https://doi.org/10.11137/2018_1_318_327

Rodrigues M, Peña-Angulo D, Russo A, et al (2021) Do climate teleconnections modulate

wildfire-prone conditions over the Iberian Peninsula? Environ Res Lett 16:44050. https://doi.org/10.1088/1748-9326/abe25d

Rodrigues RR, Taschetto AS, Sen Gupta A, Foltz GR (2019) Common cause for severe droughts in South America and marine heatwaves in the South Atlantic. Nat Geosci 12:620–626. https://doi.org/10.1038/s41561-019-0393-8

Roos N, Kovats S, Hajat S, et al (2021) Maternal and newborn health risks of climate change: A call for awareness and global action. Acta Obstet Gynecol Scand 100:566–570. https://doi.org/10.1111/aogs.14124

Rosselló J, Becken S, Santana-Gallego M (2020) The effects of natural disasters on international tourism: A global analysis. Tour Manag 79:104080. https://doi.org/10.1016/j.tourman.2020.104080

Rousi E, Kornhuber K, Beobide-Arsuaga G, et al (2022) Accelerated western European heatwave trends linked to more-persistent double jets over Eurasia. Nat Commun 13:3851. https://doi.org/10.1038/s41467-022-31432-y

Rozenberg J, Davis SJ, Narloch U, Hallegatte S (2015) Climate constraints on the carbon intensity of economic growth. Environ Res Lett 10:95006. https://doi.org/10.1088/1748-9326/10/9/095006

Ruffault J, Curt T, Moron V, et al (2020) Increased likelihood of heat-induced large wildfires in the Mediterranean Basin. Sci Rep 10:13790. https://doi.org/10.1038/s41598-020-70069-z

Ruscica RC, Menéndez CG, Sörensson AA (2016) Land surface–atmosphere interaction in future South American climate using a multi-model ensemble. Atmos Sci Lett 17:141–147. https://doi.org/10.1002/asl.635

Ruscica RC, Sörensson AA, Menéndez CG (2014) Hydrological links in Southeastern South America: soil moisture memory and coupling within a hot spot. Int J Climatol 34:3641–3653. https://doi.org/10.1002/joc.3930

Ruscica RC, Sörensson AA, Menéndez CG (2015) Pathways between soil moisture and precipitation in southeastern South America. Atmos Sci Lett 16:267–272. https://doi.org/10.1002/asl2.552

Russo A, Gouveia CM, Dutra E, et al (2019) The synergy between drought and extremely hot summers in the Mediterranean. Environ Res Lett 14:14011. https://doi.org/10.1088/1748-9326/aaf09e

Russo S, Dosio A, Graversen RG, et al (2014) Magnitude of extreme heat waves in present climate and their projection in a warming world. J Geophys Res Atmos 119:12,500-12,512. https://doi.org/10.1002/2014JD022098

Russo S, Sillmann J, Fischer EM (2015) Top ten European heatwaves since 1950 and their occurrence in the coming decades. Environ Res Lett 10:. https://doi.org/10.1088/1748-9326/10/12/124003

Russo S, Sillmann J, Sterl A (2017) Humid heat waves at different warming levels. Sci Rep 7:1–7. https://doi.org/10.1038/s41598-017-07536-7

Rusticucci M (2012) Observed and simulated variability of extreme temperature events over South America. Atmos Res 106:1–17. https://doi.org/10.1016/j.atmosres.2011.11.001

Rusticucci M, Zazulie N (2021) Attribution and projections of temperature extreme trends in South America based on CMIP5 models. Ann N Y Acad Sci. 1504(1):154–166. https://doi.org/10.1111/nyas.14591

Salomón RL, Peters RL, Zweifel R, et al (2022) The 2018 European heatwave led to stem dehydration but not to consistent growth reductions in forests. Nat Commun 13:28. https://doi.org/10.1038/s41467-021-27579-9

Salvador C, Vicedo-Cabrera AM, Libonati R, et al (2022) Effects of Drought on Mortality in Macro Urban Areas of Brazil Between 2000 and 2019. GeoHealth 6:e2021GH000534. https://doi.org/10.1029/2021GH000534

Sano EE, Rodrigues AA, Martins ES, et al (2019) Cerrado ecoregions: A spatial framework to assess and prioritize Brazilian savanna environmental diversity for conservation. J Environ Manage 232:818–828. https://doi.org/10.1016/j.jenvman.2018.11.108

Santanello JA, Dirmeyer PA, Ferguson CR, et al (2018) Land–Atmosphere Interactions: The LoCo Perspective. Bull Am Meteorol Soc 99:1253–1272. https://doi.org/10.1175/BAMS-D-17-0001.1

Sardeshmukh PD, Hoskins BJ (1988) The Generation of Global Rotational Flow by Steady

Idealized Tropical Divergence. J Atmos Sci 45:1228–1251. https://doi.org/10.1175/1520-0469(1988)045<1228:TGOGRF>2.0.CO;2

Sasaki W, Doi T, Richards KJ, Masumoto Y (2015) The influence of ENSO on the equatorial Atlantic precipitation through the Walker circulation in a CGCM. Clim Dyn 44:191–202. https://doi.org/10.1007/s00382-014-2133-5

Scalley BD, Spicer T, Jian L, et al (2015) Responding to heatwave intensity : Excess Heat Factor is a superior predictor of health service utilisation and a trigger for heatwave plans. 582–587. https://doi.org/10.1111/1753-6405.12421

Schiermeier Q (2021) Climate change made North America's deadly heatwave 150 times more likely. Nature. https://doi.org/10.1038/d41586-021-01869-0

Schifano P, Asta F, Dadvand P, et al (2016) Heat and air pollution exposure as triggers of delivery: A survival analysis of population-based pregnancy cohorts in Rome and Barcelona. Environ Int 88:153–159. https://doi.org/10.1016/j.envint.2015.12.013

Schöngart J, Wittmann F, Junk WJ, Piedade MTF (2017) Vulnerability of Amazonian floodplains to wildfires differs according to their typologies impeding generalizations. Proc Natl Acad Sci 114(41):E8550–E8551. https://doi.org/10.1073/pnas.1713734114

Schumacher DL, Hauser M, Seneviratne SI (2022a) Drivers and Mechanisms of the 2021 Pacific Northwest Heatwave. Earth's Futur 10:e2022EF002967. https://doi.org/10.1029/2022EF002967

Schumacher DL, Keune J, Dirmeyer P, Miralles DG (2022b) Drought self-propagation in drylands due to land–atmosphere feedbacks. Nat Geosci 15:262–268. https://doi.org/10.1038/s41561-022-00912-7

Schumacher DL, Keune J, van Heerwaarden CC, et al (2019) Amplification of mega-heatwaves through heat torrents fuelled by upwind drought. Nat Geosci 12:712–717. https://doi.org/10.1038/s41561-019-0431-6

Seager R, Cane M, Henderson N, et al (2019) Strengthening tropical Pacific zonal sea surface temperature gradient consistent with rising greenhouse gases. Nat Clim Chang 9:517–522. https://doi.org/10.1038/s41558-019-0505-x

Seddon AWR, Macias-Fauria M, Long PR, et al (2016) Sensitivity of global terrestrial

ecosystems to climate variability. Nature 531:229–232. https://doi.org/10.1038/nature16986

Sedlmeier K, Feldmann H, Schädler G (2018) Compound summer temperature and precipitation extremes over central Europe. Theor Appl Climatol 131:1493–1501. https://doi.org/10.1007/s00704-017-2061-5

Sen Gupta A, Thomsen M, Benthuysen JA, et al (2020) Drivers and impacts of the most extreme marine heatwave events. Sci Rep 10:19359. https://doi.org/10.1038/s41598-020-75445-3

Sen PK (1968) Estimates of the regression coefficient based on Kendall's tau. J Am Stat Assoc 63(324):1379–1389. https://doi.org/10.2307/2285891

Sena A, Freitas C, Feitosa Souza P, et al (2018) Drought in the Semiarid Region of Brazil: Exposure, Vulnerabilities and Health Impacts from the Perspectives of Local Actors. PLoS Curr 10:. https://doi.org/10.1371/currents.dis.c226851ebd64290e619a4d1ed79c8639

Seneviratne SI, Corti T, Davin EL, et al (2010) Investigating soil moisture-climate interactions in a changing climate: A review. Earth-Science Rev 99:125–161. https://doi.org/10.1016/j.earscirev.2010.02.004

Seneviratne SI, Nicholls N, Easterling D, et al (2012) Changes in Climate Extremes and their Impacts on the Natural Physical Environment. In: Field CB, Barros V, Stocker TF, Dahe Q (eds) Managing the Risks of Extreme Events and Disasters to Advance Climate Change Adaptation: Special Report of the Intergovernmental Panel on Climate Change. Cambridge University Press, Cambridge, pp 109–230

Seneviratne SI, Wilhelm M, Stanelle T, et al (2013) Impact of soil moisture-climate feedbacks on CMIP5 projections: First results from the GLACE-CMIP5 experiment. Geophys Res Lett 40:5212–5217. https://doi.org/10.1002/grl.50956

Seo Y-W, Ha K-J, Park T-W (2021) Feedback attribution to dry heatwaves over East Asia. Environ Res Lett 16:064003. https://doi.org/10.1088/1748-9326/abf18f

Seth A, Fernandes K, Camargo SJ (2015) Two summers of São Paulo drought: Origins in the western tropical Pacific. Geophys Res Lett 42: 10,816–10,823. https://doi.org/10.1002/2015GL066314

Shaposhnikov D, Revich B, Bellander T, et al (2014) Mortality related to air pollution with the Moscow heat wave and wildfire of 2010. Epidemiology 25:359–364. https://doi.org/10.1097/EDE.0000000000000090

Sharma S, Mujumdar P (2017) Increasing frequency and spatial extent of concurrent meteorological droughts and heatwaves in India. Sci Rep 7:15582. https://doi.org/10.1038/s41598-017-15896-3

Sharples JJ, Lewis SC, Perkins-Kirkpatrick SE (2021) Modulating influence of drought on the synergy between heatwaves and dead fine fuel moisture content of bushfire fuels in the Southeast Australian region. Weather Clim Extrem 31:100300. https://doi.org/10.1016/j.wace.2020.100300

Shi Z, Jia G, Zhou Y, et al (2021) Amplified intensity and duration of heatwaves by concurrent droughts in China. Atmos Res 261:105743. https://doi.org/10.1016/j.atmosres.2021.105743

Shimizu MH, Ambrizzi T (2016) MJO influence on ENSO effects in precipitation and temperature over South America. Theor Appl Climatol 124:291–301. https://doi.org/10.1007/s00704-015-1421-2

Shimizu MH, de Albuquerque Cavalcanti IF (2011) Variability patterns of Rossby wave source. Clim Dyn 37:441–454. https://doi.org/10.1007/s00382-010-0841-z

Silva Dias MAF, Dias J, Carvalho LM V, et al (2013) Changes in extreme daily rainfall for São Paulo, Brazil. Clim Change 116:705–722. https://doi.org/10.1007/s10584-012-0504-7

Silva GAM, Ambrizzi T (2006) Inter-El Niño variability and its impact on the South American low-level jet east of the Andes during austral summer − two case studies. Adv Geosci 6:283–287. https://doi.org/10.5194/adgeo-6-283-2006

Silva PS, Bastos A, Libonati R, et al (2019) Impacts of the 1.5 °C global warming target on future burned area in the Brazilian Cerrado. For Ecol Manage 446:193–203. https://doi.org/10.1016/j.foreco.2019.05.047

Silva PS, Geirinhas JL, Lapere R, et al (2022) Heatwaves and fire in Pantanal: Historical and future perspectives from CORDEX-CORE. J Environ Manage 323:116193. https://doi.org/10.1016/j.jenvman.2022.116193

Silva PS, Nogueira J, Rodrigues JA, et al (2021) Putting fire on the map of Brazilian savanna ecoregions. J Environ Manage 296:113098. https://doi.org/10.1016/j.jenvman.2021.113098

Silva WL, Nascimento MX, Menezes WF (2015) Atmospheric Blocking in the South Atlantic during the Summer 2014: A Synoptic analysis of the Phenomenon. Appl Categ Struct 05:386–393

Soares PMM, Careto JAM, Cardoso RM, et al (2019) Land-Atmosphere Coupling Regimes in a Future Climate in Africa: From Model Evaluation to Projections Based on CORDEX-Africa. J Geophys Res Atmos 124:11118–11142. https://doi.org/10.1029/2018JD029473

Solman SA, Blázquez J (2019) Multiscale precipitation variability over South America: analysis of the added value of CORDEX RCM simulations. Clim Dyn 53:1547–1565. https://doi.org/10.1007/s00382-019-04689-1

Solman SA, Sanchez E, Samuelsson P, et al (2013) Evaluation of an ensemble of regional climate model simulations over South America driven by the ERA-Interim reanalysis: model performance and uncertainties. Clim Dyn 41:1139–1157. https://doi.org/10.1007/s00382-013-1667-2

Son JY, Gouveia N, Bravo MA, et al (2016) The impact of temperature on mortality in a subtropical city: effects of cold, heat, and heat waves in São Paulo, Brazil. Int J Biometeorol 60:113–121. https://doi.org/10.1007/s00484-015-1009-7

Sousa PM, Barriopedro D, García-Herrera R, et al (2020) Distinct influences of large-scale circulation and regional feedbacks in two exceptional 2019 European heatwaves. Commun Earth Environ 1:1–13. https://doi.org/10.1038/s43247-020-00048-9

Sousa PM, Barriopedro D, Ramos AM, et al (2019) Saharan air intrusions as a relevant mechanism for Iberian heatwaves: The record breaking events of August 2018 and June 2019. Weather Clim Extrem 26:. https://doi.org/10.1016/j.wace.2019.100224

Sousa PM, Blamey RC, Reason CJC, et al (2018a) The 'Day Zero' Cape Town drought and the poleward migration of moisture corridors. Environ Res Lett 13:124025. https://doi.org/10.1088/1748-9326/aaebc7

Sousa PM, Trigo RM, Barriopedro D, et al (2018b) European temperature responses to blocking

and ridge regional patterns. Clim Dyn 50:457–477. https://doi.org/10.1007/s00382-017-3620-2

Sousa PM, Trigo RM, Russo A, et al (2022) Heat-related mortality amplified during the COVID-19 pandemic. Int J Biometeorol 66:457–468. https://doi.org/10.1007/s00484-021-02192-z

Strand LB, Barnett AG, Tong S (2012) Maternal exposure to ambient temperature and the risks of preterm birth and stillbirth in Brisbane, Australia. Am J Epidemiol 175:99–107. https://doi.org/10.1093/aje/kwr404

Strathearn M, Osborne NJ, Selvey LA (2022) Impact of low-intensity heat events on mortality and morbidity in regions with hot, humid summers: a scoping literature review. Int J Biometeorol 66:1013–1029. https://doi.org/10.1007/s00484-022-02243-z

Sun Q, Miao C, Hanel M, et al (2019) Global heat stress on health, wildfires, and agricultural crops under different levels of climate warming. Environ Int 128:125–136. https://doi.org/10.1016/j.envint.2019.04.025

Sutanto SJ, Vitolo C, Di Napoli C, et al (2020) Heatwaves, droughts, and fires: Exploring compound and cascading dry hazards at the pan-European scale. Environ Int 134:105276. https://doi.org/10.1016/j.envint.2019.105276

Svoboda M, Hayes M, Wood D (2012) Standardized precipitation index User Guide. World Meteorological Organization, Geneva, Switzerland

Swart NC, Fyfe JC, Gillett N, Marshall GJ (2015) Comparing Trends in the Southern Annular Mode and Surface Westerly Jet. J Clim 28:8840–8859. https://doi.org/10.1175/JCLI-D-15-0334.1

Tabari H, Willems P (2023) Global risk assessment of compound hot-dry events in the context of future climate change and socioeconomic factors. npj Clim Atmos Sci 6:74. https://doi.org/10.1038/s41612-023-00401-7

Taschetto AS, Ambrizzi T (2012) Can Indian Ocean SST anomalies influence South American rainfall? Clim Dyn 38:1615–1628. https://doi.org/10.1007/s00382-011-1165-3

Taschetto AS, Ummenhofer CC, Stuecker MF, et al (2020) ENSO Atmospheric Teleconnections. In: El Niño Southern Oscillation in a Changing Climate. pp 309–335.

https://doi.org/10.1002/9781119548164.ch14

Tavakol A, Rahmani V, Harrington J (2020) Temporal and spatial variations in the frequency of compound hot, dry, and windy events in the central United States. Sci Rep 10:15691. https://doi.org/10.1038/s41598-020-72624-0

Taylor CM, de Jeu RAM, Guichard F, et al (2012) Afternoon rain more likely over drier soils. Nature 489:423–426. https://doi.org/10.1038/nature11377

Taylor CM, Gounou A, Guichard F, et al (2011) Frequency of Sahelian storm initiation enhanced over mesoscale soil-moisture patterns. Nat Geosci 4:430–433. https://doi.org/10.1038/ngeo1173

Teichmann C, Jacob D, Remedio AR, et al (2021) Assessing mean climate change signals in the global CORDEX-CORE ensemble. Clim Dyn 57:1269–1292. https://doi.org/10.1007/s00382-020-05494-x

Theil H (1950) A rank-invariant method of linear and polynomial regression analysis. Indag Math 12:386–392

Thielen D, Ramoni-Perazzi P, Puche ML, et al (2021) The Pantanal under Siege—On the Origin, Dynamics and Forecast of the Megadrought Severely Affecting the Largest Wetland in the World. Water 13(21):3034. https://doi.org/10.3390/w13213034

Thielen D, Schuchmann K-L, Ramoni-Perazzi P, et al (2020) Quo vadis Pantanal? Expected precipitation extremes and drought dynamics from changing sea surface temperature. PLoS One 15:e0227437. https://doi.org/10.1371/journal.pone.0227437

Thompson DWJ, Solomon S, Kushner PJ, et al (2011) Signatures of the Antarctic ozone hole in Southern Hemisphere surface climate change. Nat Geosci 4:741–749. https://doi.org/10.1038/ngeo1296

Tomas WM, Berlinck CN, Chiaravalloti RM, et al (2021) Distance sampling surveys reveal 17 million vertebrates directly killed by the 2020's wildfires in the Pantanal, Brazil. Sci Rep 11:23547. https://doi.org/10.1038/s41598-021-02844-5

Tomas WM, de Oliveira Roque F, Morato RG, et al (2019) Sustainability Agenda for the Pantanal Wetland: Perspectives on a Collaborative Interface for Science, Policy, and Decision-Making. Trop Conserv Sci 12:1940082919872634.

https://doi.org/10.1177/1940082919872634

Tomasella J, Cunha APMA, Simões PA, Zeri M (2023) Assessment of trends, variability and impacts of droughts across Brazil over the period 1980–2019. Nat Hazards 116:2173–2190. https://doi.org/10.1007/s11069-022-05759-0

Torres RR, Benassi RB, Martins FB, Lapola DM (2022) Projected impacts of 1.5 and 2°C global warming on temperature and precipitation patterns in South America. Int J Climatol 42:1597–1611. https://doi.org/10.1002/joc.7322

Tramujas Vasconcellos Neumann L, Albert SM (2018) Aging in Brazil. Gerontologist 58:611–617. https://doi.org/10.1093/geront/gny019

Trenberth KE (2011) Changes in precipitation with climate change. Clim Res 47:123–138. https://doi.org/10.3354/cr00953

Trigo RM, Pereira JMC, Pereira MG, et al (2006) Atmospheric conditions associated with the exceptional fire season of 2003 in Portugal. Int J Climatol 26:1741–1757. https://doi.org/10.1002/joc.1333

Turco M, Marcos-Matamoros R, Castro X, et al (2019) Seasonal prediction of climate-driven fire risk for decision-making and operational applications in a Mediterranean region. Sci Total Environ 676:577–583. https://doi.org/10.1016/j.scitotenv.2019.04.296

UNESCO WHC (2022) UNESCO World Heritage Centre—World Heritage List

United Nation (2022) Spreading like wildfire: The rising threat of extraordinary landscape fires. UNEP - UN Environ Program

United Nations, Department of Economic and Social Affairs PD (2018) The World ’s Cities in 2018. World’s Cities 2018 - Data Bookl (ST/ESA/ SERA/417) 34

Vale MM, Moura DJ, Nääs IA, Pereira DF (2010) Characterization of heat waves affecting mortality rates of broilers between 29 days and market age. Rev Bras Cienc Avic / Brazilian J Poult Sci 12:279–285. https://doi.org/10.1590/S1516-635X2010000400010

van Vliet MTH, Yearsley JR, Ludwig F, et al (2012) Vulnerability of US and European electricity supply to climate change. Nat Clim Chang 2:676–681. https://doi.org/10.1038/nclimate1546

van Vuuren DP, Stehfest E, den Elzen MGJ, et al (2011) RCP2.6: exploring the possibility to keep global mean temperature increase below 2°C. Clim Change 109:95. https://doi.org/10.1007/s10584-011-0152-3

Varghese BM, Barnett AG, Hansen AL, et al (2019) Characterising the impact of heatwaves on work-related injuries and illnesses in three Australian cities using a standard heatwave definition- Excess Heat Factor (EHF). J Expo Sci Environ Epidemiol 29:821–830. https://doi.org/10.1038/s41370-019-0138-1

Vautard R, Yiou P, D'Andrea F, et al (2007) Summertime European heat and drought waves induced by wintertime Mediterranean rainfall deficit. Geophys Res Lett 34:. https://doi.org/10.1029/2006GL028001

Vicedo-Cabrera AM, Scovronick N, Sera F, et al (2021) The burden of heat-related mortality attributable to recent human-induced climate change. Nat Clim Chang 11:492–500. https://doi.org/10.1038/s41558-021-01058-x

Viganó HH da G, Souza CC de, Reis Neto JF, et al (2018) Prediction and modeling of forest fires in the Pantanal. Rev Bras Meteorol 33:306–316. https://doi.org/10.1590/0102-7786332012

Villar J, Giuliani F, Barros F, et al (2018) Monitoring the Postnatal Growth of Preterm Infants: A Paradigm Change. Pediatrics 141(2):e20172467. https://doi.org/10.1542/peds.2017-2467

Vitolo C, Di Giuseppe F, Barnard C, et al (2020) ERA5-based global meteorological wildfire danger maps. Sci data 7:216. https://doi.org/10.1038/s41597-020-0554-z

Vogel J, Paton E, Aich V, Bronstert A (2021) Increasing compound warm spells and droughts in the Mediterranean Basin. Weather Clim Extrem 32:100312. https://doi.org/10.1016/j.wace.2021.100312

Wang C, Li Z, Chen Y, et al (2023) Drought-heatwave compound events are stronger in drylands. Weather Clim Extrem 42:100632. https://doi.org/10.1016/j.wace.2023.100632

Wang H, Abajobir AA, Abate KH, Abbafati C (2017a) Global Health Metrics Global , regional , and national under-5 mortality , adult mortality , age-specific mortality , and life expectancy , 1970 – 2016 : a systematic analysis for the Global Burden of Disease Study

2016. 390:1970–2016. https://doi.org/10.1016/S0140-6736(17)31833-0

Wang R, Lü G, Ning L, et al (2021) Likelihood of compound dry and hot extremes increased with stronger dependence during warm seasons. Atmos Res 260:105692. https://doi.org/10.1016/j.atmosres.2021.105692

Wang S-YS, Yoon J-H, Becker E, Gillies R (2017b) California from drought to deluge. Nat Clim Chang 7:465–468. https://doi.org/10.1038/nclimate3330

Watch C (2024) Historical GHG emissions. Data Explor Available online https//www Clim org/data-explorer/(accessed 29 May 2024)

Watson K (2014) Drought hits Brazil's coffee industry. https://www.bbc.com/news/business-27623535

Wei Y, Ren H-L (2022) Distinct MJOs Under the Two Types of La Niña. J Geophys Res Atmos 127:e2022JD037646. https://doi.org/10.1029/2022JD037646

White RH, Kornhuber K, Martius O, Wirth V (2022) From Atmospheric Waves to Heatwaves: A Waveguide Perspective for Understanding and Predicting Concurrent, Persistent, and Extreme Extratropical Weather. Bull Am Meteorol Soc 103:E923–E935. https://doi.org/10.1175/BAMS-D-21-0170.1

WHO (2015) WHO recommendations on interventions to improve preterm birth outcomes: Highlights and key messages from the World Health Organization's 2015 global recommendations (WHO/RHR/15.16). World Health Organization

Wilks DS (2011) Statistical methods in the atmospheric sciences. 3rd Edition, Academic press, Oxford

Williams AP, Abatzoglou JT (2016) Recent Advances and Remaining Uncertainties in Resolving Past and Future Climate Effects on Global Fire Activity. Curr Clim Chang Reports 2:1–14. https://doi.org/10.1007/s40641-016-0031-0

Willmott CJ, Robeson SM, Matsuura K (2012) A refined index of model performance. Int J Climatol 32:2088–2094. https://doi.org/10.1002/joc.2419

WMO (2021) State of the climate in latin America and the caribbean 2020. https://library.wmo.int/index.php?lvl=notice_display%26id=21926 #.YXAvuRrMI2x.

Accessed 5 Nov 2021

Wohlfahrt G, Gerdel K, Migliavacca M, et al (2018) Sun-induced fluorescence and gross primary productivity during a heat wave. Sci Rep 8:14169. https://doi.org/10.1038/s41598-018-32602-z

Wood EF, Roundy JK, Troy TJ, et al (2011) Hyperresolution global land surface modeling: Meeting a grand challenge for monitoring Earth's terrestrial water. Water Resour Res 47:. https://doi.org/10.1029/2010WR010090

Wouters H, Keune J, Petrova IY, et al (2022) Soil drought can mitigate deadly heat stress thanks to a reduction of air humidity. Sci Adv 8:eabe6653. https://doi.org/10.1126/sciadv.abe6653

Wu G, Chen J, Shi X, et al (2022) Impacts of global climate warming on meteorological and hydrological droughts and their propagations. Earth's Futur 10:e2021EF002542. https://doi.org/10.1029/2021EF002542

Wu X, Hao Z, Hao F, et al (2019) Spatial and Temporal Variations of Compound Droughts and Hot Extremes in China. Atmosphere (Basel) 10(2):95. https://doi.org/10.3390/atmos10020095

Wu X, Hao Z, Zhang X, et al (2020) Evaluation of severity changes of compound dry and hot events in China based on a multivariate multi-index approach. J Hydrol 583:124580. https://doi.org/10.1016/j.jhydrol.2020.124580

Wu X, Jiang D (2022) Probabilistic impacts of compound dry and hot events on global gross primary production. Environ Res Lett 17:34049. https://doi.org/10.1088/1748-9326/ac4c5b

Xi Y, Peng S, Ciais P, Chen Y (2021) Future impacts of climate change on inland Ramsar wetlands. Nat Clim Chang 11:45–51. https://doi.org/10.1038/s41558-020-00942-2

Xu C, Kohler TA, Lenton TM, et al (2020) Future of the human climate niche. Proc Natl Acad Sci 117:11350–11355. https://doi.org/10.1073/pnas.1910114117

Xu R, Zhao Q, Coelho MSZS, et al (2019) Association between Heat Exposure and Hospitalization for Diabetes in Brazil during 2000-2015: A Nationwide Case-Crossover Study. Environ Health Perspect 127:117005. https://doi.org/10.1289/EHP5688

Xu W, Yuan W, Wu D, et al (2024) Impacts of record-breaking compound heatwave and drought events in 2022 China on vegetation growth. Agric For Meteorol 344:109799. https://doi.org/10.1016/j.agrformet.2023.109799

Yan M, Xie Y, Zhu H, et al (2022) The exceptional heatwaves of 2017 and all-cause mortality: An assessment of nationwide health and economic impacts in China. Sci Total Environ 812:152371. https://doi.org/10.1016/j.scitotenv.2021.152371

Yan Y, Piao S, Hammond WM, et al (2024) Climate-induced tree-mortality pulses are obscured by broad-scale and long-term greening. Nat Ecol Evol 8:912–923. https://doi.org/10.1038/s41559-024-02372-1

Yin J, Gentine P, Slater L, et al (2023) Future socio-ecosystem productivity threatened by compound drought–heatwave events. Nat Sustain 6:259–272. https://doi.org/10.1038/s41893-022-01024-1

Yu R, Zhai P (2020) More frequent and widespread persistent compound drought and heat event observed in China. Sci Rep 10:1–7. https://doi.org/10.1038/s41598-020-71312-3

Zanin PR, Satyamurty P (2020) Hydrological processes interconnecting the two largest watersheds of South America from seasonal to intra-monthly time scales: A critical review. Int J Climatol 40:3971–4005. https://doi.org/10.1002/joc.6443

Zhang Q, She D, Zhang L, et al (2022a) High Sensitivity of Compound Drought and Heatwave Events to Global Warming in the Future. Earth's Futur 10:e2022EF002833. https://doi.org/10.1029/2022EF002833

Zhang Y, Li Q, Ge Y, et al (2022b) Growing prevalence of heat over cold extremes with overall milder extremes and multiple successive events. Commun Earth Environ 3:73. https://doi.org/10.1038/s43247-022-00404-x

Zhao Q, Li S, Coelho MSZS, et al (2019a) The association between heatwaves and risk of hospitalization in Brazil: A nationwide time series study between 2000 and 2015. PLoS Med 16:e1002753. https://doi.org/10.1371/journal.pmed.1002753

Zhao Q, Li S, Coelho MSZS, et al (2019b) Geographic, Demographic, and Temporal Variations in the Association between Heat Exposure and Hospitalization in Brazil: A Nationwide Study between 2000 and 2015. Environ Health Perspect 127:17001.

https://doi.org/10.1289/EHP3889

Zhou S, Williams AP, Lintner BR, et al (2021) Soil moisture–atmosphere feedbacks mitigate declining water availability in drylands. Nat Clim Chang 11:38–44. https://doi.org/10.1038/s41558-020-00945-z

Zhou S, Zhang Y, Williams AP, Gentine P (2019) Projected increases in intensity, frequency, and terrestrial carbon costs of compound drought and aridity events. Sci Adv 5:eaau5740. https://doi.org/10.1126/sciadv.aau5740

Zipper SC, Qiu J, Kucharik CJ (2016) Drought effects on US maize and soybean production: spatiotemporal patterns and historical changes. Environ Res Lett 11:94021. https://doi.org/10.1088/1748-9326/11/9/094021

Zomer RJ, Xu J, Trabucco A (2022) Version 3 of the Global Aridity Index and Potential Evapotranspiration Database. Sci Data 9:409. https://doi.org/10.1038/s41597-022-01493-1

Zscheischler J, Seneviratne SI (2017) Dependence of drivers affects risks associated with compound events. Sci Adv 3:e1700263. https://doi.org/10.1126/sciadv.1700263

Zscheischler J, Westra S, van den Hurk BJJM, et al (2018) Future climate risk from compound events. Nat Clim Chang 8:469–477. https://doi.org/10.1038/s41558-018-0156-3

Zschenderlein P, Fink AH, Pfahl S, Wernli H (2019) Processes determining heat waves across different European climates. Q J R Meteorol Soc 145:2973–2989. https://doi.org/10.1002/qj.3599

Zscheischler J, Martius O, Westra S, et al (2020) A typology of compound weather and climate events. Nat Rev Earth Environ 1:333–347. https://doi.org/10.1038/s43017-020-0060-z